Evaluating the Redundancy of Steel Bridges:

Full-Scale Destructive Testing of a Fracture Critical Twin Box-Girder Steel Bridge

by

Bryce Jacob Neuman, B.S.

Thesis

Presented to the Faculty of the Graduate School of

The University of Texas at Austin

in Partial Fulfillment

of the Requirements

for the Degree of

Master of Science in Engineering

The University of Texas at Austin

May, 2009

Evaluating the Redundancy of Steel Bridges:

Full-Scale Destructive Testing of a Fracture Critical Twin Box-Girder Steel Bridge

APPROVED BY

SUPERVISING COMMITTEE:

____

Eric B. Williamson

____

Karl H. Frank

Dedication

To Amit Gupta

who recognized this ambition before anyone else

including myself

Acknowledgements

To begin, Dr. Eric Williamson and Dr. Karl Frank deserve my enormous thanks. Even before guiding me through this research project and my academic endeavors at the University of Texas, they took a chance and gave me the opportunity to participate in what turned out to be the most educational experience of my life.

My research partners also deserve recognition for their immense contribution to this project. It was a pleasure work with Vasilis Samaras: I was lucky to have him as a research partner. A great deal of the material presented in this thesis is the direct result of his hard work. Contributions from Janghwan Kim, Josh Mouras, Catherine Hovell, J.P. Sutton, Tim Barnard, Omar Espinoza, Jeremiah Fasl, Andres Stambuk, Arcan Bundur, and Jim Plantes will also not be forgotten.

On the bottom line, the staff at Ferguson Lab made this project possible. Dennis Fillip and Blake Stasney worked overtime to help realize most every part of this project, and taught me a great deal in the process. I would also like to thank Barbara Howard, Eric Schell, Andrew Valentine, Mike Wason, Jessica Hanten, and Carrie Billingsley for their continual support.

I also owe great thanks to the sponsors at the Texas Department of Transportation, who made this project possible and showed genuine interest in the results of the research.

Finally, love goes out to my family. My Mother and my Father have my utmost respect. I love them for the role they have played in where I am now, and hope they know as much. Moreover, it would be an understatement to say I am also fortunate to have my siblings and their families in my life. You are all a great part of who I am.

May 8, 2009

Abstract

Evaluating the Redundancy of Steel Bridges:

Full-Scale Destructive Testing of a Fracture Critical Twin Box-Girder Steel Bridge

Bryce Jacob Neuman, M.S.E.

The University of Texas at Austin, 2009

Supervisor: Eric B. Williamson

AASHTO defines a fracture critical member as a “component in tension whose failure is expected to result in the collapse of the bridge or the inability of the bridge to perform its function,” and requires costly bi-annual inspection of all bridges designed with fracture critical members. Failures of fracture critical members on in-service bridges, however, have demonstrated that these structures often possess sufficient capacity through redundant load paths overlooked by the fracture critical provisions of the AASHTO specifications.

The Texas Department of Transportation and the Federal Highway Administration funded a large-scale research project through the Ferguson Structural Engineering Laboratory at the University of Texas to develop methods for evaluating the redundancy of fracture critical steel bridges. Provided with new tools to estimate the redundant capacities and ultimate loads of their structures, transportation authorities will be able to tailor their maintenance and inspection schedules to their bridge inventories, appropriately managing labor and financial resources.

As part of the research project, a full-scale twin box-girder steel bridge representative of fracture critical bridges in Texas was decommissioned from the highway system in Houston, rebuilt at Ferguson Lab, and prepared for testing. Twin box-girder bridges are designed with two tension flanges, and both are designated as fracture critical members.

A series of three experiments were performed on the test-bridge to observe its response to a fracture of one of its bottom flanges. The first test used explosives to induce a complete fracture in one of the bridge's bottom flanges. Despite having a load equivalent to a 76-kip truck positioned directly above the mid-span fracture location, the fracture did not propagate into the webs of the girder, minimal deflections were observed, and there was no significant degradation in the capacity of the structure despite the loss of a fracture critical element. The second test shored the damaged girder while the fracture was manually extended to the full depth of the webs. Afterward, the same design load of approximately 76 kips used in the first test was placed above the location of the full-depth fracture. The shoring system was removed nearly instantaneously with the use of explosives, and the bridge was allowed to respond dynamically to its damaged condition. Substantial deflections and damage were observed, but the bridge resisted collapse and maintained complete serviceability. The third test incrementally over-loaded the bridge while the progressive failure mechanisms were closely observed. Loading continued until the ultimate load was reach and the bridge collapsed.

Supported by a number of its elements contributing to create a robust redundant load path, the test-bridge performed extremely well and supported the application of over four times its design load after sustaining a full-depth fracture of one of its two girders. The large concrete railing above the fractured girder transmitted force away from the fracture location when bridge deflections resulted in a closing of its expansion joints. The bridge deck also transferred significant loads in flexure, both transversely and longitudinally to the bridge span. After additional research is carried out, revisions should be considered to the current AASHTO specifications that a) can accurately predict the behavior of these bridges following the failure of a critical member, and b) subsequently prescribe appropriate inspection and maintenance requirements. Given the demonstrated redundancy in these systems beyond that for which they have been credited, the current requirement for bi-annual detailed inspections does not appear to be an effective use of labor or financial resources.

Table of Contents

List of Tables

List of Figures

CHAPTER 1

Introduction

1.1 FRACTURE CRITICAL BRIDGES: BACKGROUND

In the winter of 1967, the Silver Point Bridge in Point Pleasant, West Virginia suddenly collapsed into the Ohio River (Figure 1-1). The investigation of the failure determined that the fracture of a single eye-bar connecting the bridge's suspension chain released the primary load path, which resulted in the total collapse of the structure (Scheffey, 1971). This event demonstrated that the failure of individual members could have a significant influence on the stability of an entire bridge structure, and it led to a reconsideration of code and safety requirements for bridges theoretically susceptible to this type of failure.

Fracture critical member provisions were first introduced into the American Association of State Highway Transportation Officials (AASHTO) Bridge Design Specifications in 1978. In the current draft of that document, a fracture critical member (FCM) is defined as a "component in tension whose failure is expected to result in the collapse of the bridge or the inability of the bridge to perform its function" (AASHTO, 2004). All bridges designed with fracture critical members or components are designated as Fracture Critical Bridges (FCB).

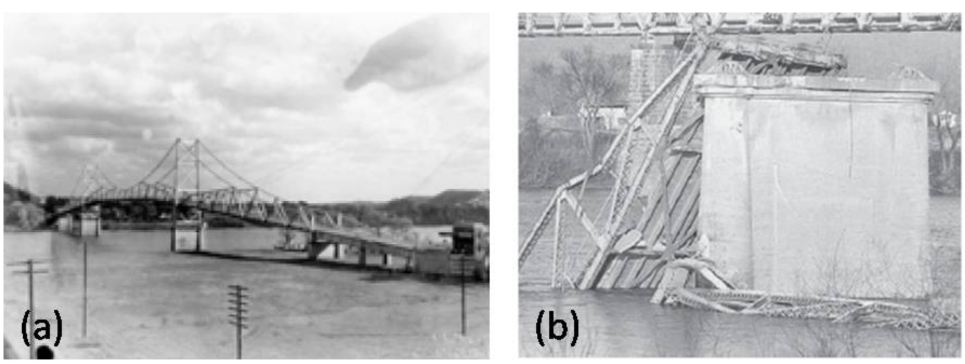

Figure 1-1: The Point Pleasant Bridge (a) In service, (b) After failure

The bridge design process is affected by many factors, including economics, aesthetics, and traffic volume, and many popular bridge structural systems are classified as fracture critical. In fact, approximately 11% of all steel bridges in the United States are fracture critical (Connor, et al., 2005).

As long as the risk of a brittle fracture of an integral component of a bridge's main load path is minimized, a fracture critical bridge is not inherently unsafe. For this reason, the design of fracture critical bridges is permitted, but a primary specification in the fracture critical member provisions requires the full inspection of all fracture critical bridges every two years. Fracture critical bridge inspections are costly, labor intensive, and often require closing of a portion of the bridge to traffic. These inspections require a hands on examination of every welded connection in a fracture critical member.

1.2 FRACTURE CRITICAL BRIDGES: IN PRACTICE

The fracture critical provisions in the AASHTO Bridge Design Specifications assume that, when a fracture critical member is lost, the remaining bridge structure lacks a redundant load path to support its loads. A number of incidents involving the full-depth fracture of in-service two-girder bridges (all designated as fracture critical) provide evidence that, in certain cases, a redundant load path does exist in these structures even though they have not been given credit for such. In 1976, the US-52 Bridge over the Mississippi River near Savanna, Illinois sustained a full-depth fracture of one of its two girders but remained in service until static deflections of 6.5 in. prompted an inspection that discovered the fracture (Fisher, 1977). In 1977, a full-depth fracture of one of the two girders on the Neville Island Bridge on I-79 in Pittsburg, Pennsylvania resulted in deflections so slight that motorists were unaffected, and the fracture remained unnoticed until it was spotted by a nearby boater (Schwendeman, 1978) (Figure 1-2). A similar case was documented in 2003, when a bird-watcher noticed a full-depth fracture in the in-service Brandywine River Bridge on I-95 in Wilmington, Delaware (Quiel, 2003). These bridges were constructed before the implementation of the Fracture Control Plan, which contains more stringent fabrication, inspection, and material requirements.

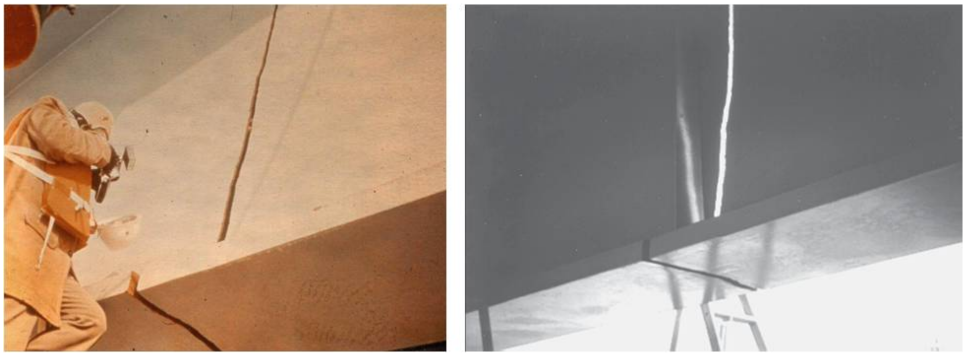

Figure 1-2: Opposing views of the Neville Island Bridge girder fracture

Conflicting evidence of how the loss of a fracture critical member affects overall bridge performance has prompted bridge owners to question the applicability of the fracture critical inspection provisions. One common concern is that, if a fracture critical bridge's stability is not always decisively linked to the performance of its fracture critical members, the increased inspection requirements require owners to utilize an unnecessarily large amount of labor and financial resources.

1.3 RESEARCH INITIATIVE

The Texas Department of Transportation (TxDOT) owns and operates a vast inventory of more than 50,000 bridges throughout the state. Many of these bridges are two-girder bridges and are classified as fracture critical by the AASHTO guidelines. Under the current schedule, TxDOT spends nearly $43 million annually on bridge inspections, and nearly $3 million of this allocation is spent on the bi-annual inspection of all the fracture critical bridges in the state. If a substantial proportion of fracture critical bridges do in fact have the redundant capacity to support their loads in the event of the loss of a fracture critical member, TxDOT may be over-utilizing their resources for the frequent inspections of these bridges.

TxDOT and the Federal Highway Administration (FHWA) co-sponsored a large-scale research program at the Ferguson Structural Engineering Laboratory (FSEL) at The University of Texas at Austin with the overall goal of providing the transportation authorities with methods for evaluating the redundancy of fracture critical steel bridges.

The research focused specifically on investigating the capacity of twin box-girder steel bridges after a fracture. Twin box-girder bridges are common throughout the state of Texas (Figure 1-3). Using tools to estimate the load carrying capacities of their structures in the event of a loss of a fracture critical element, bridge owners would be able to appropriately focus their inspection efforts on the bridges that would suffer a collapse in the event of a fracture.

Supported by significant experimental, computational, and financial resources, the comprehensive research program at FSEL continued for four years and consisted of a set of interrelated experimental initiatives. The techniques used to work toward the ultimate goals of the project included structural analyses performed through 'hand-calculation' methods, analyses performed through detailed computer-based simulations, the testing of laboratory specimens to quantify experimentally the capacity of specific bridge elements, and the full-scale testing of a twin box-girder steel bridge (i.e., a fracture critical bridge) reconstructed at FSEL for use in this project.

Figure 1-3: A typical two-box steel girder bridge in Austin, TX

1.4 SCOPE OF WORK

The full-scale destructive testing of the FSEL test-bridge that was acquired as part of the large-scale research program intended to determine methods for evaluating the redundancy of twin box-girder steel bridges is described in this thesis (Figure 1-4). Background information on the project, including additional details on the overall scope of the research and a history of the twin box-girder steel bridge utilized for testing, are described in Chapter 2. The methodology and general results of the series of three destructive tests that were carried out to observe and quantify the response of the test-bridge to a full-depth fracture of one of its two girders and determine its ultimate capacity are detailed in Chapters 3-8. A summary of the work performed, as well as some concluding remarks and recommendations, are included in Chapter 9.

Figure 1-4: The FSEL test-bridge

CHAPTER 2

Project Background

2.1 INTRODUCTION

In recent years, interest in evaluating the behavior of bridges designated as fracture critical has intensified. In particular, bridge engineers are interested in quantifying the performance of such bridges following the failure of a fracture critical member or fracture critical component. According to the AASHTO Bridge Design Specifications, a fracture on this type of bridge would result in collapse. Empirical evidence, however, has demonstrated that many fracture critical bridges have substantial reserve capacity through alternate load paths, leading bridge owners to become interested in new ways to analyze their structures. Provided with reliable tools to evaluate the redundant capacities of their structures, transportation authorities will be able to appropriately manage their assets and systematically mitigate the associated risks. Ultimately, bridge inspection and maintenance schedules could be revised and financial resources better allocated, all with greater knowledge about and assurance of the safety of the bridges within the highway infrastructure.

To address this issue, a large-scale, multi-faceted research program, sponsored by TxDOT and FHWA, was initiated at the Ferguson Structural Engineering Laboratory (FSEL) to investigate these types of structures. The full scope of the research project included numerous analyses (both 'hand-calculation' and computer based), laboratory testing to evaluate the capacity of specific bridge components, and simulated fracture tests on a full-scale decommissioned test-bridge. The research initiative was focused on twin box-girder steel bridges, which are classified as fracture critical. These structures have this designation because they have only two tension flanges in the positive moment region of the bridge. If one flange were to fracture, the bridge would not be expected to be able to support the design loads. Observations of similar structures, however, have indicated otherwise. This research seeks to determine methods of evaluating the redundant load paths possessed by these bridges in order to better understand existing structures and to guide the design of new structures.

2.2 PRELIMINARY ANALYSES

Preliminary analyses of twin box-girder bridge systems generated a model that described the way a cross-section would deform in the event of a fracture of one of its girders. Losing its flexural capacity, it was hypothesized that the fractured girder would deflect downward under gravity without significant twist due to its high torsional stiffness. This deformed position was a conceptual starting point to identify the redundant path that the loads from the disabled girder would have to travel through in order to maintain stability of the bridge as a whole.

The assumed redundant load path traces through three of the bridge components (Figure 2-1). First, the forces must be transmitted from the fractured girder through its shear studs, loaded in tension, into the concrete deck. Second, the deck would have to transfer the loads, in double curvature bending, across the width of the bridge to the intact girder. Lastly, the intact girder must resist the additional load transfer in torsion, and it must transfer the total load from both girders in strong-axis bending to the ends of the span. It

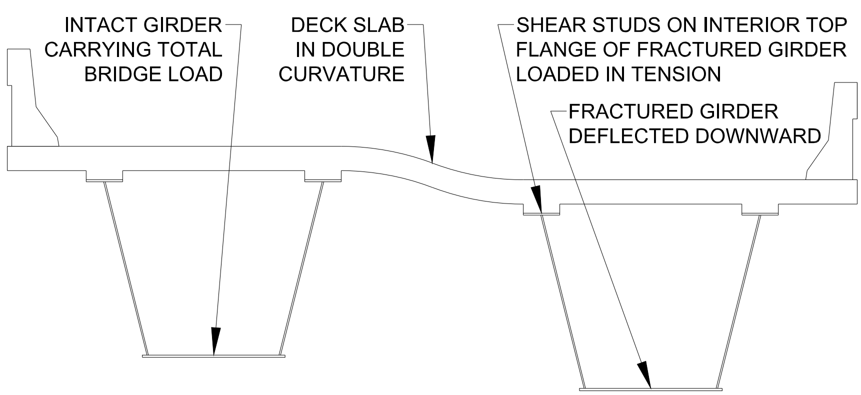

Figure 2-1: Assumed redundant load path in the event of a fractured girder

was also hypothesized that, when the bridge deflected downward, the railings above the deck could engage flexurally to transfer loads away from the fracture location.

Results obtained from the preliminary analyses suggested that a typical concrete deck would have sufficient bending capacity to transfer loads from the fractured girder to the intact girder, which in turn would have sufficient capacity to transfer the full load to its supports. The shear stud connection, however, could not be relied on as confidently (Sutton, 2007). Shear studs cast into concrete are designed for shear forces only. With the cross-section in the assumed deformed shape, some of the shear studs (in particular those along the interior top flange of the fractured girder) are required to transfer forces in tension into the main deck section through an unreinforced concrete haunch. The analysis models developed by Sutton (2007) and Samaras (2009) demonstrate that the capacity of this connection would control the ability of the deck to transfer the forces from the fractured girder to the intact girder. At the time of this writing, the hand-calculation models were still undergoing refinement. A detailed description of these models, their capabilities, and there limitations will be made available by Samaras, later in 2009.

If the connection between the shear studs on the interior top flange of the fractured girder and the deck were to fail, the deformed shape of a cross-section would change (Figure 2-2). In this configuration, preliminary analyses identified a secondary redundant load path that included the contribution of a different set of bridge elements. Tension would

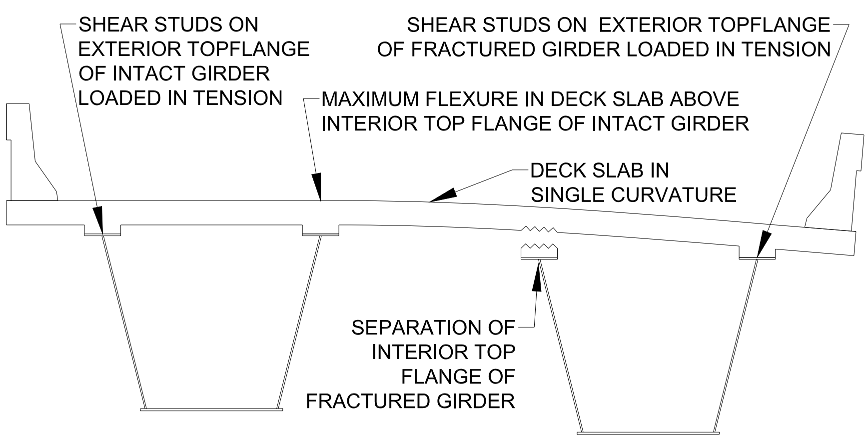

Figure 2-2: Assumed secondary redundant load path in the event of shear stud failure

again develop in the shear stud connections, this time at the exterior top flange of the fractured girder and at the exterior top flange of the intact girder. The deck slab would still transfer loads across the width of the deck, except the deformed shape would change to single curvature bending, where the maximum moment demand would occur above the interior top flange of the intact girder. The intact girder would still be required to resist the additional load transfer in torsion and transfer the total load from both girders in strong-axis bending to the ends of the span. If these load paths could be realized, the bridge should be capable of maintaining stability following a full-depth fracture of one girder.

2.3 SHEAR STUD EVALUATION

Without substantial data on how shear stud connections behave when loaded in tension, a significant research effort was channeled into a testing program to characterize their capacity and to investigate ways of improving their performance. A series of specimens were fabricated to replicate a short segment of a girder top flange, with shear studs connected to a partial width of a concrete deck (Figure 2-3). Dimensions and details of the specimens matched those from the FSEL test-bridge, which is described later in this chapter and for which the plans are included in Appendix A.1. Shear studs were welded to the top flange of WT-stubs closely approximating the dimensions of the girder top flanges, and these stubs mated with the underside of the test specimen's concrete deck. The WT-stubs were 2-ft. long to approximate the average distance at which rows of shear studs were placed on the top flanges of the girders on the test-bridge. The studs were then cast into concrete slabs with reinforcement detailing matching that from the FSEL test-bridge. The concrete section was 8 in. deep to match the thickness of the test-bridge slab, 2 ft. long to match the WT section, and 7 ft. wide based on the range of positive bending moment that would be expected to develop internal to the deck when the fractured girder deflected downward. For testing, the specimens were simply supported atop pedestals, and a ram connected through the WT-stub induced a tension force (Figure 2-4).

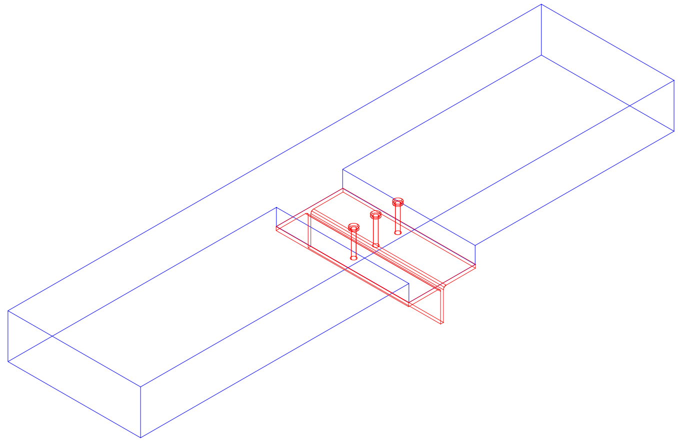

Figure 2-3: Rendering of test specimen (reinforcing bars not shown)

Figure 2-4: Test setup for shear stud tension tests

This testing program studied the effect of different specimen variations on the tensile capacity and ductility of the shear stud connections. The first set of specimens characterized the effects of a haunch and the number of transversely oriented shear studs. Subsequent test specimens varied the height of the shear studs, their arrangement (either transversely to or longitudinally to the span of the theoretical bridge), and the loading rate. The results from these tests were detailed by Sutton, Mouras, Frank, and Williamson (2008).

2.4 COMPUTER-BASED ANALYSIS MODELS

To extend the preliminary analyses, detailed computer models were developed. Finite element software was used to recreate the geometry of the bridge, the properties of its materials, and the response of the bridge resulting from a fractured girder. An elastic model of the bridge was first programmed and reported on by Hovell (2006). This original version of the computer model was later modified by Kim (2009) to account for the non-linearities associated with yielding steel, crushing and cracking concrete, and the limited tensile capacity of the shear stud connections. These models have been used to study the detailed behavior of these types of bridges and provide supporting analyses for concurrent portions of the research program. Ultimately, they have the potential to be used as aids for new bridge design and the evaluation of existing bridges. At the time of this writing, the non-linear models were still undergoing refinement. A detailed description of these models, their capabilities, and there limitations will be made available by Kim, later in 2009.

2.5 FULL-SCALE BRIDGE TESTING

2.5.1 Bridge Acquisition

In the fall of 2005, TxDOT began a reconstruction of the interchange between Interstate 10 and Loop 610 in Houston, TX (Figure 2-5). The original interchange included a twin box-girder steel bridge used as a single-lane HOV flyover exit-ramp that was to be completely removed from the highway. Because the design of this bridge was representative of the specific structures being investigated by this research project, TxDOT provided one span of the decommissioned bridge for experimentation (Appendix A.1). The availability of a reconstructed full-scale specimen opened the opportunity to design and carry out experiments that would provide observational and numerical data otherwise impossible to obtain. These results could then be used to calibrate the analysis models being developed as part of the research project and as a reference for the large-scale behavior of a fracture critical bridge.

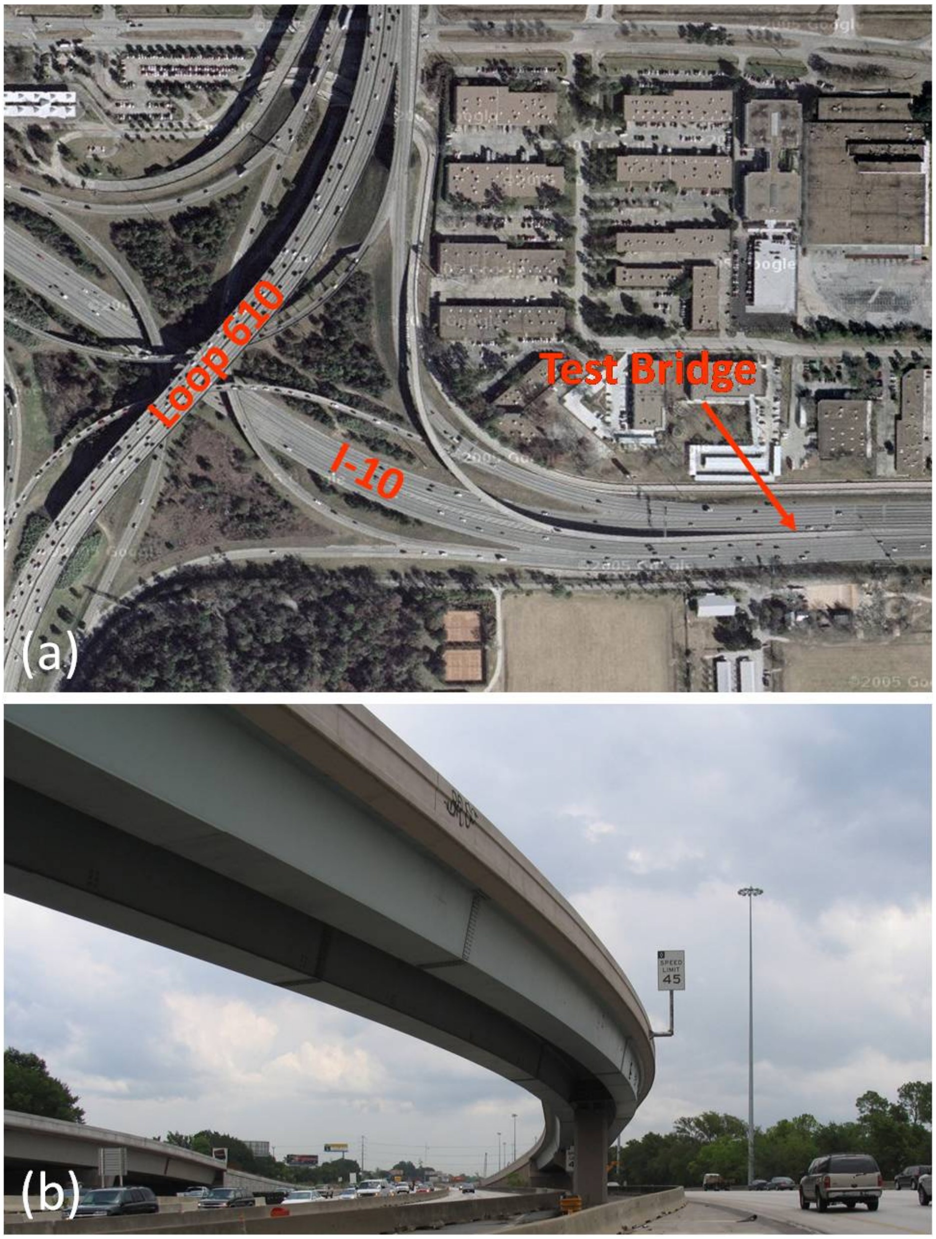

Figure 2-5: Service location of test-bridge (a) plan view, (b) elevation view

2.5.2 Transportation and Reconstruction

The steps taken between initially closing the bridge to traffic in Houston and having it ready for testing at the Ferguson Structural Engineering Laboratory were extensive (Barnard, 2006). To begin, the bridge was deconstructed from the highway in Houston. Because it was not possible to transport the complete bridge without disassembling it, only the steel girders would be utilized for the test-bridge at FSEL. Accordingly, the deck and railing had to be completely removed from the in-situ bridge. In the process of deconstructing the bridge, some damage was done to the shear studs and top flanges of the steel girders. The two girders were separated and transported to Trinity Steel Fabricators in Houston (Figure 2-6) where repairs were made (Figure 2-7). Once ready, the girders were shipped to Austin, where the reconstruction effort began in the outdoor storage area behind FSEL.

Leading up to the arrival of the girders, supports were prepared for their placement (Figure 2-8). Matching abutments were built in position at the desired end locations of the girders. These abutments, constructed of reinforced concrete, would position the test-bridge 10 ft. above the compacted road base on which they were supported. Their design

Figure 2-6 (left): Transportation of the girders

Figure 2-7 (right): Girder damage resulting from deconstruction

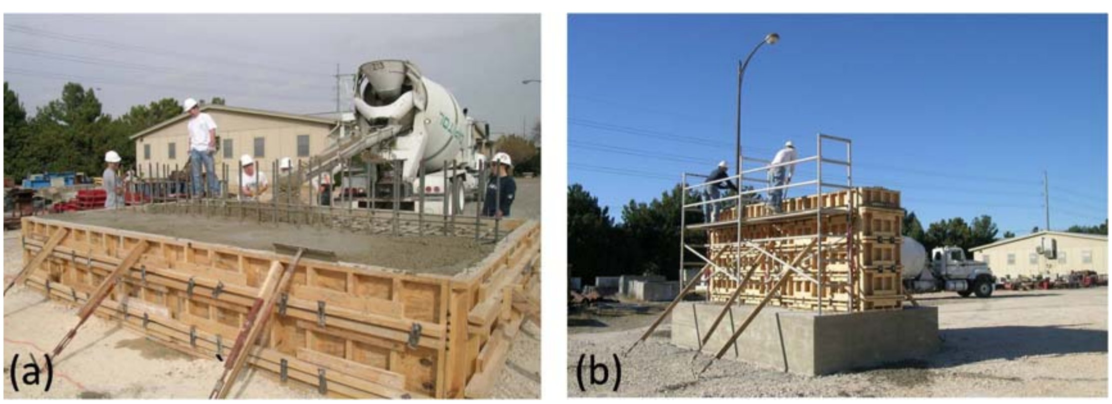

Figure 2-8: (a) Casting the base of the north foundation,

(b) Construction of the stem wall of the south pier

capacity was dependant on withstanding standard loading conditions as well as maintaining stability considering the worst-case conditions of the bridge after testing. Eccentricity from the loads following extreme deformations of the bridge was a concern, so the supports were designed with large footings at the base to maintain the stability of the system in this condition.

Four elastomeric bearing pads were used to transfer the loads from the bridge to the abutments at the ends of each of the girders. The pads were 22 in. long, 11 in. wide, and 3 in. deep. Design details for the bridge abutments and bearing pads are included in Appendix A.2.

Reconstruction of the test-bridge followed standard practices and design details in the interest of fabricating a test specimen as representative as possible of a similar bridge in service. Using two cranes, the western interior girder was placed first on the supports (Figure 2-9a). Once the end diaphragms connecting the ends of the girders were bolted to the western interior girder, the eastern exterior girder was lifted and placed so that it could be connected to the opposite edges of the end diaphragms (Figure 2-9b). To provide torsional stiffness to the girders throughout the remainder of the construction sequence, temporary cross frames were installed between the girders at two locations: one at 12 ft. to the north of the bridge centerline and the other at 12 ft. to the south of the bridge centerline. Once erection of the girders and installation of the deck was completed, the diaphragms were disconnected as they would have been on an in-service bridge.

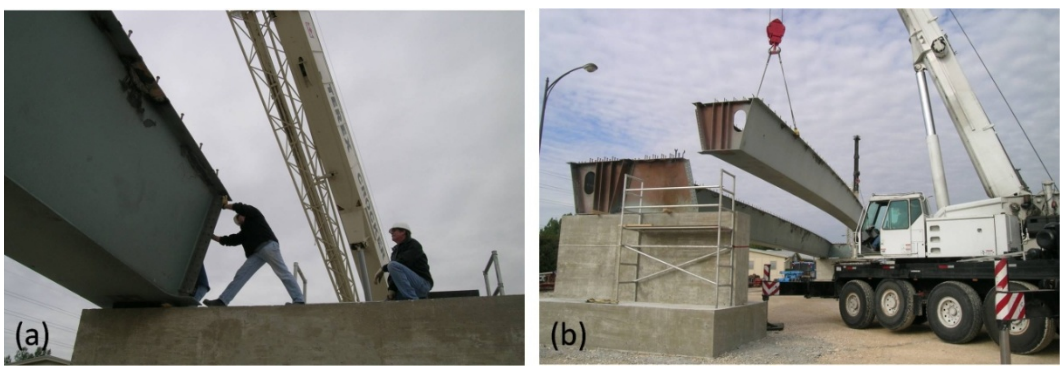

Figure 2-9: (a) Placement of the interior girder, (b) Erection of the exterior girder

The test-bridge was originally designed for unshored construction, meaning that preparations for casting the 8-in.thick deck slab required formwork capable of carrying the full load of the unhardened concrete. Stay-in-place metal deck formwork was used to span the distances between the four girder top flanges (Figure 2-10a), and built-up plywood members forming the portions of the deck overhanging both sides of the bridge were supported by metal brackets (Figure 2-10b). Standard deck reinforcement was placed in two mats both longitudinally and transversely to the bridge span (Figures Figure 2-11 and A-6). All bars were spaced at 6 in. on-center. The deck was cast following strict highway construction standards for materials, placement, and finishing (Figure 2-11). As part of this effort, subcontractors approved by TxDOT with extensive bridge construction experience were hired to construct the deck and rails. The deck

Figure 2-10: (a) Stay-in-place metal formwork, (b) Wooden formwork supported by brackets

Figure 2-11: Deck casting operation, showing (a) Concrete truck and pump beside bridge, and (b) finishing equipment and uncovered rebar mats

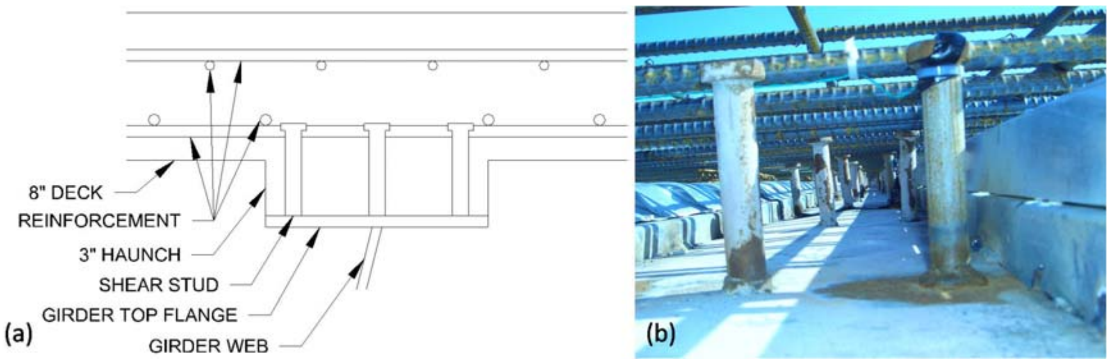

Figure 2-12: Haunch detailing (a) cross-sectional design view, (b) construction photo before deck casting

formwork and reinforcement duplicated the original details used on the bridge. A 3-in. unreinforced haunch (the maximum allowed by TxDOT) was used, also duplicating the original bridge details, and was cast in the deck directly above the top flanges of the steel girders (Figure 2-12). Haunches are typical bridge design elements included to help control super-elevation, changes in flange thickness, and variability in slab thickness (Sutton, 2007).

Preliminary analyses along with empirical evidence suggested that the railings could play a significant role in supporting the test-bridge following the intentional introduction of a fracture to one of the girder bottom flanges, and certain details selected for the construction of the railings were expected to play an important role in affecting the redundancy of the system. A variety of standard railings are used on similar bridges throughout Texas. The T501 rail was selected because of its overall prevalence and because it was the type of railing used on the bridge when it was in service in Houston (Figure 2-13 and A-9). So that the contractor could re-use the formwork for the railings, the west rail was poured first, and the east rail was poured two days later.

The original plans for the test-bridge called for expansion joints along the entire length of the railings, spaced between 10 ft. and 33 ft. Three locations were selected on each railing, which included the quarter points of the span and the centerline. Each of the expansion joints were separated by 30 ft. The expansion joints were formed by placing a 0.75-in. thick section of polystyrene foam insulation in the formwork and casting the

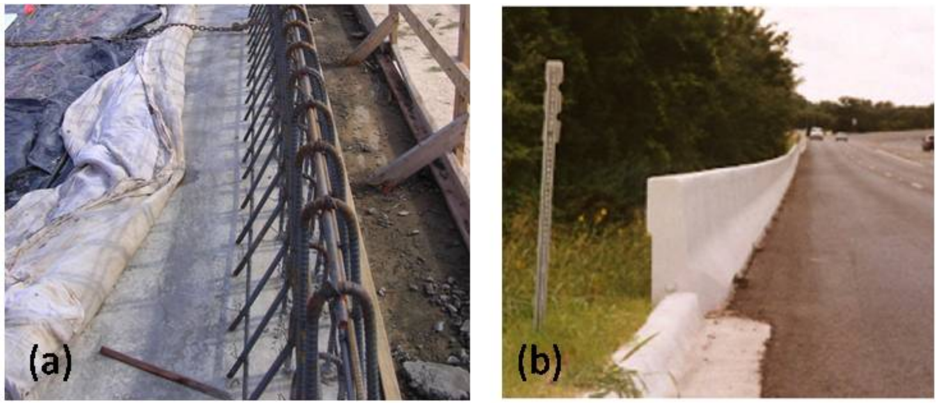

Figure 2-13: (a) Reinforcing cage for the eastern railing of the test-bridge (b) An in-service T501 railing

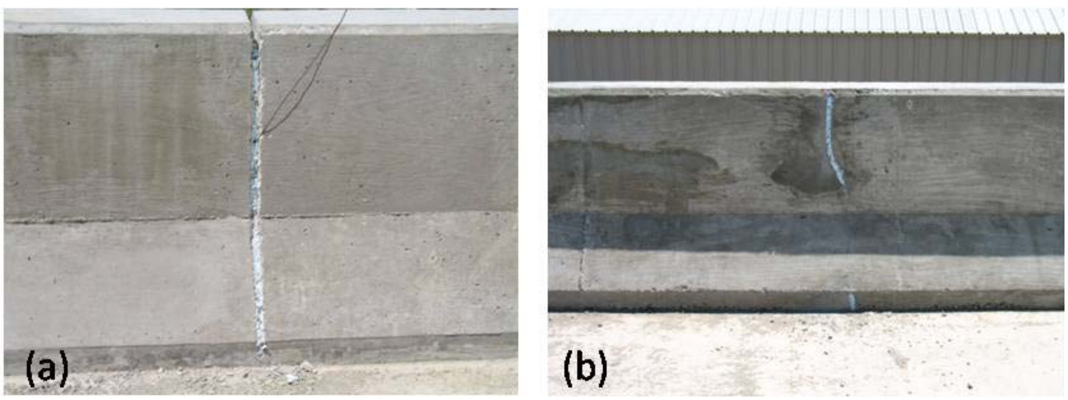

Figure 2-14: (a) Undamaged expansion joint, (b) Expansion joint skewed during rail casting

concrete around the joint location (Figure 2-14a). During casting of the railings, some of the polystyrene inserts shifted, resulting in skewed expansion joints. The most severely skewed expansion joint was at the mid-span of the exterior railing, where the top portion was offset 3 in. from the bottom (Figure 2-14b).

2.5.3 Bridge Summary

When completed, the details of the test-bridge closely matched those from the original service location (Figure 2-15). In plan, it spanned 120 ft. with a radius of curvature of 1365.4 ft. at its mid-width. The slab width extended 23 ft.–4 in. edge-to-edge and 20 ft.–6 in. between the inside bottom edges of the railings. Shear studs on the girder top flanges were in transversely oriented groups of three, spaced at 22 in. on-center. The bridge also used a 3-in. unreinforced haunch above the top flanges of the steel girders.

Important features of the test-bridge are labeled in the cross-sectional and plan views of the bridge shown in Figure 2-16 and Figure 2-17, respectively. These features will be referenced and portions of the plan and cross-sectional views will be revisited throughout this thesis. The series of cross-sections labeled in Figure 2-17 were originally determined based on the locations of internal cross-frames in the girders (Appendix A-1). The internal cross-frames are spaced every 12 ft., including at the centerline and at all cross-sections ending in .5 (e.g., N1.5, N2.5, etc.). Cross-sections denoted by whole numbers are half-way between the cross-frames (e.g., N1, N2, etc.).

Figure 2-15: Fully constructed bridge ready for testing

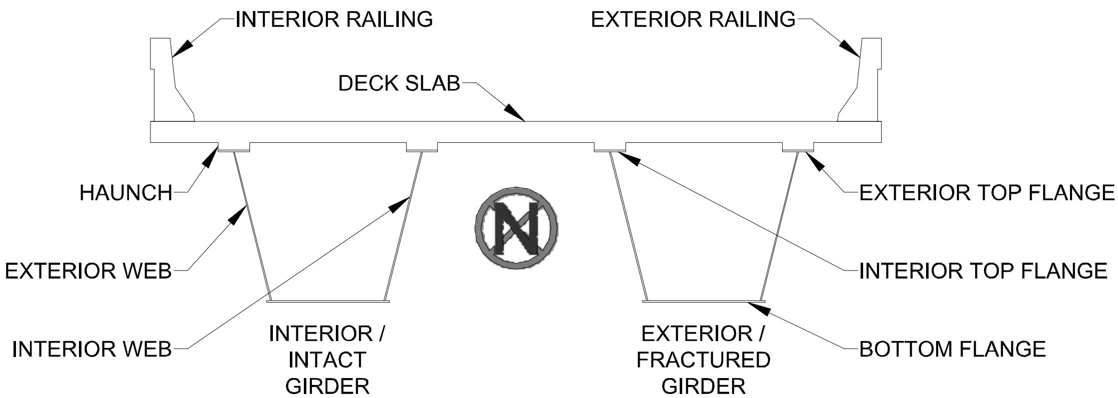

Figure 2-16: Cross-sectional view of test-bridge labeling important features

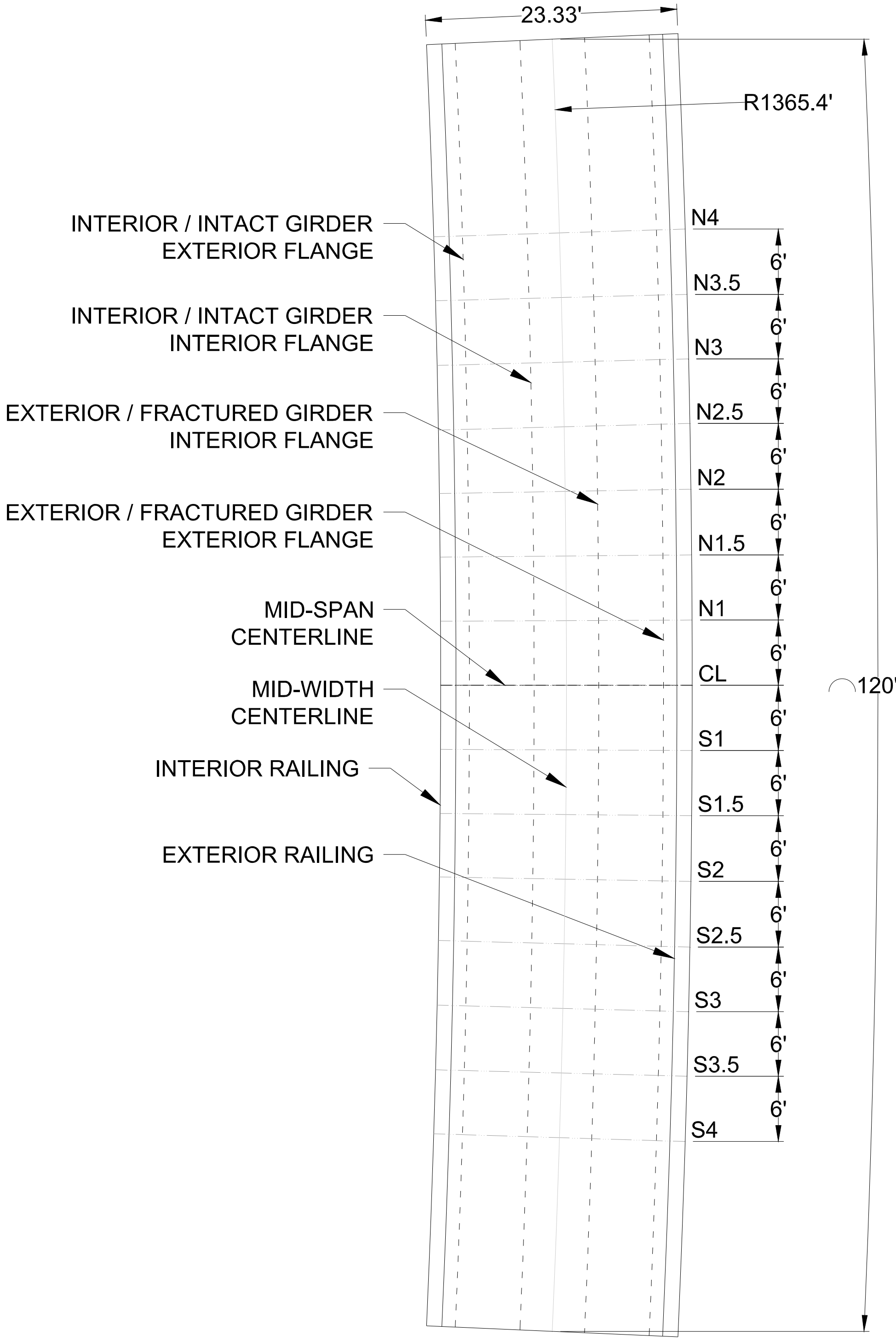

Figure 2-17: Plan view of test-bridge labeling important features

2.5.4 Preliminary Testing

Once the steel girders were in place and instrumented, non-destructive loading tests were performed. Stresses and deflections of the bridge were monitored throughout the construction sequence, including during deck casting and rail placement. After construction was completed and the bridge was serviceable and ready for experimentation, similar stress and deflection measurements were taken through a series of live load placements. Concrete blocks representing the 76,000 lb. design truck load were placed on the deck at different locations to gather data on the bridge's response to variation in the location of the live load. The tests used the same instrumentation as the first full-scale destructive test, as described in Chapter 3 of this thesis. Full reporting on the initial non-destructive tests is presented by Barnard (2006).

2.5.5 Destructive Testing

Subsequent to the non-destructive investigations, a progressive series of three destructive tests were designed and executed. The tests were intended to provide data on the behavior of the test-bridge in the event of a loss of a fracture critical tension flange. Each experiment used different methods to induce damage to the bridge and observe its response. The tests, in sequence, looked to induce a fracture, observe the bridge's dynamic response when loaded in its fractured state, and determine the ultimate capacity of the bridge in its fractured state. An extensive instrumentation plan, which evolved over the duration of the three tests, was implemented to gather data on deformations at various locations throughout the test-bridge. The remainder of this thesis focuses on the methods used in each of the tests and provides general information on the results gathered.

CHAPTER 3

Methods: Full-Scale Test 1

3.1 INTRODUCTION

Acquiring and reconstructing the full-scale test-bridge provided the opportunity to design tests that would allow the behavior of a fracture critical bridge to be observed in the event of a failure of a fracture critical component. The first full-scale test set out to simulate one of these failures by initiating a fracture in one of the two tension flanges of the test-bridge. Because each tension flange is a fracture critical component, the removal of one is expected to result in the total failure of the structure according to the AASHTO Bridge Design Specifications. By explosively cutting the full thickness and length of one of the girder bottom flanges to simulate the effects of a fracture, the subsequent behavior and damage propagation of this particular fracture critical bridge could be observed.

3.2 TEST PROCEDURE

Full-Scale Test 1 aimed to simulate an overall worst-case fracture scenario on the test-bridge. On an in-service bridge, this worst-case scenario would occur when the design truck load was passing across the bridge at the location that induced the maximum internal bending moment at the same instant that a fracture event occurred at that point of maximum moment. To simulate this situation, a design truck load was first applied to the bridge, closely approximated by a set of five concrete girders that in total weighed 76,000 lbs. The concrete girders were positioned on the bridge in a pattern corresponding to a design truck load, near mid-span and on the outside edge of the bridge curvature, in order to induce the maximum internal bending moment (Figure 3-1). Per AASHTO design guidelines, the truck load was placed 2 ft. from the exterior railing.

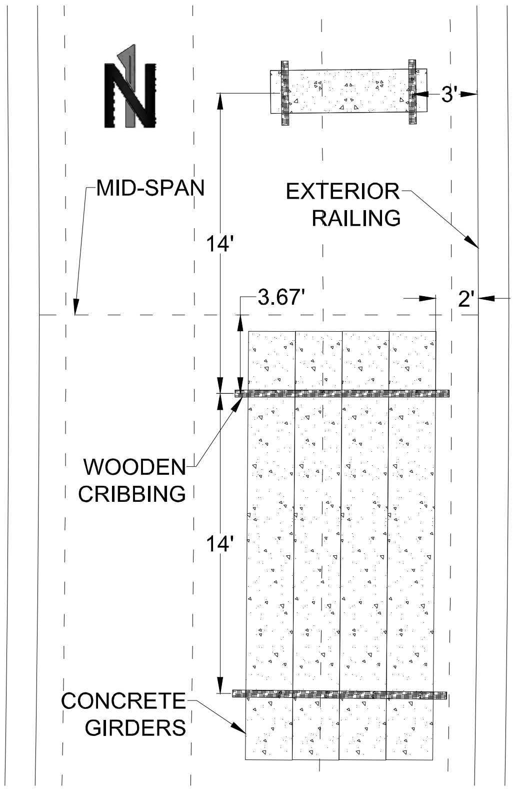

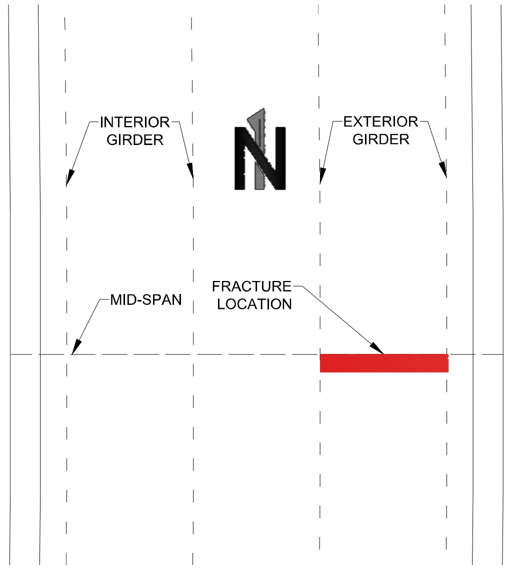

Figure 3-1 (left): Live load location for Full Scale Test 1

Figure 3-2 (right): Plan view of location selected for bottom flange fracture

The fracture location corresponded to this worst-case loading scenario on the bridge (Figure 3-2). The bridge plan had a slight curvature, and a fracture farthest to the outside of the curve was expected to induce the worst-case loading scenario, resulting in the most detrimental impact on the performance of the bridge. Therefore, the exterior of the two girders was selected for the fracture location. On that girder, a fracture location very near mid-span was desirable because the highest possible internal bending moment developed within a simply supported beam occurs at the mid-span position when it is loaded there. The exact fracture location was chosen approximately 1 in. south of the mid-span to allow for clearance beside an internal cross-frame that was positioned at the steel girder mid-span. Later, an additional cross-frame made of angle shapes was custom welded inside the girder two feet from the fracture location on the side opposite the existing cross-frame to help provide similar resistances to twisting at both open ends of the fractured girder (Figure 3-3).

Figure 3-3: Fully installed supplementary cross-frame interior to fractured girder

Explosives were chosen as the means of inducing the fracture in the bottom flange. This method would help ensure that the fracture cut all the way through the 0.75 in. thickness and across the 47 in. length of the flange, and that it happened nearly instantaneously to simulate a brittle fracture without the difficulty of trying to induce a fracture. Given the outside temperatures and the size of the specimen, the use of an explosive was believed to be a good way to simulate what a bridge such as the one tested might experience in the field should an actual fracture take place. A 50-in. long linear shape charge was positioned just below the outside face of the bottom flange of the exterior girder along the line of the selected fracture location. The full depth of the bottom flange of the fractured girder was to be severed upon detonation of the shape charge.

Southwest Research Institute (SwRI) of San Antonio was contracted to perform the explosive work, including material acquisition, testing, charge placement, and detonation. SwRI performed preliminary testing to confirm the adequacy of the explosives to completely sever the bottom flange of the test-bridge (Figure 3-4). In addition to successfully demonstrating shape charge capacity, the preliminary tests also

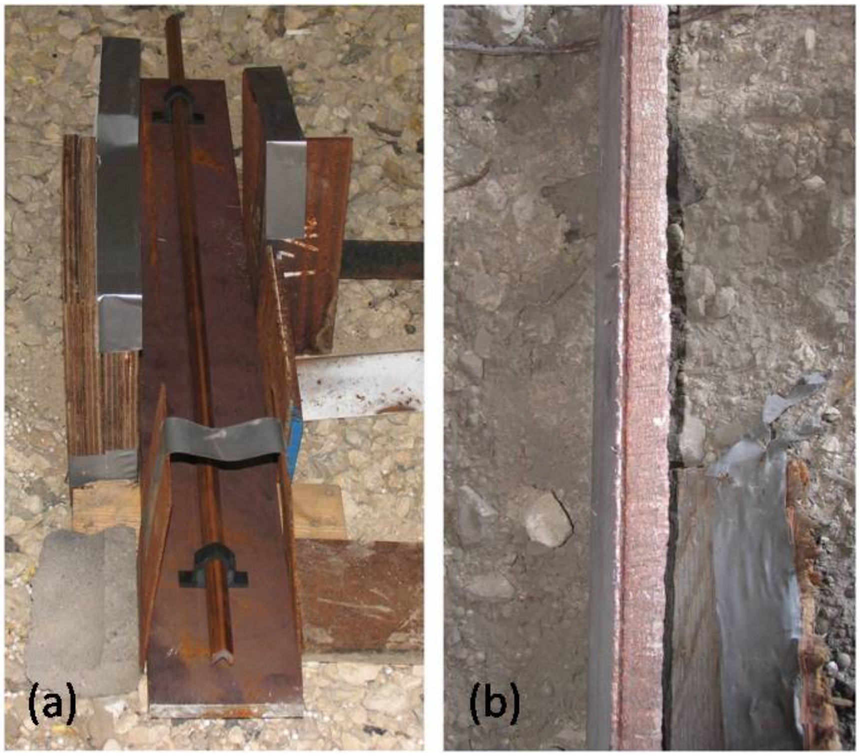

Figure 3-4: Shape charge testing at Southwest Research Institute, showing (a) test set-up, and (b) successful results

demonstrated the need to control fragments: the test explosion produced large metal shards that were capable of embedding themselves into concrete.

3.2.1 The Use of a Custom Blast-Shield

A custom steel blast-shield was designed and constructed for Full-Scale Test 1. The shield had a number of features that together were intended to position and to support the shape charge up until detonation and to contain debris following the explosion. Design consideration was also given to ensuring that the blast-shield could not act as a redundant load path once the girder had lost its bottom flange. Connecting chords were anchored into a concrete block sitting beneath the bridge to limit the possibility of the blast-shield becoming a projectile itself. Details of the blast shield design and construction are provided in the subsections below and in Appendix A.3.

3.2.1.1 Design Details

The blast-shield was constructed using a channel section and flat plates of various thicknesses. A 0.375-in. thick, 12-in. wide channel formed the underside of the shield. To add depth to the containment zone, 0.5-in. plates were welded along the outside faces of the channel flanges. Above the regions where the shape charge was overhanging the flange, 2-in. thick plates were used to close the section and to help contain fragments from the linear shape charge. One of the 0.5-in. thick end caps was welded directly to the channel, but the other was designed with a bolted connection, allowing the blast shield to be installed ahead of the test. When ready, the shape charge was placed inside the installed blast shield, and the second end cap was attached to seal the blast shield. A design schematic of the blast shield is shown in Figure 3-5, and a photograph of the fabricated blast shield is shown in Figure 3-6.

To connect the blast-shield to the girder, the design took advantage of a 1.75-in. extension of the girder flange width beyond the locations where to the webs intersected the bottom flange. The end portions of the blast-shield, including the 2-in. closing plates, were designed as built-up angles that could hang from the bottom flange protrusions.

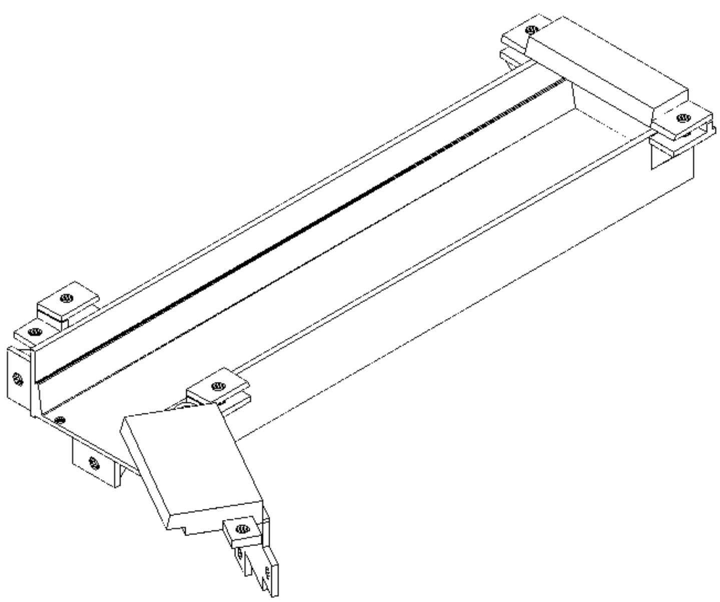

Figure 3-5: Design schematic for the blast shield used in Full-Scale Test 1

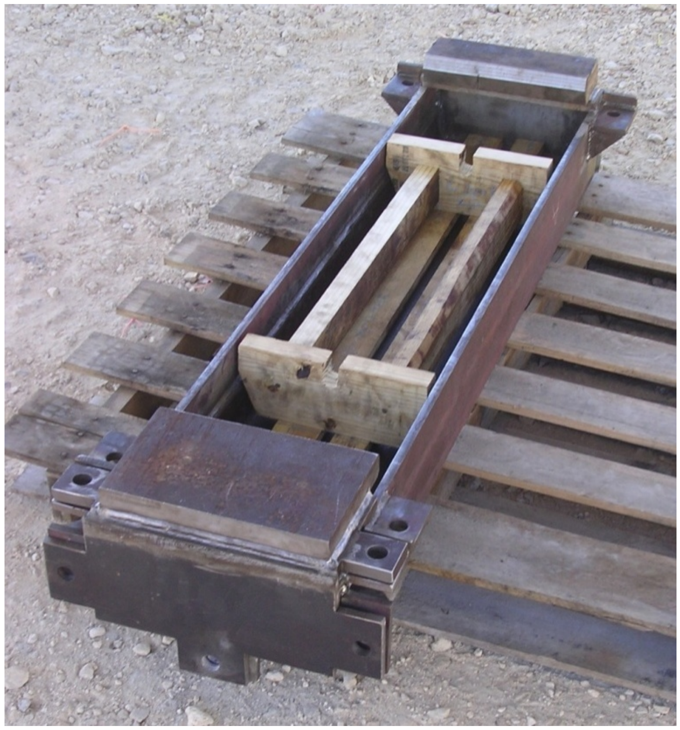

Figure 3-6: Fully constructed blast shield housing the wooden pedestal to hold the shape charge

Without any mechanical connection between the blast-shield and the girder, no significant load transfer between the two would be possible. This passive locking would allow the blast shield to simply fall away from the girder flange in the case of large deflections of the bridge.

As a precaution for the case where it might be forcefully ejected from the bottom flange during the explosion, the blast-shield was tethered with high-strength steel wire rope to a heavy concrete block sitting beneath the bridge (Figure 3-7). On each end of the shield, the steel wire rope connected through stub plates on the shield end-caps to anchors installed into the concrete block. A small amount of slack was left in the steel tethers. If the blast-shield gained significant momentum during the test, the tethers would engage and prevent any significant motion of the assembly.

A small wooden pedestal was built to hold he shape charge in its desired position up until detonation (Figure 3-8). The pedestal was sized to fill the cross-section of the

Figure 3-7: Blast shield installed to fracture location and connected to safety tethers

Figure 3-8: Shape charge held by the wooden pedestal, ready to be inserted into the blast shield

containment zone within the blast-shield and to position the shape charge against the outside face of the bottom flange of the girder. Once the pedestal and charge were slid together into the containment zone, the bolted end plate and second capping angle were secured.

3.3 DATA-ACQUISITION AND INSTRUMENTATION

Equally as important as executing the full-scale test safely and to specification was ensuring that data were acquired during the experiment so that the behavior of the bridge could later be analyzed. The instrumentation plan was designed and implemented to measure deflections and material strains, which could then be used to help quantify material stresses along portions of the hypothesized redundant load paths. Strain gages attached directly to bridge components took measurements of material deformations. In addition to the information provided in this chapter, Appendix B includes details about the gages used, the locations of the gages, and the acquisition set-up. Direct measurements of bridge displacements were also acquired through surveys of the bottom flanges of the girders before and after each major step of the experimental procedure (Figure 3-9). Survey points were taken at both edges of the bottom flange of each girder at 6-ft. intervals along the length of the bridge to capture translational, rotational, and twisting deflections.

3.3.1 Instrumentation Cast Into the Bridge Deck

Before construction of the test-bridge was completed, instrumentation was installed on reinforcing bars and shear studs that were later cast into the concrete deck. Planning

Figure 3-9: Capturing the bridge position by surveying the underside of the two girders

ahead for these instrumentation locations was important to ensure the availability of measurements from bridge elements that would not be accessible once construction was completed.

3.3.1.1 Shear Stud Gages

The shear studs were a critical part of the redundant load path expected to transfer loads from the fractured girder to the intact girder. Relative deflection between the girders would induce tension forces in the studs for which the connections were not designed. To help quantify the amount of axial force transferred, uni-axial bolt gages were installed into small holes drilled into the shaft of a limited number of shear studs. The installation procedure required drilling a very narrow hole down the axis of a shear stud, which could not be performed on a shear stud already welded to the girder top flange.

The girders were delivered to FSEL with a number of damaged studs. The shear stud gage locations were therefore dependent upon the positions of studs that were required to be replaced. Fifteen of the replacement studs, distributed among all four girder top flanges and within a 46 ft. range at the center of the span, were instrumented. A map of the shear stud gage locations is shown in Figure 3-10, and a sample photograph of an instrumented shear stud appears in Figure 3-11.

On a simply supported beam loaded symmetrically about its mid-span, no shear demands are imposed at the center of the span. For Full-Scale Test 1, the dead weight of the bridge plus the design truck load approximated this case. Though shear studs at locations far from the bridge centerline must restrain shear and tensile forces should a fracture occur, the gage measurements taken near the critical fracture location at the middle of the span where shear demands were fairly small would provide an accurate indication of the simple uni-axial tension forces in the studs.

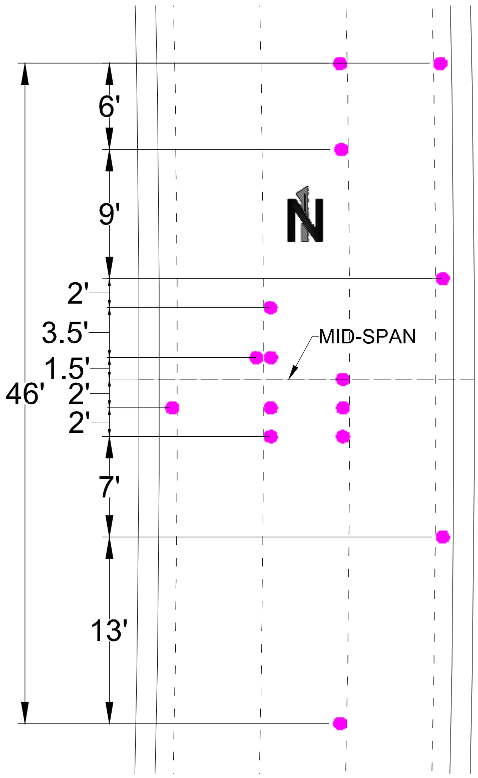

Figure 3-10 (left): Plan view of shear stud gage locations

Figure 3-11 (right): A fully instrumented shear stud

3.3.1.2 Reinforcing Bar Gages

The bending action of the 8-in. thick reinforced concrete deck was also expected to play a critical role in transferring loads from the fractured girder to the intact girder. Axial strain readings from reinforcing bars would help estimate the magnitude of the bending moments in the deck and their contribution to the redundant load path.

All of the reinforcing bars selected for instrumentation were oriented transversely to the bridge span and were intended to provide information on the bending action across the width of the deck. Eleven locations above the interior flanges of the two steel tub girders, spanning the central 80 ft. along the length of the bridge, were used. At all eleven locations, matching bars on the top and bottom reinforcing mats were instrumented. A map of the reinforcing bar gage locations is shown in Figure 3-12, and a sample photograph of an instrumented pair of bars appears in Figure 3-13.

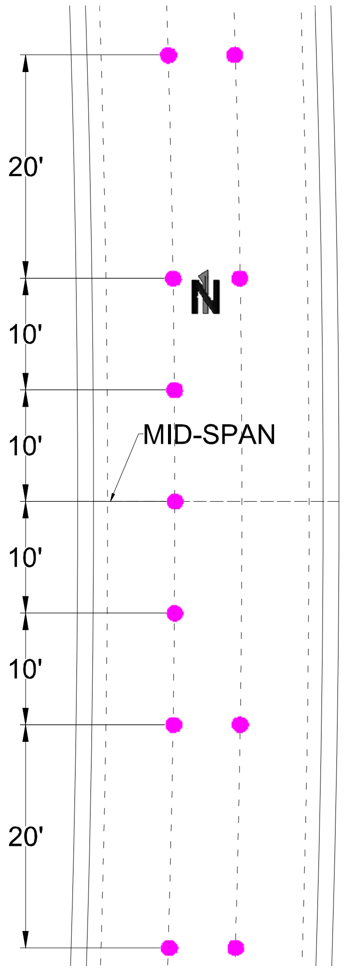

Figure 3-12 (left): Plan view of the reinforcing bar gage locations

Figure 3-13 (right): A pair of fully instrumented reinforcing bars

3.3.2 Girder Instrumentation

The two steel box-girders were also heavily instrumented to help provide information on their contribution in redistributing loads after the bottom flange of the exterior girder was fractured. The intact girder was expected to carry the full load in longitudinal bending to the supports at the end of the span. There was also expected to be substantial torsional loading of the intact girder as the loads were transferred transversely from the fractured girder. To help quantify the complex stress states in the girders, uni-axial gages were used alongside 0˚-45˚-90˚ rosette gages on the girders' webs and bottom flanges.

Stiffening cross-frames internal to the girders were spaced at 12 ft. along their length, with one of the cross-frames positioned to coincide with the mid-span location of each girder. The cross-sections selected for instrumentation were halfway between these internal diaphragms at N1, 6 ft. to the north and S1, 6 ft. to the south of the bridge mid-span location (Figure 2-17). The highest force demands were expected at mid-span where the fracture was induced, and it was desirable to get strain readings as close to this location as possible. Placement between the stiffening elements would help minimize their effects on the stress state readings of the primary load transfer elements.

An array of gages was used to help determine the full stress state of the girders. 0˚-45˚-90˚ rosette gages were positioned halfway across the bottom flange and at the mid-height of the two webs of both girders to measure the axial and shear strains of these elements. In addition, uni-axial gages aligned in the direction of the bridge length were placed symmetrically at the 1/4- and 3/4-point locations along the width of the bottom flanges and the height of all four webs. Data collected from these gages were intended to help fill in details of the strain profile through the full depth of the girders. Both girders at the S1 cross-section, 6 ft. south of the centerline, were fully instrumented. At the N1 cross-section, 6 ft. north of the centerline, only the interior girder was instrumented, and only rosette gages were installed. A diagram of the instrumentation at a typical cross-section is shown in Figure 3-14, and a photograph of a typical strain gage placed on one of the steel plates of the bridge girders, fully installed, is shown in Figure 3-15.

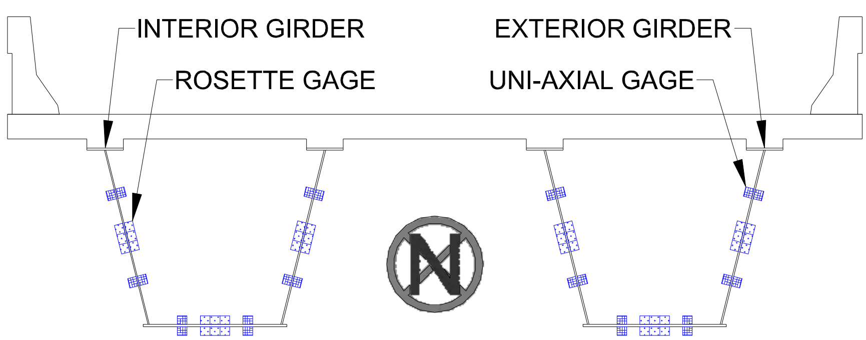

Figure 3-14: Instrumentation of the bridge elements for Full-Scale Test 1 at a typical cross-section

Figure 3-15 (left): A fully installed strain gage on a steel plate

Figure 3-16 (right): Instrumentation of the inside of the north end diaphragm

The diaphragms connecting the two girders at the ends of the span were also expected to transfer load from the fractured girder to the intact girder. The connection at the ends of the girders was likely to restrain two kinds of relative deformation between the girders. In-plane stiffness of the diaphragms would resist relative twist along the longitudinal axes of the girders, and twisting stiffness of the diaphragms would resist relative longitudinal rotation at the girder ends. To gain information about the contribution of the diaphragms, 0˚-45˚-90˚ rosette gages were attached to the center of the plates (Figure 3-16).

In every case where a steel section was instrumented, gages were placed identically on opposite faces of the plates so that an average strain value through the plate thickness could be determined. Because the steel elements were deformed out of plane to varying degrees, global deformations could have induced localized bending. On one side of a deformed plate, the localized bending strains would be additive to the global bending strains. On the other side, the localized bending strains would have subtracted from the effects of global bending. Calculating the average of the values of the strains from opposite sides of the plates would eliminate these localized effects.

3.3.3 Data-acquisition

Wires connected to each piece of instrumentation were run to the southern end of the bridge where a small hut housed all of the data-acquisition equipment (Figure 3-17). For the first full-scale test, a high-speed data-acquisition system was configured for all 127 channels of instrumentation (Tables 3-1 and B-3). Because the loading and subsequent bridge response was expected to be dynamic, it was important to sample the data rapidly, accurately, and in a synchronized manner. The system used for the test employed equipment from National Instruments and was set up to sample data simultaneously from all 127 channels, 1000 times each second.

The wires from the 127 instrumentation channels were connected into sixteen National Instruments SCXI-1314 8-channel terminal blocks. Each terminal block hooked into its own SCXI-1520 8-channel universal strain module. Two SCXI-1001 12-slot chassis were used to house the sixteen modules, leaving eight slots empty. The two chassis were connected through a PC that was equipped with a National Instruments PCI-6250 data-acquisition card. LabVIEW was used on the PC to view and organize the incoming data.

3.4 FINAL PREPARATIONS

Leading up to test-day, relevant authorities including the research campus facilities crew, local law enforcement, and those responsible for the nearby train tracks were notified of

Figure 3-17: (a) Instrumentation wires running from the bridge into the instrumentation hut, (b) Data-acquisition equipment in the instrumentation hut

Table 3-1: Instrumentation count for Full-Scale Test 1

Gage Type	# of Gages / Channels	
Reinforcing Bar	22	22
Shear Stud	15	15
Girder (Uni-axial)	24	24
Girder (Rosette)	18	54
End Diaphragm (Rosette)	4	12
Total	**83**	**127**

the test plan. Before the explosives were triggered, the area was completely cleared of personnel and spectators, and all other safety concerns were addressed. A live web-cast streamed the event online, and video monitoring was set up inside FSEL because there was no safe location to observe the test with a direct line of sight to the test-bridge. Once all the preparations were completed for Full-Scale Test 1, the execution of the experiment took only a few seconds and required only a remote detonation command.

3.5 SUMMARY

Full-Scale Test 1 was designed to simulate a fracture event on the FSEL test-bridge by explosively inducing a fracture in the bottom flange of the exterior girder. Preparations for this test required recreating a worst-case loading scenario in the event of an actual fracture event, and arranging for the explosives to be used both safely and effectively. 127 channels of instrumentation were prepared to acquire strain data that would help characterize the behavior of the bridge in response to the fracture event. The results of the full-scale explosive test are presented in the following chapter.

CHAPTER 4

Results: Full-Scale Test 1

4.1 INTRODUCTION

Full-Scale Test 1 was performed on October 21, 2006. Upon detonation, the shape charge positioned on the bottom flange of the exterior girder successfully induced a fracture through the full thickness and full width of the bottom flange steel plate. The fracture, however, did not propagate into the webs of the girder, and minimal damage to the bridge was observed beyond the localized effects of the explosives (Figure 4-1). The blast shield successfully limited the amount of debris ejected as a result of the explosion, and no serious collateral damage was recorded at any distance away from the bridge. The instrumentation equipment near the fracture location, however, was severely damaged by the blast. Due to the small deflections experienced by the test-bridge, along with a human error associated with the initiation of data collection after the detonation of the explosives, the amount of strain data recorded during the test was limited.

Figure 4-1: FSEL test-bridge after Full-Scale Test 1

4.2 TEST RESULTS

4.2.1 Creating a Bottom Flange Fracture

The explosion successfully induced a fracture in the bottom flange of the exterior girder. The fracture extended the complete width and depth of the bottom flange, and was a consistent 0.25-in. thick across its length (Figure 4-2). The fracture did not extend into the webs of the girder. Thus, despite losing one of its primary tension resisting elements (i.e., a fracture critical component), the fractured girder was able support the load without any further material failures. The tension forces previously carried by the flange were simply transferred to the intact components of the bridge system, including the webs in the area of the fracture, which showed minimal signs of distress (Figure 4-3).

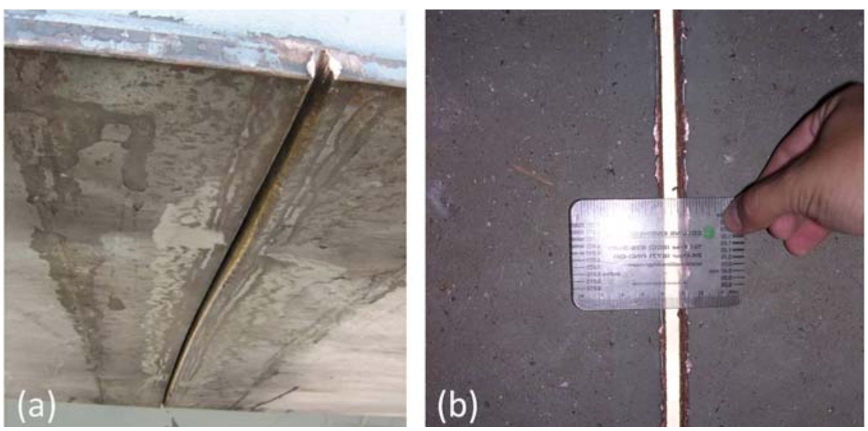

Figure 4-2: (a) Underside view of the fracture showing its full depth and length, (b) Inside view of the fracture showing its width

Figure 4-3: Side view of the fracture showing minimal distress in the adjacent girder web

4.2.2 Bridge Deflections

The test-bridge was positioned with an overall incline, climbing approximately 1 ft. vertically across its 120-ft. length. The surveys of the bottom flanges of the girders were taken relative to a benchmark away from the bridge, and reviewing the raw data would have emphasized this overall incline, thus deemphasizing deflections due to applied loads and sustained damage. Throughout this thesis, all surveyed deflections presented were normalized to eliminate the effects of overall bridge incline. Reported deflections along the length of the bridge therefore represent the amount that individual sections deflected below a straight line connecting the north and south ends of the span.

The static deflections of the intact and fractured girders sustained during various stages of Full-Scale Test 1, as determined by surveys of the bottom flanges, are shown in Figures 4-4 and 4-5, respectively. The survey data indicate small deflections along both girders throughout the experimental steps. The mid-span of the intact girder deflected downward 0.5 in. under the initial application of the simulated truck live load, then deflected an imperceptible amount following the fracture of the opposite girder, and finally rebounded 0.25 in. when the live load was released, according to the survey data. The deflection of the mid-span of the fractured girder follows a similar pattern. It first deflected downward 1.25 in. under the live load, then deflected a very small amount following the fracture of its own bottom flange, and finally rebounded 0.4 in. when the live load was released.

The surveyed deflections do not indicate bridge behavior consistent with the expected results associated with the load steps performed for Full-Scale Test 1. Though the fracture induced in the bottom flange of the exterior girder did not propagate up the webs and no significant damage was observed elsewhere on the bridge, the loss of an entire tension flange should have led to a stiffness reduction that was expected to have resulted in downward deflection of the fractured girder. Significant downward deflection was not recorded for either girder after the explosion, implying that the system was unaffected by the loss of the bottom flange. Furthermore, if the bridge system was unaffected by the

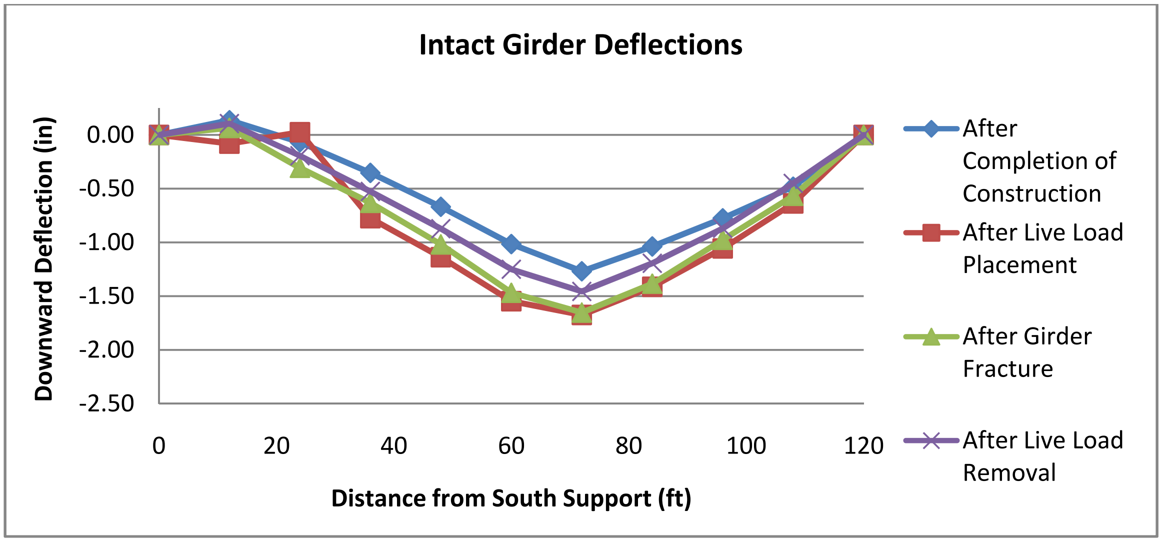

Figure 4-4: Intact girder deflections during Full-Scale Test 1

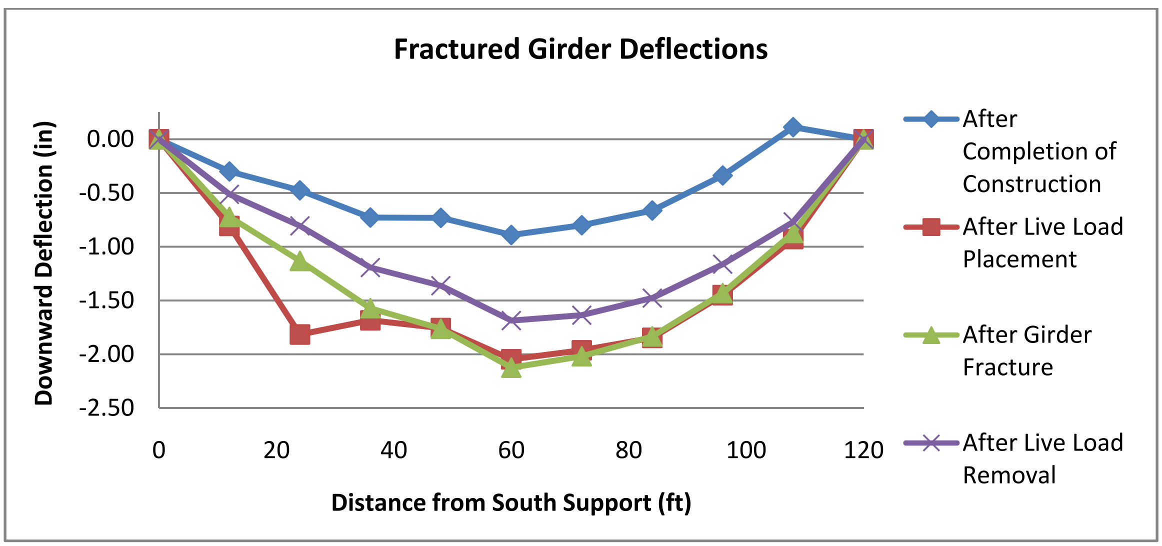

Figure 4-5: Fractured girder deflections during Full-Scale Test 1

loss of the bottom flange of the fractured girder, when the live load was released, the bridge should have rebounded to its original position before the live load was applied. According to the survey data, the rebound of both girders following release of the live load was half or less than the original deflection that resulted from the application of the live load.

A total deflection of 1 in. – 2 in. across a 120 ft. span is small. The surveys reported in Figures 4-4 and 4-5 were taken by different people over the course of a month. Though the methods should have been consistent, there is no record to indicate one way or the other. Furthermore, the surveys were taken on different days at different times of the day, increasing the probability that thermal effects influenced the overall deflection of the bridge. A temperature gradient through the depth of the bridge deck and girders would induce a curvature due to variable thermal expansion, and a small amount of curvature over a large span could certainly result in noticeable deflections. Basic calculations show that a uniform temperature gradient of only 5˚ Fahrenheit through the depth of one of the girders could result in deflections exceeding 0.25 in. at the mid-span location. Given the right environmental conditions, a temperature gradient 5-10 times this magnitude would not be considered unusual. At the times the surveys were conducted to collect the deflection data, no records were taken of the ambient temperatures, or of the temperatures of the steel, so the effects of temperature variation on bridge deflection cannot be easily estimated. Despite these issues, the recorded displacements were small, and the bridge performed exceedingly well relative to the AASHTO fracture critical designation.

4.2.3 Blast Shield Performance

Overall, the blast shield was successful at containing the vast majority of the shrapnel created by the shape charge, thus minimizing damage to the surroundings. The blast shield was ejected from the bottom flange of the fractured girder and was severely damaged during the explosion, eliminating the possibility that it acted as a redundant load path for the bridge. Also, the steel wire tethers ultimately restrained the blast shield after its ejection from the bottom flange.

The damage sustained by the blast shield during the explosion was extensive, failing both individual components and connections between components. The main channel used for the base of the blast shield ruptured along the joint between the web and one of the flanges (Figure 4-6). The 0.375-in. thick channel components were the thinnest plates used in the blast shield. Selecting a channel with 0.5-in. thick plates, matching the thickness of the majority of the other blast shield components, could have reduced the extent of this failure.

The 2-in. thick plates used to close the ends of the channel section where the shape charge and blast shield were overhanging the bottom flange were significantly damaged from the upward force applied by the explosives (Figure 4-7). A partial fracture, consistent with the fracture induced on the bottom flange of the test-bridge, extended into but not through the full thickness of the 2-in. plates. This was consistent with their design, so that the explosives did not cut through the full thickness of the shield and spray the area with debris. Also, the welds that connected the short ends of the 2-in. channel closing section to the bolt tabs at the channel flanges ruptured, peeling the plates back and leaving them connected only by the welds to the end caps along the longer back edges (Figure 4-7). Inspection revealed that the longitudinal welds did not penetrate deeply into the metal at the locations of the ruptures. Beveling the longitudinally welded parts would allow for greater weld penetration, reducing the risk of similar weld failures in future applications.

As the blast shield was ejected from the bottom flange of the girder, one of the bolts that connected the built-up angles that hung onto the girder overhang to the main blast shield

Figure 4-6 (left): Rupture of the web to flange connection of the channel section

Figure 4-7 (right): Damage to the 2 in. capping sections, including partial fracture and weld rupture

body ruptured, turning pre-tensioned bolt fragments into high-speed projectiles. A subsequent, safer design would include notches in the tabs through which the bolts are secured to reduce their net area. This modification would increase the likelihood that the bolt tabs, rather than the bolts themselves, would fail (Figure 4-8).

Ultimately, the steel wire tethers were successful in preventing the blast shield from traveling a great distance upon its ejection. The restraining process, however, did not proceed precisely according to design. As the blast shield came away from the bottom flange, it did so asymmetrically, allowing one of the steel wire tethers to engage before the other one did. The force from this first engagement ripped the anchorage at the opposite end of the steel wire tether completely out of the concrete block into which it was secured, resulting in a cable with one loose end whipping through the air. When the second steel wire tether engaged, it was successful at restraining further movement of the blast shield. Stronger anchorage is recommended for future applications of this steel tethering concept.

While the blast shield was successful in containing most of the debris, a few small slivers of explosive casing did escape out the sides of the shield and travel up to seventy feet down the length of the bridge. These pieces were small, but it is preferable to contain them if at all possible. Containment could be improved by adding “lips” to the top faces

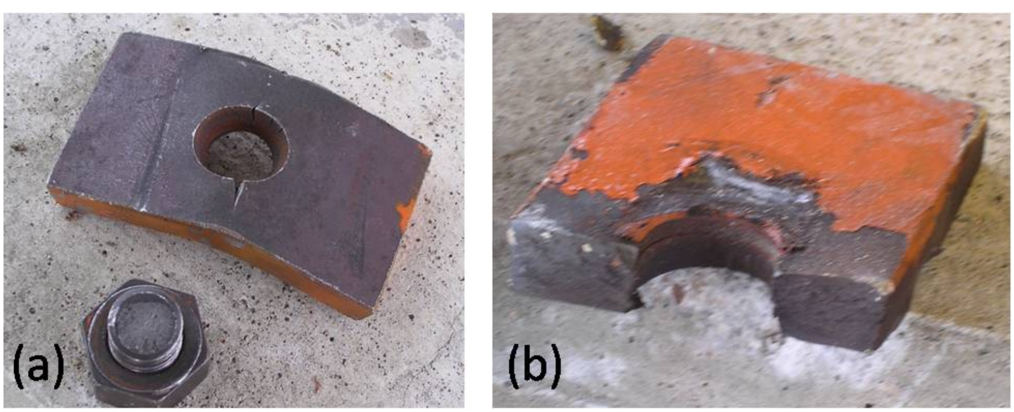

Figure 4-8: (a) Undesirable bolt rupture at tab of hanging angle connection, (b) Desirable tab rupture

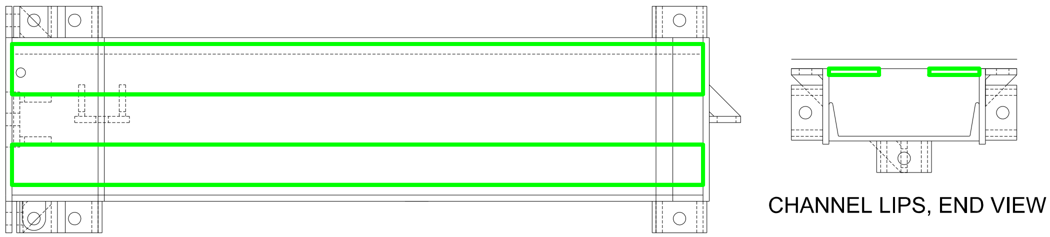

Figure 4-9: Proposed blast shield modification to limit projectile debris

of the shield that press up against the bottom flange of the test-bridge. These lips would help restrain the fragments within the volume of the shield, preventing their escape. The added lips, shown emboldened in green in Figure 4-9, would reduce the area of the opening at the top of the containment box, limiting the number of fragments that could escape once the shield was no longer pressed against the bottom flange of the test-bridge.

4.3 Instrumentation Performance

When online, the data-acquisition system successfully captured data from all viable gages. Without a propagation of the bottom flange fracture, however, minimal relative deflection occurred between the two girders, and significant load transfer from the fractured girder to the intact girder was not perceptible through the readings taken. Wiring in the vicinity of the explosion was not properly protected and was severely damaged during detonation, limiting the number of channels that were able to capture data on the bridge’s response to the fracture. In addition, a communication error resulted in the data-acquisition system not initiating data recording until after the detonation took place and the initial pulse had passed. The data that were recorded, however, were effectively captured at the desired rate from the intact channels.

4.3.1 Damage to Equipment

The impulse from the explosion near the fracture location and the shrapnel that was projected inside the girder damaged nearby instrumentation. The wires connected to the strain gages on the S1 cross-section of the fractured girder were torn loose during the detonation by the impulse of the blast (Figure 4-10a). Inside the fractured girder, shrapnel from the explosion shredded a number of gage wires that were crossing near to the fracture location (Figure 4-10b). The wires affected inside the girder included those connecting shear stud, reinforcing bar, and steel plate gages. The shrapnel propelled into the girder had so much energy it pierced the permanent metal deck forms at the top of the girder and pitted the concrete underneath it (Figure 4-11). In future tests where explosives are used, better protection of sensitive equipment near the detonation location will help ensure the resilience of the equipment and result in more complete data-acquisition than was achieved in Full-Scale Test 1.

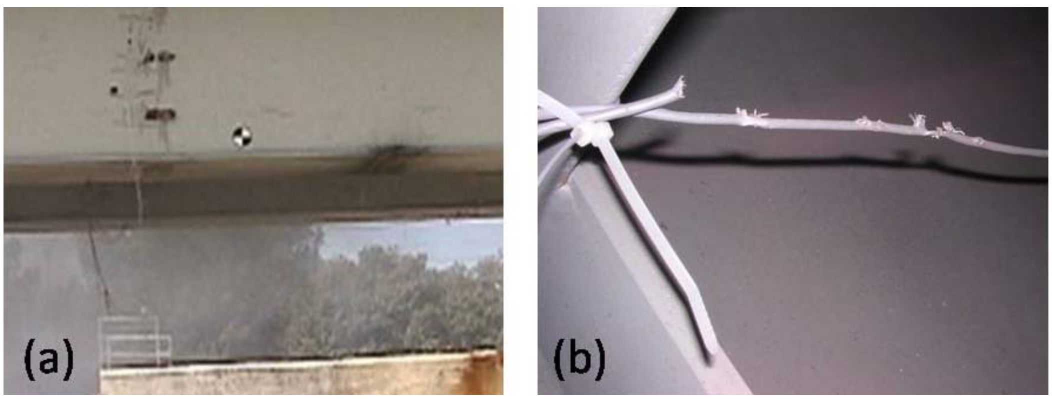

Figure 4-10: (a) Disconnected wires just south of the fracture location,
(b) Shredded wires inside the fractured girder near the fracture location

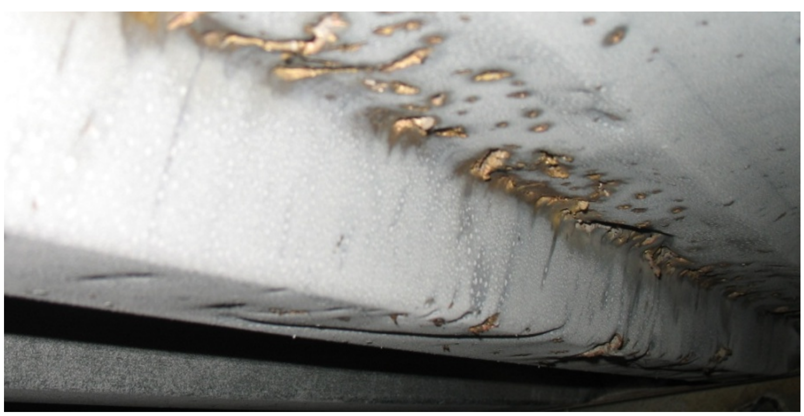

Figure 4-11: Damage to the permanent metal formwork and the underside of the concrete slab

4.3.2 Loss of Data

Because data sampled 1000 times each second from 128 channels required a significant amount of disk space, it was important to limit the time during which the data was recorded. A countdown to detonation was planned, but a miscommunication resulted in the explosives being fired before the instrumentation system began recording data. Shortly after the detonation, the data-acquisition system began saving data readings, but the initial pulse was lost. In future tests, a clearer communication method should signal the initiation of the test, and ample hard drive space should be secured so that the material demands of recording data for an extra few seconds do not affect the experimental results.

4.4 SUMMARY

Full-Scale Test 1 was executed, successfully creating a bottom flange fracture in the exterior girder of the test-bridge. The expected consequences of this fracture, however, were not realized. The fracture in the bottom flange did not propagate into the girder webs, minimal relative deflection occurred between the two girders, and no significant loads were perceivably transferred from the fractured girder to the intact girder. Furthermore, a lack of protection for the instrumentation resulted in severe damage sustained during the detonation, and a communication error resulted in no data being recorded until after the detonation took place.

The intent of Full-Scale Test 1 was to observe the behavior of the bridge and the subsequent participation of redundant load paths in the event of a full-depth fracture of a fracture critical component. Because a full-depth fracture did not result and redundant load paths were not engaged, this goal was not realized. To make the desired observations and gather the necessary data, subsequent tests would have to be designed and executed to fabricate a fracture event, making use of the test-bridge in its partially damaged state.

CHAPTER 5

Methods: Full-Scale Test 2

5.1 INTRODUCTION

After the bridge sustained minimal damage during Full-Scale Test 1, the opportunity to observe the behavior of the structure in the case of a girder fracture was still available. The second full-scale test set out to accomplish the same general goals as the first, but without the uncertainty surrounding the propagation of the bottom flange fracture into the webs of the girder. The test methods differed: in the first test, a fracture event was simulated by a rapid cutting of the flange. The second test focused on dynamically releasing the energy from a fracture using an external jack system.

5.2 TEST PROCEDURE

As an initial step, the second testing sequence required the displaced bridge to be repositioned and held at the approximate height where it stood prior to the bottom flange fracture sustained during Full-Scale Test 1. While supported in that position, the bottom flange fracture was manually extended up the web height using an acetylene torch (Figure 5-1). The web cuts were terminated 10 in. below the weld to the top flange. Next, concrete girders closely approximating the geometry and weight of a 76-kip. design truck load were placed on the bridge deck, longitudinally near the centerline and biased transversely toward the fractured girder (Figure 5-2). This position simulated a worst-case-loading scenario at the fracture location when considering both longitudinal bending of the girders along the span and transverse bending of the deck across its width. Lastly, the support system that was installed to hold the bridge throughout the loading process was forced to very quickly release the entirety of the load it was supporting. The use of a small amount of explosives helped realize this rapid change in support conditions, simulating a dynamic fracture of the bridge girder. Loading the bridge in its already

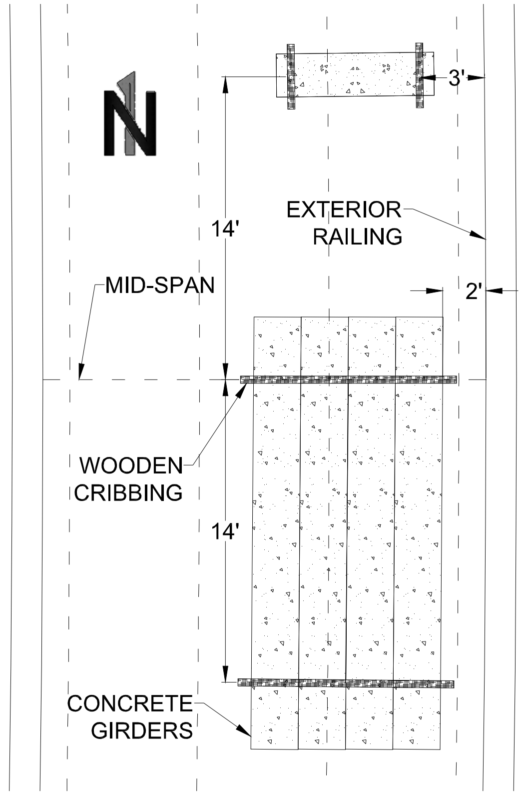

Figure 5-1 (left): Manual fracture of girder web

Figure 5-2 (right): Simulated truck load position

damaged state contributed to the worst-case loading scenario. In the event of an actual fracture, energy would be dissipated as the fracture propagated. For the procedure used in Full-Scale Test 2, none of the internal energy of the test-bridge and jack system would be dissipated through propagation of the fracture because the damage had already been imposed. Thus, the test set-up utilized for Full-Scale Test 2 was envisioned to place demands on the redundant load paths that would be in excess of what a bridge in service would be expected to withstand in the event of an actual fracture.

5.2.1 The Use of a Custom Scissor-Jack System

A custom scissor-jack system was designed and constructed to assist with a number of stages of the test sequence. The jacks were used to raise the fractured girder to its undeformed position and hold it there as damage was induced and live load was added. It was then disabled on command by explosively removing a tension link, resulting in a dynamic response of the bridge in its fractured condition. Full design details of the scissor-jacks are included in Appendix A.4.

The scissor-jack system was comprised of two hexagonal assemblies symmetrically placed 2.5 ft. on either side of the fracture location and connected to each other using x-bracing for stability. The jacks were bolted to the bottom flange of the fractured girder and to the concrete slab approximately 10 ft. below, and were pinned with solid steel rounds at the base plates, at mid-height, and to the upper connection plates. Tension-ties on each jack connected to the mid-height pins completed the stable load path from the girder through the jack system and into the ground. A design schematic of the structure is shown in Figure 5-3, and photographs of the completed system are shown in Figure 5-4.

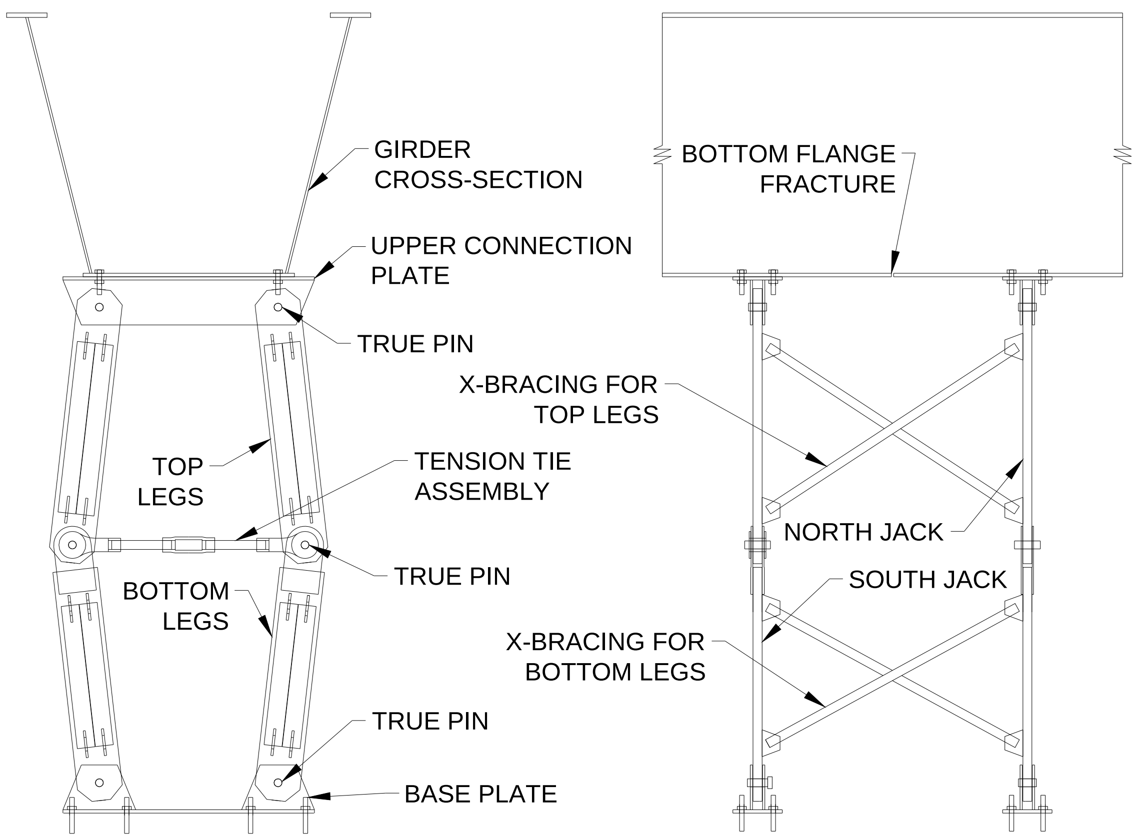

Figure 5-3: Scissor-jack schematic, shown longitudinal to the span (left) and transverse to the span

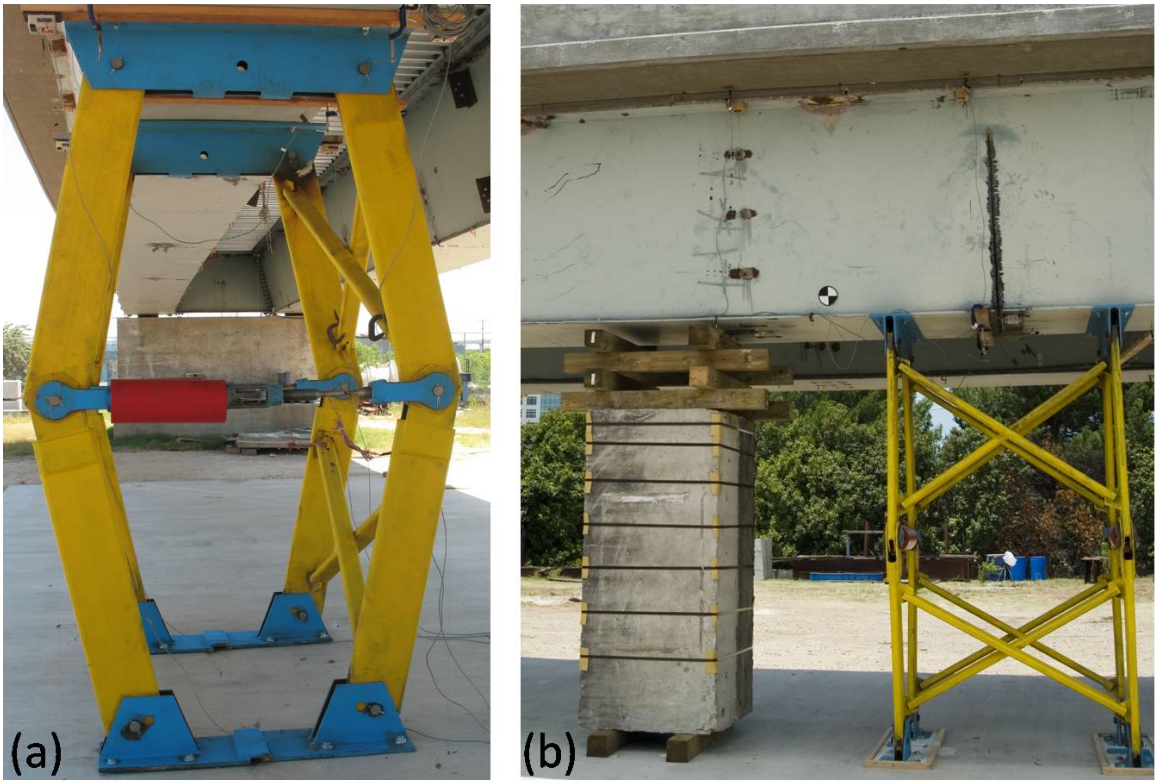

Figure 5-4 (a): Longitudinal view of the fully installed scissor-jacks, (b): Transverse view of the fully installed scissor-jacks, shown with the southern concrete and cribbing safety pillar.

5.2.1.1 Design for Operation

The scissor-jack system in its operation phase was designed to be able to raise the fractured girder 0.25 in. at mid-span and hold the bridge in place for an extended period in its progressively damaged, increasingly loaded state. The scissor-jack support allowed for the transfer of loads from the fractured girder to the underlying slab through truss-like action. The inclined legs were loaded in compression and connected at mid-height to a tension-tie that counteracted the horizontal component of the force in the inclined legs. The geometry of the scissor-jacks positioned the inclined legs at nearly vertical angles to minimize the horizontal components of the forces held by the mid-height tension rod assemblies.

The scissor-jacks were used to raise the fractured girder and hold it in the approximate position where it stood before sustaining the bottom flange fracture induced during Full-

Scale Test 1. As discussed in Chapter 4, survey data from the bottom flanges of the two girders taken throughout Full-Scale Test 1 indicated girder deflections that were not completely credible based on the observed response of the bridge. Video evidence of the experiment was not sufficiently detailed to provide more accurate data than that collected from the surveys, so the exact downward displacement of the fractured girder resulting from the loss of its bottom flange was unknown. Ultimately, it was decided that the scissor-jacks would be designed and used to recover 0.25 in. of vertical displacement at the mid-span of the fractured girder. This value was selected because it correlated reasonably well with the measurements taken during Full-Scale Test 1.

Each of the mid-height tension assemblies included a clevis at each end, two custom-machined threaded solid steel rounds, and a central left-hand, right-hand turnbuckle. Schematics for the tension assembly components are shown in Figures 5-5 and 5-6, and a photograph of the installed assembly is shown in Figure 5-7. The clevis at each end of each tension assembly shared the pin connection joining the top and bottom inclined legs of the scissor-jacks. The central turnbuckle, when adjusted, changed the distance between the pins connecting the ends of the tension-tie, and therefore the total height of the

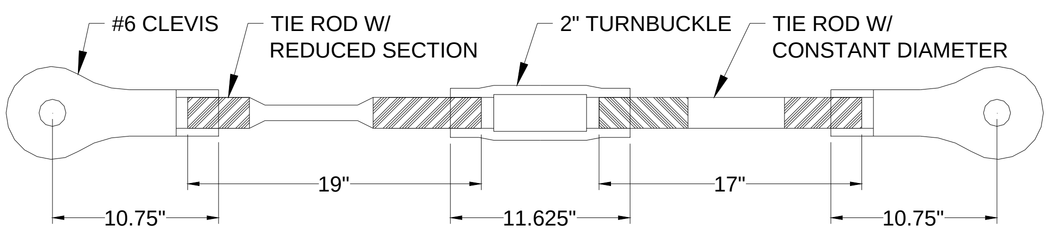

Figure 5-5: Tension assembly component detail

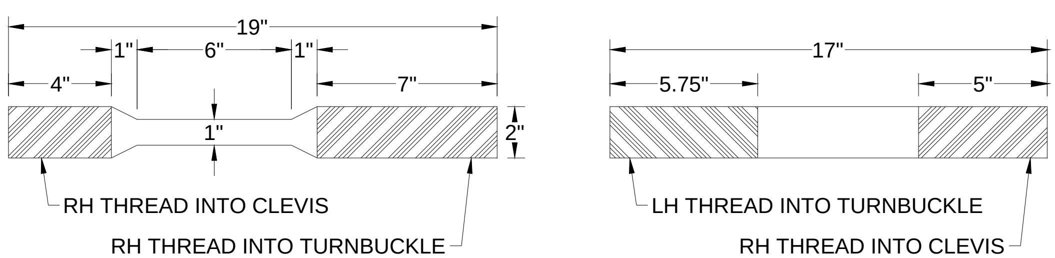

Figure 5-6: Tension rod details

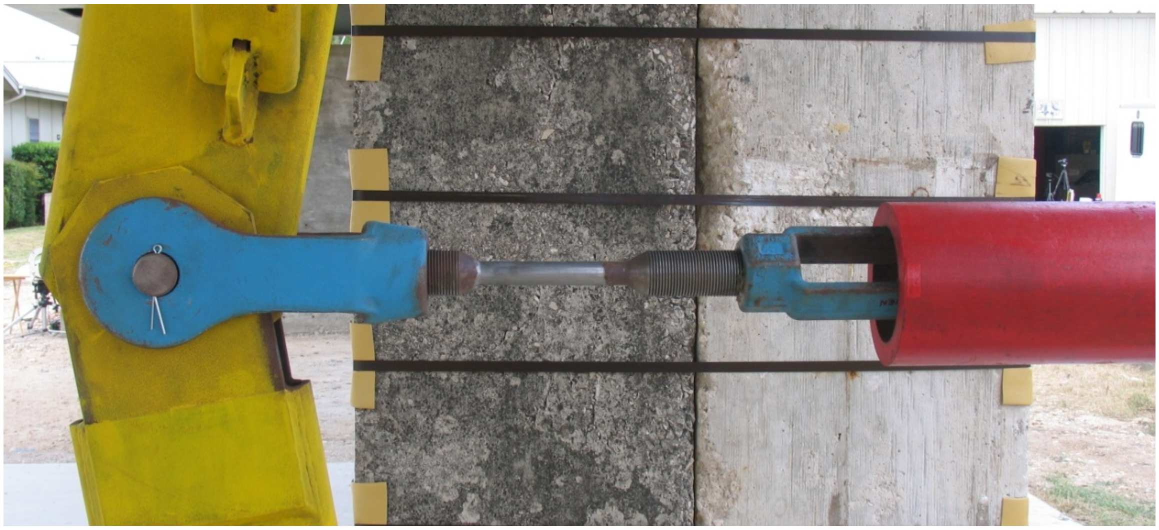

Figure 5-7: Tension rod assembly, showing (from left to right) a true pin connection through a clevis, the reduced tension-tie section, the turnbuckle, and the protective piping in the open position.

scissor-jacks. Large wrenches were used to manipulate the turnbuckles and adjust the position of the bridge, based on the number of screw turns necessary to alter the geometry of the scissor-jacks appropriately. To help control the tie adjusting procedure, a thread locking agent fixed the screw threads between the clevises and the rods, and wax lubricated the threads between the rods and the turnbuckle. The clevises and turnbuckles were ordered to specification from Cleveland City Forge.

Ultimate force demands on the scissor-jacks to shore the fractured girder were predicted analytically through the non-linear finite element model of the test-bridge (Kim, 2009), into which the full progression of bridge damage and load staging was programmed. Design forces were determined by multiplying the force demands predicted by the finite element model by a factor of safety of 2.0. The supporting concrete slab was also designed and constructed to have the capacity to resist factored versions of the ultimate forces determined by the analysis model. Design details of the slab-on-grade are included in Appendix A.5.

5.2.1.2 Design for Failure

Equally as important as the design of the scissor-jacks for their operation phase was the design for their failure. To have the test-bridge respond in way that simulated a dynamic fracture event, the supports would have to fail in a controlled manner, on command, and in a way that nearly instantaneously released the full load that was being carried. The use of true pins in a non-redundant truss system created a situation where the failure of one connecting member would mean the failure of the entire assembly. Because of their tension-only loading, the horizontal ties were not designed for buckling resistance. This led to section selections that considered material area but not moment of inertia, resulting in sections that were small compared to the compression members of the scissor-jacks. The tension-ties were therefore chosen as the members to be eliminated. As with Full-Scale Test 1, explosives were used in Full-Scale Test 2. The use of explosives allowed the load in the tension rods to be released nearly instantaneously, which allowed the bridge to respond dynamically as one of its supports was released in a sudden manner. The same precautions for safety were used for the second round of testing as were implemented during the first test.

The overall jack design required clevises with a 3-in. grip to fit around the connecting elements of the top and bottom legs, and clevises with grips this large were only available with a minimum 2-in. diameter thread. Design forces traveling through the tension assemblies, however, demanded steel rods with diameters just less than 1 in. To minimize the explosive requirements, one of the rods in each tension assembly was turned down from 2 in. to 1 in. in diameter (Figure 5-6). The rods were designed so that this modification could be placed where ample space existed between threaded regions so that the section could be reduced at a reasonable angle and so that an appropriate length of 1-in. diameter section could be provided for the explosives to be attached.

The top plates of the scissor-jacks were initially bolted to the fractured girder’s bottom flange to facilitate installation, but these bolts were removed prior to severing the tension-ties to allow for the jacks and the bridge to deflect and respond independently. Separating the structures helped reduce the possibility that the scissor-jacks, once disabled, would act as an alternate load path for the bridge load, and observations of independent responses would help support the claim that the experiment allowed for the test-bridge to respond dynamically in carrying the entire load previously held by the scissor-jacks.

For the final step in the test sequence, the reduced sections on each of the two tension-ties were severed with approximately 1/4-lb of explosives (Figure 5-8). Because all of the connections within the scissor-jack system were constructed as true pins, a rapid failure of the tension assembly would effectively take the bridge from being held in its undeformed position to being unsupported at mid-span with one of its two girders having a full-depth fracture at that location.

The use of explosives to cause the nearly instantaneous disabling of the scissor-jack support was critical to achieve a dynamic response. All of the planning and execution of the explosives work, including preliminary testing, installation at the test site, and detonation, was again contracted to Southwest Research Institute. Samples of the steel tension-ties with reduced sections were provided for preliminary testing so that the appropriate amount of explosives could be used during Full-Scale Test 2.

Figure 5-8: Explosives attached to the reduced section of the tension assembly

5.2.1.3 Construction and Installation

Construction of the scissor-jack components took place at the Ferguson Structural Engineering Laboratory. The components consisted of HSS sections, solid steel rounds, built-up members that used 0.375-in. and 0.5-in. plates, and a small selection of prefabricated parts. Project team members cut, punched holes in, machined, or otherwise modified all steel components, and they also tack-welded all built-up sections in place with a mig-welder until a certified welder could complete the structural welds.

The installation of the jack system began from the top and proceeded downward. The top connection plates were first bolted onto the bottom flange of the fractured girder through custom punched holes (Figure 5-9a). Next, the top legs were pinned into and suspended from the top plates (Figure 5-9b). The clevises were then installed as the bottom legs were pinned into and suspended from the top legs. Come-alongs were used to stabilize the legs from swinging while the remainder of the tension assembly was installed between the clevises (Figure 5-9c). The bottom legs could then be pinned into the individually drilled connection holes in the base plates, which were lastly bolted into anchors installed in the concrete slab (Figure 5-9d).

Special attention was paid during installation of the jacks to the fitting of the base plates. The bottom flange of the fractured girder was not perfectly level, nor was the concrete slab on which the jacks were supported, resulting in variability of nearly 1 in. in the overall heights the jacks spanned between their four top and bottom connecting corners. After the two base plates were separated into four individual feet, a second set of connection-holes were drilled individually into each base plate to ensure correct height and a proper connection at all locations (Figure 5-10). Despite these steps, local irregularities in the concrete slab and warping of the steel plates produced a situation where each base plate did not bear continuously on the slab. Washers were used as spacers to provide a bearing load path through the base plates and into the slab at each of the four bolt locations on each foot of the scissor-jack assemblies. Grout was then poured into small dammed up areas surrounding the base plates to fill the remaining gaps

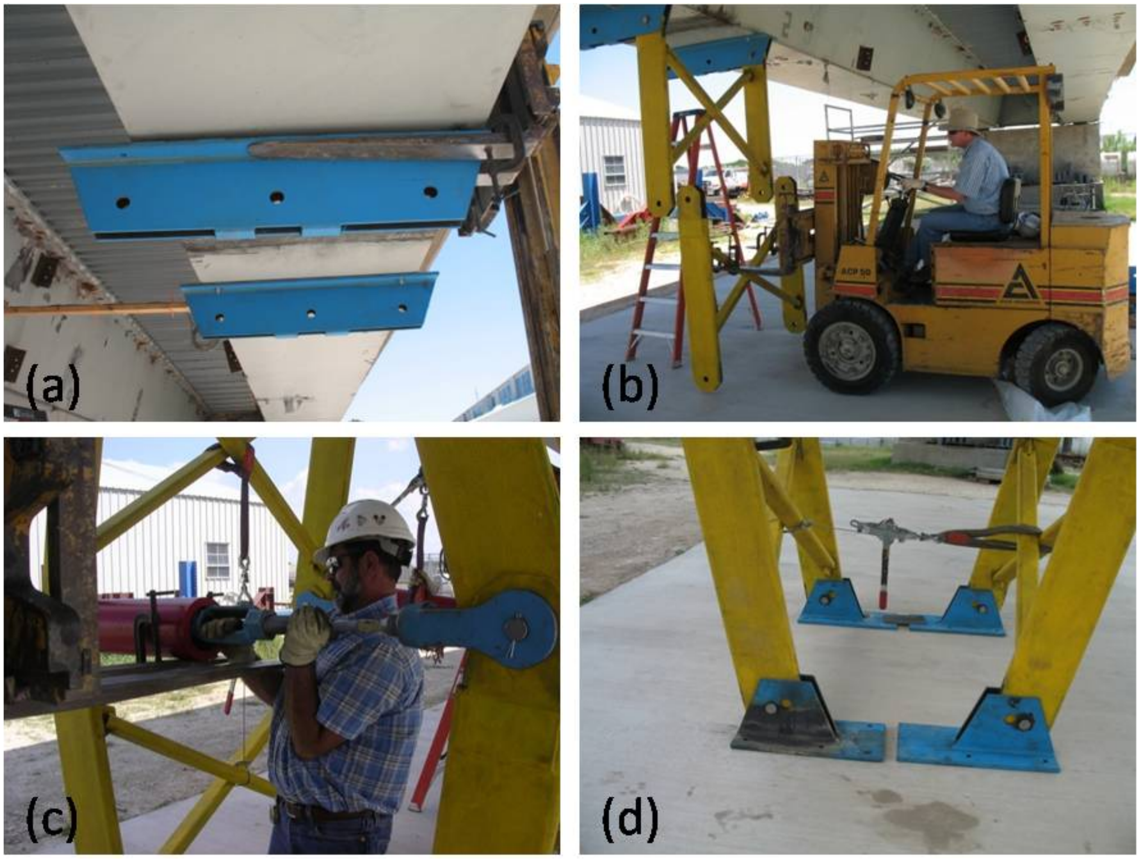

Figure 5-9 (a, top left): Installing the top connection plates, (b, top right): Installing the legs, (c, bottom left): Installing the tension assembly, (d, bottom right): The pinned custom fitted base plates

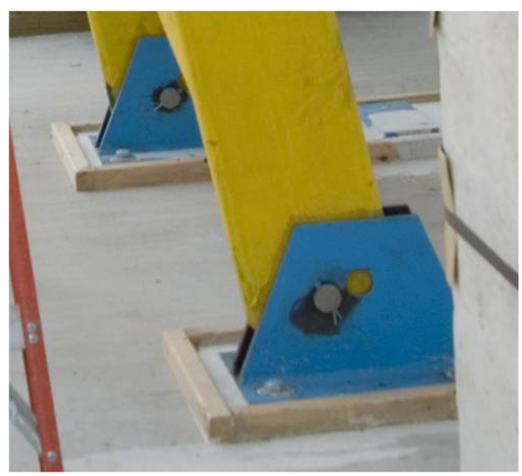

Figure 5-10 (left): Custom-drilling pin holes into scissor-jack base plates

Figure 5-11 (right): The scissor-jack base plates after grouting to the concrete slab

between the steel and the concrete (Figure 5-11). Grouting the gaps provided complete bearing surfaces between the scissor-jacks and the slab, eliminating the effect that bending of the base plates would have had on the stiffness of the overall system response.

5.2.2 Safety

Because of the large size of the test specimen, the uncertainty of dealing with a severely damaged bridge, and the danger of using explosives, a number of safety precautions were taken throughout the test procedure. Prior to cutting the girder webs, concrete pillars topped with wooden cribbing reaching within a few inches of the fractured girder bottom flange were placed on both sides of the fracture (Figure 5-4b). These pillars were left in place until just before the explosives were detonated to ensure that, in case of an unexpected failure, the bridge could not deflect to a degree that would be dangerous to workers nearby.

As a precaution against debris from the explosion, heavy 1-in. thick steel pipe was installed around the tension-tie assembly. The thickness of the pipe was recommended by Southwest Research Institute based on preliminary testing of the sample tie rods and efforts to contain unwanted fragments and debris. The length of the pipe allowed for it to be slid to one side of the tension assembly to allow access to the turnbuckle and detonation location (the open position), or it could be positioned to completely cover the explosives (the closed position). In the closed position, the ends of the pipe were almost completely blocked by the clevis and turnbuckle, further reducing the risk of flying debris.

5.3 DATA-ACQUISITION AND INSTRUMENTATION

The instrumentation setup from the first full-scale test was repaired and significantly extended to cover critical locations of the assumed primary and alternate load paths more completely than before (Figure 5-12). The arrangement of gages attached to the steel girders was modified and extended to six cross-sectional locations along the length of the bridge. In addition, an array of uni-axial concrete gages was placed on the concrete deck, and a number of direct displacement gages were installed.

5.3.1 Repairs to Existing Instrumentation

Because a significant amount of time passed between the first full-scale test and the second, it was important to review the existing instrumentation setup and to determine the extent of the repairs required. All of the existing gages were inspected visually as well as electronically. Certain gages required new wiring, and others required complete replacement. A small number of shear stud and reinforcing bar gages, which were non-functional and unable to be repaired, were not utilized for Full-Scale Test 2.

5.3.2 Girder Instrumentation

The typical instrumentation of the steel girders through a cross-section was significantly modified for the second full-scale test. The fractured girder was not expected to resist significant torsional load, so the use of rosette gages was, after further discussion, determined to be unnecessary. To capture the strong-axis bending behavior of the fractured girder with a minimum number of data channels, uni-axial gages were used only at the mid-width of the bottom flange. The uni-axial gages at the quarter points of the flange and webs were also consuming a number of valuable data channels and were eliminated. Rosette gages were still used at the mid-width position of the bottom flange

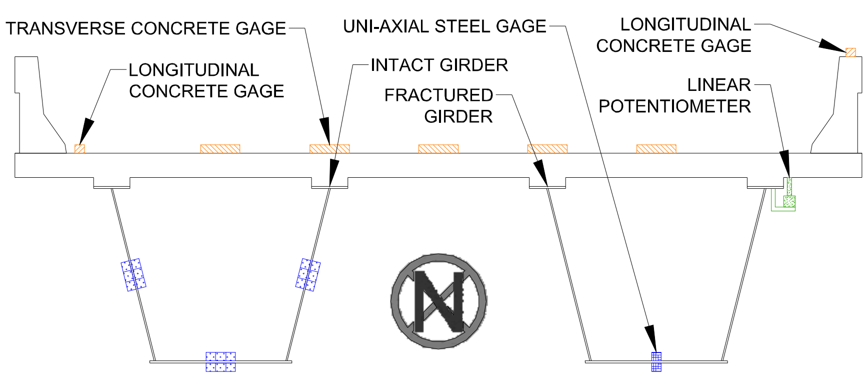

Figure 5-12: Instrumentation of the bridge elements for Full-scale Test 2 at a typical cross-section

and at the mid-height location of the two webs of the intact girder to help determine the overall stress state throughout the intact girder's cross-section.

For the extended gaging plan, six cross-sections (including S3, S2, S1, N1, N2, N3) of the steel girders were instrumented, spanning the central 60 ft. of the bridge. The cross-sections were spaced 12 ft. apart, each lying half-way between internal cross-frames. A plan view showing the cross-section designations along the length of the test-bridge is included in Figure 2-17.

Data from the non-linear finite element analyses indicated that the mid-span cross-frame internal to the intact girder would see high levels of stress during Full-Scale Test 2. Accordingly, four uni-axial strain gages were attached to the angle members comprising the cross-frame to capture deformations in the members. The results were intended for use in calibrating the non-linear computer analyses.

5.3.3 Concrete Instrumentation

The approximately 20 reinforcing bar gages cast into the concrete that were still functioning correctly were determined to be insufficient to capture the bending behavior of the deck effectively. Consequently, an array of uni-axial concrete gages was installed, oriented both longitudinally and transversely to the bridge span. Though these gages could not be used to determine the complete strain profile throughout the deck thickness, they would be able to provide an appropriate estimation of extreme tension or extreme compression fiber strain in the direction they were oriented.

To help provide an accurate reading of the strain at a discrete location on a concrete member, long gage lengths are used to average the readings across the non-uniform material. The concrete gages selected for Full-Scale Test 2 were 60 mm. long. It was important to prepare appropriate locations to reliably attach the gages and provide a bond stiff enough to transfer equal strain from the concrete material into the strain gage. The concrete at the gaging locations was polished with a grinder and then primed with a thin layer of fast drying epoxy that, once hardened, was again smoothed with a grinder. Once

Figure 5-13: A pair of fully installed uni-axial gages on the surface of the concrete deck

each concrete gage was attached with the standard adhesive, it was waterproofed with a layer of wax and a layer of silicon (Figure 5-13).

Concrete gages oriented transversely to the bridge span were placed on the deck surface half-way between the flanges of the intact girder, above the interior flange of the intact girder, half-way between the two girders, above the interior flange of the fractured girder, and half-way between the two flanges of the fractured girder. This series of five evenly spaced gages would help determine the bending behavior of the concrete deck across the width of the four girder top flanges on which it was supported. Three longitudinally oriented gages were placed at four cross-sections on the girder. These gages were positioned at the interior railing, between the top flanges of the intact girder, and between the top flanges of the fractured girder. These longitudinal gages would help determine the bending behavior of the deck along the span of the bridge, particularly in the region near the fracture location.

The cross-sections instrumented with concrete gages corresponded to those on which the steel gages were placed. Eight cross-sections were used, including S3, S2, S1.5, S1, N1, N1.5, N2, and N3, in total spanning the central 60 ft. length of the bridge. A map of the concrete gage locations is shown in Figure 5-14.

In the event of significant deflection of the bridge, the expansion joints in the railings could close, causing the concrete rail sections to engage. To provide information on the

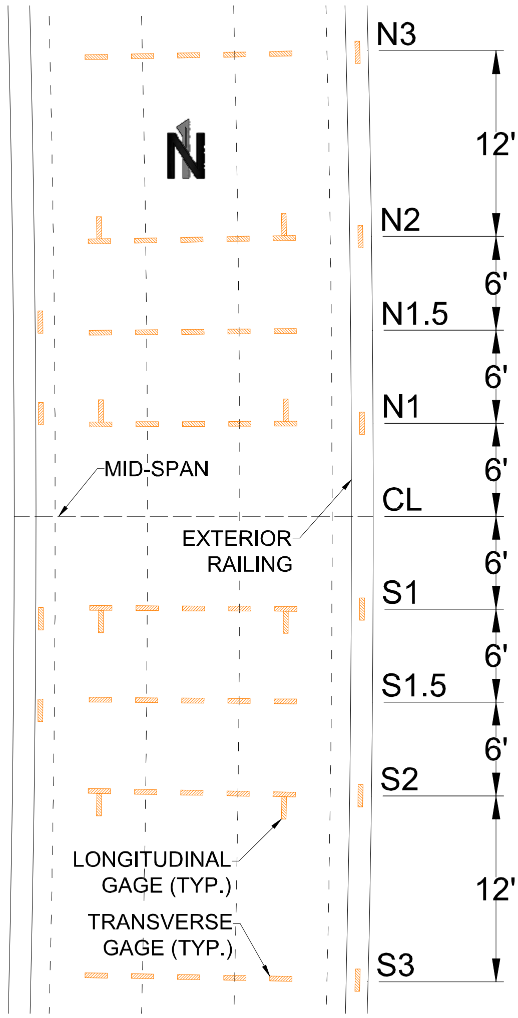

Figure 5-14: Plan view of the surface concrete gage locations for the second test

magnitude and nature of the forces that would develop in the event of an expansion joint closing, the exterior railing above the fractured girder was instrumented at S3, S2, S1, N1, N2, and N3. All of these gages were positioned on the top face of the railing oriented in line with the span of the bridge to measure extreme fiber axial strains (Figure 5-15).

5.3.4 Direct Measurements and Observations

Linear potentiometers were installed at seven locations between the exterior flange of the fractured girder and the overhanging concrete deck on cross-sections S3, S2, S1, CL, N1, N2, and N3. To position the potentiometers, clamps were secured to wooden blocks that were attached to the girder bottom flanges with epoxy (Figure 5-16). Small glass plates

Figure 5-15: A concrete gage installed to the top face of the exterior railing

were glued to the underside of the deck at the contact point to minimize frictional effects on the potentiometer readings. These gages would help measure the amount of separation between the girder and the deck as the bridge displaced. Similar gages along the inside flange of the fractured girder would have provided beneficial data, but the permanent metal formwork that spanned between the two girders would have interfered with the acquisition of any reliably accurate readings. A pair of linear potentiometers was also installed at opposite ends of the bottom flange of the fractured girder across the fracture location to measure its change in width as the bridge deflected (Figure 5-17).

Four linear potentiometers were installed between the southern end diaphragm and the abutment that supported it (Figure 5-18). Measurements of the change in height between the bottom corners of the girders and their supports would provide data on any twisting of

Figure 5-16 (left): Linear potentiometer measuring separation between girder flange and concrete deck

Figure 5-17 (right): Two linear potentiometers measuring change in width of fracture at bottom flange

Figure 5-18 (left): Linear potentiometer measuring change in position of the end of the girder span

Figure 5-19 (right): String potentiometer measuring the change in height of the fractured girder

the girders about their longitudinal axes at the ends of the bridge span. These data would provide information that could be used to determine the force transfer between the girders through the end diaphragms, supplementing the strain gage data from the center points on the diaphragms.

One string potentiometer was installed for the second full-scale test that was intended to provide data on the overall deflection of the fractured girder once the jacks were released. The housing base of the string potentiometer was attached immediately adjacent to one side of the fracture location at the mid-point of the bottom flange, and the end of the instrument's string was attached to the concrete slab immediately underneath (Figure 5-19).

As was the case in Full-Scale Test 1, surveys were taken of the girder bottom flanges before and after every major step in the testing sequence. A survey across the deck slab was also taken to provide information on local deformations as well as to offer a secondary reference of overall bridge deflection (Figure 5-20). Differences between the measurements in the deck and girder surveys could be used to determine separation of the girders from the deck due to shear studs pulling out as the bridge deflected.

A number of video cameras were set up, two of which recorded at high frame-rates, to capture visuals of Full-Scale Test 2 from a variety of angles. Additionally, to provide

Figure 5-20: Surveying the bridge deck

another means of visual observation of the deformation of the concrete deck, cracks on the top surface of the deck were traced with permanent markers before and after the scissor-jacks were disabled.

5.3.5 Real-Time Monitoring

To provide a means of immediately observing the state of the test-bridge during test preparations, a mobile computer system was set up to help monitor the instrumentation at critical locations. Once the scissor-jacks were operational, the loads they carried changed as the steps in the testing procedure proceeded. Progressive test steps, including raising the fractured girder to its original height, extending the fracture to the full depth of the girder, and placing the live load on the bridge deck, all increased demand on the scissor-jacks. Real-time measurements would help ensure that the scissor-jacks were functioning as expected while transferring loads similar to those predicted by the non-linear finite element model. These measurements could also be used to identify any immediate safety concerns. To supplement these data, direct measurements of the geometry of the scissor-jacks were taken as the load steps progressed. Length measurements were taken along its height from the top pins to the bottom pins and across its width between the pins on either end of the tension assemblies.

To estimate force transfer, four strain gages were installed on the reduced 1-in. diameter sections of the scissor-jacks' tension-ties (Figure 5-21). Two of the gages were mounted longitudinally and two were mounted transversely and then wired together to form a full bridge circuit. The forces through the tension-ties were used to predict the overall loads carried by the scissor-jacks. These accurate, real-time readings of the demands on the support were actively compared with the loads predicted from an analytical study of the jacking scenario. To measure deflections, string potentiometers were also temporarily installed near the four corners of the scissor-jacks between the bottom flange of the fractured girder and the concrete slab (Figure 5-22). Measurements from these gages

Figure 5-21: The tension-tie with reduced section, instrumented with a full bridge to act as a load cell.

Figure 5-22: String potentiometers measuring the change in height of the corners of the scissor-jacks

were used to observe the height and movement of the bridge, both as the fractured girder was raised and as the load through the scissor-jacks was increased.

5.3.6 Data-acquisition

For Full-Scale Test 2, a high-speed data-acquisition system was again used (Figure 5-23). To capture dynamic response of the test-bridge, rapid, accurate, and synchronized data-acquisition from all 244 channels of instrumentation was important (Table 5-1 and B-4). After reviewing the data from the first full-scale test, it was determined that when viewing and analyzing readings incremented every thousandth of a second, similar clarity was reached by eliminating half or even more of the data points. Therefore, the system set-up for the second test sampled data simultaneously from all 244 channels, 500 times each second.

The data-acquisition system used for the 127 channels from Full-Scale Test 1 was expanded to accommodate the addition of 117 channels for Full-Scale Test 2, bringing

Figure 5-23: The main data-acquisition system, fully connected for Full-scale Test 2

Table 5-1: Instrumentation count for Full-Scale Test 2

Gage Type	# of Gages / Channels	
Reinforcing Bar	22	22
Shear Stud	14	14
Girder (Uni-axial)	12	12
Girder (Rosette)	36	108
End Diaphragm (Rosette)	4	12
Interior Diaphragm (Uni-Axial)	4	4
Top Deck (Transverse)	40	40
Top Deck (Longitudinal)	12	12
Exterior Railing	6	6
Linear Potentiometer	13	13
String Potentiometer	1	1
Total	**164**	**244**

the total number of channels to 244. National Instruments manufactured all of the hardware used. The two 12-slot SCXI-1001 chassis used in Full-Scale Test 1 were both filled to capacity with a total of 24 SCXI-1520 8-channel universal strain modules. Two new SCXI-1000 4-slot chassis were also purchased. Filling the eight new slots were five additional SCXI-1520 8-channel universal strain modules, and three SCXI-1121 4-channel isolation amplifiers. SCXI-1314 8-channel terminal blocks were connected to each of the twenty-nine SCXI 1520 modules, and three SCXI-1321 4-channel terminal blocks were connected to the SCXI-1121 isolation amplifiers. All four of the chassis were connected through the National Instruments PCI 6250 data-acquisition card into the PC, configured with LabVIEW.

5.4 FINAL PREPARATIONS

The use of explosives for Full-Scale Test 2 again required communication with relevant authorities and observation of the test from a distance. In this case, however, because the explosion was well contained and significantly smaller than what was used in Full-Scale Test 1, live observation of the test event was allowed from approximately 150 ft. away.

Streaming video was also broadcast on the internet for remote viewing. Once all preparations were completed and the test location was secured, executing the test, as with Full-Scale Test 1, took a matter of seconds and required only a remote detonation command.

5.5 SUMMARY

Full-Scale Test 2 was designed to produce a dynamic response of the test-bridge after it had been held in position while damage comparable to what it would have sustained in the event of an actual fracture was induced. Preparations for this test were extensive. A scissor-jack system was designed, constructed, and installed to raise the mid-span of the fractured girder 0.25 in. and support it there while damage was induced on the bridge. The support structure was also capable of immediate collapse when a critical link was severed with explosives. Coordinating for the appropriate and safe use of the explosives was an integral part of the test preparations. 244 channels of instrumentation equipment were prepared to gather data that would help characterize the response of the bridge to the simulated dynamic fracture event. The results of the full-scale dynamic fracture simulation are described in the following chapter.

CHAPTER 6

Results: Full-Scale Test 2

6.1 INTRODUCTION

Full-Scale Test 2 was performed during the first week of June 2008. Once the scissor-jacks were installed and operational, the webs of the fractured girder were cut on June 4, the live load was placed on June 5, and the scissor-jacks were explosively disabled on June 6. The scissor-jacks performed as designed, releasing their load when the tension-ties were cut (Figure 6-1). The resulting dynamic response of the bridge led to substantial deflections of the girders and the deck, and damage was recorded, particularly in the shear stud connections between the interior flange of the fractured girder and the concrete deck. Despite the damage the bridge sustained, it resisted total collapse. Extensive and meaningful data were recorded by both the strain-reading equipment and the various direct displacement measurement methods.

Figure 6-1: FSEL test-bridge after Full-Scale Test 2

6.2 TEST RESULTS

The explosives successfully cut through the tension-ties nearly instantly, releasing the load held by the scissor-jack structure, which in turn caused the dynamic response of the bridge in its fractured state (Figure 6-2). Immediately after the detonation, the bridge deflected downward and began to oscillate until its energy was dissipated and it came to rest. The fractured girder deflected downward farther than the intact girder (Figure 6-3) by a visually perceptible amount, but only minimal damage was apparent during preliminary inspection. As more measurements were taken and as more results were analyzed, the extent of the damage sustained by the bridge was revealed.

6.2.1 Dynamic Impact Factor

The dynamic response of the bridge to the release of the scissor-jacks was characterized by initial downward displacement followed by decaying oscillations until the all of the dynamic energy was dissipated. The initial pulse and subsequent oscillations could be observed both visually and in the strain gage data captured. An average impact factor of the test-bridge’s dynamic response was calculated to be 1.3 by analyzing the strain data captured by different types of gages at different locations. The maximum strain value

Figure 6-2 (left): Completely severed tension-tie

Figure 6-3 (right): Rear view of the test-bridge showing differential deflection between the two girders

during the initial pulse was compared with the minimum value following the peak strain, and the average of the two was compared with the static value once the total energy had been dissipated. In cases where the average strain following the initial pulse matched with the static value at the end of the test, the dynamic impact factor could be calculated as the ratio between the maximum and the average strain values, without bias from progressive damage sustained at that gage location or overall tracking of the gage readings.

Figure 6-4 presents two representative examples of the above-described calculation of the dynamic impact factor. The series on the left shows data taken from a reinforcing bar gage and the values used to calculate a dynamic impact factor of 1.23. The series on the right shows data taken from a surface concrete gage and the values used to calculate a dynamic impact factor of 1.36. The calculations based on the responses at these two and many other gage locations were in agreement of an average dynamic impact factor of approximately 1.3.

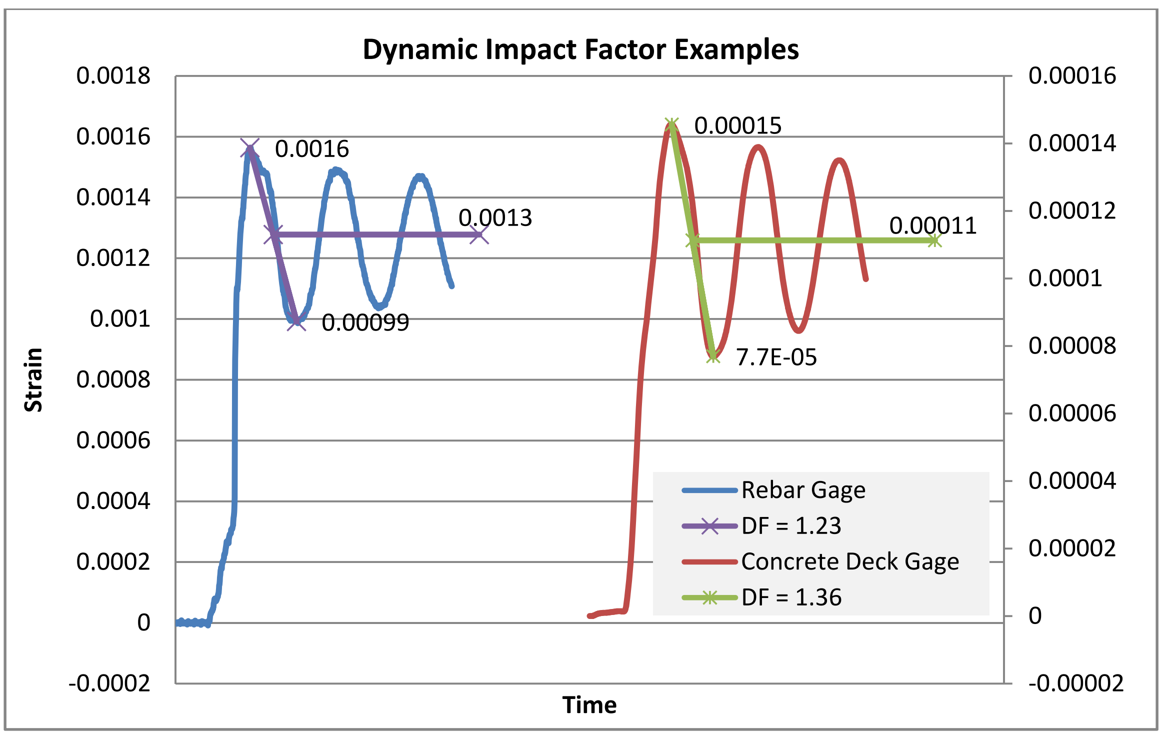

Figure 6-4: Dynamic impact factor examples

6.2.2 Scissor-Jack Performance

Upon detonation of the explosives, the tension-ties were severed, and the scissor-jacks collapsed. The strain energy released caused the scissor-jacks to collapse very quickly, and the top connection plates moved away from the bottom flange of the fractured girder much faster than the fractured girder deflected downward. High-speed video shows that, after detonation, the scissor-jacks immediately began to move downward (Figure 6-5).

When the legs impacted the clevises at the mid-height pins in the scissor-jacks' lowest possible position, approximately 0.24 seconds after detonation, the bridge was still moving downward. By the time the bridge reached the lowest point of its first oscillation, 0.31 seconds after detonation, the scissor-jacks had already begun to recoil upward.

Because of the geometry of the clevis at the mid-height connection between the top legs, the tension assembly, and the bottom legs, the scissor-jacks were only able to collapse downward 2.5 ft. Had the bridge deflected a similar amount downward, it could have impacted the scissor-jacks, which would have provided some restraint to additional deflection. If, in the future, a similar scissor-jack assembly is to be used and disabled, and the supported structure is expected to deflect downward more than the scissor-jack assembly is capable of collapsing, a reconfiguring of the central joint is recommended to provide additional deformation capacity over that realized by the configuration used in this test program.

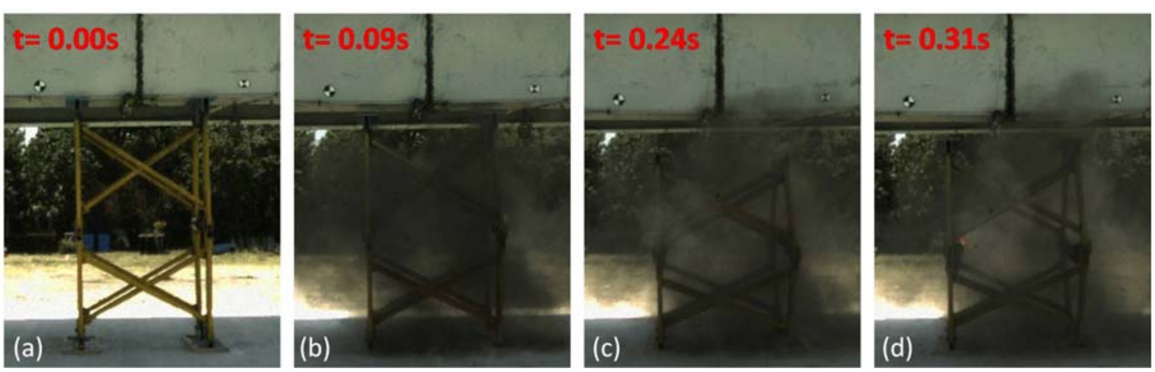

Figure 6-5: (a) Before detonation, (b) Immediately after detonation, (c) The lowest position of the scissor-jacks, (d) The lowest position of the bridge on its first oscillation

6.2.3 Fracture Opening

When the fractured girder deflected downward, the fracture widened an additional amount compared to its width prior to the cutting of the tension-ties on the scissor-jacks. Before the scissor-jacks were released, the fracture was 0.25 in. wide at the bottom flange (Figure 6-6a). When the bridge came to rest after Full-Scale Test 2, the fracture had opened an additional 0.91 in. to a total of 1.16 in. (Figure 6-6b). On the exterior web of the fractured girder, the top of the fracture propagated an additional 1 in. toward the top flange (Figure 6-6c). The area of steel immediately above and around the tops of the fractures on both webs visibly yielded. This yielding was discernible by the extent of paint that peeled in the region.

6.2.4 Damage at the Exterior Top Flange of the Fractured Girder

Substantial damage was immediately noticeable in the connection between the exterior flange of the fractured girder and the concrete deck (Figure 6-7). Cracks appeared along the length of the haunch above the fracture location, for a distance of 7 ft. in both

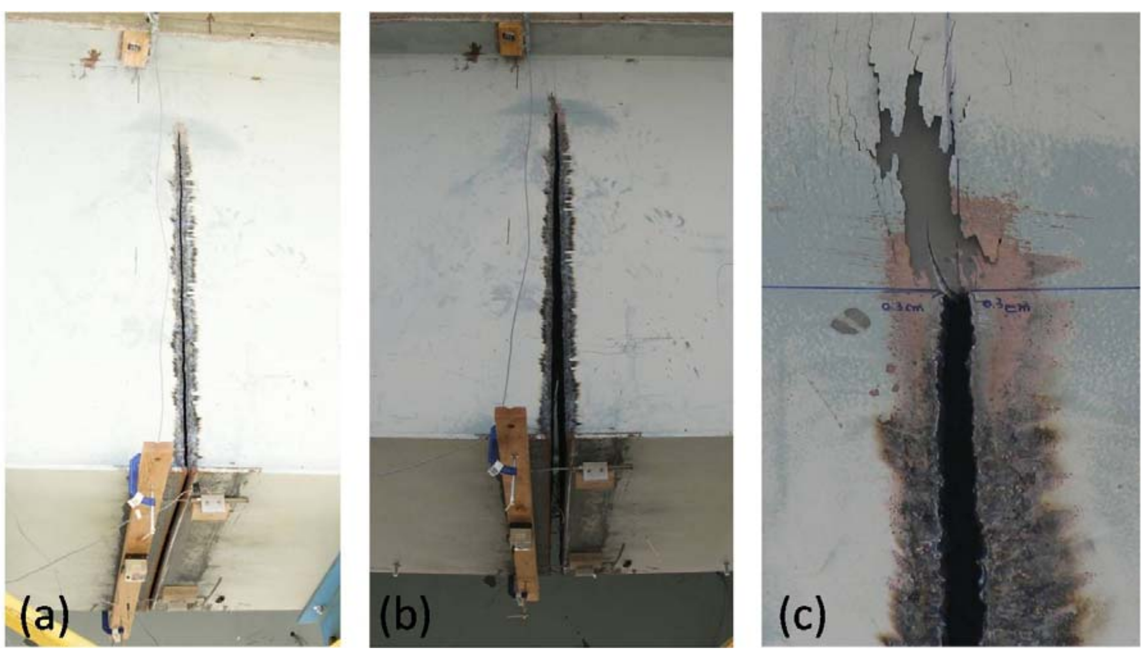

Figure 6-6: View of (a) the fracture before releasing the scissor-jacks, (b) the fracture after releasing the scissor-jacks, (c) the 1 in. propagation of the fracture on the exterior web of the fractured girder

Figure 6-7: Cracks separating the exterior top flange of the fractured girder and the deck

directions from mid-span. The cracks were as wide as 1 in. at their largest at the mid-span of the bridge.

6.2.5 Cracking of the Concrete Deck

Extensive cracking was observed on the top surface of the concrete deck. Before the scissor-jacks were released, cracks were traced with black permanent marker. After the scissor-jacks were released, new cracks and the propagation of existing cracks were traced in red marker. After all of the cracks were marked, a crack map was composed using 22 individual photographs of the top of the bridge deck (Figure 6-8). The crack map was intended to record the location of the cracks and allow future observation of the cracking patterns. Most prominently, cracks were densely spaced along the longitudinal line above the interior flange of the intact girder (Figure 6-9). Moving away from the mid-span of the bridge, these longitudinal cracks extended toward the ends of the span and curved toward the exterior railing. Some transverse cracks were also recorded, starting at the toe of the exterior railing and progressing toward the interior railing.

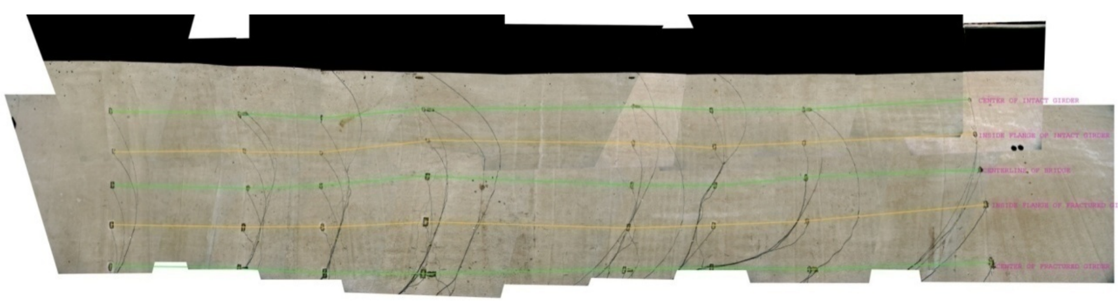

Figure 6-8: Composite map showing crack patterns on concrete deck

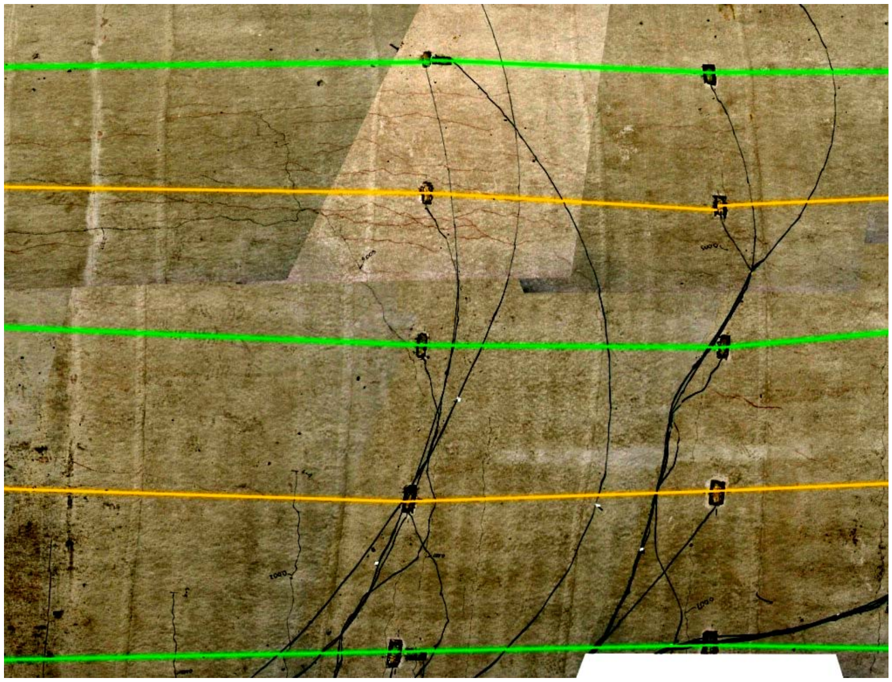

Figure 6-9: Crack map section, faintly showing cracks above the interior flange of the intact girder

This method for recording information on the deck cracking was precise but inefficient. Using permanent marker allowed for very accurate following of the cracks, but the process was time consuming, exhausted a large supply of markers, and left only relatively fine lines on the deck that were difficult to capture on camera. The composite crack map effectively captured a significant proportion of the trace marks, but the cracks do not appear boldly in the photographs, if at all. For instance, the brightness and contrast of the image of the crack map shown in Figure 6-9 were adjusted to help embolden the crack markings. Despite these manipulations, the markings are still difficult to discern. Subsequent methods for mapping concrete cracks on an unfinished surface of this scale should produce a more defined visual result (using brighter colors or bolder markings), even if some of the precise details of the cracks are sacrificed.

6.2.6 Girder Twist

Because of the torsional rigidity of closed sections, the box girders on the test-bridge had high resistance to twist and were expected to deflect directly downward. Using the data from the surveys of their bottom flanges, the change in twist along the length of the

Figure 6-10: Change in girder twist after during Full-Scale Test 2

girders was calculated, comparing their positions before and after the jacks were released (Figure 6-10). At no location did the calculated change in twist exceed 0.5˚. Data from the linear potentiometers that measured the change in height of the southern ends of the girders above the piers were in agreement, showing virtually zero twist of the girders at that location. The minimal twist of the girders throughout Full-Scale Test 2 sufficiently justified using the average surveyed heights between the edges of the girder bottom flanges for deflection analyses.

6.2.7 Girder Deflections

Surveys taken along the bottom flanges of the fractured girder before and after critical steps of the testing procedure provided a significant amount of information about the response of the test-bridge following the full-depth fracture of one of its girders. All girder deflection measurements presented were averaged between the two edge readings on each of the bottom flanges. This averaging did not impose an inappropriate skew to the data because all girder twists were relatively small. The deflections were again normalized to eliminate overall incline of the bridge, with each end of the span set to zero deflection.

Throughout the final loading steps of Full-Scale Test 2, the deflected shape of the intact girder resembled that of a simply supported beam, rotating at the ends of the span and mostly maintaining upward curvature throughout its length (Figure 6-11). With the live load applied, and prior to releasing the scissor-jacks, the intact girder deflected downward by a maximum of 1.2 in. from the normalized level of the bridge near its mid-span. After the jacks were released and the dynamic energy dissipated, the mid-span of the intact girder deflected downward an additional 2.9 in. to a total static deflection of 4.1 in. below the ends of the span. After the test when the simulated truck live load was removed from the bridge so that the girders only needed to support the self-weight of the test-bridge, the central portion of the intact girder rebounded 0.6 in., displaying a maximum of 3.5 in. deflection with the opposite girder fractured.

The deflections of the fractured girder were markedly different from that of the intact girder (Figure 6-12). Before releasing the jacks, the fractured girder's mid-span deflected 1.5 in. downward from the end supports. After the jacks were released, the center point deflected an additional 7.0 in. downward to a total static displacement of 8.5 in. below its support points. The deflected shape of the fractured girder resembled that of two partially restrained cantilevers pinned at the center. The ends of the span rotated downward toward the mid-span, and the two halves of the girder were curved downward toward the center-point where they met. When the simulated truck live load was removed, the central portion of the fractured girder rebounded 1.0 in., displaying a maximum of 7.5 in. of deflection when the bridge was supporting only its self-weight.

Differential deflection between the two girders varied as these steps progressed. Before the scissor-jacks were released, the fractured girder hung 0.3 in. below the intact girder. After release of the jacks, that difference grew to 3.9 in. Upon removing the simulated truck live load, the differential deflection between the two girders under the self-weight of the bridge was 3.5 in.

Considering the inconsistencies of the survey results from Full-Scale Test 1, the survey results from Full-Scale Test 2 appeared more credible. This set of results displayed larger

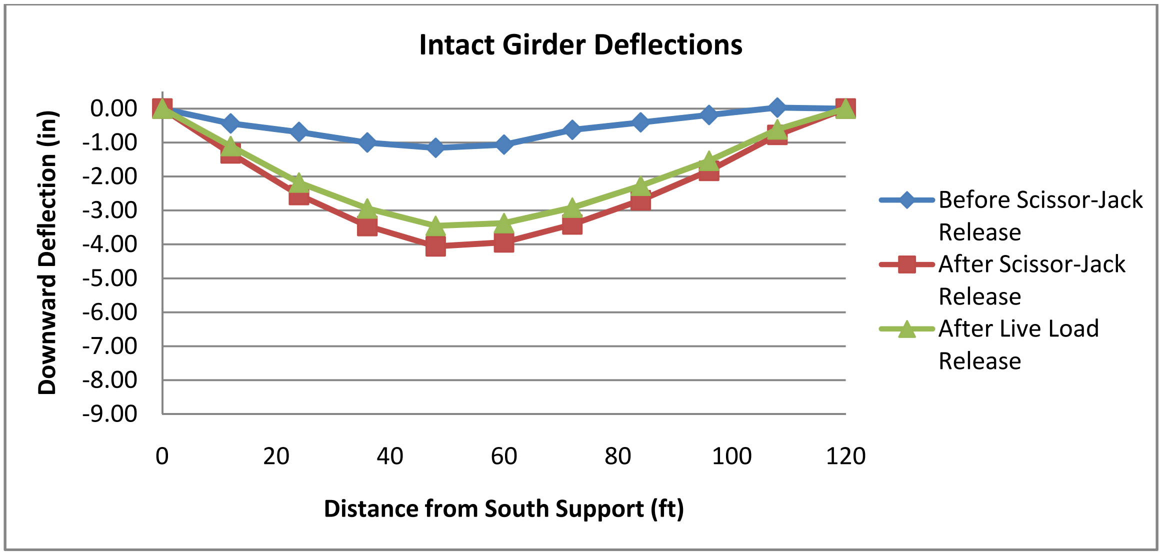

Figure 6-11: Intact girder deflections during Full-Scale Test 2

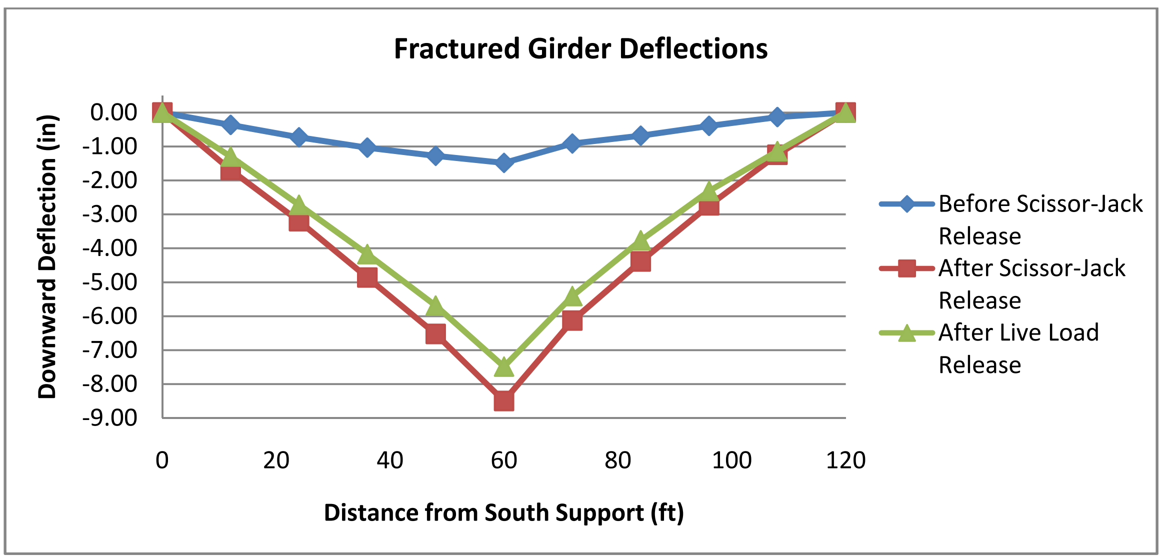

Figure 6-12: Fractured girder deflections during Full-Scale Test 2

overall deflections than Full-Scale Test 1, and hence they were not as sensitive to the factors that could affect the readings by fractions of an inch. Furthermore, the standardization of measurement procedures was more properly documented than in previous tests. Still, temperature readings of the girders were not taken during Full-Scale Test 2, and temperature gradients through the depth of the girders could have influenced the deflection data that was collected.

6.2.8 Deck Deflections

A survey taken across the top of the bridge deck after the release of the scissor-jacks provided meaningful data for the deflection of the deck after the test-bridge sustained a full-depth fracture of one of its girders (Figure 6-13). Similarly to the way the girder survey data was adjusted, the deck deflection measurements were normalized to eliminate overall slope from one end of the bridge to the other. For the three-dimensional graph shown in Figure 6-13, normalized downward deflection in inches was plotted along the vertical axis, location along the length of the bridge in feet north from the centerline was plotted along the long axis, and location along the width of the bridge in feet east from the outside flange of the intact girder appears on the other axis.

The largest displacement of the deck surface was along the exterior railing over the fracture location. This point was approximately 3.8 in. below the normalized plane of the

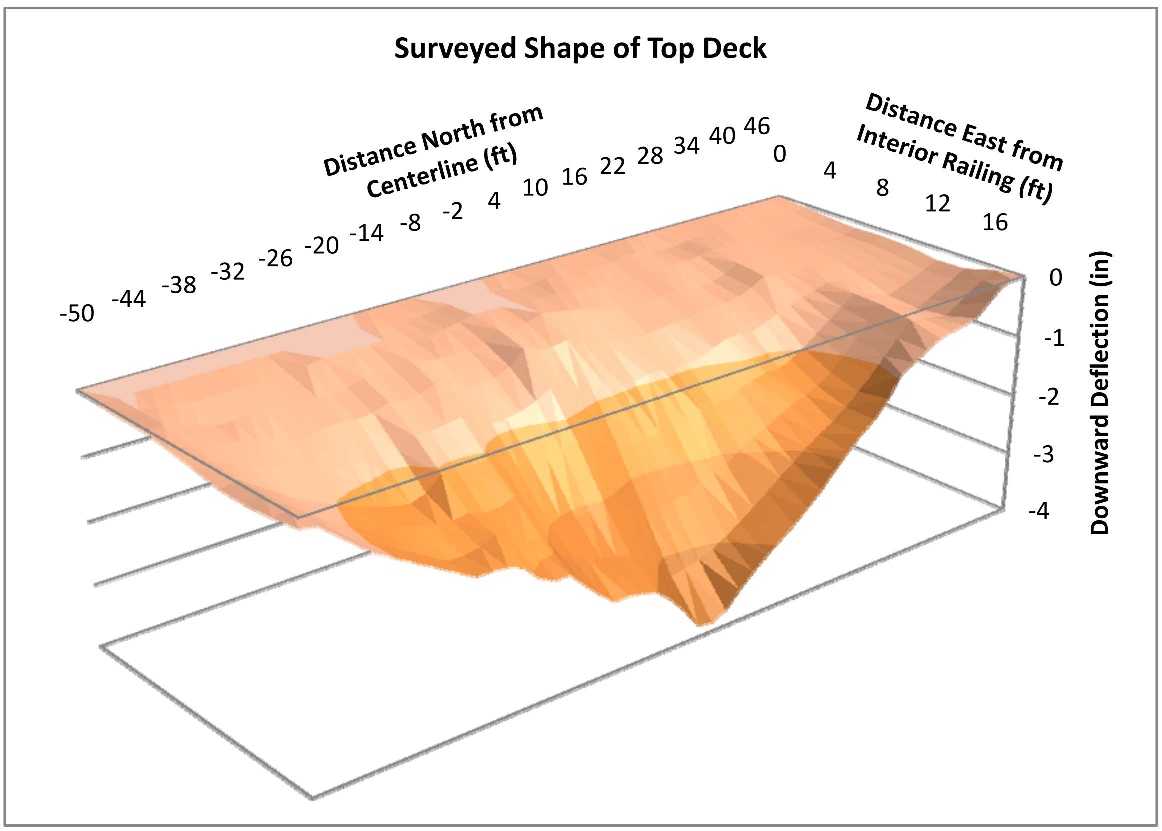

Figure 6-13: 3-D deflected shape of deck surface after Full-Scale Test 2

bridge surface. Transverse cross-sections of the deck width deflected in strongly defined double curvature near the ends of the span. Near the center of the span, however, the deflected shapes of these cross-sections were approximately in single curvature.

6.2.9 Separation of the Interior Top Flange of the Fractured Girder

The permanent metal formwork that spanned between the two girders was directly attached to the interior top flange of the fractured girder. As such, the interface between that flange and the concrete deck to which it was connected was not readily visible from ground level. Without a better perspective on the flange to deck connection, it appeared as if the interface was essentially intact (Figure 6-14a). Deflections measured through surveying, a strip model developed by Samaras (2009), and the non-linear finite element model all suggested the contrary. Upon closer inspection, it became apparent that there was, in fact, wide separation between the top flange of the fractured girder and the concrete deck along a significant length of the bridge (Figure 6-14b and c).

To gain better visual and physical access to the damaged connection between the inside top flange of the fractured girder and the concrete deck, portions of the permanent metal formwork were removed (Figure 6-14d). Deflection between the deck and the girders de-bonded the metal formwork from the concrete, facilitating removal. Pneumatic powered rotary cutting tools were used to remove strips of the metal formwork, starting at the bridge mid-span and moving toward the ends of the span through the region where the deck and fractured girder were separated (Figure 6-15). Once the extent of the separation was uncovered from the metal formwork, the gap was measured directly with a tape measure (Figure 6-16).

A second independent method, based on the data from surveys of the girder bottom flanges and the bridge deck, was used to estimate the separation between the fractured girder and the deck. At each bridge cross-section section where the surveys were taken, the deformed location and shape of the deck was plotted along with the deformed location and shape of the girders (Figure 6-17). At the cross-sections near the mid-span of

Figure 6-14: (a) Ground view showing no clear signs of damage, (b) Deck level view showing deflection, (c) View into metal formwork showing separation, (d) Cutting away the metal formwork

Figure 6-15: Extent of separation of fractured girder apparent after removal of metal formwork

Figure 6-16: Directly measuring the separation between the fractured girder and the deck

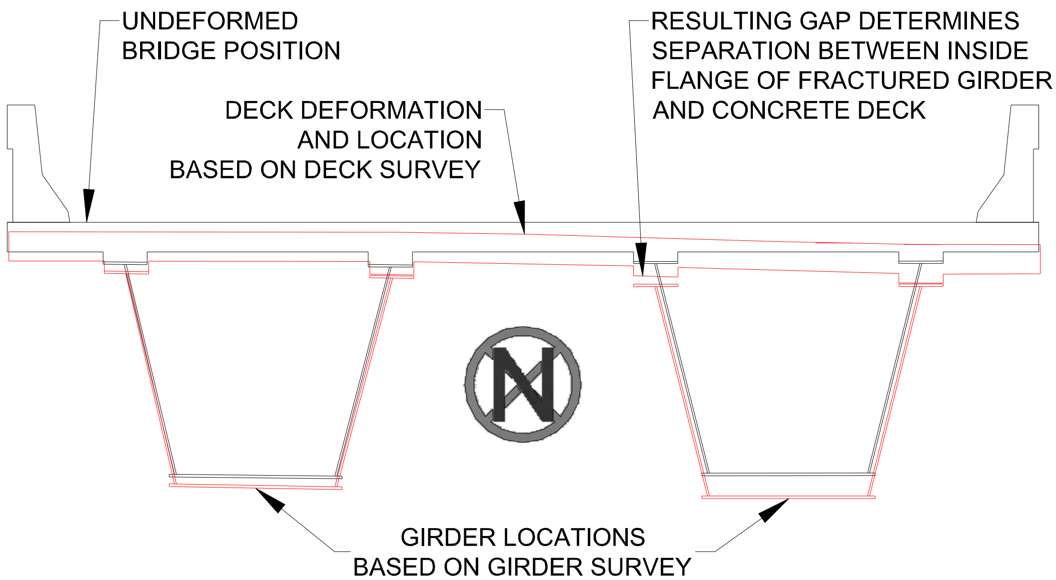

Figure 6-17: Indirect method for estimating fractured girder separation using survey data

the bridge, the deformed positions of the bridge elements identified an unaccounted for gap between the concrete deck and the interior top flange of the fractured girder. This gap directly represented the separation distance between the interior top flange of the fractured girder and the concrete deck.

Direct measurements of the separation distance between the deck and the interior top flange of the fractured girder were compared with the indirect survey analysis and are plotted in Figure 6-18. Data from the two methods were in agreement considering both the extent and the magnitude of damage. The maximum separation between the inside

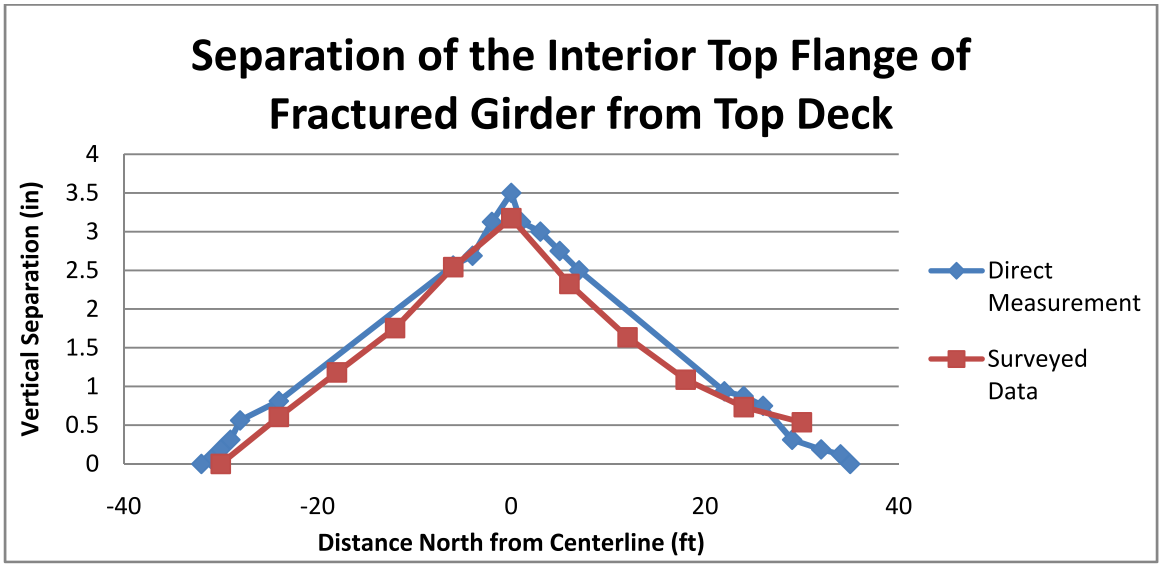

Figure 6-18: Separation of the fractured girder and concrete deck during Full-Scale Test 2

top flange of the fractured girder and the concrete deck occurred at mid-span and was nearly 3.5 in., and the cracks extended more than 30 ft. from the mid-span in each direction, spanning more than half of the total bridge length.

6.2.10 Engagement of the Exterior Railing

As the fractured girder deflected downward, the expansion joint in the exterior railing above the fracture location closed, and the concrete sections on both sides of the expansion joint came into contact with each other (Figure 6-19a). Small fragments of concrete spalled along the height of the expansion joint, and larger pieces broke loose on the top face of the railing, indicating significant force was being transmitted across the joint. Compared to the contact at the mid-span expansion joint, the expansion joints at the 1/4- and 3/4- points along the exterior railing did the opposite, opening up wider than their original separation (Figure 6-19b). This pattern is consistent with the deflected shape of the fractured girder and concrete deck. Because the two halves of the fractured girder curved downward from the abutments toward the mid-span, tension would occur on the top face where the expansion joints at the 1/4 and 3/4 point were located.

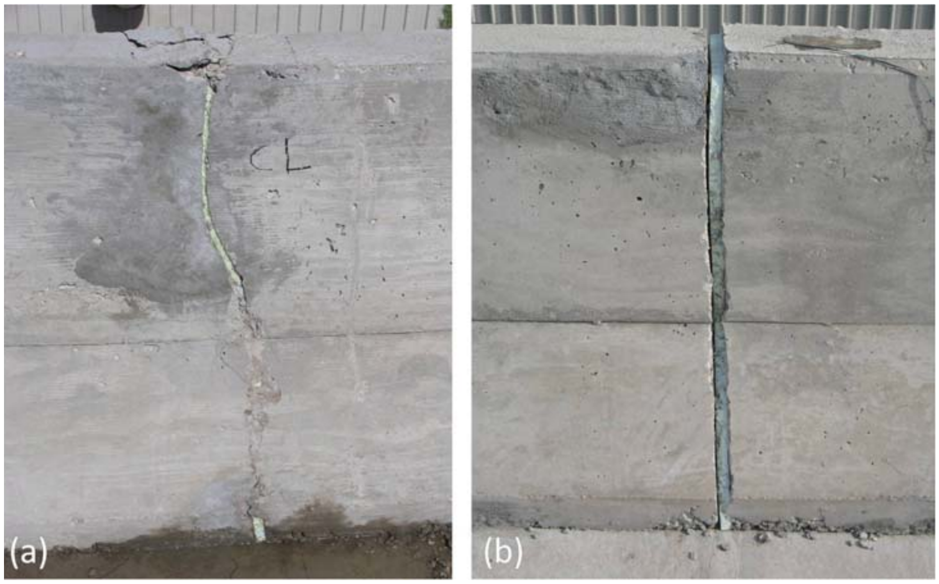

Figure 6-19: (a) Contact at the central expansion joint above the fractured girder,

(b) Slight opening of the N3 expansion joint above the fractured girder

6.2.11 Unzipping of the Interior Top Flange of the Fractured Girder

Preliminary analyses of the test-bridge theorized that downward deflection of the fractured girder would result in double curvature bending of the deck across its width between the two girders (Figure 6-20). This deformed shape was dependent upon a downward force transmitted to the deck through tension in the shear stud connections on the interior top flange of the fractured girder. If the tensile capacity of this section was reached and a brittle failure occurred, this downward force on the deck would be lost and the deformed shape of deck at that location would change to approximately single curvature bending.

If an individual cross-section were in the assumed deformed shape with all of its shear stud connections intact, the portion of deck above the interior flange of the fractured girder would be curved upward. This upward curvature would result, in part, due to the downward force applied by the tension in the shear stud connection at the interior top flange of the fractured girder. In this configuration, the top fiber of the concrete deck above the interior flange of the fractured girder would be in compression. If the tensile

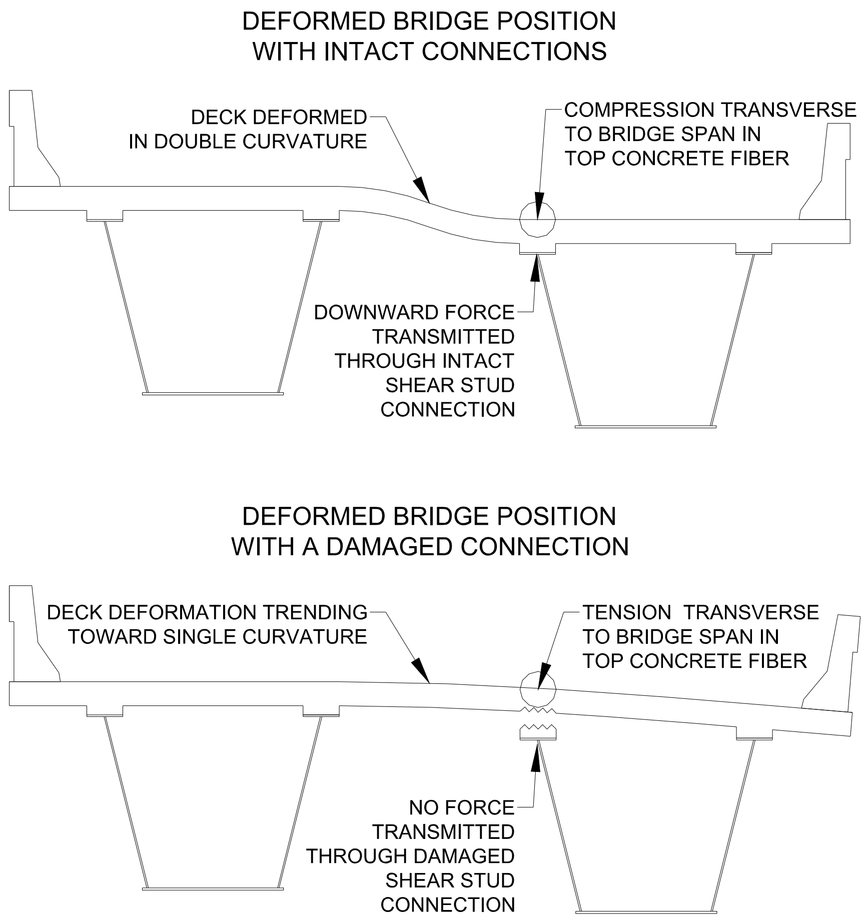

Figure 6-20: Deformed shape of bridge before (top) and after (bottom) shear stud connection damage

load through the shear studs reached capacity, there would be a brittle failure of the connection. The downward force on the deck at the location of the ruptured connection would be suddenly lost, and the deformed shape of the cross-section would be affected instantaneously. Without the downward force applied to the concrete deck by the shear stud connection, the portion of the deck immediately above the damaged connection would trend more toward downward curvature. In this configuration, the stress state in the top fiber of the concrete deck above the interior flange of the fractured girder would trend more toward tension.

The strain readings taken on the deck surface transverse to the bridge span above the interior top flange of the fractured girder provide evidence of the behavior described above. Figure 6-21 shows these strain readings during the first 0.6 seconds following the release of the scissor-jacks. The blue lines plot strain transverse to the concrete deck above the interior top flange of the fractured girder at the N1 and S1 sections, 6 ft. away from the mid-span fracture location. The red lines plot similar values for the N1.5 and S1.5 gages, 12 ft. from the fracture location. The green lines represent readings taken at the N2 and S2 sections, 18 ft. from the mid-span, and the purple lines are data from the gages at N3 and S3, 30 ft. from the fracture.

In a very short amount of time following the release of the scissor-jacks, the readings from the gages 6 ft., 12 ft., and 18 ft. away from the fracture underwent abrupt reversals in rate of change of strain. These strain readings were rapidly becoming increasingly compressive until a defined point at which the compressive strains quickly relaxed. Despite the punctuated slope change, these strain measurements did not completely reverse to indicate tensile strains in the top fiber of the concrete section above the damaged shear stud connections.

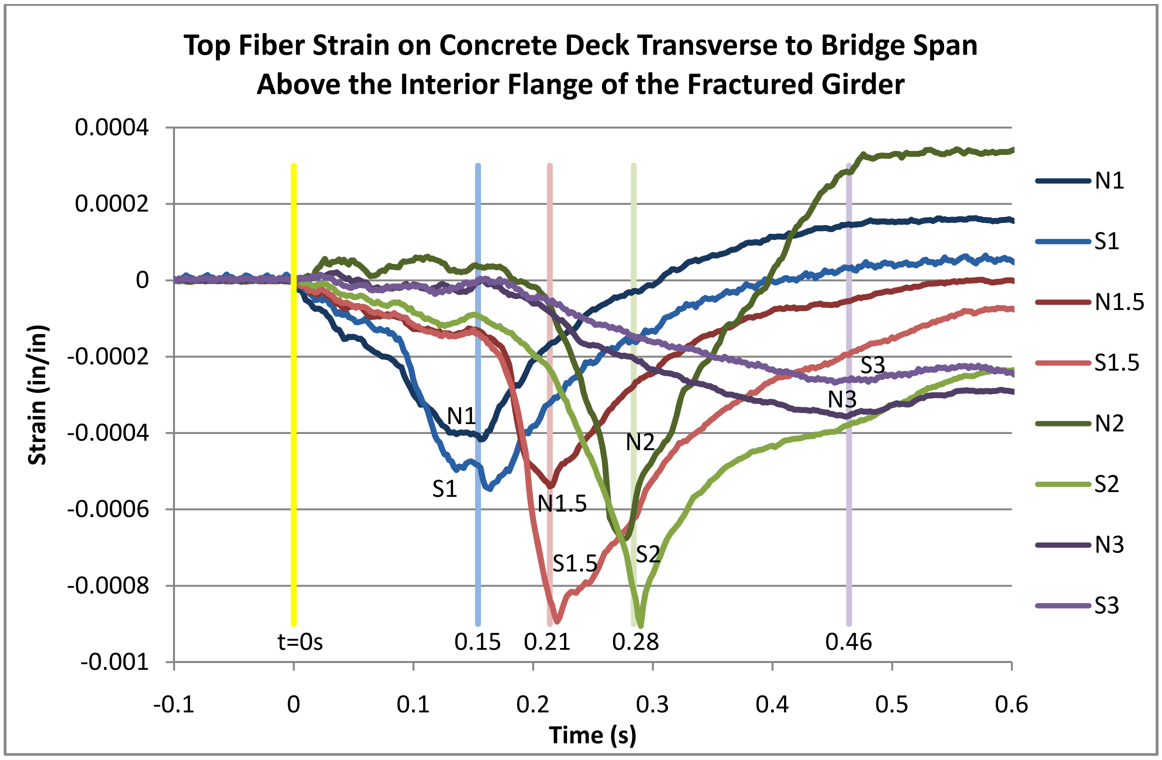

Figure 6-21: Strain reversals transverse to bridge span above interior flange of fractured girder

This model does not account for inertial effects of the dynamically responding bridge, which may have influenced details of this behavior. Still, the demonstrated trend in the axial strains of these concrete fibers was consistent with a change in deck curvature resulting from the loss of the shear stud connection at the interior top flange of the fractured girder. Furthermore, the reversals in strain rate occurred in time symmetrically about the mid-span of the bridge, and occurred in sequence starting near the fracture location and moving toward the ends of the bridge. The strain readings at the N3 and S3 sections, 30 ft. from the fracture location did not undergo similarly abrupt reversals.

The pattern of strain rate reversals illustrated in Figure 6-21 implies that, when the bridge was dynamically responding in its fractured state, the shear stud connections along the interior top flange of the fractured girder failed in sequence beginning at the fracture location and moving outward. This progressive “unzipping” of the girder from the deck continued past the gage locations 18 ft. from mid-span, but was arrested before reaching the gage locations 30 ft. from mid-span. The range of the unzipping process as indicated by the strain measurements is consistent with the measurements taken of the separation between the interior top flange of the fractured girder and the deck (Figure 6-18).

Figure 6-22 shows the compressive strain in the top fiber of the exterior concrete railing in the direction longitudinal to the bridge span for the first 0.6 seconds following the release of the scissor-jacks. Shortly after the scissor-jacks were released, the concrete railing began to experience compression, indicating that the expansion joint at mid-span had closed and force was being transmitted between the two adjacent portions of the railing. Approximately 0.33 seconds after the scissor-jacks were released, the strain in the concrete railing reached a peak compressive value and began to decline. This peak compressive strain corresponded closely to the time at which downward deflection of the fractured girder during its first oscillation reached its peak, 0.31 seconds after the jacks were released (Figure 6-5).

Relating the time sequence of the aforementioned events highlights an important aspect of the bridge behavior during Full-Scale Test 2. 0.28 seconds after the jacks were

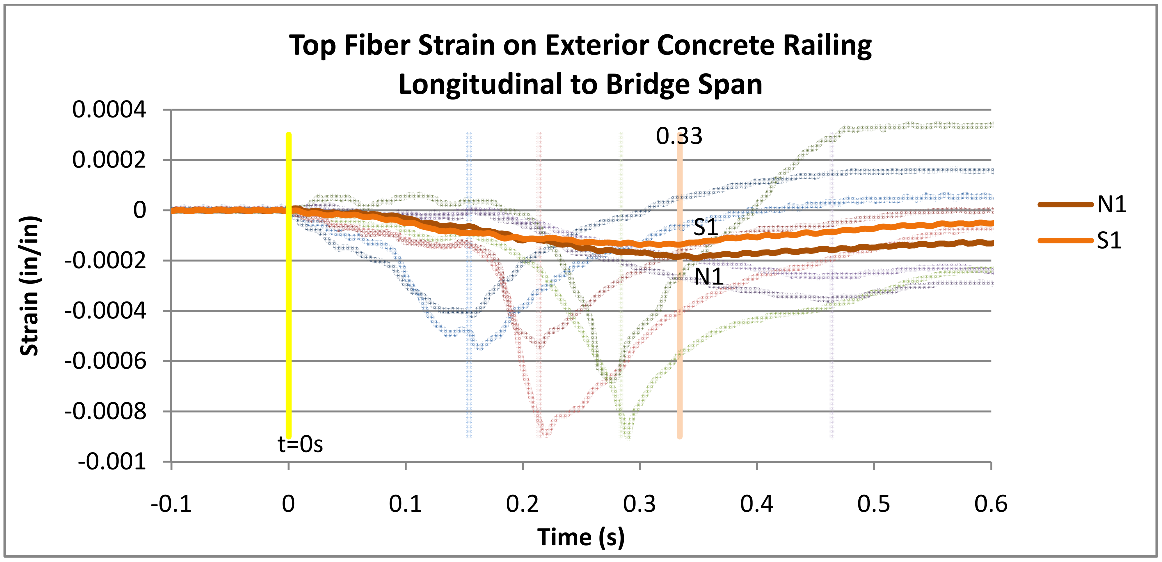

Figure 6-22: Peak compressive strain in concrete railing

released, the bridge was deflecting downward and strain readings in the concrete deck indicated that the shear stud connections at the N2 and S2 sections were damaged. Less than 1/20 of a second later, the dynamic displacement of the girder reached its peak (0.31 seconds after the jacks were released), and the compressive streak in the concrete railing reached its peak (0.33 seconds after the jacks were released). Peak compressive strains in the deck at the N3 and S3 sections occurred 0.46 seconds after the scissor jacks were released, but did not exhibit the abrupt reversals that had indicated earlier damage at sections closer to the mid-span of the bridge. This sequence suggests that, as the fractured girder deflected downward, the unzipping pattern continued outward from the fracture location until the concrete railing arrested downward deflection, limiting the extent to which further tensile failures occurred in the shear stud connections.

6.2.12 Other Bridge Components

The remaining components of the test-bridge showed no signs of damage or distress. The intact girder did not yield at any location: peak dynamic tensile strains in the bottom flange at the N1 and S1 sections 6 ft. from the mid-span reached 0.0011 in/in, which is approximately 53% of the static yield strain. If the effect of dynamic loading rates on material strength were considered, the measured strain in the bottom flange of the intact

Figure 6-23: Undamaged connection to the exterior top flange of the intact girder and interior railing

girder would be an even smaller percentage of the yield strain. The end diaphragms connecting the two girders were not visually distressed, and peak strains in these components were measured at 0.00036, which is less than 20% of the static yield strain. Observationally, the connections between the top flanges of the intact girder and the concrete deck remained intact (Figure 6-23). No significant changes were observed at the expansion joints along the interior railing above the intact girder.

6.3 INSTRUMENTATION PERFORMANCE

Overall, the instrumentation and the data-acquisition system performed well during Full-Scale Test 2. Data were recorded throughout the duration of the experiment, starting with all of the preparatory steps and proceeding through the dynamic response of the bridge following the detonation of the tension-ties on the scissor-jacks. The high-speed data-acquisition equipment produced clear and closely spaced data, allowing for the analysis of short increments of time on the order of hundredths of a second, as was demonstrated in Section 6.2.10.

In the case of the gages attached to the concrete deck, data were effectively collected, though not all of it can be considered numerically accurate. Observations of the cracking pattern on the deck show that, in a number of locations, cracks passed directly underneath strain gages. For these gages, the strain values recorded can provide qualitative data, but their reliability in a quantitative sense is not comparable to those gages that were not directly affected by cracks.

Repeating one of the lessons learned during Full-Scale Test 1, one channel of instrumentation was damaged as a result of the detonation of the explosives that disabled the scissor-jacks. The blast impulse destroyed the connection between the string potentiometer on the bottom flange of the fractured girder at the fracture location and the concrete deck immediately below. The string that was torn passed through the immediate vicinity of both explosives. The difficulty of protecting equipment in this zone would likely prevent reasonable data-acquisition of any kind.

6.4 SUMMARY

Full-Scale Test 2 was executed, successfully loading the test-bridge after it sustained a full-depth fracture in one of its girders. The residual static downward deflection of the fractured girder was as much as 7 in. in locations, and the bridge sustained significant damage to the shear stud connections between the top flanges of the fractured girder and the concrete deck. Despite the displacements and damage sustained, the test-bridge unequivocally resisted collapse, maintaining complete serviceability in its fractured state with the design truck load positioned directly above the fracture location.

Components of the theorized redundant load paths were engaged, including the concrete deck, which contributed to load transfer from the fractured girder to the intact girder and the exterior railing, which began to transfer force when the expansion joint at its centerline closed. Because deflections were not large enough to fully engage or cause failure in the components of the redundant load paths, data to quantify the full extent to which they could contribute to resisting more extensive movements and damages than those observed during Full-Scale Test 2 were not acquired. In addition to remaining uncertainty about the contribution of the redundant components, the ultimate capacity of the system had not been reached, nor could it have been identified from the data recorded during the first two full-scale tests. To acquire the necessary data to help complete the broad analysis of fracture critical twin box-girder bridges, another experiment was designed and executed, making use of the test-bridge in its substantially damaged state, and bringing it to failure.

CHAPTER 7

Methods: Full-Scale Test 3

7.1 INTRODUCTION

During the second full-scale experiment, the test-bridge resisted collapse when loaded with a simulated truck in its fractured state. Because the test-bridge was still capable of supporting additional loads following completion of Full-Scale Test 2, a third full-scale test was planned as a follow-up to extend the results from the dynamic test. The goal was to observe the sequence of failure mechanisms and to determine the ultimate load required to induce a total collapse of the bridge. The experimental procedure for Full-Scale Test 3 was designed as a load-controlled test, where additional load in excess of the design truck load was applied incrementally and without significant dynamic effects. While the process would not allow for unloading as damage was incurred, it would allow for gradual observation of the failure sequence as load was slowly added.

7.2 TEST PREPARATION

The five concrete girders used in the previous full-scale tests to simulate the design truck load were rearranged with a sixth additional girder to form a rectangular bin on the bridge deck weighing a total of 82,100 lbs. (Figure 7-1). The open rectangle was designed as a receptacle for the incremental load so that it could be accurately placed and analyzed. The bin was shaped by pairing the four 20-ft. long pre-stressed girders as the bin edges along the length of the bridge and by using the two 8-ft. long concrete blocks as the ends of the bin spanning in the transverse direction of the bridge. The rectangle was centered longitudinally about the mid-span to maximize the overall bending moment on the fractured girder. Transversely, the bin was placed 2 ft. from the railing above the fractured girder, biasing the loading effects toward the damaged portion of the bridge while still allowing physical and visual access to the exterior railing and matching the

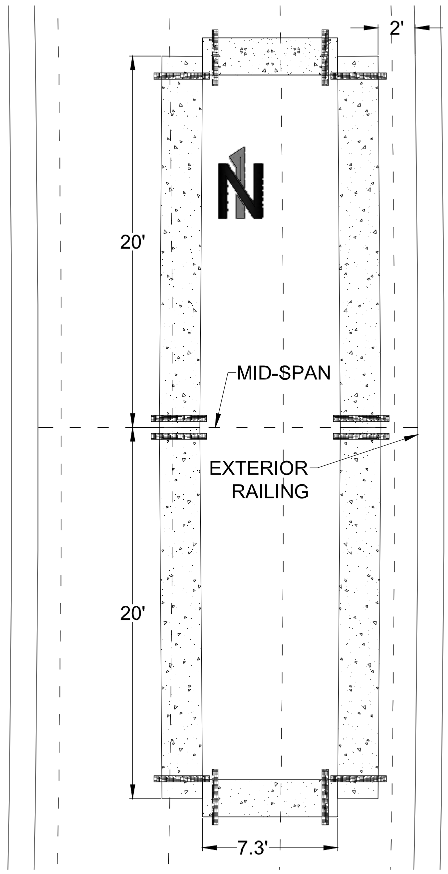

Figure 7-1 (left): Bin location

Figure 7-2 (right): Placing the bin on the bridge deck

AASHTO design recommendations of placing the design loads 2 ft. from the outside edge of the bridge.

Arranging the concrete girders into the bin required a small number of workers to be on the test-bridge deck to unhook each beam from the crane as they were hoisted into position (Figure 7-2). Loading the bridge in its damaged state presented a potential hazard to the people on the deck because the failure load of the bridge was not known precisely. Consideration of this hazard was especially critical, because an additional sixth girder was being used to complete the bin, increasing the total live load applied to the bridge relative to the previous test by more than 6 kips. Because of the geometry of the bin, however, flexural demand on the bridge, particularly at the damaged sections, did not exceed that from the second test. Longitudinally, the load from the bin was more biased toward the ends of the bridge span relative to the live-load placement in Full-Scale Test 2, reducing the total internal bending moment. The placement of the bin had a similar effect transversely, as a significant portion of the weight was laid toward the intact girder and was expected to be transferred there. Still, extra precaution was taken during bin placement. Once each girder was positioned and held a few inches above its final placement location, the crew on top of the bridge moved toward the end of the span. They remained there until the load was completely transferred from the crane to the deck with no apparent damage incurred by the bridge. After achieving this condition, the workers on the bridge deck would unhook the girders from the crane.

7.3 TEST PROCEDURE

After placing the concrete girders on the bridge deck, additional load was applied by incrementally dumping material into and eventually around the bin. Road base was chosen as the loading material for its ease of acquisition, low cost, and relatively high density. The material, mostly gravel and dirt, was delivered in 12-cubic-yard truckloads, and was stored within a holding area bounded on three sides by concrete blocks. This containment area helped keep the work site organized and allowed a front-end loader to efficiently take from and manage the large volume of road base. The front-end loader was used to fill a 1-cubic-yard concrete lift bucket, which was hung from a truck-mounted crane (Figure 7-3). The bucket was then lifted into place just above the bridge, and the contents were dropped onto the deck (Figure 7-4). As the loading process repeated, the weight increments were placed approximately symmetrically about the mid-span, biased toward the damaged girder.

7.3.1 Special Equipment

Obtaining a lifted weight measurement for each crane pass, from the placement of the concrete girders through the placement of each bucket of the road base, was critical. To measure the weights quickly and easily, a load-cell was attached to the crane load line above the lift bucket. A wireless transmitter was connected to the load cell so that the load data could be easily read and recorded from across the work-site (Figure 7-5). A

Figure 7-3: The front-end loader dumping road base into the crane-mounted lift bucket

Figure 7-4: The loaded lift-bucket in place above the bin ready to be emptied onto the bridge deck

Figure 7-5: Remote load cell monitoring setup

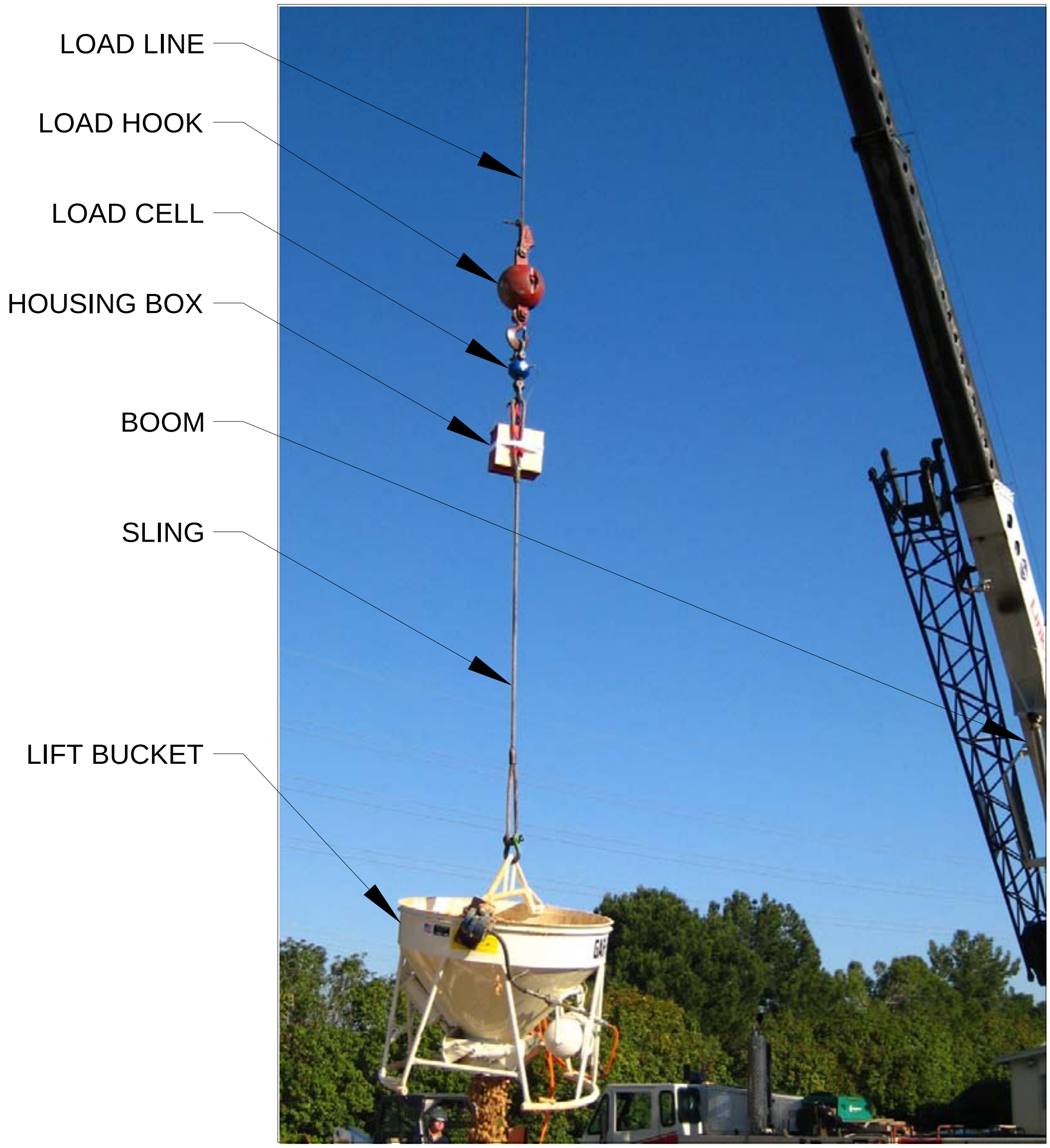

Figure 7-6: The load line setup with labeled components

small wooden box was built to house the wireless transmitter and its power supply, which was hung on the crane near the load cell. Lastly, a steel sling was connected between the load cell and the lift bucket to provide sufficient clearance so that the road-base being dumped into the bucket would not damage the load cell or associated equipment. A photograph labeling the lifting setup is shown in Figure 7-6.

To ensure a safe testing procedure, it was important to implement a loading method that did not require any personnel to be on the bridge deck. To achieve such an arrangement, an air-operated lift bucket was acquired from GAR-BRO Manufacturing (Figure 7-7). The system operated with a piston controlling the discharge position, supported by an onboard reserve air tank. The setup required the air supply to be connected through a custom operating valve to a built-in system on the bucket. The valve directly controlled the discharge position on the lift bucket so that it could be operated from a distance away from the bridge (Figure 7-8).

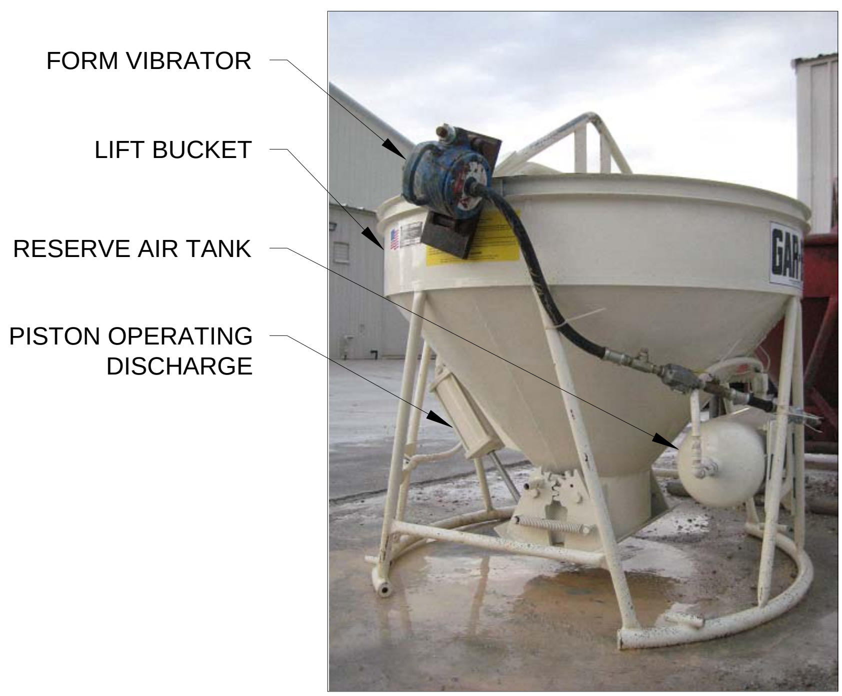

Figure 7-7: The air-operated lift bucket and attached form vibrator

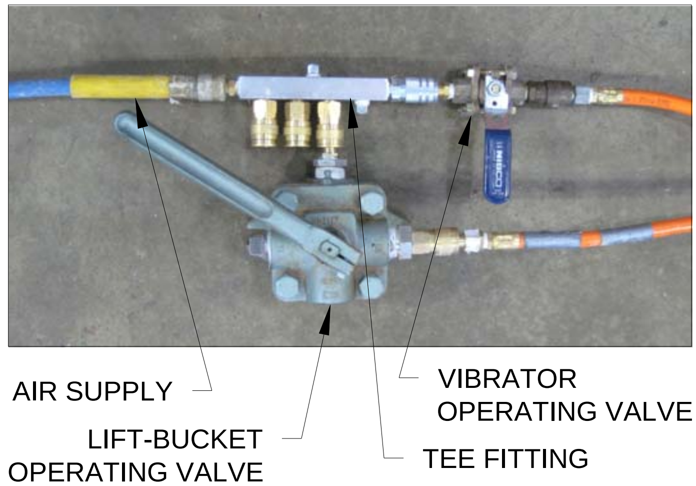

Figure 7-8: Operating controls for lift bucket and form vibrator

Once the lift bucket was acquired, preliminary tests were performed to assess the ability of the bucket to discharge the road base (Figure 7-9). Because the road base did not flow as easily as concrete typically would, the contents of the bucket would not always completely empty without assistance. To improve control of the dumping procedure, a vibrator designed for concrete forms was welded to a plate that was then bolted to the

Figure 7-9: Testing the lift bucket discharge

outside rim of the concrete bucket (Figure 7-7). The vibrator was also air operated, so a tee fitting was used to split the air source, and a second valve to toggle the vibrator power was connected right beside the operating valve for the bucket discharge (Figure 7-8).

7.3.2 Labor

A man-lift was situated next to the bridge to allow researchers to see the deck from above during testing (Figure 7-10). One person in the man-lift signaled the crane operator to help position the lift bucket and a second person in the man-lift operated the valves for the lift bucket and attached vibrator. A helper on the ground ensured that the hoses connecting the air supply, the pendant on the man-lift, and the moving lift bucket were safe. Other personnel on the ground assisted the front-end loader and crane operators.

It was critical that the load readings from the wireless system be integrated with the data set being recorded by the full data-acquisition system at the appropriate time, even though the systems were set up in different locations. Integrating the data required active

Figure 7-10: The man-lift, the crane boom carrying the lift-bucket, and the air hoses connecting the equipment

communication among the person operating the wireless system, the person operating the larger data-acquisition system, and a third person observing the activities on the bridge, who specifically reported on the time when the load was transferred from the lift bucket onto the deck.

Overall, the procedure required up to ten total workers with responsibilities ranging from operating heavy machinery to monitoring and recording critical data points. To protect the workers, all of the major equipment and duties were set up on the intact side of the bridge. The testing space was compact, therefore requiring constant communication and coordination among the required tasks to maintain a safe and efficient testing environment. A full site plan indicating all major testing features is shown in Figure 7-11.

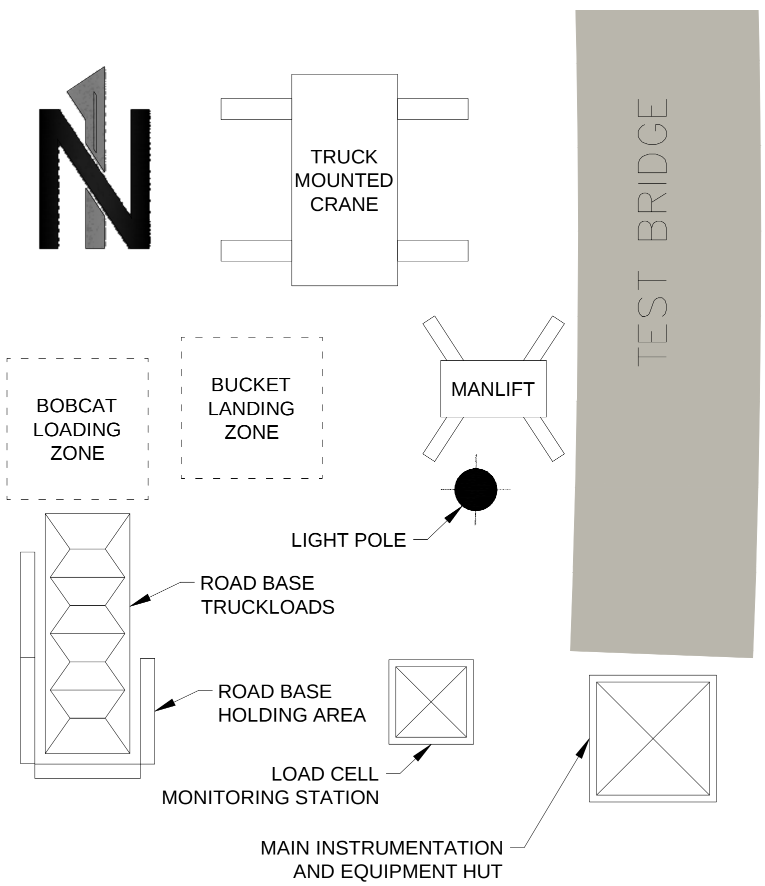

Figure 7-11: Work site plan view

7.4 INSTRUMENTATION AND DATA-ACQUISITION

As with Full-Scale Test 2, the instrumentation on the test-bridge was repaired and expanded upon for the third full-scale test. Similarly to the changes implemented in preparation for the second test, these modifications were made to improve the continuity of the deflection measurements and to collect data representing the participatory behavior of a larger percentage of the bridge elements maintaining equilibrium, as compared to previous tests. These improvements were made by adding gages, using a more balanced variety of gages, and instrumenting more cross-sections of the bridge than had previously been monitored (Figure 7-12).

7.4.1 Girder Instrumentation

The steel girder gage layout at individual cross-sections did not change from the second test: rosette gages were still used at the mid-points of the bottom flange and webs of the intact girder, and uni-axial gages remained at the mid-width of the bottom flange of the fractured girder. The number of cross-sections instrumented, however, was expanded. For the third test, two additional cross-sections were covered, again spaced at 12 ft. relative to the other cross-sections that had been instrumented. In total, eight cross-sections of steel were identically instrumented, including S4, S3, S2, S1, N1, N2, N3, and N4, spanning the central 84 ft. of the girders. The full cross-sectional layout is detailed in Figure 2-17.

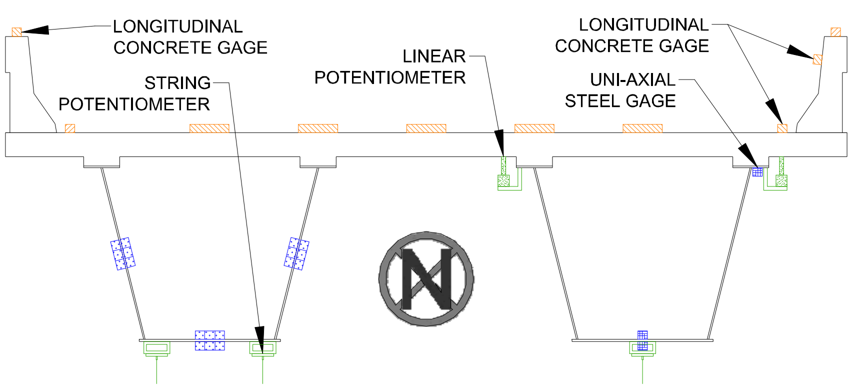

Figure 7-12: Instrumentation of the bridge elements for Full-scale Test 3 at a typical cross-section

Figure 7-13: Steel gage on the outside flange of the fractured girder

It was hypothesized that, in the case where the concrete railing above the fractured girder acted flexurally to help support the loaded bridge deck, the outside top flange of the fractured girder could provide a tensile contribution to the composite beam. To help observe this behavior, the underside of the flange was instrumented with uni-axial steel gages oriented longitudinally to the bridge span (Figure 7-13). These gages were placed at the S1, CL, and N1 cross-sections.

7.4.2 Deck Instrumentation

The gages on top of the concrete deck and rails had been directly exposed to severe weather in the months between the second and third full-scale tests. When preparing for the instrumentation plan update, a large portion of the concrete gages were found to be non-functional and required replacement.

Similarly to the changes made on the steel girders, the philosophy behind the positioning of the concrete gages did not change as significantly as did the extent of their placement (Figure 7-14). On the deck, repetitively patterned gages oriented transversely to the bridge span were included at all cross-sections spanning between S4 and N4, covering in total the central 84 ft. of the bridge. The number of longitudinally oriented concrete gages used was also significantly increased. The majority of the longitudinal gages in this new arrangement were spaced across the width of the deck at the mid-points above the girders and between them, and along the length of the bridge at the S3, S2, S1, N1, N2, and N3

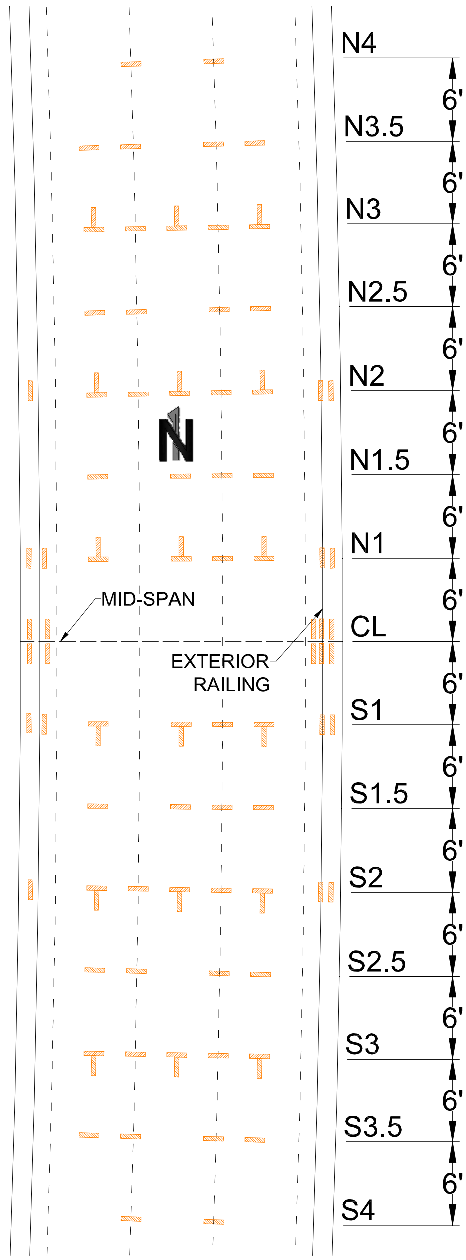

Figure 7-14: Plan view of the surface concrete gages for the third test

cross-sections. A few select longitudinal gages on the deck surface were concentrated at mid-span near the railings to help identify the onset of compressive crushing at these critical sections.

Instrumentation of the concrete railings for the third test was also expanded as compared to the previous test. Data was sought to help quantify the strain profile of the exterior railing above the fractured girder, the change in its stress state moving farther away from the contact point at the central expansion joint, and the transfer of these forces into the composite deck. Gages were added on the inside face of the exterior railing at cross-sections just north and south of the expansion joint at mid-span and at the S2, S1, N1, and N2 cross-sections. On the cross-sections just north and south the centerline, two side-face gages were placed 6 in. and 12 in. below the top edge of the railing (Figure 7-15). Farther from mid-span, at S2, S1, N1, and N2, one side-face gage was placed at mid-height of the railing at each cross-section. Gages were also added to the top face of the railing above the intact girder on identical cross-sections to help estimate its contribution to the redundant load path in the event of a closure of one of its expansion joints.

Figure 7-15: Instrumentation of the railing just north of the centerline expansion joint

7.4.3 Direct Measurements and Observations

A significant number of linear potentiometers and string potentiometers were added to the instrumentation setup for Full-Scale Test 3. Because of the de-bonding of the permanent metal-formwork on the underside of the deck between the two girders, it was possible to cut windows into the sheet metal and add linear potentiometers to measure the changes in separation between the inside top flange of the fractured girder and the concrete deck (Figure 7-16). Nine linear potentiometers were installed along the inside flange of the fractured girder, at the S4, S3, S2, S1, CL, N1, N2, N3, and N4 cross-sections. On the outside flange, the seven linear potentiometer locations from the second full-scale test were unchanged. Two other linear potentiometers were added at S3 and N3, crossing the expansion joints in the railing above the fractured girder to measure the change in width of the expansion joint as the bridge deflected (Figure 7-17).

An extensive array of string potentiometers were connected between the bottom flanges of the girders and the concrete deck below (Figure 7-18). The safety of surveying the bottom flanges of the girders was uncertain once loading began; the measurements provided by the string potentiometers would provide a means for monitoring the overall

Figure 7-16 (left): Linear potentiometer installed between the inside top flange of the fractured girder and the underside of the concrete deck

Figure 7-17 (right): Linear potentiometer across an expansion joint in the exterior railing

Figure 7-18: A pair of linear potentiometers at the edges of the intact girder bottom flange

deflection of the girders as the testing proceeded. Measurements were taken at both edges of the bottom flange of the intact girder to capture linear translation and twisting of the girder. On the fractured girder, one transverse location was instrumented at mid-width of the bottom flange, capturing only average translation. These string potentiometers were positioned at five cross-sections, including S3, S2, CL, N2, and N3, which in total spanned the central 60 ft. of the span.

Throughout the testing process, video and photographs were captured from various positions at ground level and from the man-lift. To record the extent of concrete cracking on the deck and on the railings, marking paint was used to trace visible cracks. This method was less time consuming than using permanent markers, provided a sufficiently accurate qualitative view of the cracking, and the results could be captured clearly in photographs.

7.4.4 Data-acquisition

Because the load increments were placed at approximately ten-minute intervals, high-speed recording was not required for Full-Scale Test 3, and a standard-speed data-acquisition system was used to capture data from a total of 306 instrumentation channels (Tables 7-1 and B-5). During testing, the data were recorded at three-second intervals, and critical measurements were closely observed to help anticipate material failures of bridge components that would lead to a loss of load carrying capacity of the bridge.

The significant expansion of the instrumentation plan exceeded the capacity of any one data-acquisition system owned by FSEL. To accommodate all 306 desired readings, the 244-channel National Instruments system used for Full-Scale Test 2 was set up concurrently with an Agilent Systems scanner and custom-built equipment to take data readings during Full-Scale Test 3. An Agilent Systems 70-channel 34980a scanning voltmeter hooked directly into the USB card of the PC. A custom-built 8-connector scanner interface was attached between the scanning voltmeter and eight custom-built pods. Six of the pods housed eight instrumentation channels, while the remaining two

Table 7-1: Instrumentation count for Full-Scale Test 3

Gage Type	# of Gages / Channels	
Reinforcing Bar	21	21
Shear Stud	8	8
Girder (Uni-axial)	22	22
Girder (Rosette)	36	108
End Diaphragm (Rosette)	4	12
Top Deck (Transverse)	56	56
Top Deck (Longitudinal)	24	24
Exterior Railing	14	14
Interior Railing	6	6
Linear Potentiometer	18	18
String Potentiometer	17	17
Total	**226**	**306**

housed seven. An external power supply connected through the scanner interface to dedicated excitation channels in each of the pods.

7.5 CONTINUATION OF THE EXPERIMENT

The experiment proceeded with the repetition of the loading procedure once the researchers were confident that the test-bridge could sustain additional load without collapsing. Because the failure load and precise failure mode were unknown (i.e., unzipping of shear studs, plastic hinging of the concrete deck, crushing of the bridge railing), it was important to prepare the site for a number of conditions that could have resulted from the loading procedure. Concrete blocks were arranged in a bed beneath the fractured girder, leaving approximately 4.5 ft. of vertical distance between the bottom flange of the fractured girder and the top of the cribbing that sat on the concrete blocks (Figure 7-19). The bridge was to be declared collapsed and failed once a load was reached that caused deflection substantial enough to rest the fractured girder on the cribbing bed below.

Figure 7-19: The bridge ready for testing with the bin loaded on top and the concrete bed below

7.6 SUMMARY

Full-Scale Test 3 was designed to load the test-bridge statically in its significantly damaged state until it collapsed. Preparations for the test required acquiring the equipment and organizing the labor necessary to carry out a safe and efficient loading procedure. Remote weight readings of each loading increment were recorded, and 308 channels of instrumentation were prepared to gather data on the behavior of the bridge and its failure sequence as the loading continued. The results of the collapse load test are presented in the following chapter.

CHAPTER 8

Results: Full-Scale Test 3

8.1 INTRODUCTION

Full-Scale Test 3 was performed over the course of two weeks in March 2009. The concrete blocks were placed on the bridge deck to form the containment bin on March 11, and the additional load increments were placed over the course of three days on March 16, 23, and 24. The incremental loading process was successfully implemented and was repeated 104 times before the bridge lost capacity and came to rest on the bed of concrete blocks that had been positioned underneath (Figure 8-1). Including the concrete girders used to form the bin, the total load applied to the bridge before its collapse was 363,300 lbs, which is more than four times greater than the legal truck load of 80 kips. A complicated sequence of failure mechanisms was observed, and various bridge elements participated in demonstrating significant redundant capacity of the system as a whole. Once again, extensive and meaningful data were recorded by the strain-reading equipment and the various direct displacement measurement methods.

Figure 8-1: FSEL test-bridge after Full-Scale Test 3

8.2 TEST RESULTS

The various components used to realize the loading process and the different tasks required to execute the experiment combined to carry out a safe, effective, and efficient loading sequence. The loading sequence was repeated on average every 10 minutes, but in certain instances, a single cycle was completed in as short a time as five minutes. The front-end loader was able to fill the 1-cubic-yard lift bucket in three to four dumps. The wireless load readings were taken reliably and quickly, except for a few cases when the loading process was paused for the equipment to be reset. Communication between the crane operator and personnel on the man-lift was clear, providing for the bucket contents to be positioned at or very near to the desired location. Additionally, the two-valve setup controlling the air-operated lift bucket discharge and the attached vibrator allowed for excellent control over the release of the road base. Finally, personnel on the ground level were effective at guarding equipment, recording data, and providing general assistance.

8.2.1 Estimation of the Collapse Load

Including efforts to position the bin on the bridge deck, the loading process from initiation to failure took four working days. A summary of the loading steps is shown in Table 8-1. The ultimate load lifted and placed on the bridge deck was 363,300 lbs, which is more than four times the 76,000 lb. truck load applied during Full-Scale Tests 1 and 2. Considering that the bridge held this load despite having already suffered damage in the form of a full-depth fracture and stud pullout from the previous tests, the fact that it carried so much load clearly illustrates, at least for this particular bridge, that sufficient capacity exists to question whether or not the bridge is truly fracture critical.

Table 8-1: Loading Steps for Full-Scale Test 3

Date	Activity	Load Added (kips)	Total Load (kips)
March 11, 2009	Placing the bin	82.1	82.1
March 16, 2009	Loading road base	152.4	234.5
March 23, 2009	Loading road base	105.9	340.4
March 24, 2009	Loading road base	22.9	**363.3**

After a substantial number of loading cycles, the road base filled the bin on the bridge deck to its approximately 40-cubic-yard capacity. Though the bin was initially designed to help contain the road base and simplify analyses, the bridge had not yet reached its capacity by time the bin was filled, and it was important to continue loading until collapse. After the bin had been filled, the road base was placed directly on top of the bin, creating a pile that could grow as large as the natural angle of repose of the material would allow (Figure 8-2). When the road base could no longer be placed on top of the bin, it was carefully dumped in the area between the bin and the exterior railing (Figure 8-3). Placement at this location required extra precision so that a minimal amount of material was lost off the edge of the bridge, which would have affected the accuracy of the weight measurements taken at the start of the loading cycles. Before the total area between the bin and the exterior railing was exhausted, the bridge collapsed.

To calculate the total internal bending moment developed within the deck and intact girder at the point of collapse, the total load and the placement of that load had to be

Figure 8-2: View of the applied load from the man-lift when the bin was filled to capacity

Figure 8-3: Filling the area between the exterior railing and the bin with road base

identified. Because the load was placed irregularly in various box and pyramid shapes, it was important to estimate its location and distribution at collapse. Based on measurements of the road base pile, typical cross-sections of the road base volume were drawn in AutoCAD (Figure 8-4). Observations of the road base behavior during its placement and storage suggested an angle of repose that was approximated 40˚, and this angle was used in estimating the geometry of road base that was piled on top of the bin and spilled to each side. The resulting volumes were divided and simplified, and they were then approximated as distributed or point loads.

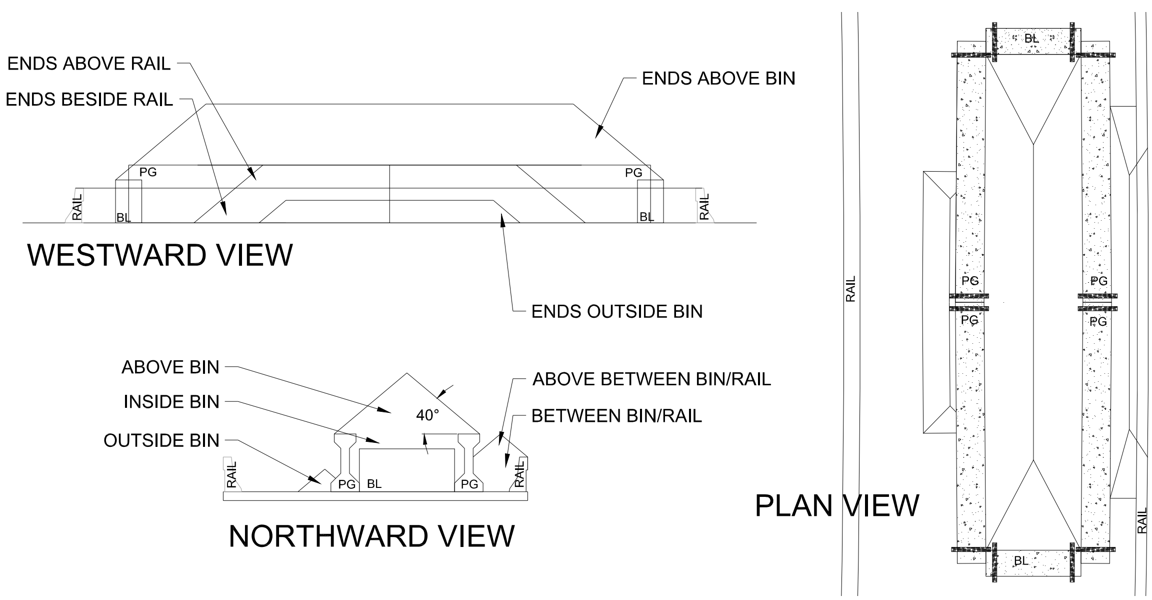

Figure 8-4: Estimating the placement of the road base

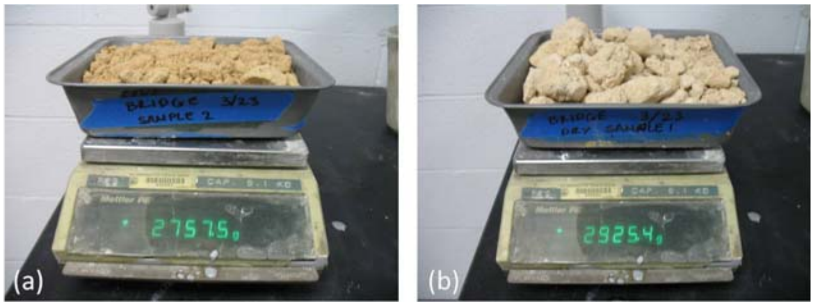

Figure 8-5: Measuring the water content of the road base, showing (a) wet and (b) dry samples

The process of loading the road base took place over the course of more than a week, including some days when it was particularly hot, and other days when it rained. These environmental factors led to uncertainty about the total load on the bridge once the roadbase had been placed. If the water content of the road based changed during the extended experiment, the sum of the measurements taken by the load cell on the crane when each load was lifted would not exactly match the actual load applied to the bridge at failure. To help quantify these effects on the total bridge load, soil samples were taken, and the water content was measured throughout the week leading up to the collapse of the bridge (Figure 8-5). The changing water content of the soil was determined to have had an ultimately small effect on the total applied load, and a final load of 363,300 lbs was determined to be accurate and correct.

8.2.2 Load-Deflection Response

Representative load-deflection plots from the intact and fractured girders are shown in Figure 8-6. The deflection values for the fractured girder were taken at mid-width of the bottom flange at the S2 cross-section, 18 ft. south of mid-span. The values for the curve showing the downward deflection of the intact girder were taken as the average between the deflections measured at both edges of the bottom flange, also at the S2 cross-section. Deflection data from the mid-span of the fractured girder were incomplete: the string potentiometers could not be connected when loading the containment bin because an additional safety block was placed immediately beneath the fractured location, and the stroke of the string potentiometers was exhausted during the days when the road base was

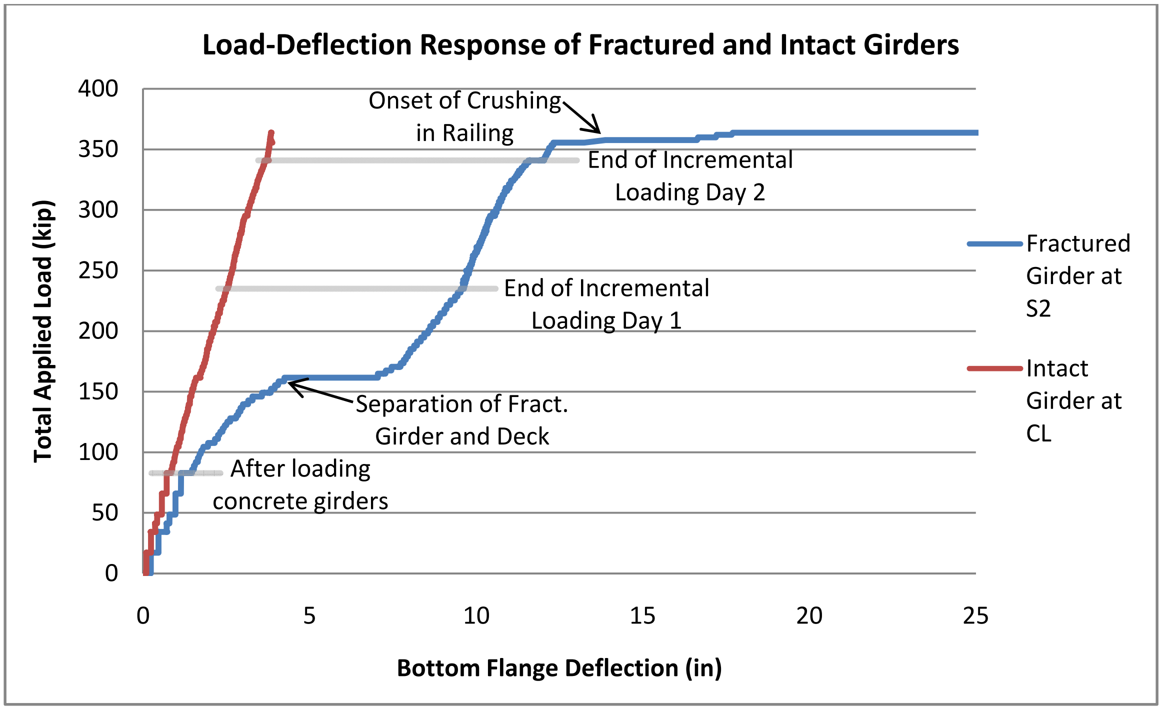

Figure 8-6: Load-deflection response of bridge girders during Full-Scale Test 3

loaded. Without complete mid-span deflection data, deflections from the S2 cross-section were selected as representative samples of bridge behavior only 18 ft. from the mid-span.

The load-deflection response at the S2 cross-section of the fractured girder was relatively linear between punctuated points of large displacement. When the total load reached 161,500 lbs., the fractured girder separated from the deck and displaced without additional load. This event is discussed in more detail in Section 8.2.3.2. The data preceding this distinct separation indicated a softening of the response as the cracks between the exterior flange of the fractured girder and the concrete haunch began to grow. After the separation, the response regained linearity at a stiffness similar to that which it exhibited before the separation. When the total load reached 360,200 lbs., the exterior railing began to crush, initiating collapse of the bridge. This event is discussed in more detail in Section 8.2.4.1. Before the railing failed, the fractured girder maintained a downward displacement of nearly 14 in. at the cross-section 18 ft. south of the fracture location. The load-deflection response of the intact girder is remarkably linear throughout the duration of Full-Scale Test 3. The behavior showed a slightly stiffer response than that of the fractured girder, and only minor deviations from linearity were observed at the load levels that caused rapid downward deflection of the fractured girder. When the exterior railing began to crush, no significant changes in deflection of the intact girder were recorded. At the time of collapse, the average downward deflection of the intact girder 18 ft. south of the centerline was approximately 3.3 in.

8.2.3 Component Failures Preceding Collapse

As the load applied to the bridge increased over the course of the experiment, the bridge components experienced a series of failures. Following these intermediate failures, the bridge was able to redistribute the applied loads, suggesting the contribution of redundant load paths in maintaining equilibrium of the bridge in its progressively damaged state.

8.2.3.1 Propagation of the Fracture on the Exterior Web of the Fractured Girder

When the bin was being positioned on the deck, the fracture on the exterior web of the fractured girder propagated up to the top flange. During Full-Scale Test 2, this specific fracture propagated 1 in. upward from the point where the torch cut was terminated. As the load from the third concrete block used as the southern end of the bin was transferred to the bridge, bringing the total applied load to 40,900 lbs, the remaining height of the exterior web fractured (Figure 8-7a). This event caused a dynamically applied incremental downward deflection of the fractured girder, resulting in some oscillatory movement. The dynamic energy was quickly dissipated, and no further damage resulting from the fracture extension was apparent. At that point in time, the fracture on the inside web of the fractured girder had still not propagated beyond the location where the torch cut was terminated (Figure 8-7b).

8.2.3.2 Separation of the Exterior Top Flange of the Fractured Girder from the Deck

On the first day of loading the road base, the outside top flange of the fractured girder separated from the concrete deck across a substantial central portion of the bridge span. The extent of cracking along the haunch at the exterior flange of the fractured girder grew

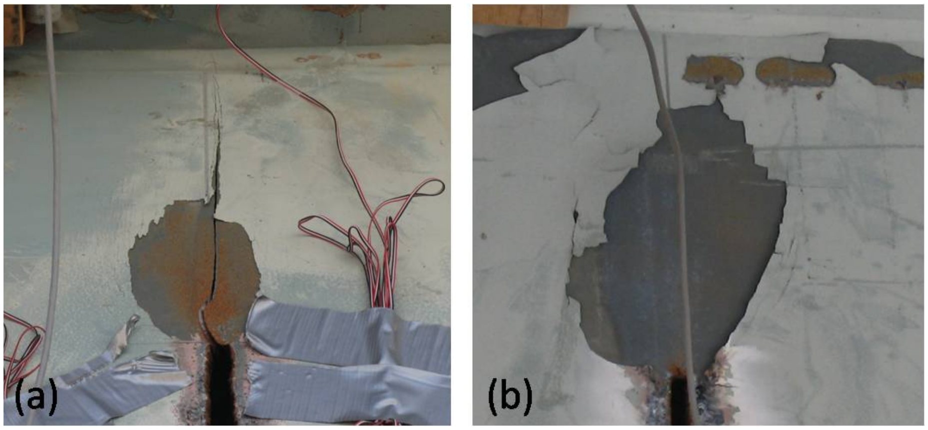

Figure 8-7: (a) Propagation of the fracture on the exterior web of the fractured girder, (b) No change in the fracture on the interior web of the fractured girder

Figure 8-8: Close-up view of the initial separation between the fractured girder and the concrete deck

Figure 8-9: Wide view of the initial separation between the fractured girder and the concrete deck

as the load was incrementally applied, but there was a punctuated separation between the two components when the total applied load reached 161,500 lbs (Figure 8-8). The cracks separating the exterior flange of the fractured girder and the deck extended 20 ft. in both directions from the fracture location, spanning the central 1/3 of the bridge (Figure 8-9).

When the components separated, the fractured girder deflected downward slightly. The concrete deck, conversely, rebounded upward. This response was attributed to the fact that the downward tensile force applied through the shear stud connections from the fractured girder was released, thereby reducing the total load applied to the slab and increasing the total load carried by the fractured girder.

8.2.3.3 Progressive Damage to Other Bridge Components

Through the second full day of loading the road base, the only punctuated failure event that occurred was the separation of the outside flange of the fractured girder from the bridge deck as described above. As the load increased, however, progressive but non-catastrophic damage was observed across a number of the bridge components.

The extent and magnitude of the separation between each of the top flanges on the fractured girder and the concrete deck continued to grow. By the end of the first day of loading, the interior top flange of the fractured girder had unzipped from the deck across essentially the entire span of the bridge (Figure 8-10). The stroke of the linear potentiometers measuring the separation along this flange had been exhausted, as the separation at the centerline had grown to 11 in. (Figure 8-11). A similar increase in separation from the concrete deck was observed along the outside top flange of the fractured girder. The cracks that had initially extended across the central 40 ft. of the bridge span soon grew to cover 60 ft., equivalent to the middle half of the bridge span (Figure 8-12). As was the case along the interior top flange, the stroke of the linear potentiometers near mid-span of the exterior flange was exhausted, as the separation at the mid-span of the bridge increased to 6.5 in. (Figure 8-13). After the experiment resumed on the second full day of loading road base, similar measurements were not taken to avoid the potential hazards of performing work so close to the severely damaged bridge elements.

As the load was incremented, the fractured girder deflected downward, hinging at its top flanges and opening wider at the bottom of the fracture. By the end of the first day of loading the road base, this fracture, which had started out 1.16 in. wide at its base, grew to 4.5 in. at the bottom flange (Figure 8-14). Similarly to the case with the measurements of the separation between the top flanges of the fractured girder and the concrete deck,

Figure 8-10: Separation at the interior top flange of the fractured girder extending the full bridge span

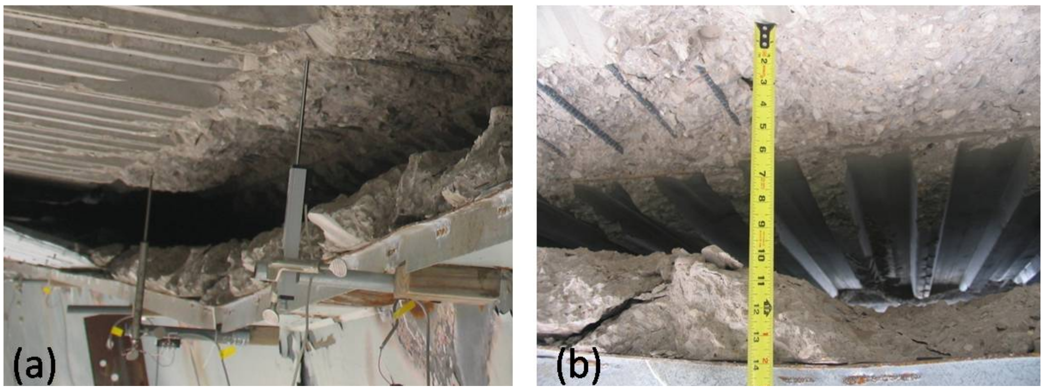

Figure 8-11: (a) Exhausted stroke of the linear potentiometers on the interior top flange of the fractured girder, (b) 11 in. separation at the interior top flange of the fractured girder

Figure 8-12: Separation at the exterior top flange of the fractured girder extending half the bridge span

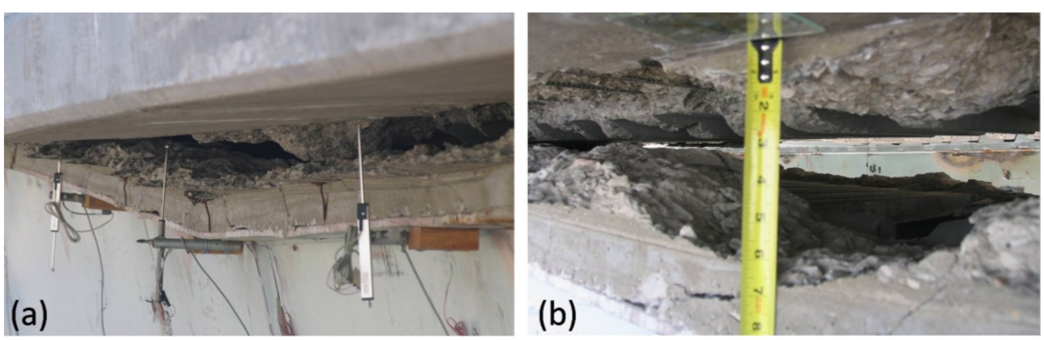

Figure 8-13: (a) Exhausted stroke of the linear potentiometers on the exterior top flange of the fractured girder, (b), 6.5 in. separation at the exterior top flange of the fractured girder

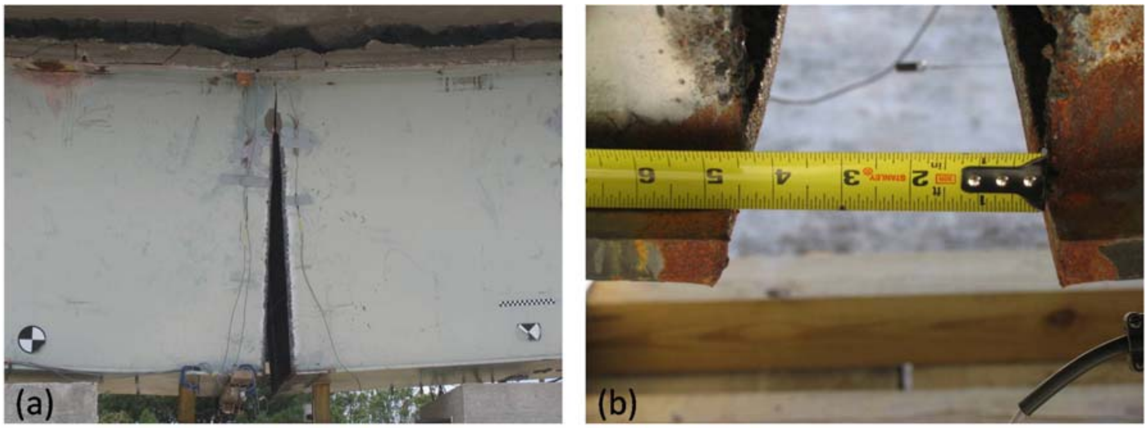

Figure 8-14: (a) Wide view of the opened fracture, (b) Close-up of the width of the fracture at its base

direct measurements of the width of the girder fracture were not taken after additional load was placed to maintain the safety of the researchers.

The downward deflection of the fractured girder was significant. Just as the stroke of many of the linear potentiometers between the fractured girder top flanges and the concrete deck was exhausted by the magnitude of the separation of the girder, the magnitude of the downward deflection of the fractured girder exceeded the capacity of many of the string potentiometers measuring the change in its height. For safety reasons, it was not possible to reset the string potentiometers mid-test, and some of the deflection data were lost.

The extent of concrete cracking on the deck surface significantly increased with the applied load. Before each major loading cycle, new cracks were marked with spray-paint, providing a clear visual reference of the cracking patterns (Figure 8-15). The crack trends that developed as a result of Full-Scale Test 2 were directly extended during the loading sequence of Full-Scale Test 3. Wide, closely spaced cracks grew along the length of the bridge above the interior flange of the intact girder. Moving away from the centerline, cracks curved from the longitudinal orientation toward the exterior railing. As the loading progressed, the cracks extended closer to the ends of the span. New transverse cracks also formed in the previously lightly cracked area between the inside flange of the intact

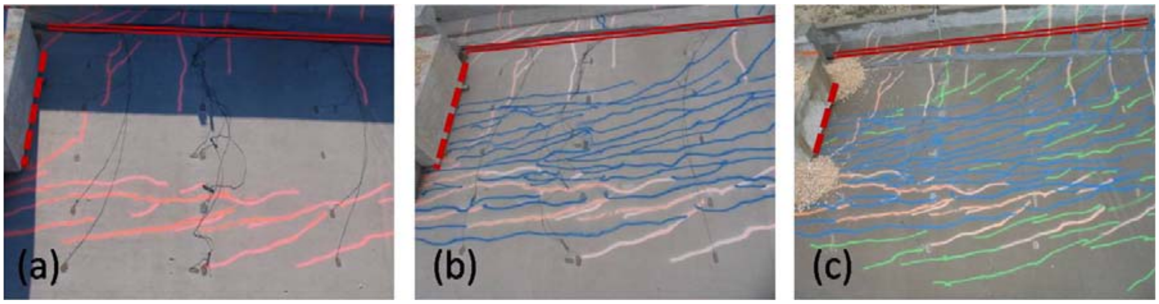

Figure 8-15: Top views of the deck, showing crack patterns (a) After loading the bin, (b) After the first day loading road base, (c) After the second day loading road base. The dashed line indicates the southern end of the containment bin, and the double line indicates the inside foot of the exterior railing

girder and the exterior railing. Other new cracks appeared between existing cracks resulting in a densely cracked deck.

With the increasing load applied to the bridge, cracking also increased around the contact point at the expansion joint on the exterior railing at mid-span (Figure 8-16). Significant spalling of concrete cover on the rail was also observed. The railing, however, did not unload with the loss of the cover concrete. The increased compression through the height of the polystyrene pad that was used to form the expansion joint indicated that contact forces were extending through the height of the railing as the loading progressed.

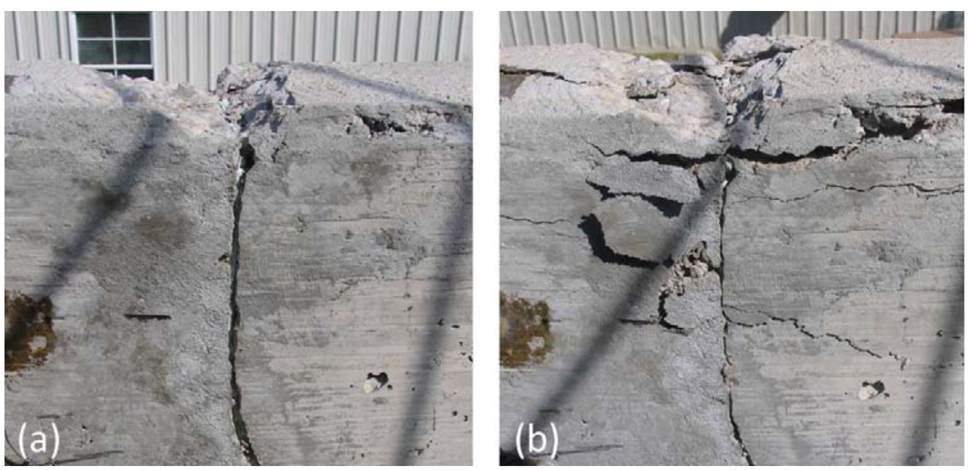

Figure 8-16: Deck views of the mid-span expansion joint in the exterior railing
(a) After loading the bin, (b) After the first day loading road base

Through the second day of loading road base, the load-deflection response of the bridge was relatively linear (Figure 8-6). The fractured girder and the concrete deck above it continued to deflect downward with increasing load, but without any sudden or apparent stiffness changes. A clear space remained between the fractured girder and the concrete deck through the central half of the bridge span until the exterior railing crushed.

8.2.4 Collapse

On the third day of incremental loading, the ultimate capacity of the bridge was reached. Significant portions of the exterior railing surrounding the mid-span expansion joint began to spall. As the railing failure progressed, the mid-span portion of the concrete deck came back into contact with the fractured girder that had been hanging underneath it since the two had separated on the first day of loading road base. A shear transfer failure between the exterior top flange of the fractured girder and the concrete deck along the northern half of the bridge allowed the fractured girder to slip relative to the concrete deck. The two halves of the fractured girder rotated downward about their support points until they came to rest at the fracture location on the bed of concrete blocks positioned underneath the bridge for safety reasons (Figure 8-1). As the concrete deck deflected downward on top of the fractured girder, a plastic hinge along the length of the deck above the interior flange of the intact girder underwent significant rotation.

8.2.4.1 Crushing of the Exterior Railing at the Mid-Span Expansion Joint

Large portions of concrete at the mid-span expansion joint of the exterior railing began to spall when the total load applied to the bridge reached 360,200 lbs. After the onset of major material losses, three additional lift bucket loads were placed on the bridge before the bridge came to rest on the concrete bed below. Video evidence shows, however, that the railing was deflecting downward between loads and losing material without the addition of load (Figure 8-17). It is possible that, given enough time, the railing could have creeped to ultimate failure without the addition of the final three buckets of road base. With the progressive crushing of the rail, the concrete deck deflected downward, eventually coming back into contact with the exterior top flange of the fractured girder

Figure 8-17: Video stills showing progressive failure of the railing

Figure 8-18 (left): Extensive crushing of the exterior railing at mid-span following bridge collapse

Figure 8-19 (right): Close-up top view of the failed railing showing a fractured reinforcing bar

(Figure 8-17). When the bridge collapsed, the railing had lost a significant proportion of its concrete area through the upper 2/3 of its depth (Figure 8-18). Close-up inspection of the remaining railing post-failure revealed that the first vertical reinforcing bar south of the mid-span expansion joint had fractured (Figure 8-19 and A-9).

8.2.4.2 Shear Transfer Failure between the Fractured Girder and the Concrete Deck

When the crushing of the exterior railing allowed the concrete deck to deflect downward and come in contact with the exterior top flange of the fractured girder, the load on the fractured girder increased. Throughout the majority of Full-Scale Test 3, the fractured girder had not seen an increase in load, as it had remained disconnected from the concrete deck in the area where the incremental loads were being added. The added vertical load on the two halves of the fractured girder increased the demand on these components, which was at least partially resisted through the composite action of the girder and the deck near the ends of the span where the shear stud connection on the exterior flange of the fractured girder had not yet been completely lost.

Soon after the concrete deck applied additional load to the fractured girder, the remaining connection between the exterior top flange and the concrete deck failed. The girder slipped relative to the concrete deck, releasing a critical amount of restraint against collapse of the girder through rotation about its support points and the hinge point at the fracture location. Once the fractured girder was completely separated from the concrete deck, the only elements restraining it from rotating were the end diaphragms. The diaphragms, however, did not provide the capacity to prevent the rotation of the fractured girder, and the diaphragms twisted along with the girder rotations at failure (Figure 8-20).

The magnitude of the slip between the fractured girder and the concrete deck was at a maximum at the north end of the girder, where the exterior top flange slipped 3.0 in. and

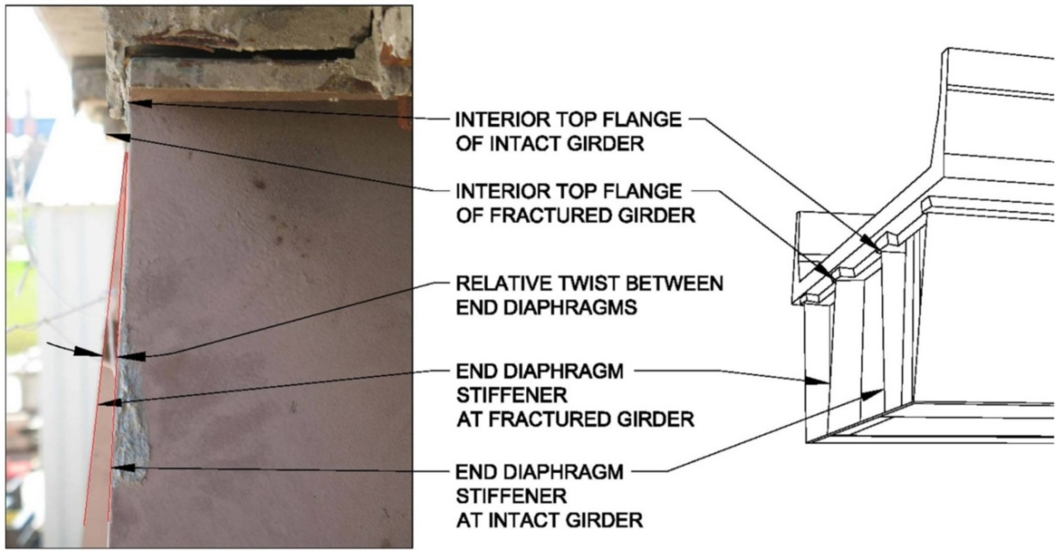

Figure 8-20: Relative twist between end diaphragms after collapse, shown transverse to bridge span

the interior top flange slipped 2.75 in. (Figure 8-21). The slip was apparent along the length of the bridge at a number of locations. Shear studs on the exterior top flange of the fractured girder bent in the direction of the slip, and breakout cones of concrete slid relative to each other along the length of the top flanges (Figure 8-22). In addition, the permanent metal formwork near the northern end of the bridge span crumpled, and deck reinforcing bars engaged in the haunch bent in the direction of the bridge slip (Figure 8-23).

Figure 8-21 (left): Slip between the fractured girder and the concrete deck at the north support

Figure 8-22 (right): Shear stud on the fractured girder bent due to slip between the girder and the deck

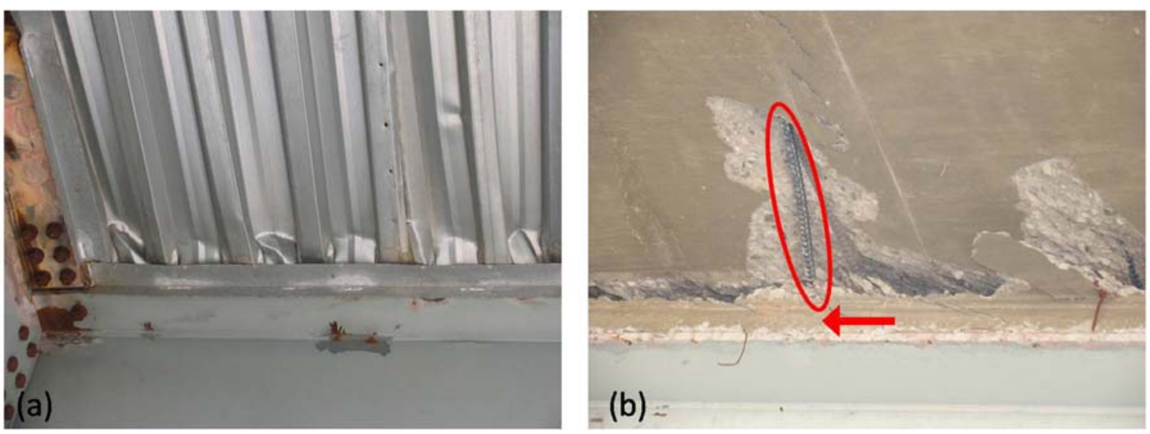

Figure 8-23: Evidence of slip from (a) crumpling of the metal formwork, and (b) rebar bending

8.2.4.3 Flexural Hinging of the Deck above the Interior Flange of the Intact Girder

Preliminary analysis of the assumed redundant load path and observational evidence throughout the series of full-scale tests predicted that the ultimate failure of the bridge would include flexural hinging of the concrete deck along the line above the interior flange of the intact girder (Figure 2-2). After the flanges of the fractured girder separated from the deck during the early stages of Full-Scale Test 3, transverse strips of the deck acted as overhanging slab sections. In this configuration, the bending moment is at a maximum above the interior flange of the intact girder. Once the redundant load path was engaged after Full-Scale Test 2, a series of parallel cracks formed in the concrete deck along the line above the interior flange of the intact girder, indicating tension in the top concrete fibers and high negative bending stresses transverse to the bridge span.

As the loading continued, the cracks in this region became prominent. The hinge, however, was restrained from significant rotation until the fractured girder deflected downward more significantly than was possible before the failure of the exterior railing and the slip between the fractured girder and the deck took place. By the time collapse occurred, the deck had limited ability to redistribute these loads, and the flexural hinge along the line above the interior flange of the intact girder rotated approximately 20˚ over a 45 ft. length of the bridge deck (Figure 8-24).

Figure 8-24: Effects of deck hinging shown (a) With load applied, (b) After load removed

8.2.5 Damage to Other Bridge Components

The exterior railing experienced significant deflection at locations away from the mid-span expansion joint. Along its length, the railing exhibited both flexural and torsional cracking. At the 1/4 and 3/4 expansion joints, the two railing sections opened outward, as well as shifted out of plane (Figure 8-25). The flexural cracks along the length of the railing, starting at the top face of the railing and moving downward, were consistent with the cantilevered deflected shape of the deck and the outward opening of the expansion joints. Torsional cracking is characterized by inclined cracks extending in opposite directions on opposing faces of a concrete member and was displayed on the exterior

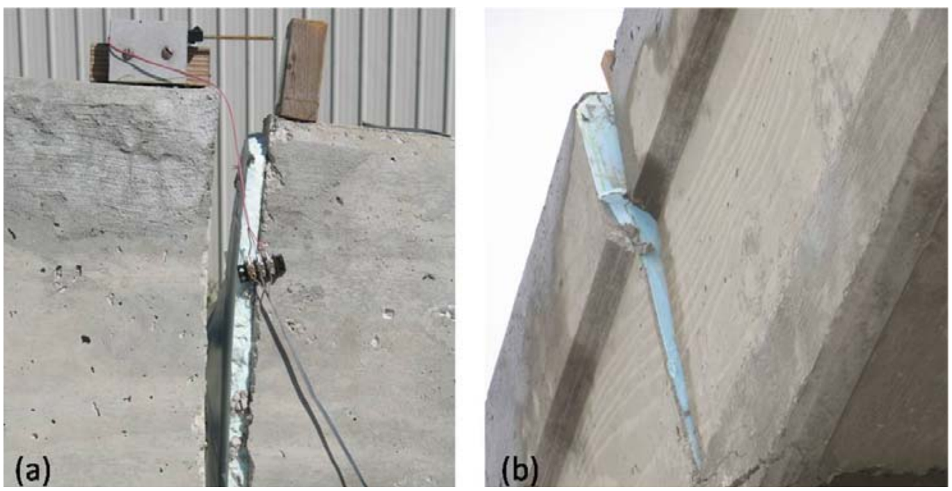

Figure 8-25: Deformation of the 1/4 expansion joint showing (a) opening shift, and (b) out of plane shift

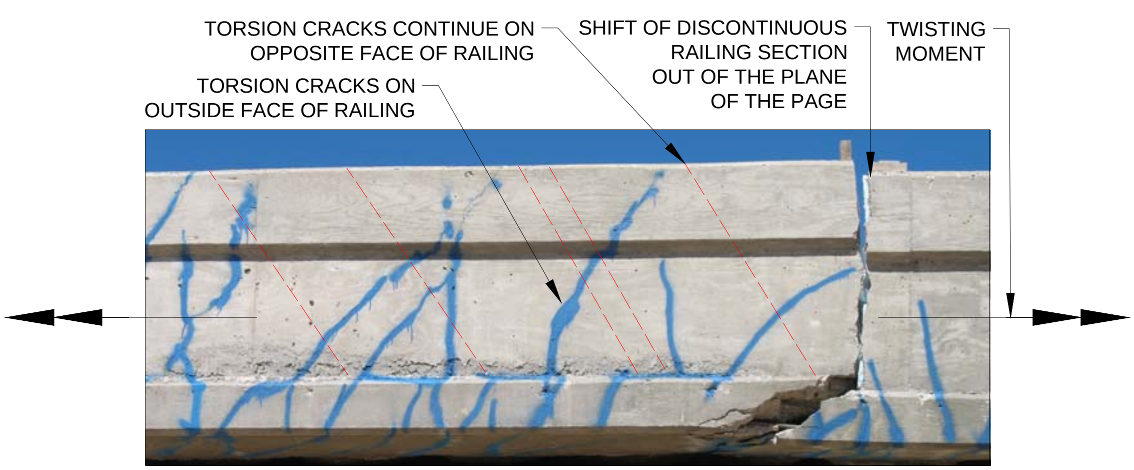

Figure 8-26: Torsional effects on exterior railing

railing after Full-Scale Test 3 (Figure 8-26). The orientation of the torsional cracks along the length of the exterior railing and the out-of-plane shift of the railing at the discontinuous expansion joints were consistent with the same twisting moment.

At the locations of the 1/4 and 3/4 expansion joints in the exterior railing, the concrete deck experienced shear failure (Figure 8-27). At these locations, the exterior railing was discontinuous. Shear transfer just inches away from the expansion joint could be achieved by a 40-in. deep concrete section that included the deck and the railing. At the expansion joint, however, the concrete section was only 8-in. thick, and it did not have adequate shear capacity to resist the applied loads.

When the bridge had ultimately collapsed, the fracture at the interior web of the fractured girder propagated through the remaining depth of the web (Figure 8-28). The area around

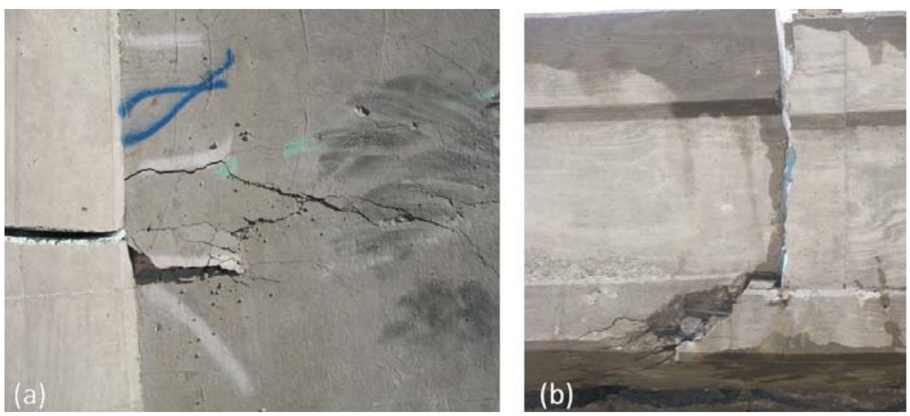

Figure 8-27: Deck shear failure at the expansion joint, shown (a) from above, and (b) from the side

Figure 8-28: Fracture propagation at the interior web of the fractured girder

the fracture also experienced significant yielding during Full-Scale Test 3, as the location acted as a plastic hinge in the fractured girder.

8.2.6 Undamaged Bridge Components

The redundant load path originally hypothesized to maintain equilibrium of a twin box-girder bridge in the event of a full-depth fracture of one of its girders relied on the intact girder to accept transfer of the loads originally carried by the fractured girder in torsion and carry those loads in strong axis bending to the supports. During Full-Scale Test 3, the intact girder remained undamaged, and there were no apparent signs of yielding at any point along the span (Figure 8-29). Because deflection of the intact girder was never substantial enough to close any of the expansion joints along the interior railing, the interior railing also remained undamaged throughout Full-Scale Test 3.

8.3 INSTRUMENTATION PERFORMANCE

The instrumentation and data-acquisition was again an overall success for Full-Scale Test 3. Data were recorded during all four days of testing from the intended sources, amassing

Figure 8-29: Side view of the intact girder, showing small deflection relative to the fractured girder, and lack of distress on the steel and on the railing

a significant amount of strain, displacement, load, photo, and video evidence of the experiment. The regular-speed data-acquisition equipment produced clear and appropriately spaced data, allowing for the analysis of various increments of time, ranging from a few minutes to a whole day.

As was previously described, a number of the direct displacement gages were not able to record data for the full duration of testing. Several portions of the test-bridge experienced deflections that far exceeded the capacity of the linear potentiometers and string potentiometers that were installed. Still, data from the beginning portions of the experiment were recorded, which would be available for use as a starting-point for analysis.

Data from a small number of strain gages were also lost during the test. Six surface concrete gages were installed adjacent to the mid-span expansion joint of the exterior railing. As the bridge deflected, portions of the concrete railing to which these gages were attached spalled off, eliminating the potential for any strain readings. Some of these concrete gages were lost as soon as the first day of loading road base. Strain measurements were still taken 6 ft. from the mid-span expansion joint through the entire experiment, but a set of gages spaced closer to the expansion joint just outside the range of the potential concrete break-out would have helped ensure the acquisition of meaningful data on the strain behavior of the railing near the contact point.

8.4 SUMMARY

Full-Scale Test 3 was executed, successfully loading the test-bridge to collapse. The labor-intensive loading procedure was successfully repeated over 100 times over the course of three days, bringing the total applied load resisted before collapse to 363,300 lbs, which is over four times the legal design truck load. Leading up to collapse, a number of bridge components were damaged or destroyed. In response, a redundant load path engaged to maintain stability of the overloaded system well beyond the point at which standard design methodologies would predict collapse.

The ultimate collapse of the bridge was initiated after the concrete in contact at the mid-span expansion joint of the exterior railing crushed, deflecting the deck downward and re-loading already damaged elements that were unable to sustain the increase in applied force. A shear transfer failure between the fractured girder and the concrete deck ultimately allowed for rapid downward deflection of the bridge elements, and a flexural hinge in the concrete deck underwent significant plastic rotation.

Many aspects of the damage sustained to the test-bridge were documented in this chapter, but detailed analyses of the components that failed and the components that successfully resisted the applied loads were not presented. The particulars of the redundant load path that sustained the enormous load applied to the test-bridge must be evaluated to fully understand the ultimate capacities of the system. The substantial amount of data taken during Full-Scale Test 3, during post-failure observations, and during all of the experimental work that preceded this experiment will serve as a reference for those evaluations. This work is currently ongoing and will be presented by Samaras (2009).

CHAPTER 9

Conclusions

9.1 PROJECT SUMMARY

The AASHTO Bridge Design Specifications a) define a fracture critical member as a "component in tension whose failure is expected to result in the collapse of the bridge or the inability of the bridge to perform its function," and b) require costly bi-annual hands on inspections of all bridges designed with a fracture critical member. Observations of member failures on in-service bridges have shown, however, that the overall response of a fracture critical bridge is not always controlled by the performance of its fracture critical members. As evidence has amassed suggesting inherent redundancy for which these bridges have not been given credit, bridge owners have begun to question the applicability of the fracture critical provisions, seeking in particular to redefine the inspection requirements that consume significant labor and financial resources.

To investigate the behavior of twin box-girder fracture critical steel bridges and develop methods for estimating their redundant capacities in the event of a loss of a fracture critical member, the Texas Department of Transportation and the Federal Highway Administration co-sponsored a large-scale research program at the Ferguson Structural Engineering Laboratory at The University of Texas at Austin. The broad scope of the research project included analyses of the bridge system based on both hand-calculations and computer simulations, laboratory experiments to test the tensile capacity of the shear stud connections between the steel girders and the concrete deck, and a series of three destructive tests performed on a full-scale twin box-girder steel bridge relocated from its service location to an outdoor area immediately adjacent to FSEL.

9.2 FULL-SCALE TESTING SUMMARY

Full-scale testing of the FSEL test-bridge was designed to gather information on the behavior and capacity of the system in the event of a full-depth fracture of one of its two girders. Testing procedures and data-acquisition setups were designed to identify and to characterize the redundant load paths that participated in maintaining the stability of the bridge in its damaged state. The results would be used to calibrate the analytical models that were concurrently developed, and also as a reference for the full-scale behavior of these types of bridges.

- Full-Scale Test 1 used an explosive shape charge to induce a fracture in the bottom flange of one of the box-girders at a mid-span location, representing a worst-case loading scenario. Despite having had a 76-kip simulated truck live load placed directly above the fracture location, the fracture did not propagate into the webs of the girder, the bridge experienced only minor deflections, and redundant load paths were not significantly engaged in supporting the applied loads.

- Full-Scale Test 2 instantaneously released existing loads to generate the dynamic response of the test-bridge after damage comparable to a full-depth fracture was manually induced. A custom-built support structure was used to shore the fractured girder at mid-span while the fracture sustained during Full-Scale Test 1 was extended with a torch-cut and while the truck load was applied to the bridge deck. The support structure was then suddenly disabled using an explosive charge at a critical tension rod location. In response, the bridge displayed residual static deflections as large as 7 in. and sustained considerable damage to the connections between the fractured girder and the concrete deck. A redundant load path, which received contribution from the exterior railing and the concrete deck, was engaged and helped limit the overall damage to the bridge, which remained serviceable following the experiment.

- Full-Scale Test 3 applied incremental loads statically to the bridge deck until the system collapsed. The bridge sustained substantial damage to the connections between the fractured girder and the concrete deck, but was able to maintain overall stability as the applied load increased to more than four times the legal truck load. Failure was initiated when the exterior railing suffered extensive crushing, and collapse occurred when plastic hinging of the concrete deck and a shear-transfer failure between the fractured girder and the deck allowed for rapid downward deflection of the fractured girder.

9.3 CONCLUSIONS

The results gathered from full-scale testing were extensive, and a number of conclusions can be drawn with respect to performance of the test-bridge, instrumentation of a test specimen of this scale, and the complications of large-scale testing in general.

9.3.1 Behavior of the FSEL Test Bridge

- The dynamic response of the FSEL test-bridge was characterized by an initial pulse followed by decaying oscillations until the full dynamic energy was dissipated. The dynamic impact factor resulting from the sudden release of the scissor-jacks during Full-Scale Test 2 was calculated to be approximately 1.3.

- The FSEL test-bridge had significant redundant capacity after sustaining a full-depth fracture in one of its girders. When the test-bridge dynamically responded to the presence of a full-depth fracture in one of its girders with the 76-kip design load applied, the damage sustained would not have prevented the safe clearing of the deck surface, nor would it have endangered people or property nearby. Under static loads, the test-bridge was able to support more than four times its design truck load before ultimate collapse.

- The exterior railing above the fractured girder played a significant role in the post-fracture stability of the FSEL test-bridge. As the test-bridge began its dynamic response immediately following the release of the loads being held by the specially designed temporary shoring system, the fractured girder began deflecting downward. The continuation of this downward deflection was arrested when the expansion joint in the railing closed and the concrete section began carrying load. During Full-Scale Test 3, the failure of the concrete railing initiated the collapse of the test-bridge. Shear failures occurred in the concrete deck at sections where the railing was discontinuous.

- The bending capacity of the concrete deck played a major role in transferring loads away from the fracture location. Throughout the majority of Full-Scale Test 3, a large portion of the concrete deck at the bridge mid-span was overhanging without support from the fractured girder. In this state, the deck continued to transfer increasing static loads away from the fracture location to other components in the bridge system.

9.3.2 Instrumentation of a Full-Scale Specimen Tested to Failure

- When instrumenting a large-scale test specimen, it is critical to protect all of the data-acquisition equipment as best as possible. If a material failure occurs at a gage location or the stroke of a direct displacement device is exhausted before a test is completed, information from that location cannot be subsequently collected. Furthermore, instrumentation equipment must be adequately protected when using any testing procedure that can energize dangerous fragments or create a force pulse capable of damaging the equipment.

- The use of a high-speed data-acquisition system was essential in capturing thorough details of dynamic behavior. Because data points were recorded at such a rapid rate during Full-Scale Test 2, events that had occurred only 0.05 seconds apart could be distinguished when observing the data, and rapidly transpiring patterns could be identified.

9.3.3 Full-Scale Testing in General

- When taking data over an extended period of time, it is important to take a record of factors that can affect the measurements on different time scales. During this research project, survey and instrumentation measurements were taken to characterize the displacement of the test-bridge with respect to loading and damage conditions, but temperature measurements that would have affected the measured displacements were not taken. Thus, environmental factors that may have affected the overall bridge displacements could not be quantified.

- In the case of large-scale structures tested to failure, the opportunity for repeat trials is rare, and it is critical that all methods and data-acquisition procedures be sufficiently prepared for testing. In the case of this research project, three tests were performed due to the resilience of the test specimen. Performing a series of tests provided the opportunity to make observations and to implement modifications to the instrumentation plan at various stages of bridge damage. In this type of research, these opportunities will not always be available.

9.4 CONCURRENT STRUCTURAL ANALYSES

Two methods of structural analysis that can be used to model the response of the test-bridge were taking place concurrently at the time of this thesis writing. The first method, which is a hand-based analysis procedure (Samaras, 2009), will provide a means of quickly and conservatively estimating the ultimate capacity of bridges similar to the one tested at FSEL. The second approach, which is based on a non-linear finite element analysis (Kim, 2009), will be used to capture detailed aspects of response that cannot be accounted for by the simple, hand-based procedure. The finite element model considers a broad range of behaviors observed during the full-scale tests, and it is capable of accounting for the load-deformation response, component failures, and the collapse sequence that was observed in the test-bridge. Specific quantitative data from the full-scale tests will be compared to output from the computer simulations. These comparisons will be used to calibrate the model so that its results mimic the actual behavior of the test-bridge.

9.5 RECOMMENDATIONS

The overall scope of this research project was to determine methods for evaluating the redundancy of fracture critical bridges, with a focus on twin box-girder designs. The full-scale tests performed as part of this research provided multi-faceted data on the behavior and capacity of the FSEL test-bridge. While the specimen was representative of twin box-girder steel bridges used in the State of Texas, the results from these tests cannot be immediately or directly extrapolated to predict the behavior of every twin box-girder steel bridge.

- The FSEL test-bridge was tested as a single-span structure. In practice, these bridges are commonly constructed as multi-span structures. Though the results from a simple span test should be conservative compared to those from tests of a multi-span structure, it is recommended that the effect of the number of spans on the behavior and capacity of these bridges be investigated.

- The FSEL test-bridge had only a slight curvature. Twin box-girder steel bridges can be designed and exist in service with significantly smaller radii of curvature than that of the test-bridge. The most notable effect of this variation is that torsional demand on a bridge section is inversely proportional to the radius of curvature of the bridge plan. The consequences of an increase in curvature on the performance and capacity of a bridge that has lost a fracture critical member must be considered before the results gathered from the full-scale tests at FSEL can be applied to other bridges.

- The FSEL test-bridge was built with stocky-shaped T501 concrete railings, which were constructed with 0.75-in. wide expansion joints spaced at 30 ft. Details of in-service bridges, including the material, size, and shape of the railings, as well as the geometry and distribution of their expansion joints, are highly variable. Especially considering the demonstrated contribution of the railing during the full-scale tests at FSEL, it is important to characterize the effects of various railing designs on the behavior and ultimate capacity of a bridge that has lost a fracture critical member.

The effects of variations in number of spans, curvature, and railing specifications on twin box-girder performance in the event of a full-depth fracture of one of the girders are currently being addressed analytically. The results of this parametric study will be made available by Kim (2009).

9.6 CLOSING COMMENTS

Through three full-scale tests, the FSEL test-bridge performed much better than the AASHTO Bridge Design Specifications suppose, particularly given the fact that it was a simply-supported span, had expansion joints in its railings, and had all external cross-frames removed. After sustaining a full-depth fracture of one of its box-girders, the test-bridge demonstrated sufficient redundancy through alternate load paths to maintain loads far exceeding those for which it was designed. After additional research is carried out, revisions should be considered to the current AASHTO specifications that a) can accurately predict the behavior of these bridges following the failure of a critical member, and b) subsequently prescribe appropriate inspection and maintenance requirements. Given the demonstrated redundancy in these systems beyond that for which they have been credited, the current requirement for bi-annual hands on inspections does not appear to be an effective use of labor or financial resources.

APPENDIX A

Drawings and Design

A.1 BRIDGE DETAILS

Table A-1: Deck reinforcing bar properties

Bar Designation	Nominal Yield Strength Fy (ksi) (specified)	Nominal Yield Strength Fy (ksi) (measured)	Nominal Ultimate Strength Fu (ksi) (measured)
#4	60	60	102
#5	60	68	101

Table A-2: Bridge concrete properties

Deck Slab - Cast 8/17/06 TxDOT Class-S-Type (4 ksi)		
Test Date	Age (days)	Average f'c (ksi)
9/14/2006	28	4.84
10/24/2006	68	5.37
8/16/2008	669	6.26
4/2/2009	898	6.26

Interior Railing - Cast 8/22/06 Austin Class-S-Type (4 ksi)		
Test Date	Age (days)	Average f'c (ksi)
9/19/2006	28	5.34
10/24/2006	63	5.95
8/16/2008	664	6.63
4/2/2009	893	6.60

Exterior Railing - Cast 8/24/06 Austin Class-S-Type (4 ksi)		
Test Date	Age (days)	Average f'c (ksi)
9/19/2006	26	4.74
10/24/2006	61	4.90
8/16/2008	662	6.27
4/2/2009	891	5.49

The compression tests performed on 4/2/2009 indicate a decrease in concrete strength, which is not expected. The cylinders that remained for testing in this fourth round of measurements, on average, had poor capping surfaces, which would have affected measured compressive strength.

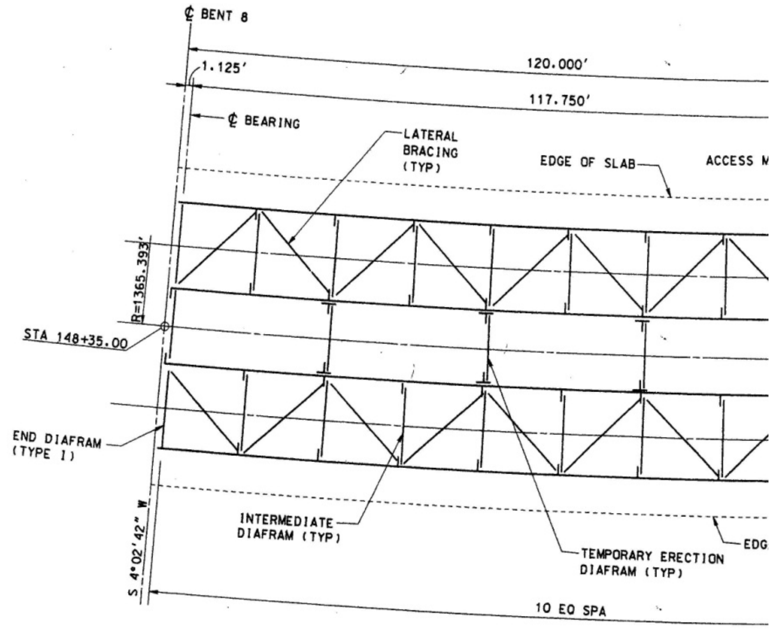

FRAMING PLAN

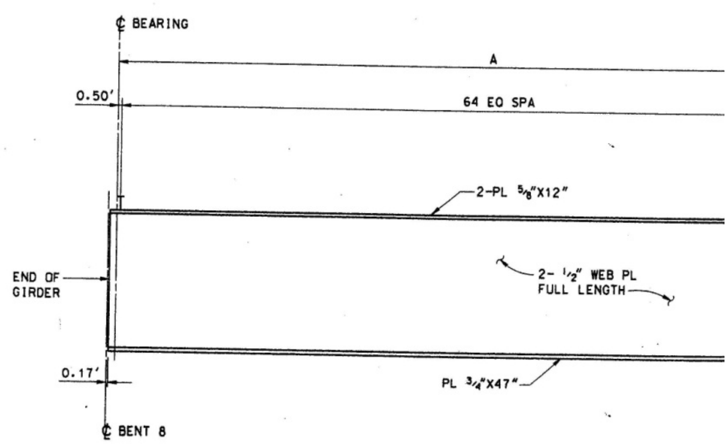

BOX GIRDER ELEVATION (TYP)
(DIMENSIONS SHOWN ARE ALONG ℄ GIRDER)

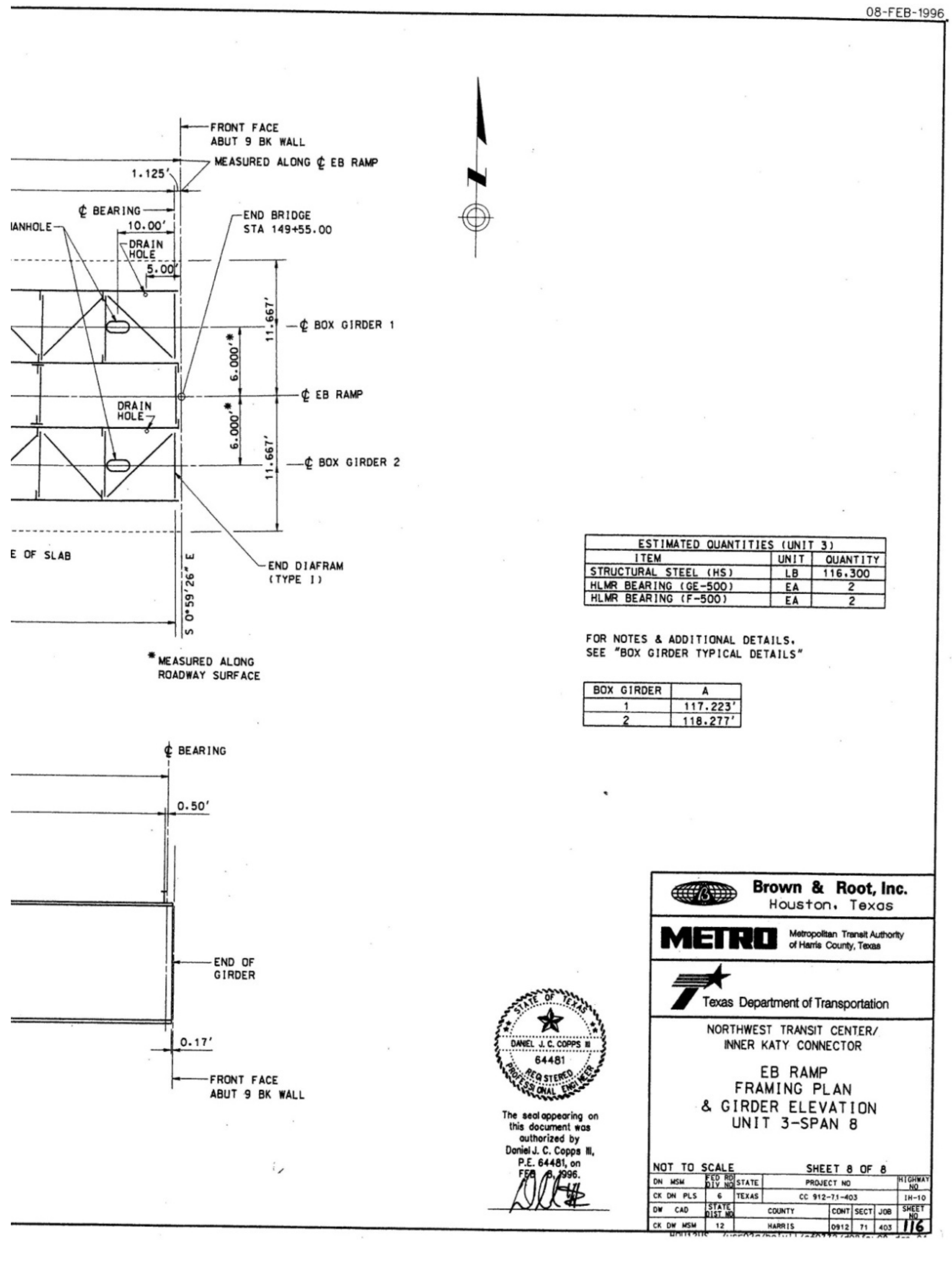

Figure A-1: Bridge Framing Plan

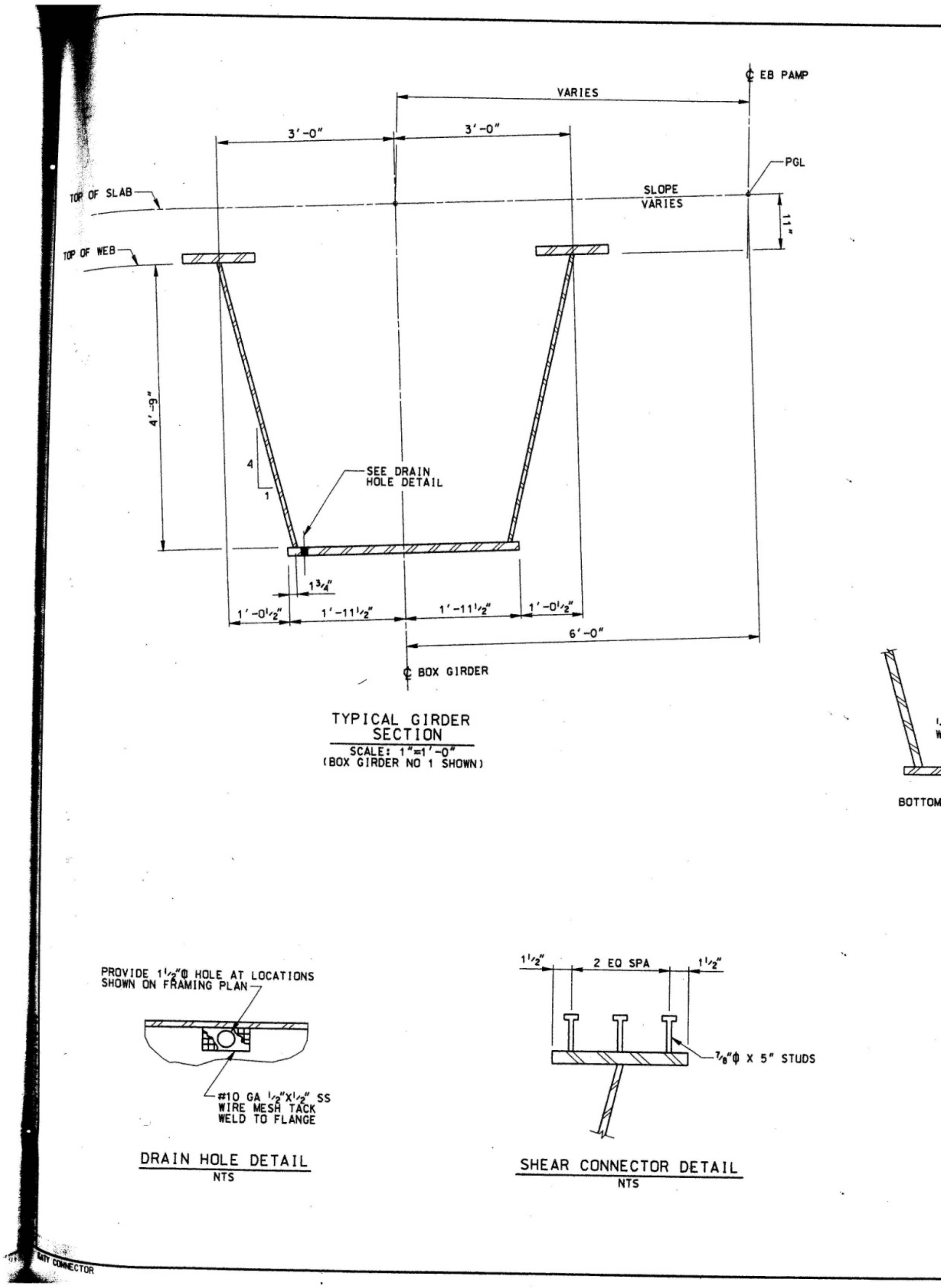

℄ EB PAMP
VARIES
3'-0"
3'-0"
PGL
TOP OF SLAB
SLOPE VARIES
11"
TOP OF WEB
4'-9"
4
1
SEE DRAIN HOLE DETAIL
1 3/4"
1'-0 1/2"
1'-11 1/2"
1'-11 1/2"
1'-0 1/2"
6'-0"
℄ BOX GIRDER
TYPICAL GIRDER SECTION
SCALE: 1"=1'-0"
(BOX GIRDER NO 1 SHOWN)
BOTTOM
PROVIDE 1 1/2"Φ HOLE AT LOCATIONS SHOWN ON FRAMING PLAN
#10 GA 1/2"X1/2" SS WIRE MESH TACK WELD TO FLANGE
DRAIN HOLE DETAIL
NTS
1 1/2"
2 EQ SPA
1 1/2"
7/8"Φ X 5" STUDS
SHEAR CONNECTOR DETAIL
NTS

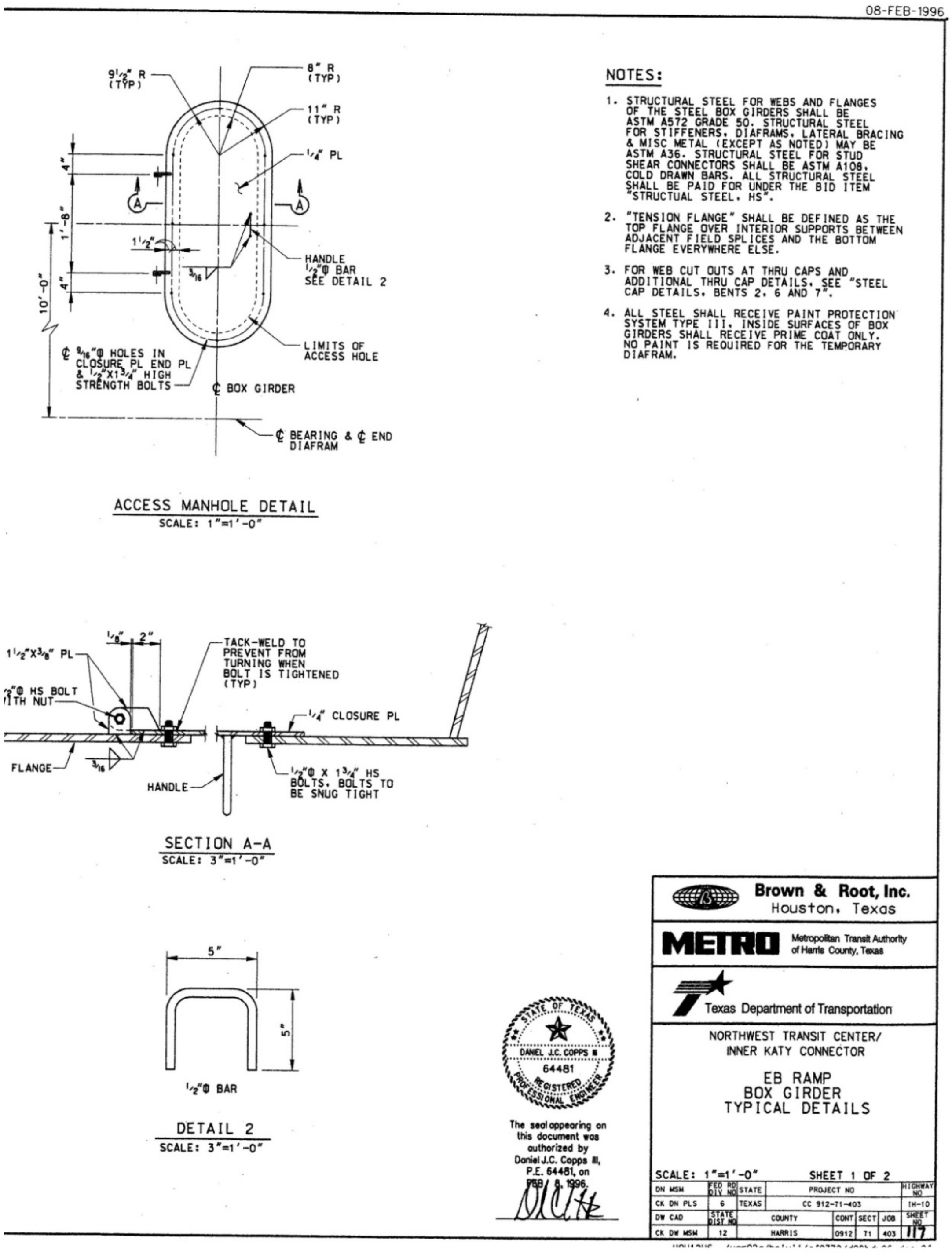

Figure A-2: Box girder typical details page 1

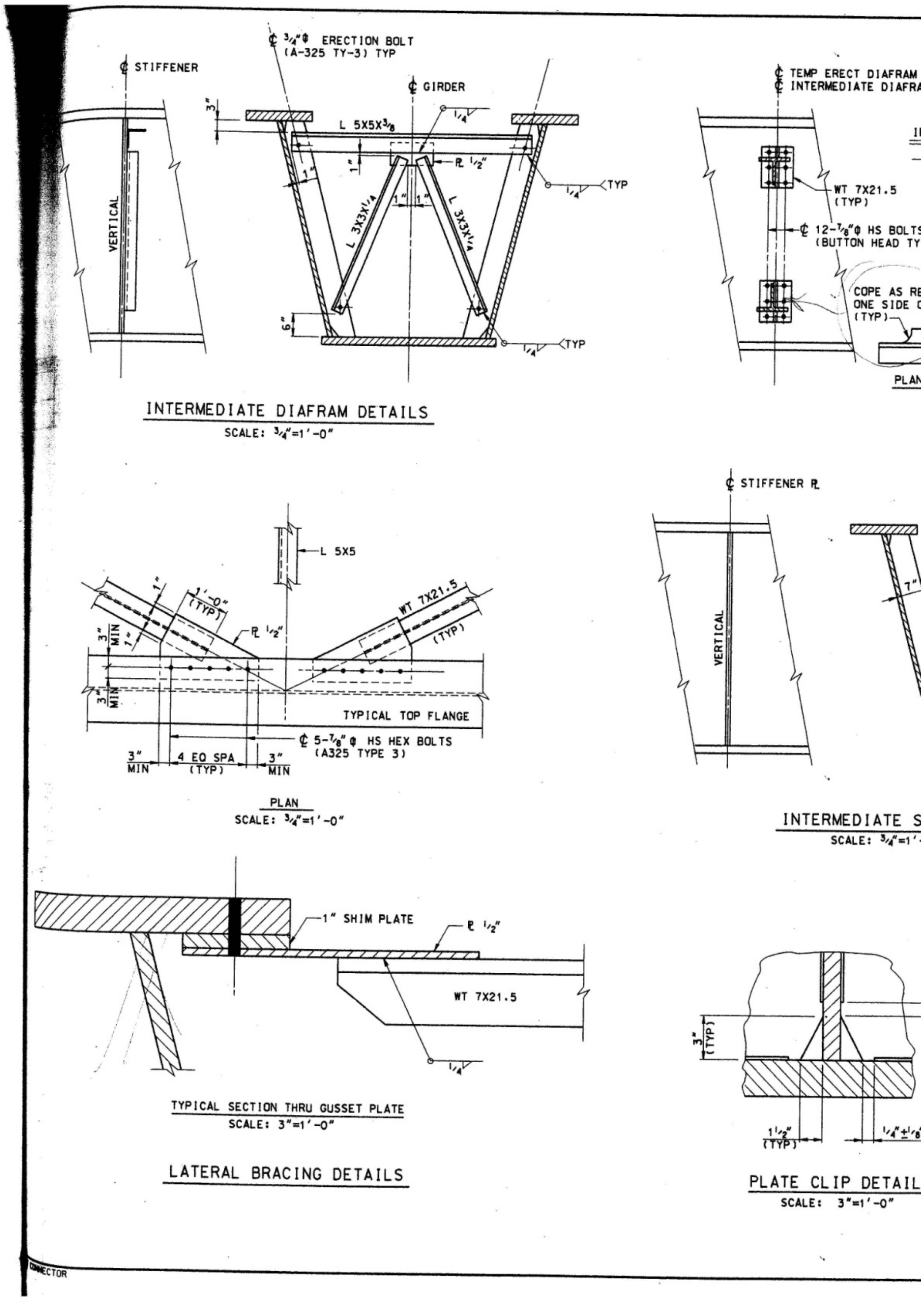

℄ STIFFENER
℄ 3/4"φ ERECTION BOLT (A-325 TY-3) TYP
℄ GIRDER
L 5X5X3/8
℄ 1/2"
L 3X3X1/4
L 3X3X1/4
TYP
TYP
VERTICAL
℄ TEMP ERECT DIAFRAM
℄ INTERMEDIATE DIAFRA
WT 7X21.5 (TYP)
℄ 12-7/8"φ HS BOLTS (BUTTON HEAD TY
COPE AS RE ONE SIDE (TYP)
PLAN
INTERMEDIATE DIAFRAM DETAILS
SCALE: 3/4"=1'-0"
L 5X5
1'-0" (TYP)
WT 7X21.5
℄ 1/2"
(TYP)
3" MIN
3" MIN
TYPICAL TOP FLANGE
℄ 5-7/8"φ HS HEX BOLTS (A325 TYPE 3)
3" MIN
4 EQ SPA (TYP)
3" MIN
PLAN
SCALE: 3/4"=1'-0"
℄ STIFFENER ℄
VERTICAL
INTERMEDIATE S
1" SHIM PLATE
℄ 1/2"
WT 7X21.5
TYPICAL SECTION THRU GUSSET PLATE
SCALE: 3"=1'-0"
LATERAL BRACING DETAILS
3" (TYP)
1 1/2" (TYP)
PLATE CLIP DETAIL
SCALE: 3"=1'-0"
CONNECTOR

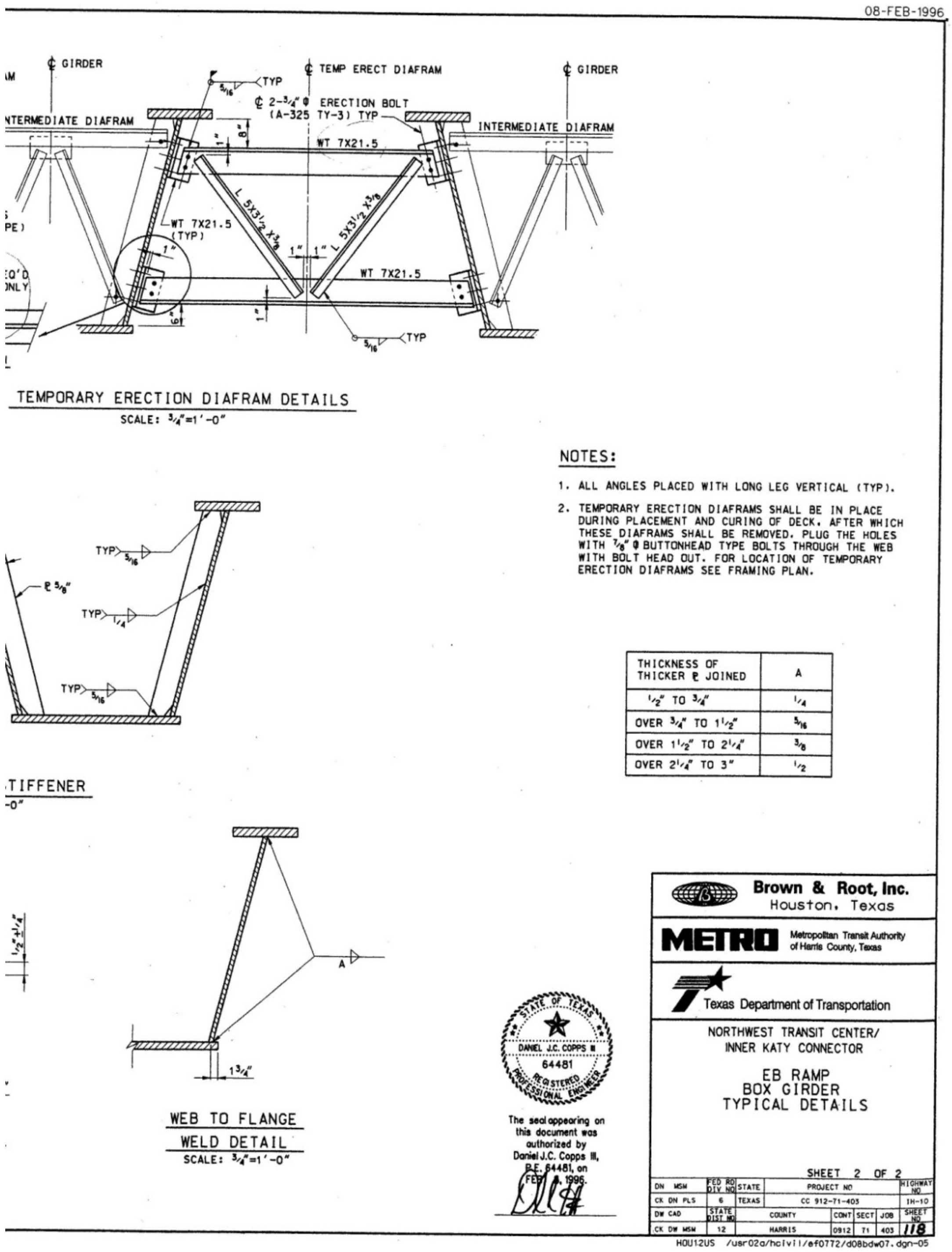

Figure A-3: Box girder typical details page 2

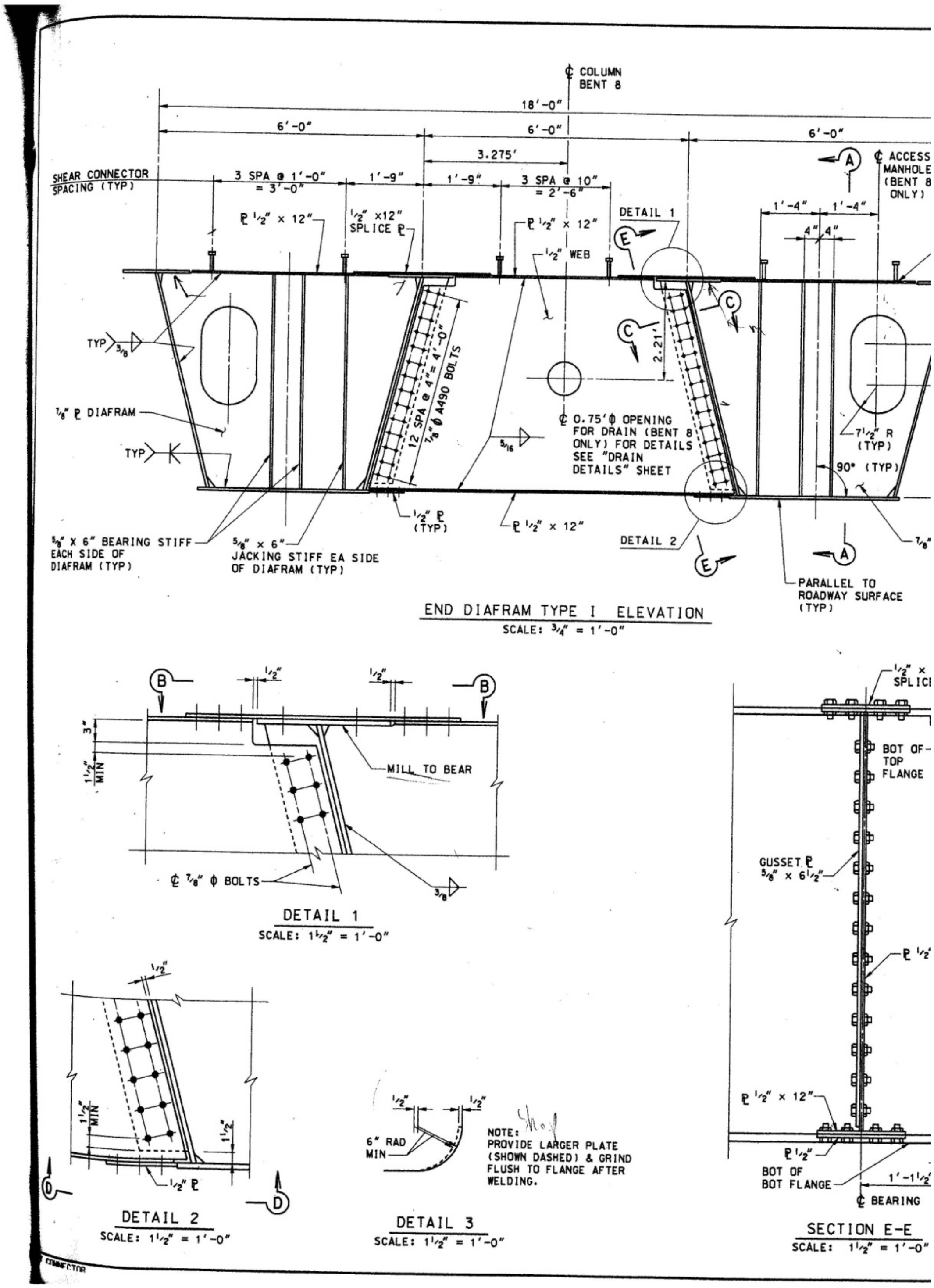

℄ COLUMN BENT 8
18'-0"
6'-0"
6'-0"
6'-0"
3.275'
SHEAR CONNECTOR SPACING (TYP)
3 SPA @ 1'-0" = 3'-0"
1'-9"
1'-9"
3 SPA @ 10" = 2'-6"
℄ ACCESS MANHOLE (BENT 8 ONLY)
1'-4"
1'-4"
4"
4"
℄ 1/2" × 12"
1/2" ×12" SPLICE ℄
℄ 1/2" × 12"
1/2" WEB
DETAIL 1
TYP
7/8" ℄ DIAFRAM
12 SPA @ 4" = 4'-0"
7/8" ϕ A490 BOLTS
2.21'
℄ 0.75' ϕ OPENING FOR DRAIN (BENT 8 ONLY) FOR DETAILS SEE "DRAIN DETAILS" SHEET
7 1/2" R (TYP)
90° (TYP)
5/8" X 6" BEARING STIFF EACH SIDE OF DIAFRAM (TYP)
5/8" × 6" JACKING STIFF EA SIDE OF DIAFRAM (TYP)
1/2" ℄ (TYP)
℄ 1/2" × 12"
DETAIL 2
PARALLEL TO ROADWAY SURFACE (TYP)
END DIAFRAM TYPE I ELEVATION
SCALE: 3/4" = 1'-0"
1/2"
1/2"
3"
1 1/2" MIN
MILL TO BEAR
℄ 7/8" ϕ BOLTS
DETAIL 1
SCALE: 1 1/2" = 1'-0"
1/2"
1 1/2" MIN
1 1/2"
1/2" ℄
DETAIL 2
SCALE: 1 1/2" = 1'-0"
6" RAD MIN
NOTE: PROVIDE LARGER PLATE (SHOWN DASHED) & GRIND FLUSH TO FLANGE AFTER WELDING.
DETAIL 3
SCALE: 1 1/2" = 1'-0"
1/2" × SPLICE
BOT OF TOP FLANGE
GUSSET ℄ 5/8" × 6 1/2"
℄ 1/2" × 12"
℄ 1/2"
BOT OF BOT FLANGE
1'-1 1/2"
℄ BEARING
SECTION E-E
SCALE: 1 1/2" = 1'-0"

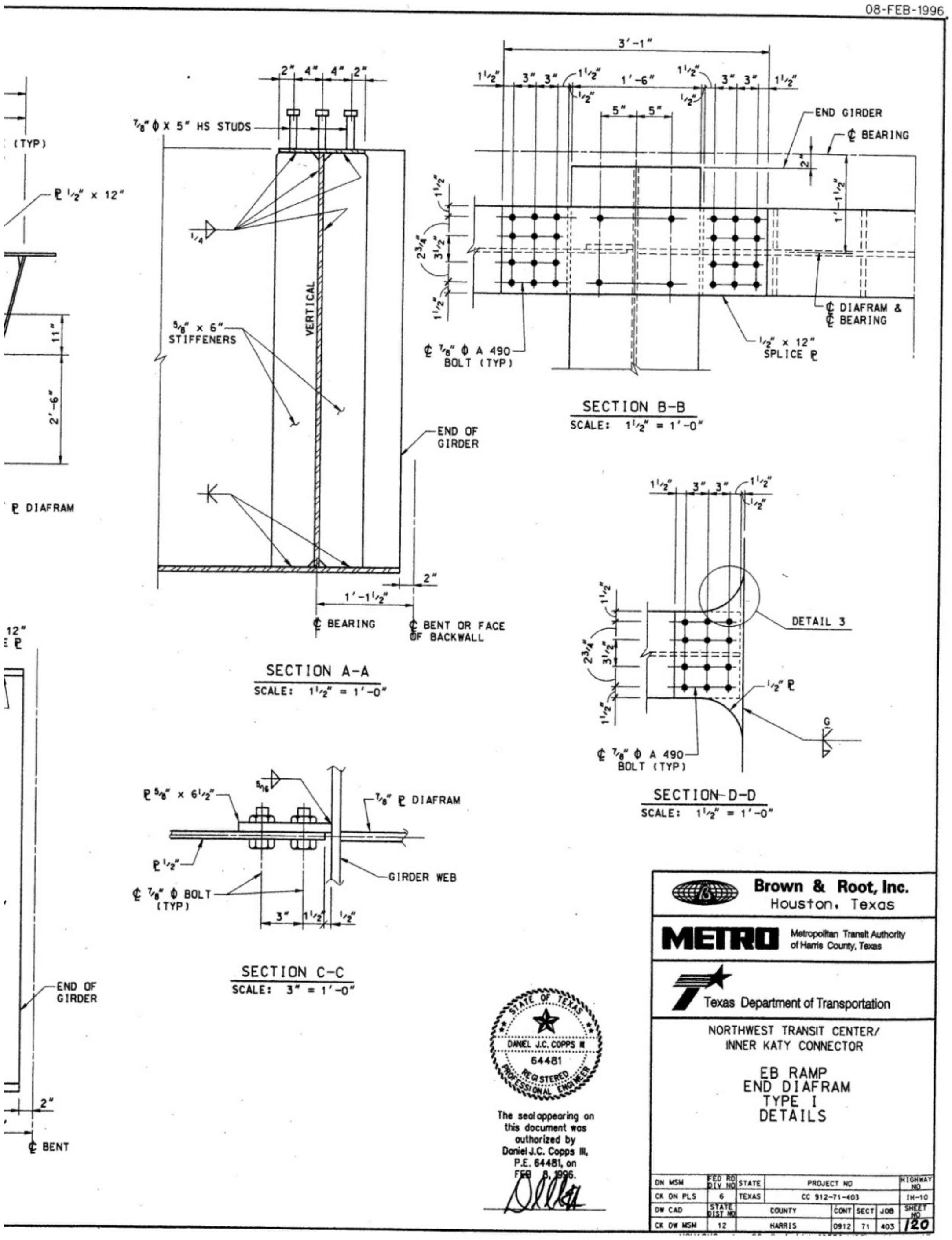

Figure A-4: End diaphragm details

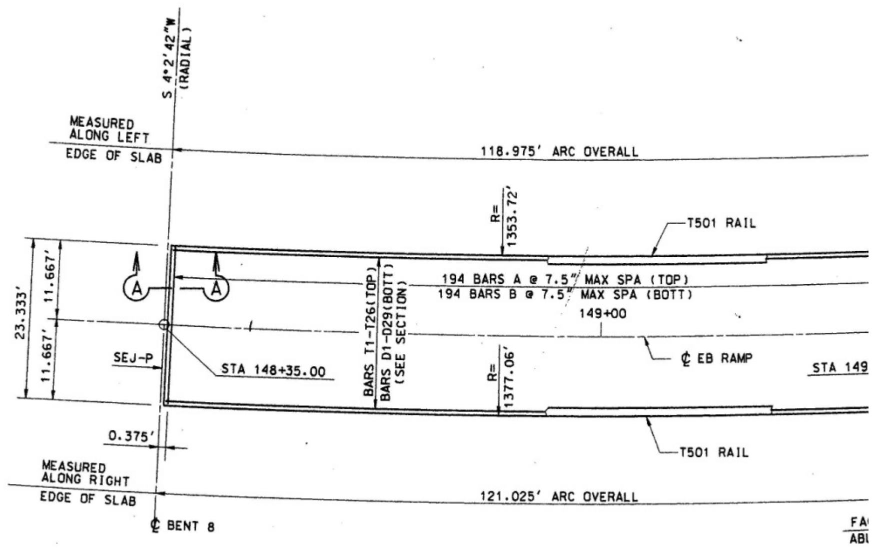

PLAN
SCALE: 1"=10'-0"

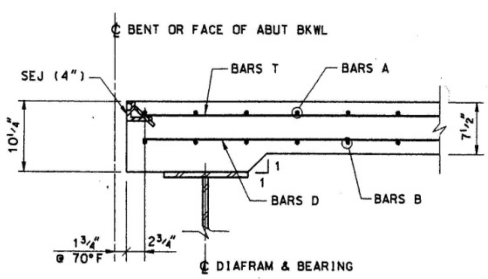

SECTION A-A
SCALE: 1"=1'-0"

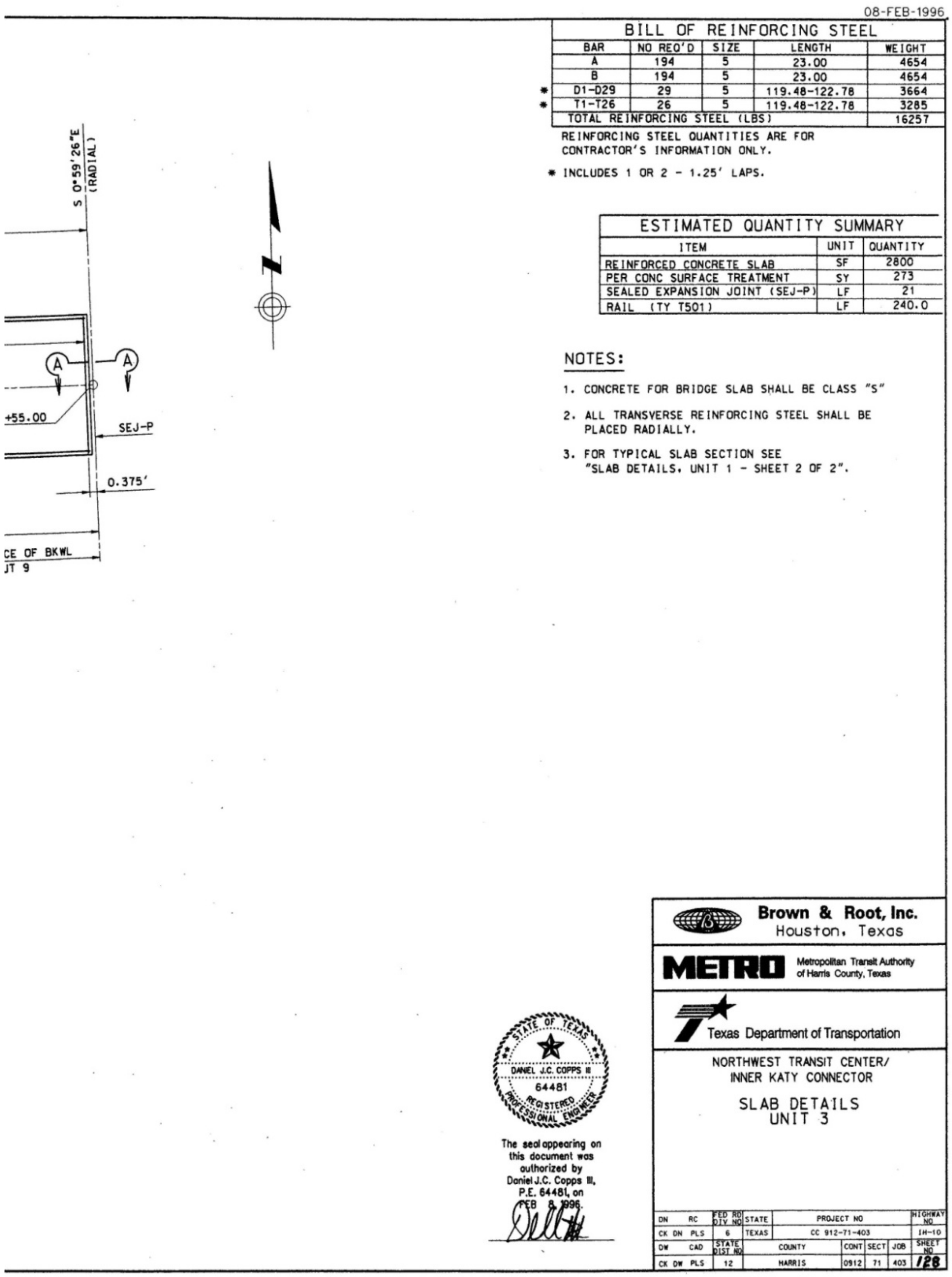

Figure A-5: Slab details page 1

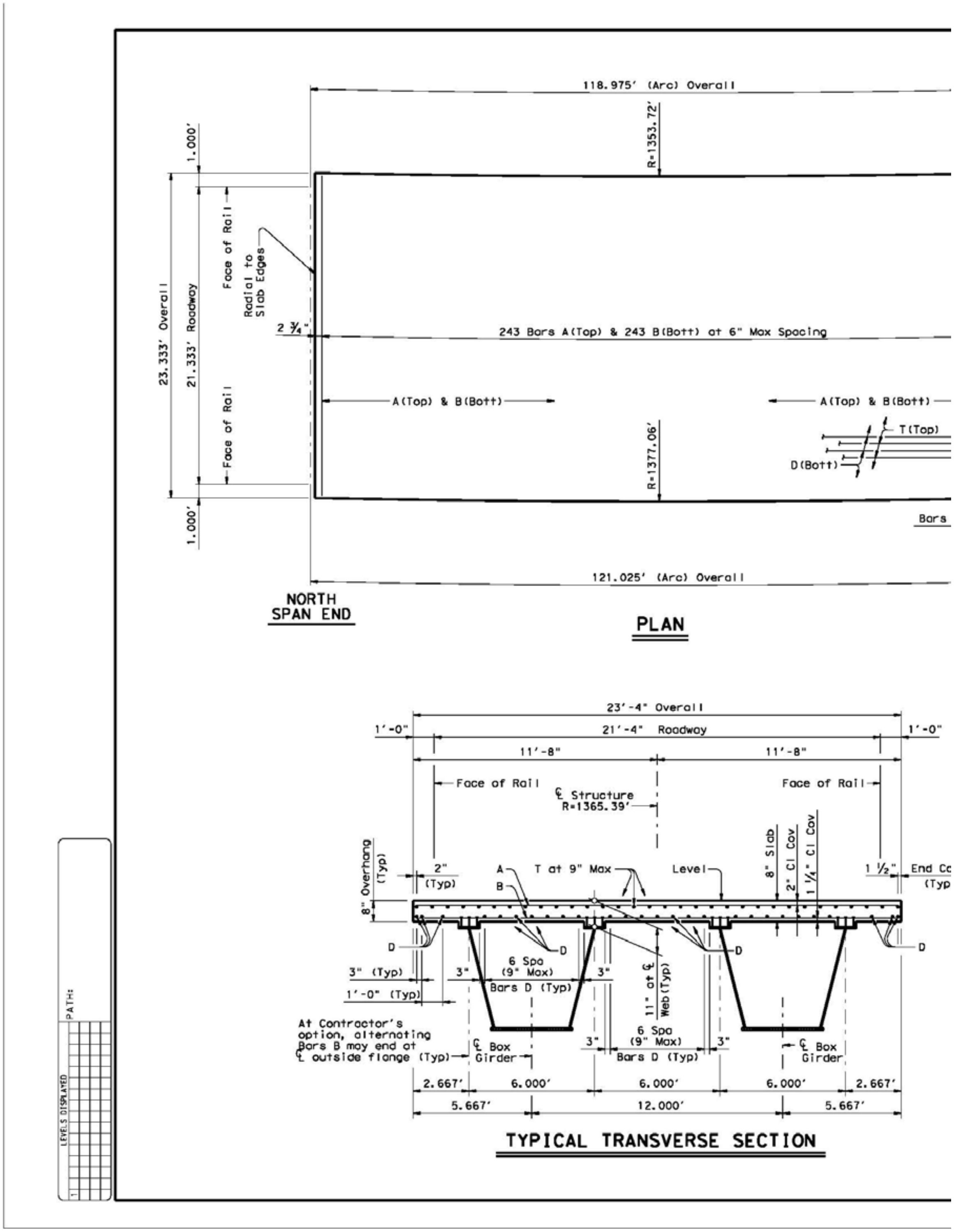

118.975' (Arc) Overall
R=1353.72'
1.000'
23.333' Overall
21.333' Roadway
Face of Rail
Radial to Slab Edges
2 ¾"
243 Bars A(Top) & 243 B(Bott) at 6" Max Spacing
A(Top) & B(Bott)
T(Top)
D(Bott)
R=1377.06'
Bars
121.025' (Arc) Overall
NORTH SPAN END
PLAN
23'-4" Overall
1'-0"
21'-4" Roadway
11'-8"
Face of Rail
℄ Structure R=1365.39'
8" Overhang (Typ)
2" (Typ)
T at 9" Max
Level
8" Slab
2" Cl Cov
1 ¼" Cl Cov
1 ½"
End Cc (Typ
8"
D
3" (Typ)
1'-0" (Typ)
6 Spa (9" Max) Bars D (Typ)
11" at ℄ Web (Typ)
At Contractor's option, alternating Bars B may end at ℄ outside flange (Typ)
℄ Box Girder
2.667'
6.000'
5.667'
12.000'
TYPICAL TRANSVERSE SECTION
LEVELS DISPLAYED
PATH:

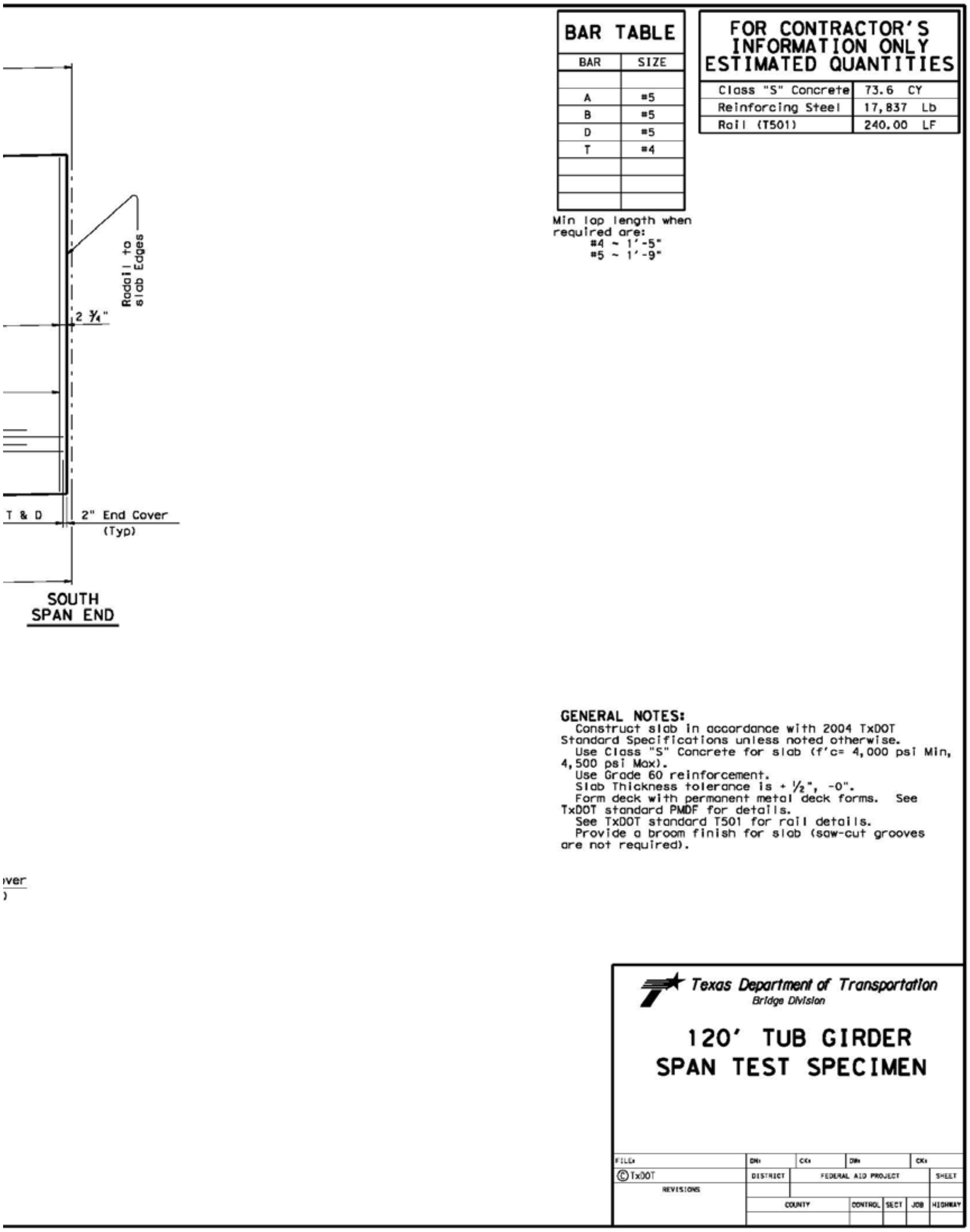

Figure A-6: Slab details page 2

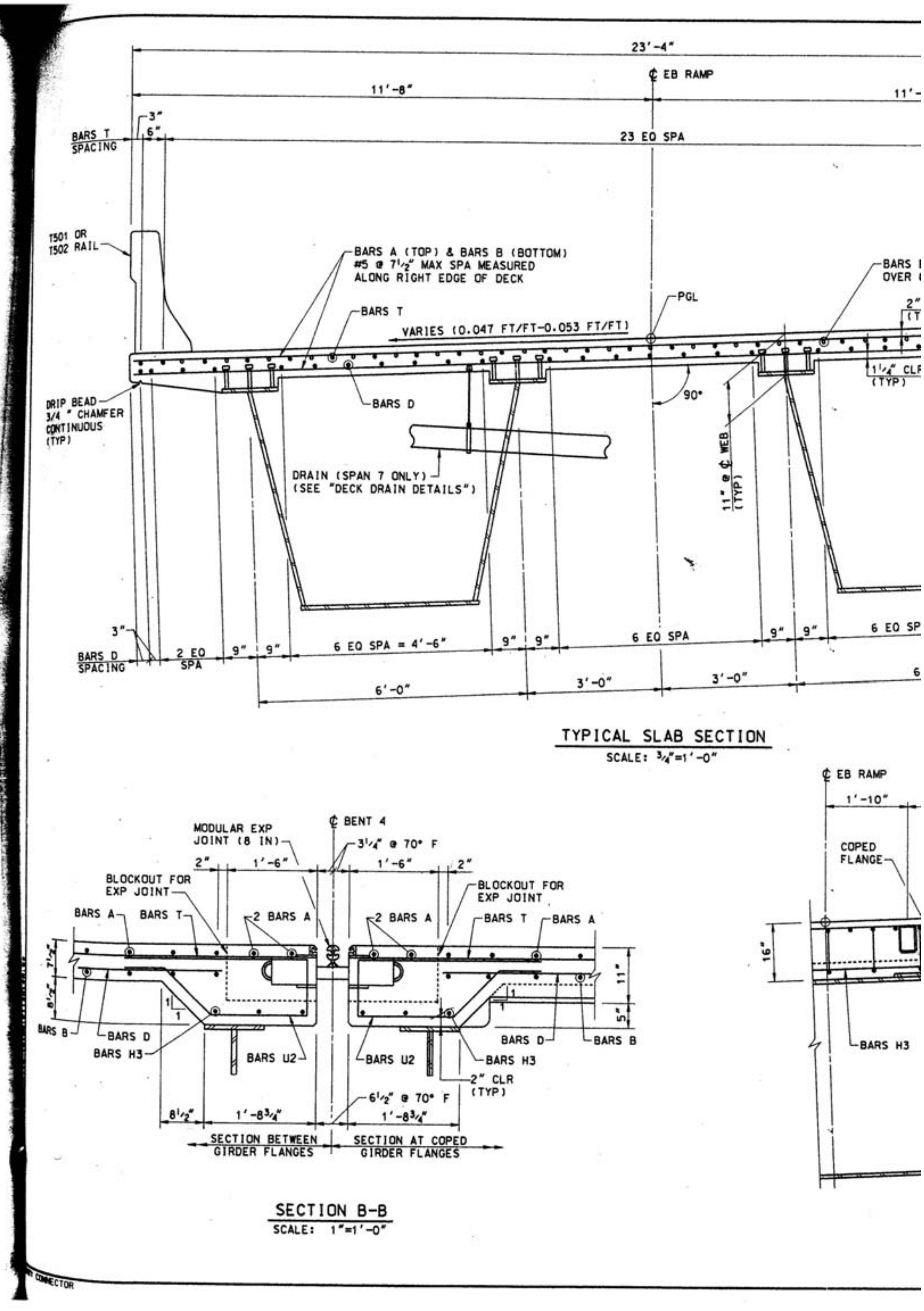
23'-4"
℄ EB RAMP
11'-8"
BARS T SPACING
3"
6"
23 EQ SPA
T501 OR T502 RAIL
BARS A (TOP) & BARS B (BOTTOM) #5 @ 7½" MAX SPA MEASURED ALONG RIGHT EDGE OF DECK
BARS T
PGL
VARIES (0.047 FT/FT-0.053 FT/FT)
DRIP BEAD 3/4" CHAMFER CONTINUOUS (TYP)
BARS D
90°
11" @ ℄ WEB (TYP)
1¼" CLR (TYP)
DRAIN (SPAN 7 ONLY) (SEE "DECK DRAIN DETAILS")
BARS D SPACING
2 EQ SPA
9"
6 EQ SPA = 4'-6"
6 EQ SPA
6'-0"
3'-0"
TYPICAL SLAB SECTION
SCALE: ¾"=1'-0"
MODULAR EXP JOINT (8 IN)
℄ BENT 4
3¼" @ 70° F
1'-6"
2"
BLOCKOUT FOR EXP JOINT
BARS A
BARS T
2 BARS A
BARS B
BARS D
BARS H3
BARS U2
2" CLR (TYP)
6½" @ 70° F
8½"
1'-8¾"
11"
5"
SECTION BETWEEN GIRDER FLANGES
SECTION AT COPED GIRDER FLANGES
SECTION B-B
SCALE: 1"=1'-0"
℄ EB RAMP
1'-10"
COPED FLANGE
16"
BARS H3

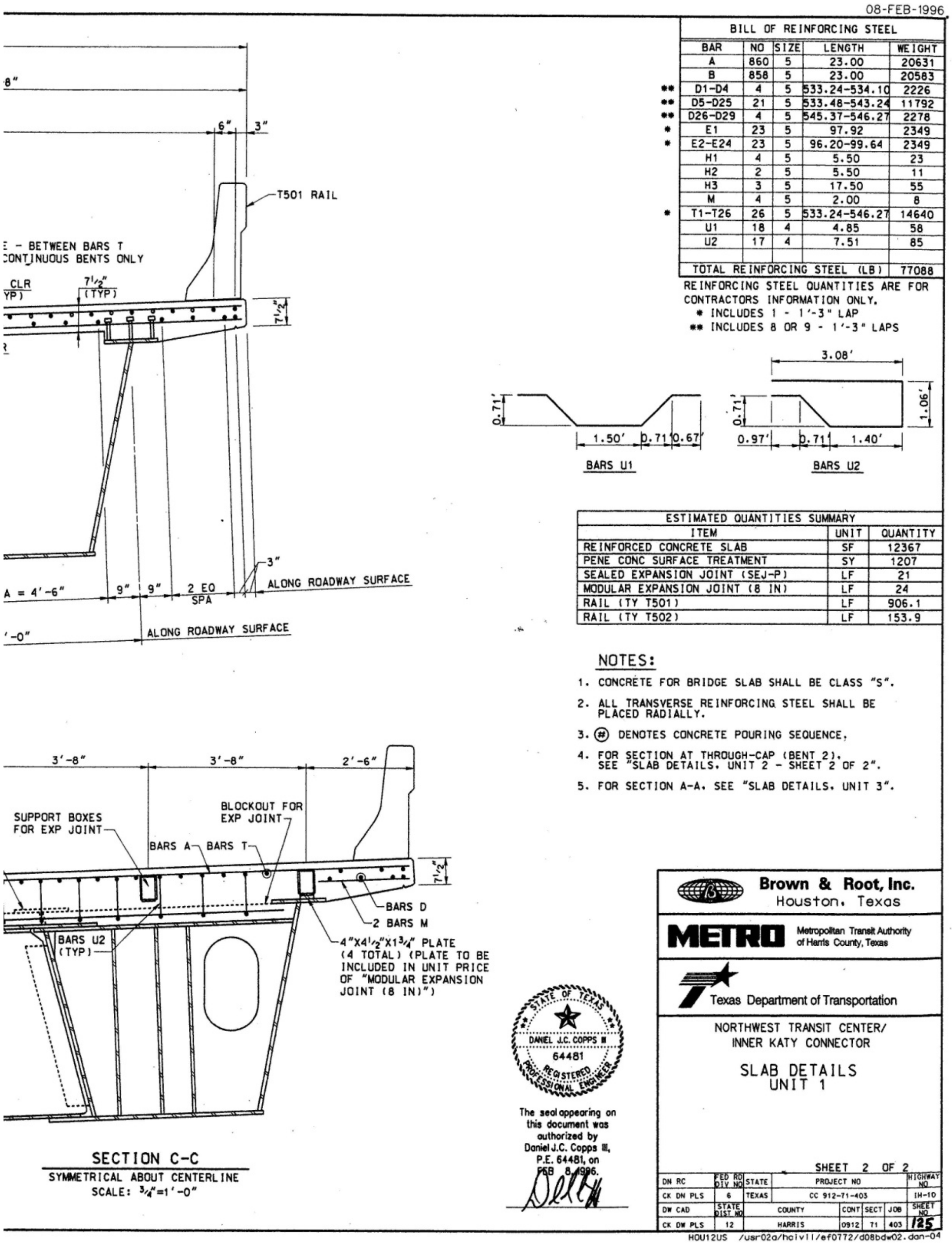

	BAR	NO	SIZE	LENGTH	WEIGHT
	A	860	5	23.00	20631
	B	858	5	23.00	20583
**	D1-D4	4	5	533.24-534.10	2226
**	D5-D25	21	5	533.48-543.24	11792
**	D26-D29	4	5	545.37-546.27	2278
*	E1	23	5	97.92	2349
*	E2-E24	23	5	96.20-99.64	2349
	H1	4	5	5.50	23
	H2	2	5	5.50	11
	H3	3	5	17.50	55
	M	4	5	2.00	8
*	T1-T26	26	5	533.24-546.27	14640
	U1	18	4	4.85	58
	U2	17	4	7.51	85
	TOTAL REINFORCING STEEL (LB)				77088

BILL OF REINFORCING STEEL

REINFORCING STEEL QUANTITIES ARE FOR CONTRACTORS INFORMATION ONLY.
* INCLUDES 1 - 1'-3" LAP
** INCLUDES 8 OR 9 - 1'-3" LAPS

ESTIMATED QUANTITIES SUMMARY

ITEM	UNIT	QUANTITY
REINFORCED CONCRETE SLAB	SF	12367
PENE CONC SURFACE TREATMENT	SY	1207
SEALED EXPANSION JOINT (SEJ-P)	LF	21
MODULAR EXPANSION JOINT (8 IN)	LF	24
RAIL (TY T501)	LF	906.1
RAIL (TY T502)	LF	153.9

NOTES:

1. CONCRETE FOR BRIDGE SLAB SHALL BE CLASS "S".
2. ALL TRANSVERSE REINFORCING STEEL SHALL BE PLACED RADIALLY.
3. (#) DENOTES CONCRETE POURING SEQUENCE.
4. FOR SECTION AT THROUGH-CAP (BENT 2), SEE "SLAB DETAILS, UNIT 2 - SHEET 2 OF 2".
5. FOR SECTION A-A, SEE "SLAB DETAILS, UNIT 3".

Figure A-7: Slab details page 3

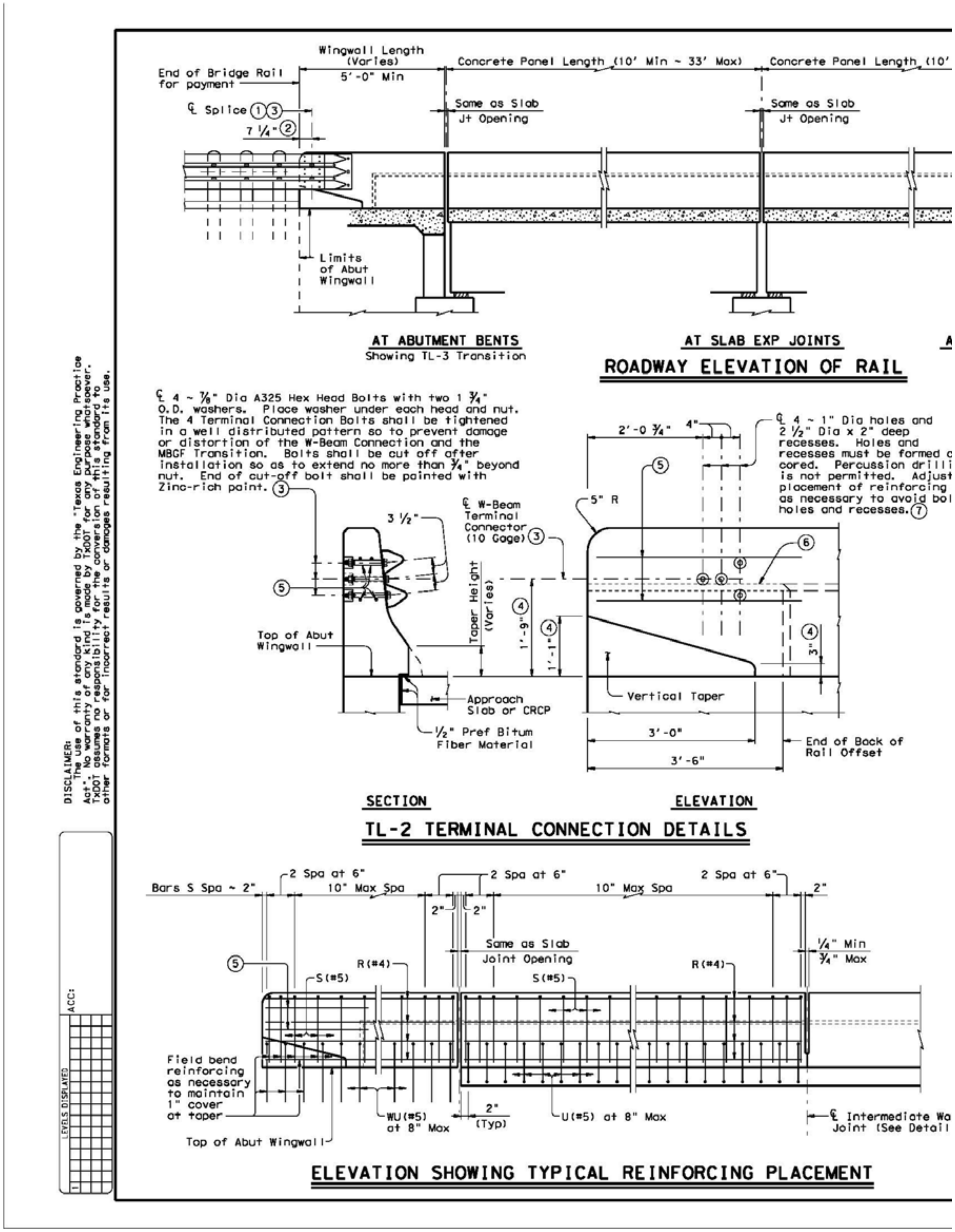
AT ABUTMENT BENTS
Showing TL-3 Transition
AT SLAB EXP JOINTS
ROADWAY ELEVATION OF RAIL
SECTION
ELEVATION
TL-2 TERMINAL CONNECTION DETAILS
ELEVATION SHOWING TYPICAL REINFORCING PLACEMENT
DISCLAIMER: The use of this standard is governed by the "Texas Engineering Practice Act". No warranty of any kind is made by TxDOT for any purpose whatsoever. TxDOT assumes no responsibility for the conversion of this standard to other formats or for incorrect results or damages resulting from its use.

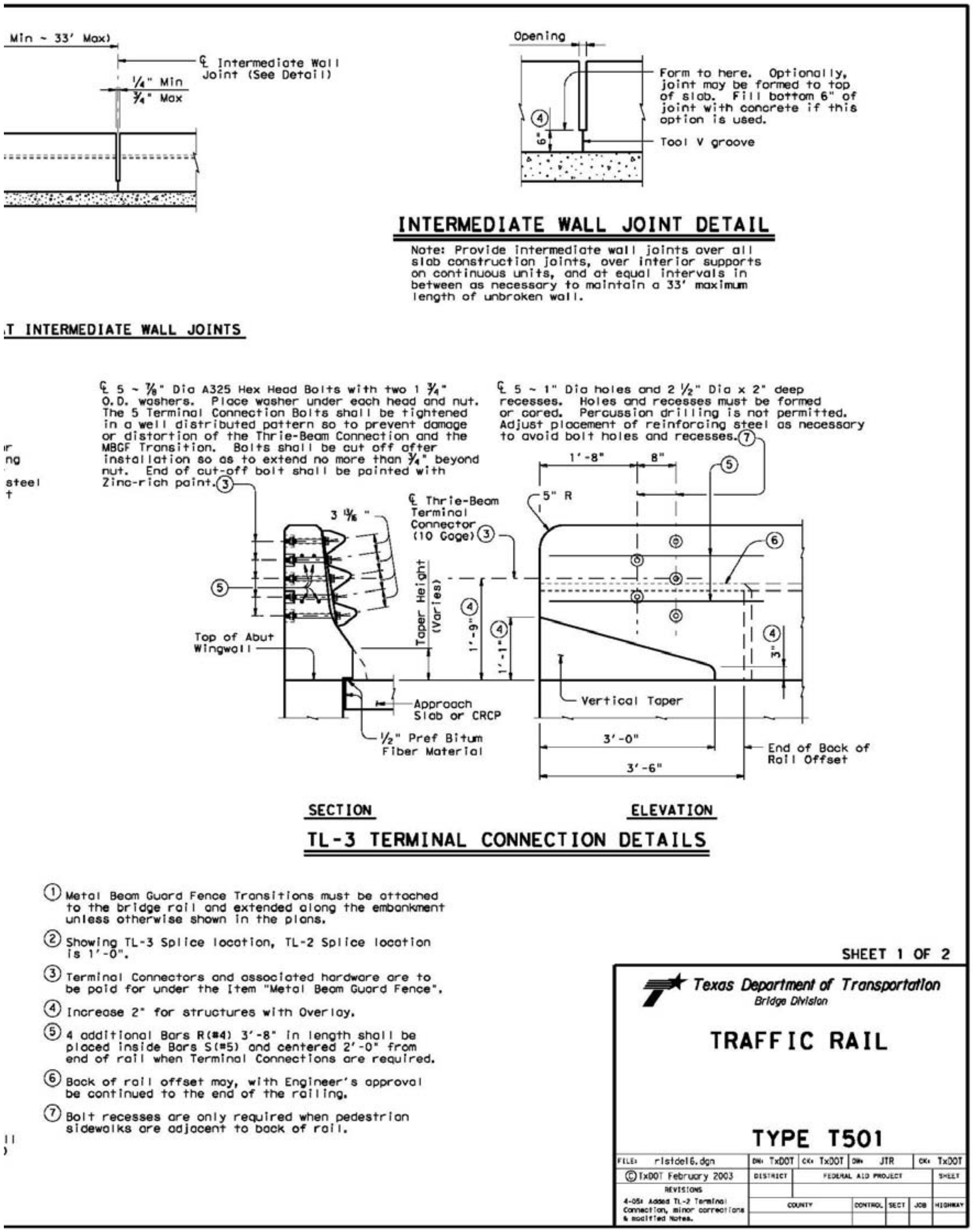

Figure A-8: T501 railing details page 1

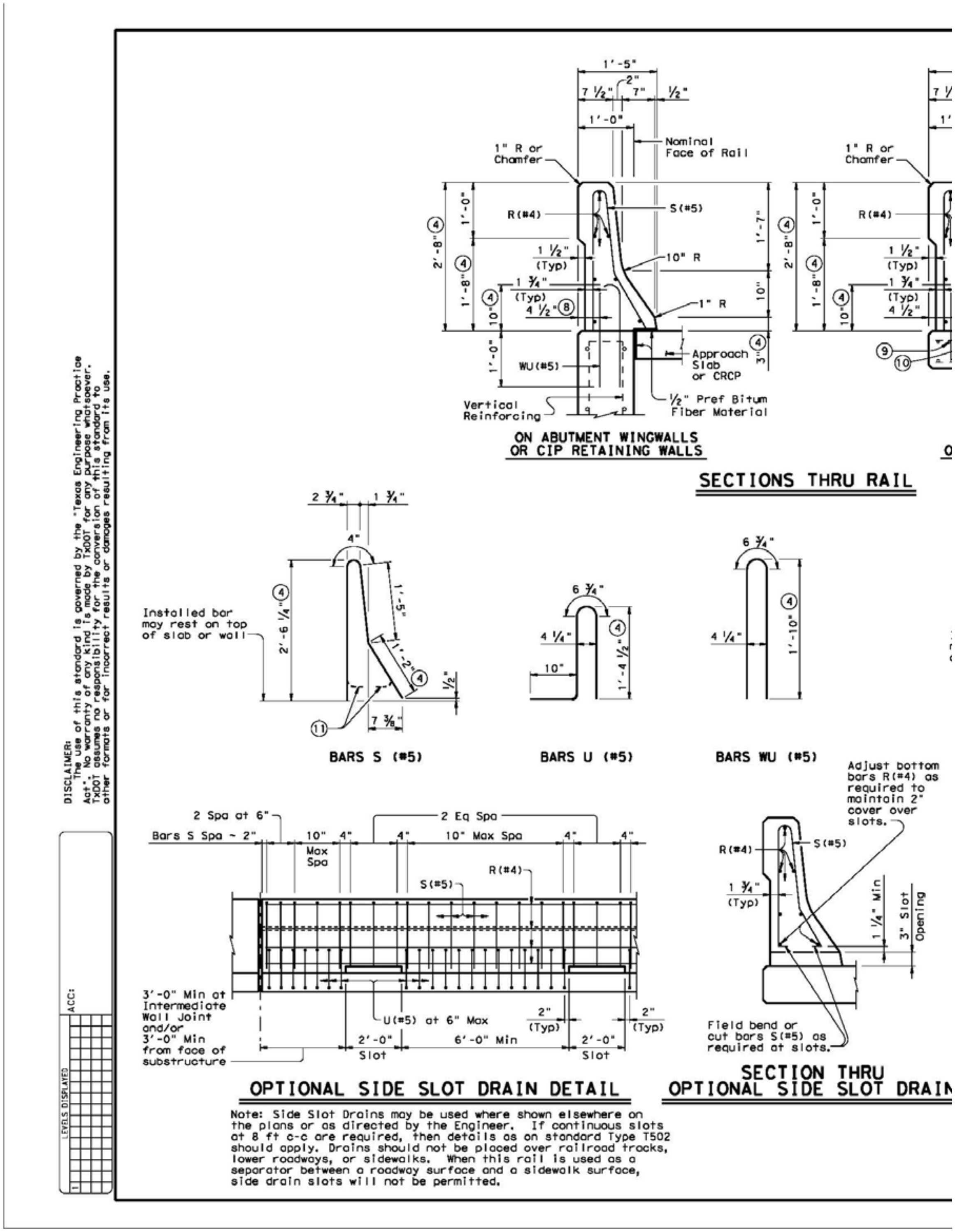
DISCLAIMER:
The use of this standard is governed by the "Texas Engineering Practice Act". No warranty of any kind is made by TxDOT for any purpose whatsoever. TxDOT assumes no responsibility for the conversion of this standard to other formats or for incorrect results or damages resulting from its use.
LEVELS DISPLAYED
ACC:
1" R or Chamfer
Nominal Face of Rail
R(#4)
S(#5)
10" R
1" R
WU(#5)
Approach Slab or CRCP
½" Pref Bitum Fiber Material
Vertical Reinforcing
ON ABUTMENT WINGWALLS OR CIP RETAINING WALLS
SECTIONS THRU RAIL
Installed bar may rest on top of slab or wall
BARS S (#5)
BARS U (#5)
BARS WU (#5)
Adjust bottom bars R(#4) as required to maintain 2" cover over slots.
2 Spa at 6"
2 Eq Spa
Bars S Spa ~ 2"
10" Max Spa
U(#5) at 6" Max
3'-0" Min at Intermediate Wall Joint and/or 3'-0" Min from face of substructure
2'-0" Slot
6'-0" Min
Field bend or cut bars S(#5) as required at slots.
3" Slot Opening
OPTIONAL SIDE SLOT DRAIN DETAIL
SECTION THRU OPTIONAL SIDE SLOT DRAIN
Note: Side Slot Drains may be used where shown elsewhere on the plans or as directed by the Engineer. If continuous slots at 8 ft c-c are required, then details as on standard Type T502 should apply. Drains should not be placed over railroad tracks, lower roadways, or sidewalks. When this rail is used as a separator between a roadway surface and a sidewalk surface, side drain slots will not be permitted.

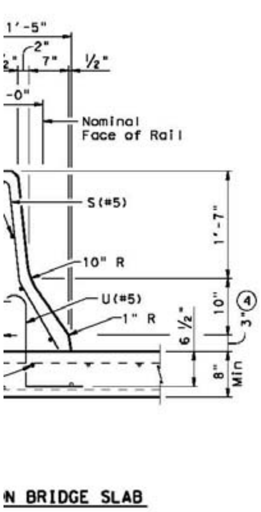

④ Increase 2" for structures with Overlay.

⑧ 5 ½" when vertical reinforcing has closer clear cover over horizontal reinforcing in abutment wingwalls or retaining walls on traffic side of wall.

⑨ As an aid in supporting reinforcement, additional longitudinal bars may be used in the slab with the approval of the Engineer. Such bars shall be furnished at the Contractors expense.

⑩ Top longitudinal slab bar may be adjusted laterally 3" ± to tie reinforcing.

⑪ Bend or cut as required to clear drain slots.

⑫ No longitudinal wires may be within upper bend.

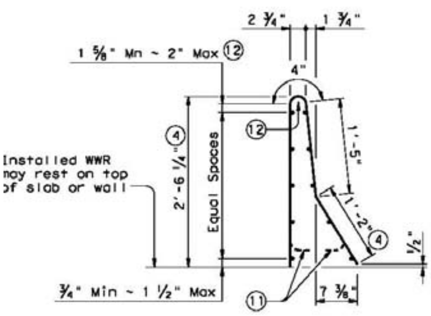

OPTIONAL WELDED WIRE REINFORCEMENT (WWR)

DESCRIPTION	LONGITUDINAL WIRES	VERTICAL WIRES
Minimum (Cumulative Total) Wire Area	0.933 Sq In.	0.248 Sq In. per Ft
	No. of Wires	Spacing
Minimum	6	4"
Maximum	11	12"
Maximum Wire Size Differential	The smaller wire shall have an area of 40% or more of the larger wire.	

GENERAL NOTES:

This rail has been evaluated and approved to be of equal strength to railings with like geometry, which have been crash tested to meet NCHRP Report 350 TL-4 criteria. This rail can be used for design speeds of 50 mph and greater when a TL-3 rated guard fence transition is used. When a TL-2 rated guard fence transition is used, this rail can only be used for design speeds of 45 mph and less.

Rail anchorage details shown on this standard may require modification for select structure types. See appropriate details elsewhere in plans for these modifications.

All steel components except reinforcing shall be galvanized unless otherwise shown on plans.

All concrete shall be Class "C".

All reinforcing steel shall be Grade 60.

Shop drawings will not be required for this rail.

This railing may be constructed with slip-forms when approved by the Engineer, with equipment approved by the Engineer. Sensor control for both line and grade must be provided. Tack welding to provide bracing for slip-form operations is acceptable. Welding can be performed at a minimum spacing of 3 ft between the cage and the anchorage. It is permissible to weld to U, WU and S bars at any location on the cage. If increased bracing is needed, additional anchorage devices must be added and welding must be performed in the upper two thirds of the cage.

The back of railing shall be vertical unless otherwise shown on the plans or approved by the Engineer.

Deformed welded wire reinforcement (WWR) may be used as an option to conventional reinforcement and shall be made in accordance with ASTM A497 (Deformed Wire). Combinations of Reinforcing Steel and WWR or configurations of WWR other than shown will be permitted when the conditions in the table are satisfied and the dimension from end of section to first welded vertical wire does not exceed 3".

Epoxy coat bars U and WU if slab bars are epoxy coated.

Average weight of railing with no overlay is 326 plf.

SHEET 2 OF 2

Texas Department of Transportation
Bridge Division

TRAFFIC RAIL

TYPE T501

FILE: rlstde16.dgn	DN: TxDOT	CK: TxDOT	DW: JTR	CK: TxDOT
© TxDOT February 2003	DISTRICT	FEDERAL AID PROJECT		SHEET
REVISIONS 4-05: Added TL-2 Terminal Connection, minor corrections & modified Notes.	COUNTY	CONTROL	SECT	JOB / HIGHWAY

Figure A-9: T501 railing details page 2

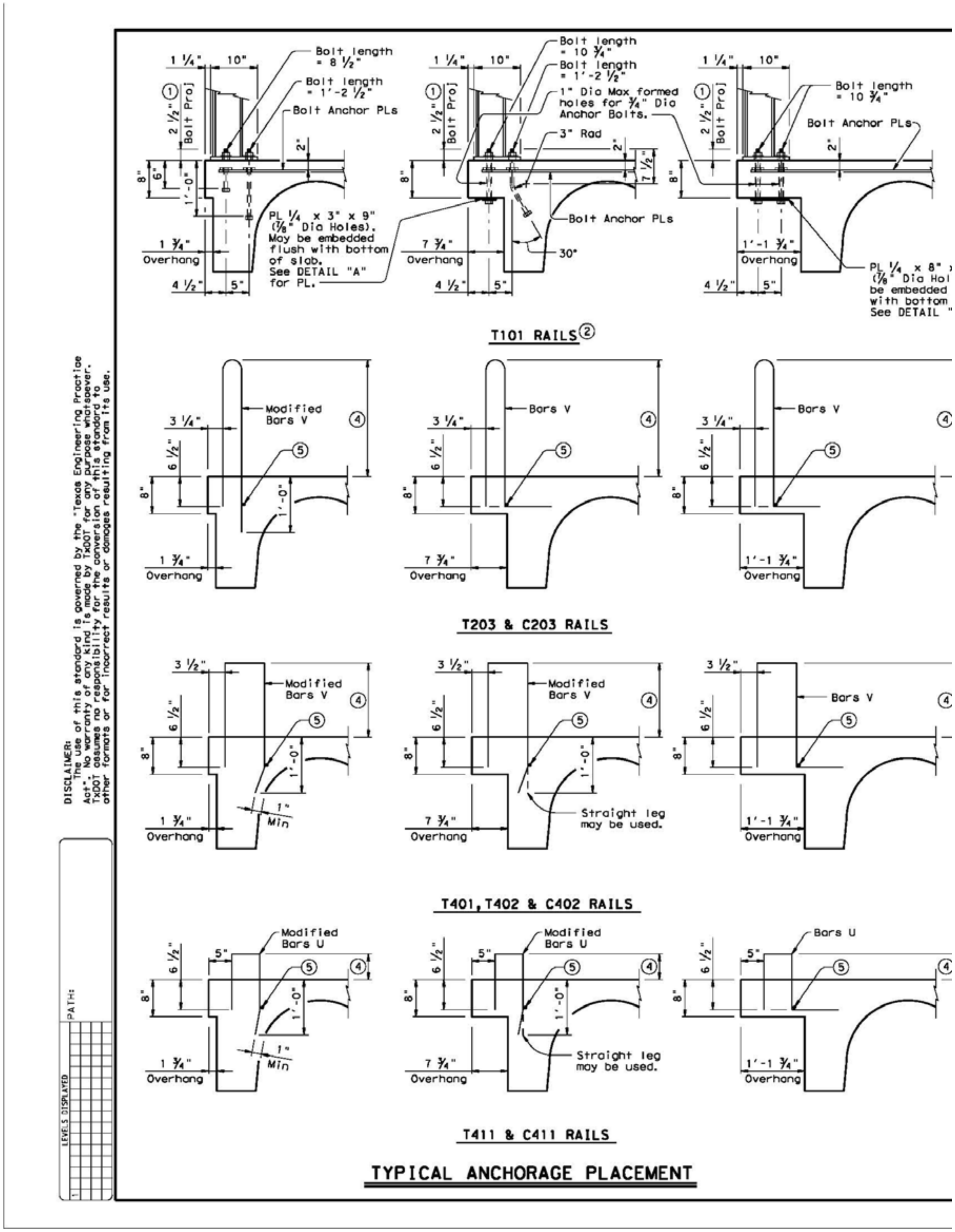

DISCLAIMER:
The use of this standard is governed by the "Texas Engineering Practice Act". No warranty of any kind is made by TxDOT for any purpose whatsoever. TxDOT assumes no responsibility for the conversion of this standard to other formats or for incorrect results or damages resulting from its use.
LEVELS DISPLAYED
PATH:
Bolt length = 8 1/2"
Bolt length = 1'-2 1/2"
Bolt Anchor PLs
Bolt length = 10 3/4"
Bolt length = 1'-2 1/2"
1" Dia Max formed holes for 3/4" Dia Anchor Bolts.
3" Rad
Bolt Anchor PLs
30°
PL 1/4 x 3" x 9" (7/8" Dia Holes). May be embedded flush with bottom of slab. See DETAIL "A" for PL.
Bolt Pro j
Overhang
T101 RAILS ②
Modified Bars V
Bars V
T203 & C203 RAILS
Straight leg may be used.
1" Min
T401, T402 & C402 RAILS
Modified Bars U
Bars U
T411 & C411 RAILS
TYPICAL ANCHORAGE PLACEMENT

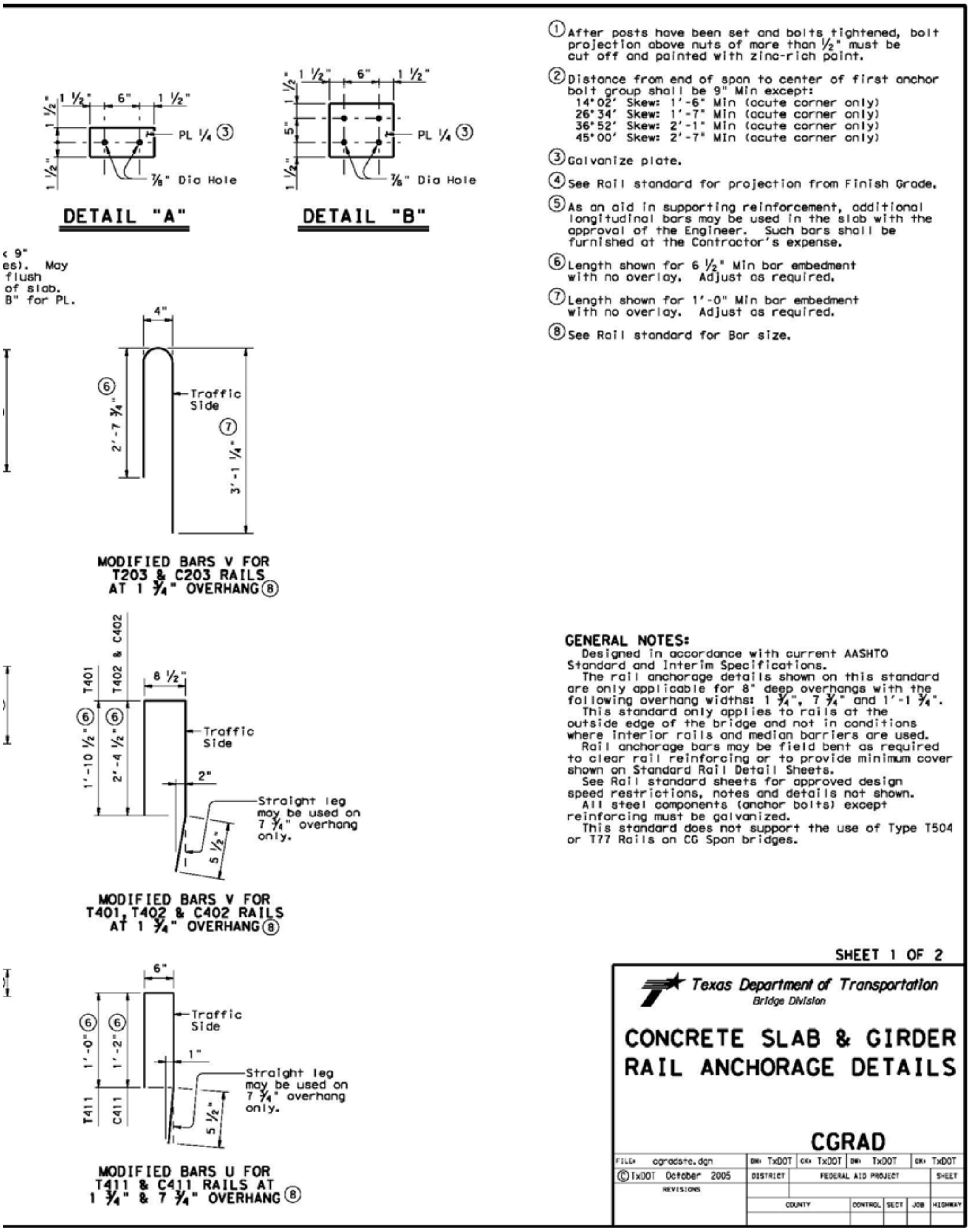

Figure A-10: Railing anchorage details page 1

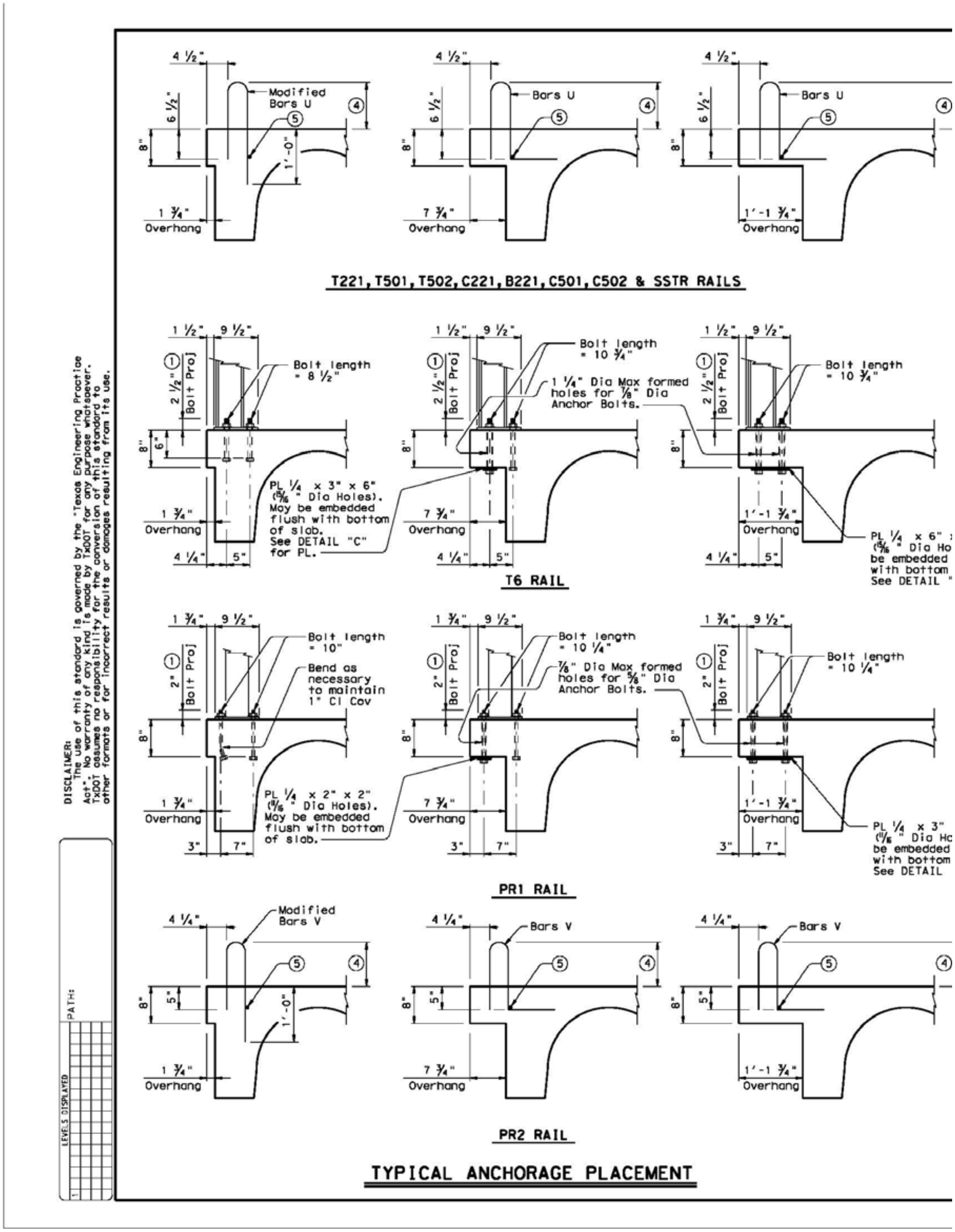
T221, T501, T502, C221, B221, C501, C502 & SSTR RAILS
T6 RAIL
PR1 RAIL
PR2 RAIL
TYPICAL ANCHORAGE PLACEMENT
Modified Bars U
Bars U
Bolt length = 8 1/2"
Bolt length = 10 3/4"
1 1/4" Dia Max formed holes for 7/8" Dia Anchor Bolts.
PL 1/4 x 3" x 6" (15/16" Dia Holes). May be embedded flush with bottom of slab. See DETAIL "C" for PL.
Bolt length = 10"
Bend as necessary to maintain 1" Cl Cov
Bolt length = 10 1/4"
7/8" Dia Max formed holes for 5/8" Dia Anchor Bolts.
PL 1/4 x 2" x 2" (11/16" Dia Holes). May be embedded flush with bottom of slab.
Modified Bars V
Bars V
Overhang
Bolt Proj
DISCLAIMER: The use of this standard is governed by the "Texas Engineering Practice Act". No warranty of any kind is made by TxDOT for any purpose whatsoever. TxDOT assumes no responsibility for the conversion of this standard to other formats or for incorrect results or damages resulting from its use.
PATH:
LEVELS DISPLAYED

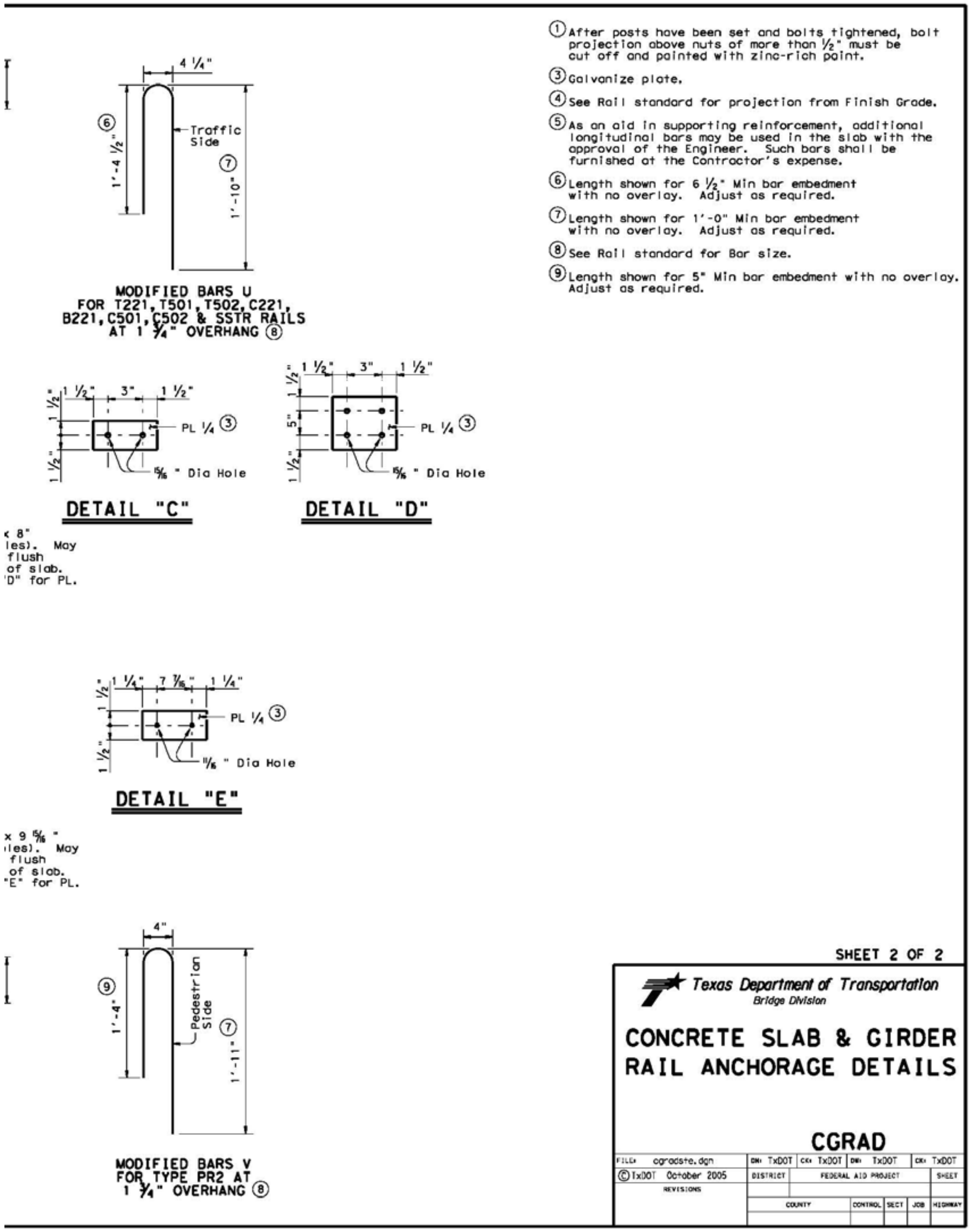

Figure A-11: Railing anchorage details page 2

A.2 SUPPORTING ELEMENT DETAILS

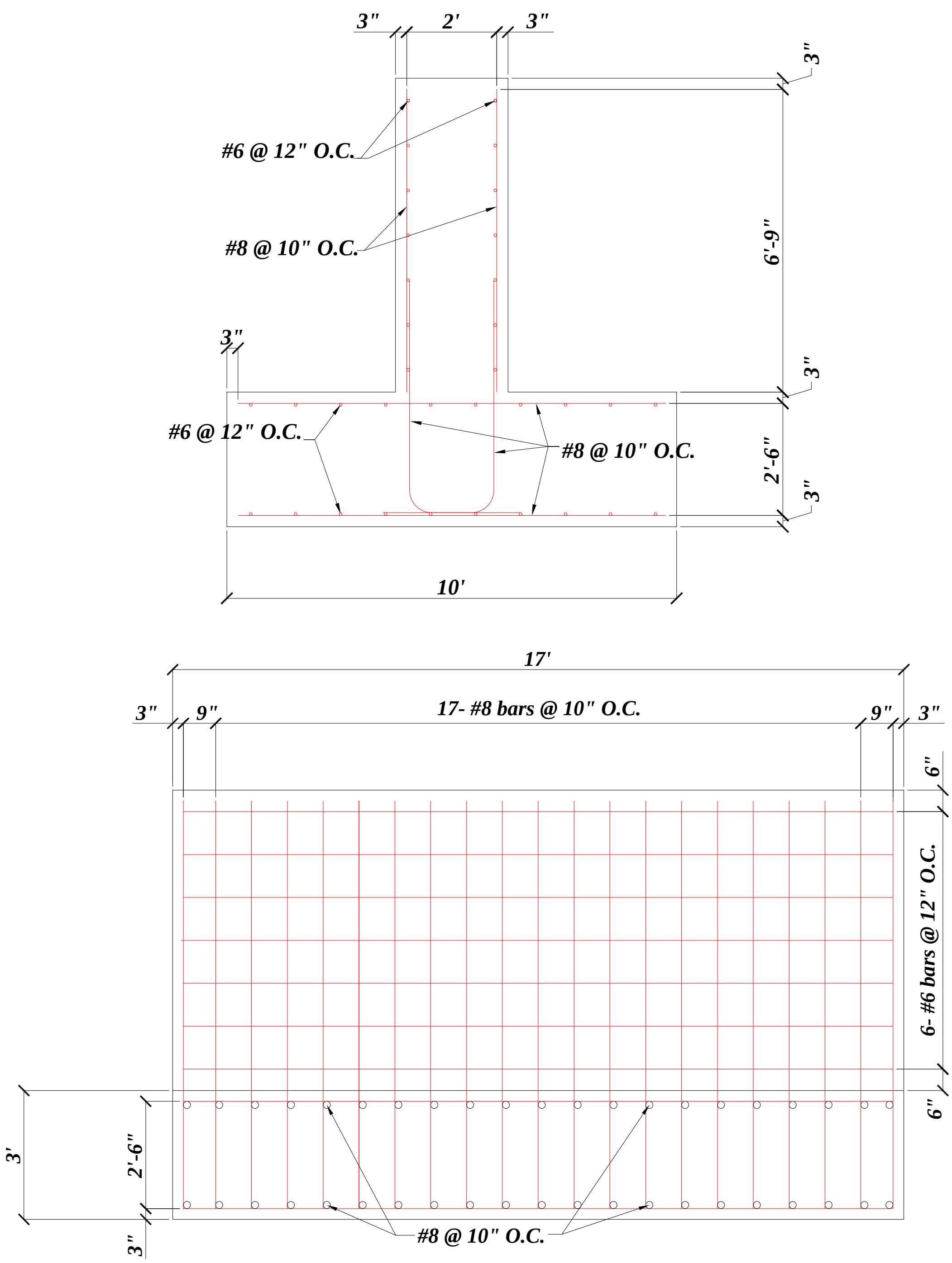

Figure A-12: Abutment design, (top) cross-section, (bottom) elevation view

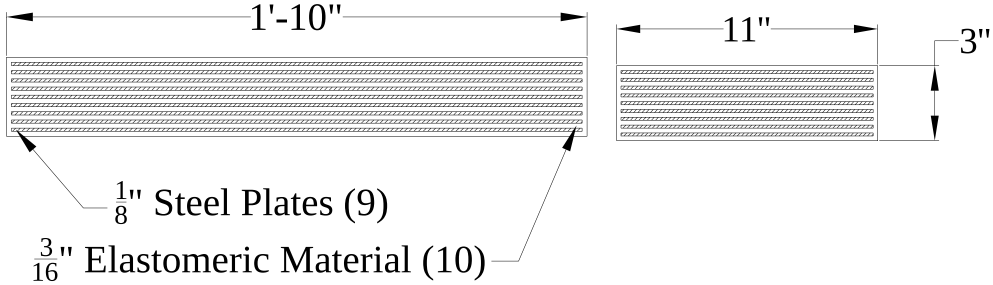

Figure A-13: Bearing pad design

A.3 BLAST SHIELD DESIGN

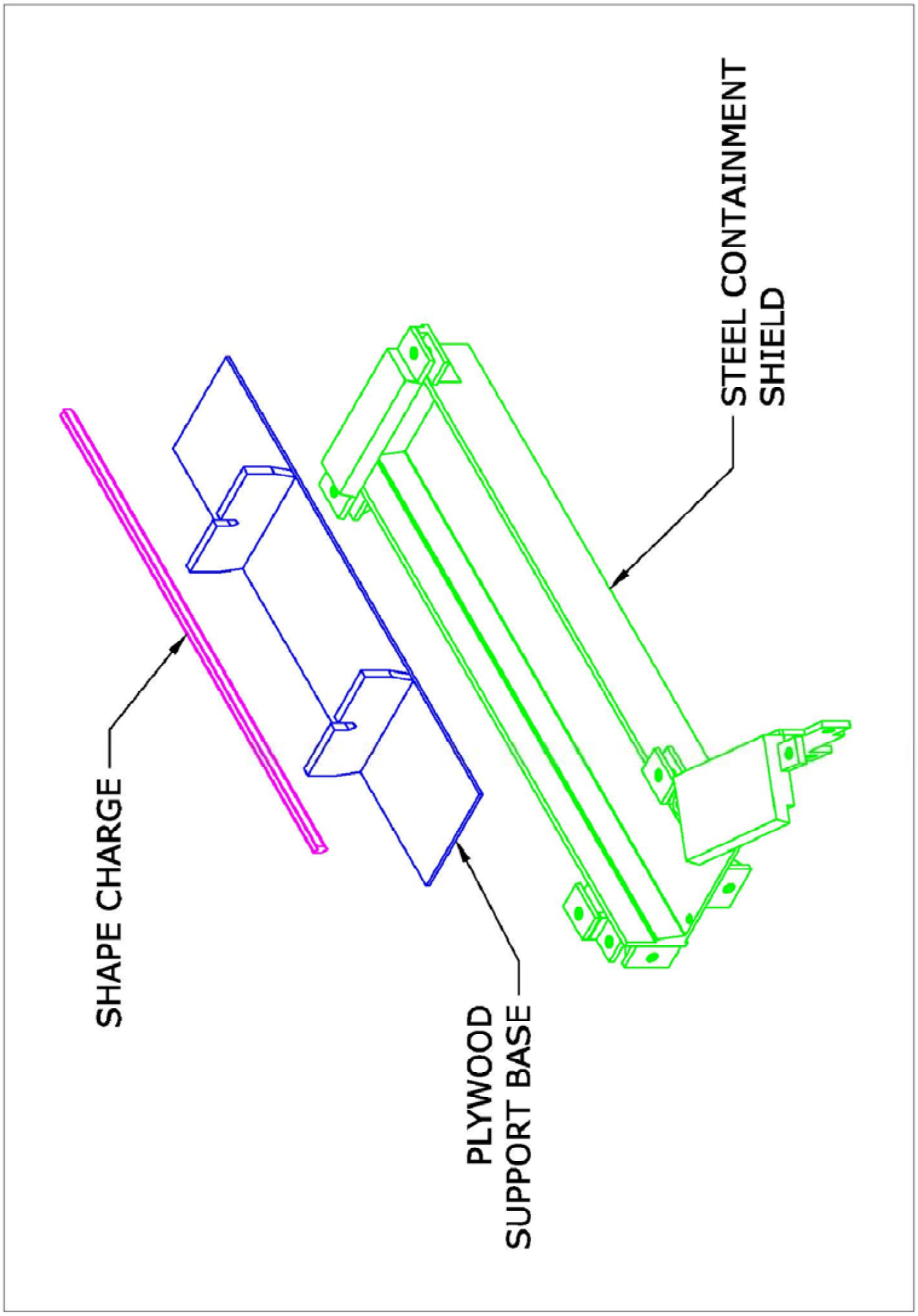

Figure A-14: Containment shield components

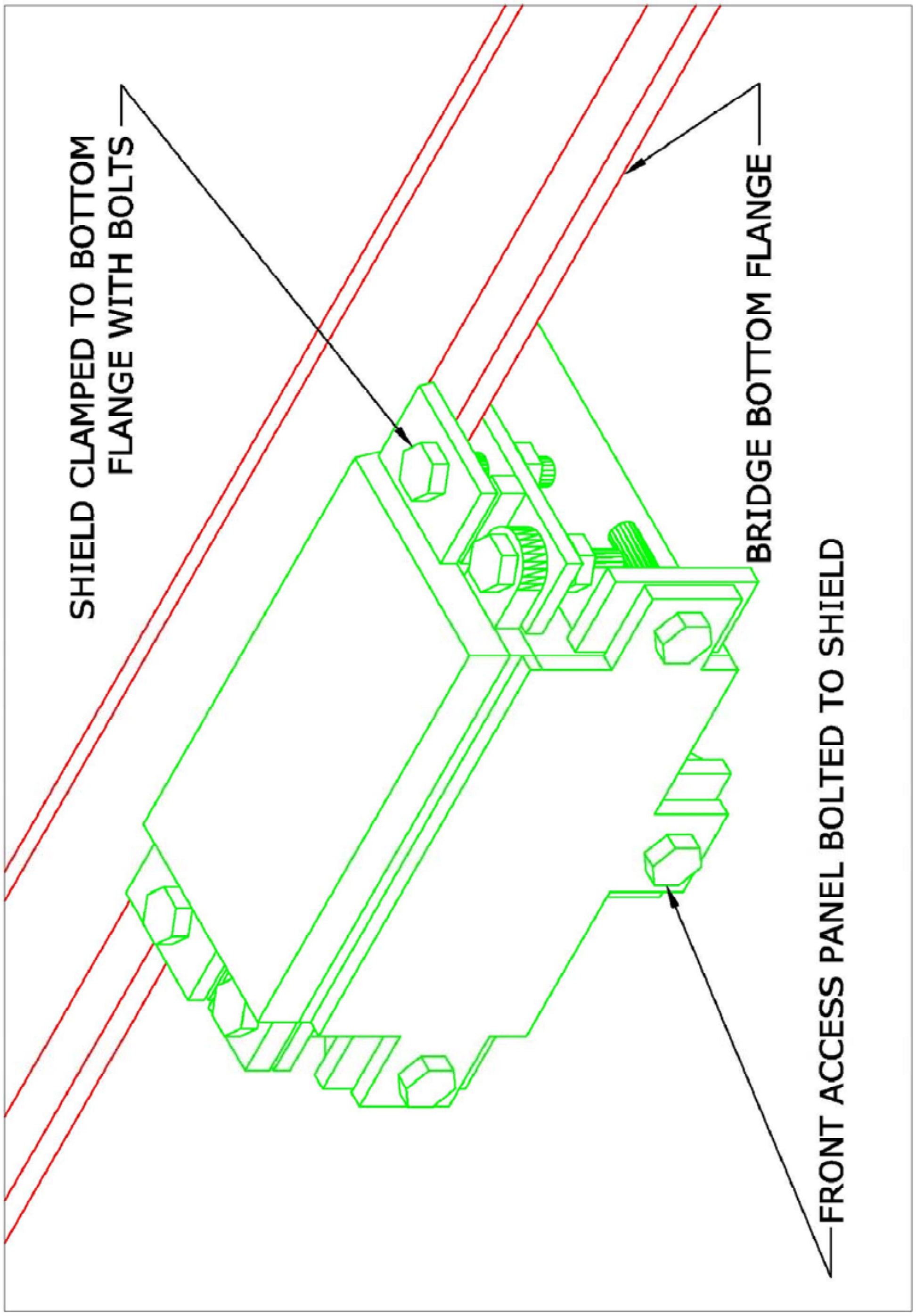

Figure A-15: Containment shield attachment

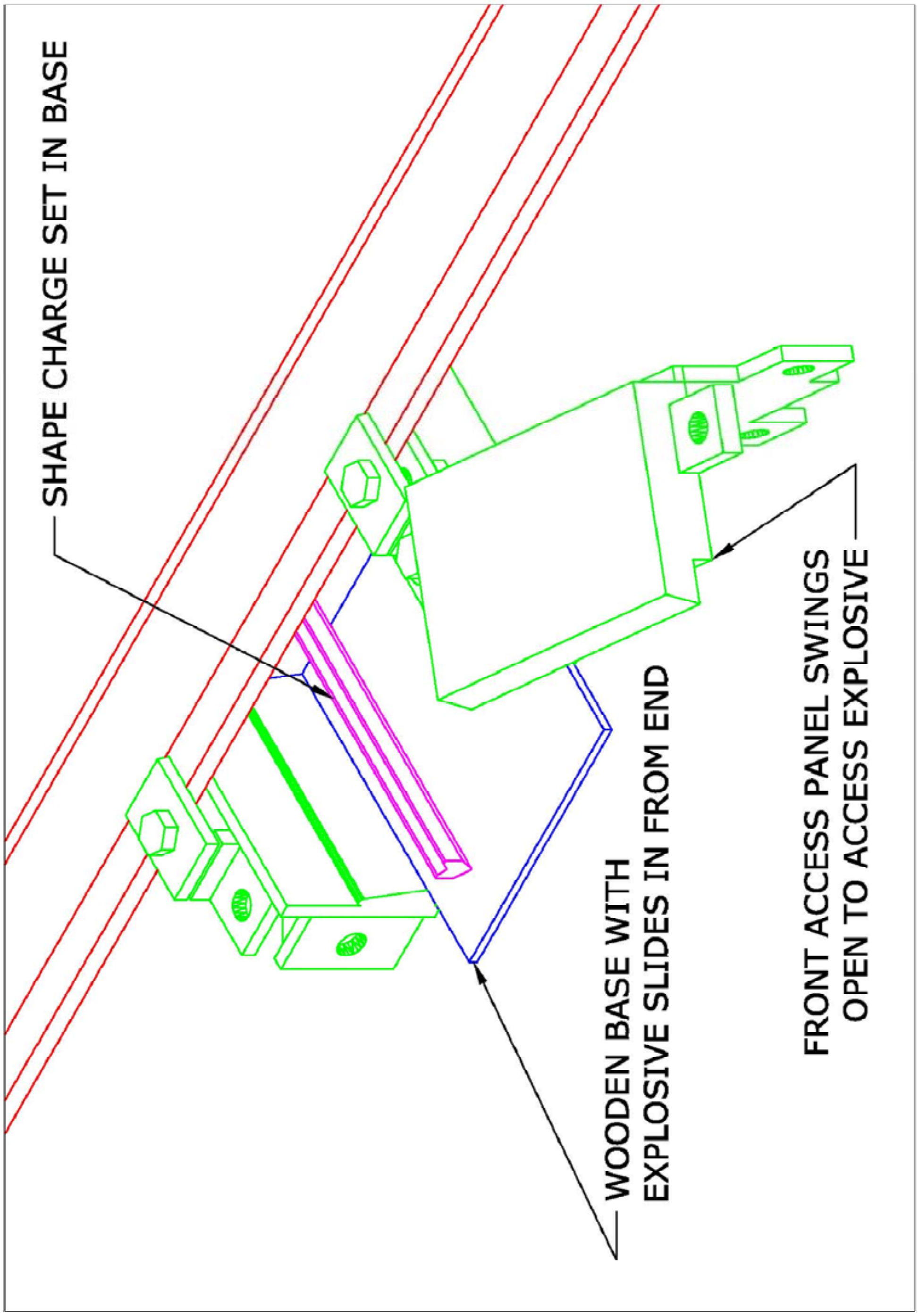

Figure A-16: Containment shield front access panel detail

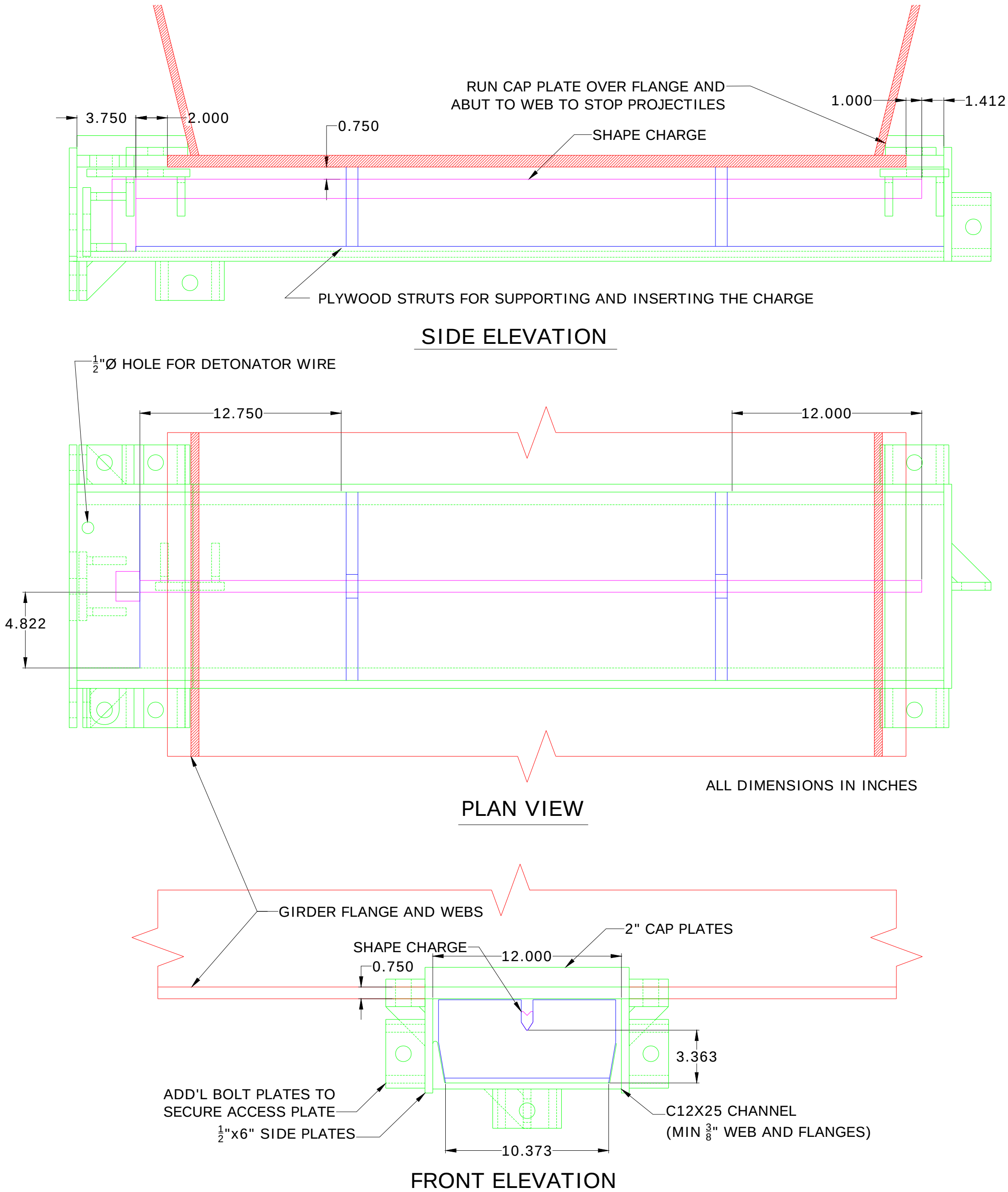

Figure A-17: Containment shield design details

A.4 SCISSOR JACK DESIGN

Table A-3: Scissor-jack component specifications

Section	Material Specification	Fy (ksi)
HSS 10 X 2X 3/8	A500 GDB	46
HSS 4 X2 X 3/8	A500 GDB	46
3/4" PLATE	A36	36
1/2" PLATE	A36	36
1.75"D Rounds	A193 GDB7 Cold Rolled Alloy Unthreaded	100
2.0"D Rounds	A193 GDB7 Cold Rolled Alloy Unthreaded	100

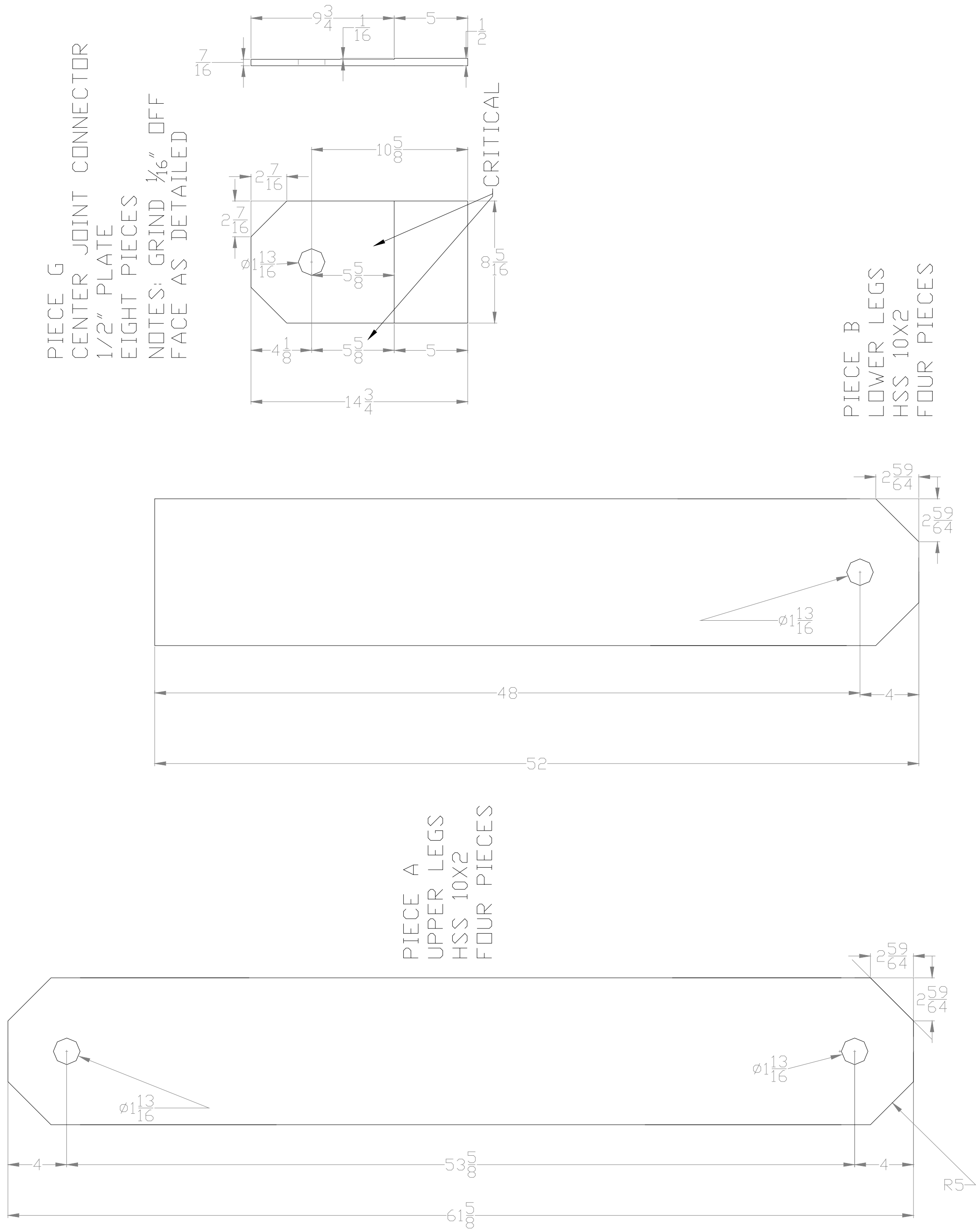

Figure A-18: Scissor-jack components, page 1

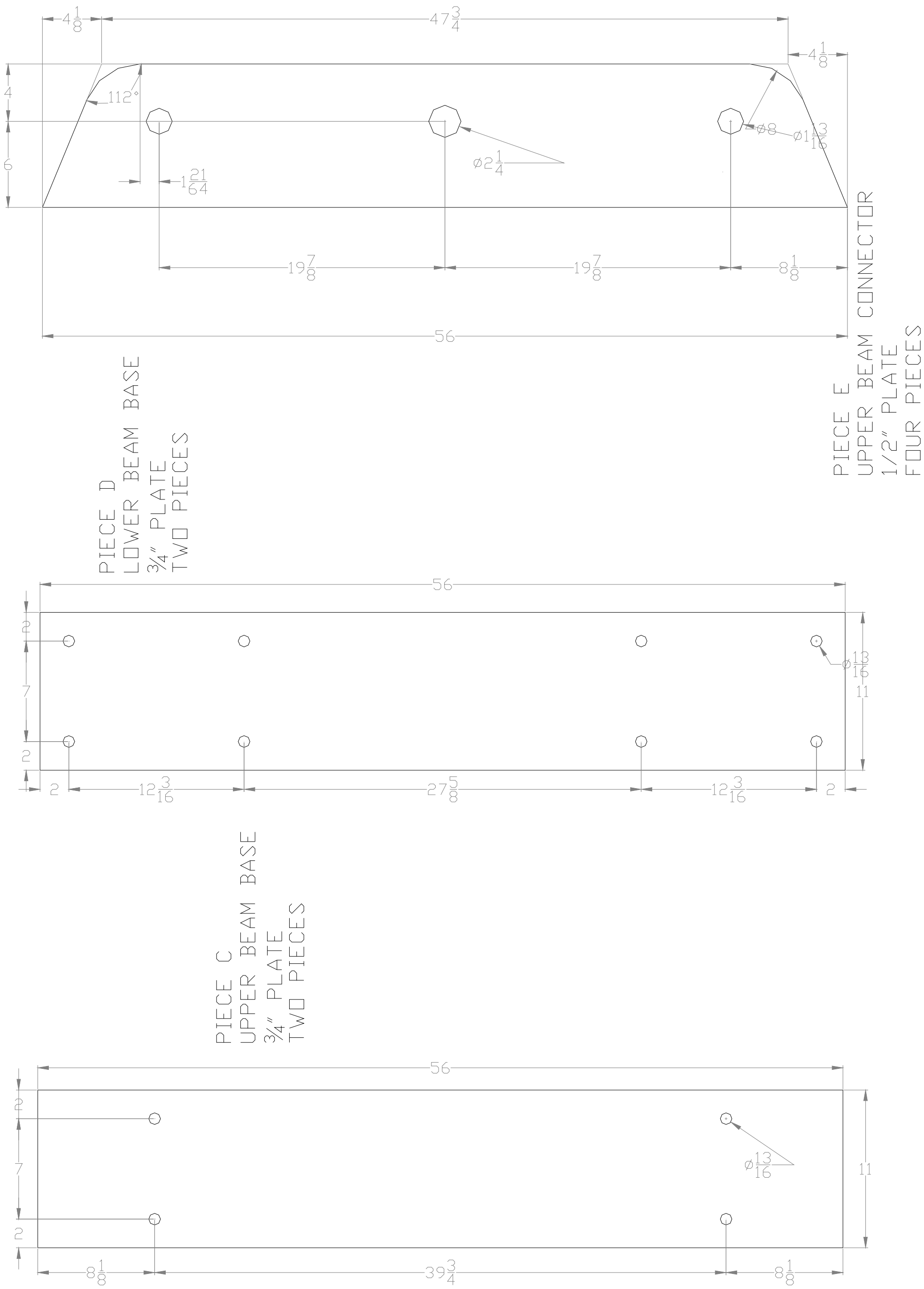

Figure A-19: Scissor-jack components, page 2

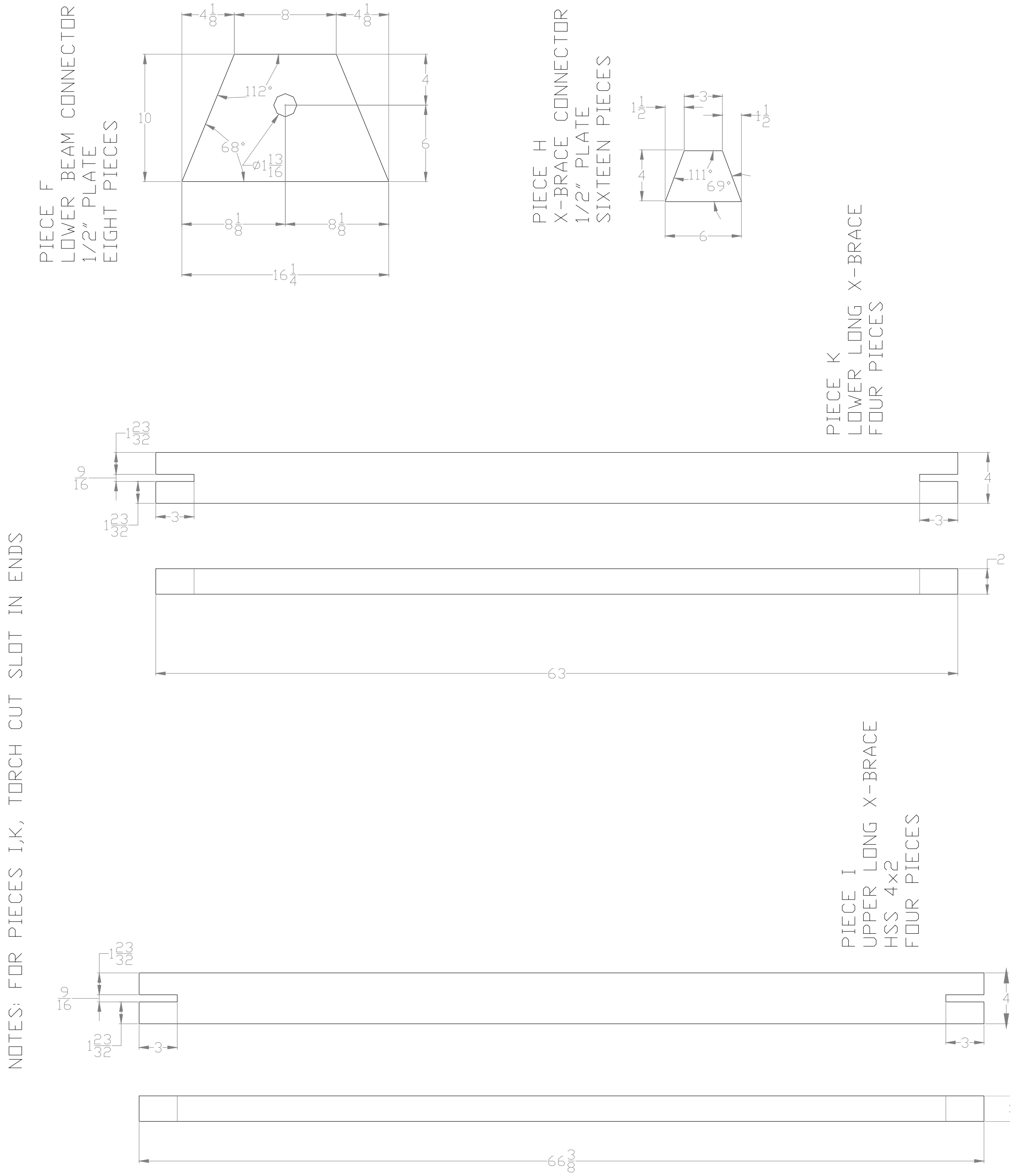

Figure A-20: Scissor-jack components, page 3

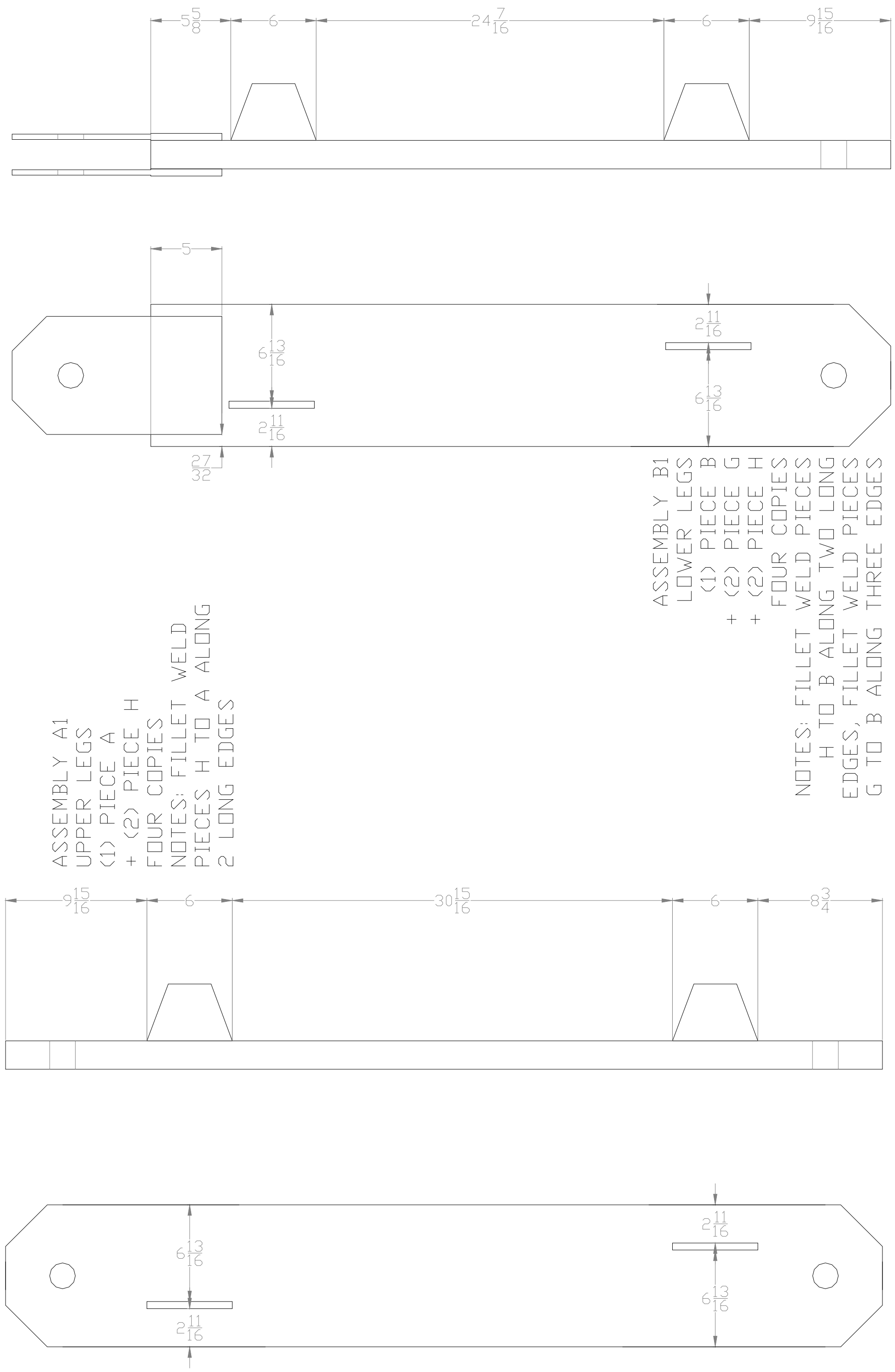

Figure A-21: Scissor-jack assemblies, page 1

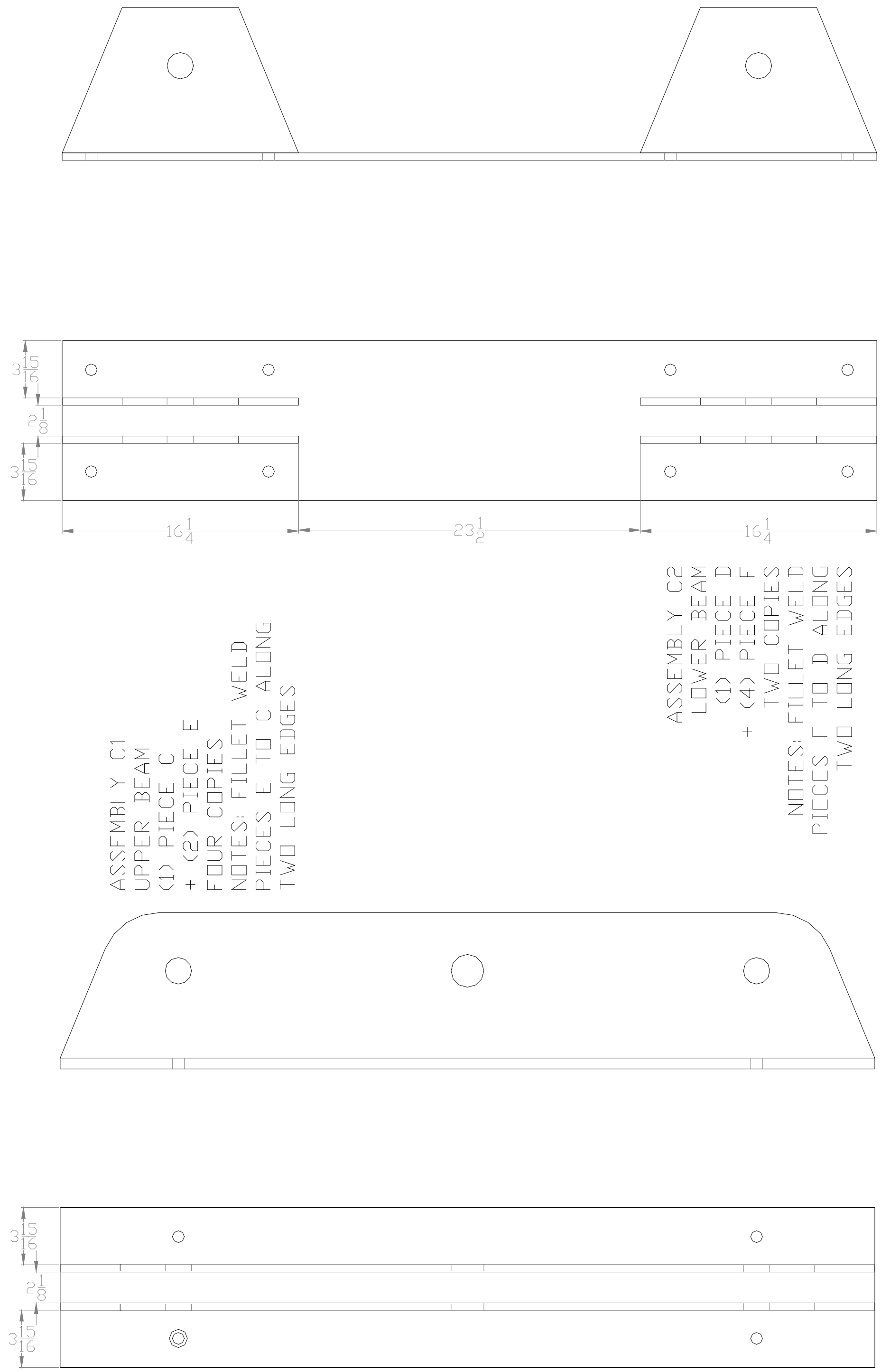

Figure A-22: Scissor-jack assemblies, page 2

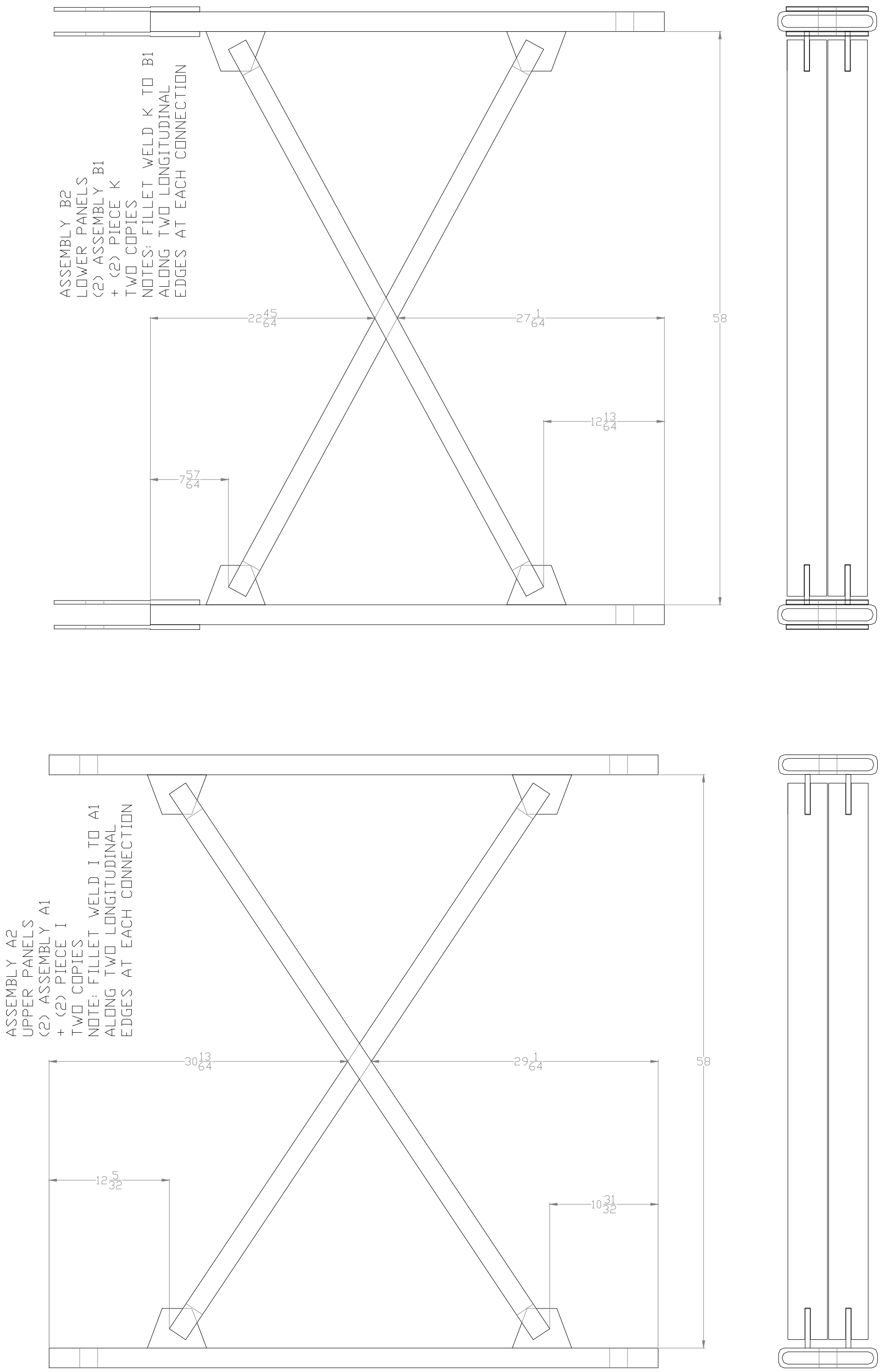

Figure A-23: Scissor-jack assemblies, page 3

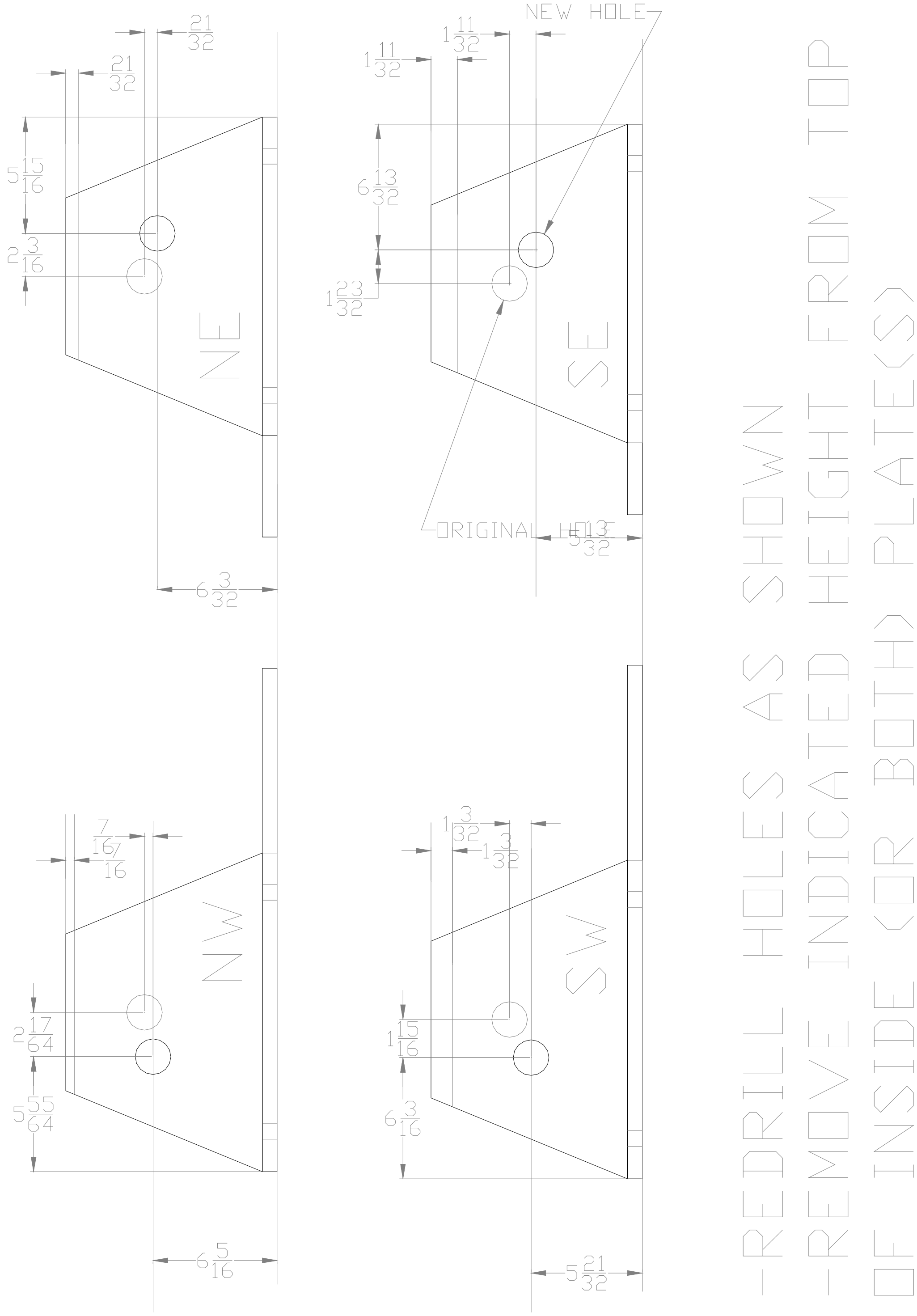

Figure A-24: Modifications to scissor-jack base plates

A.5 SLAB DESIGN

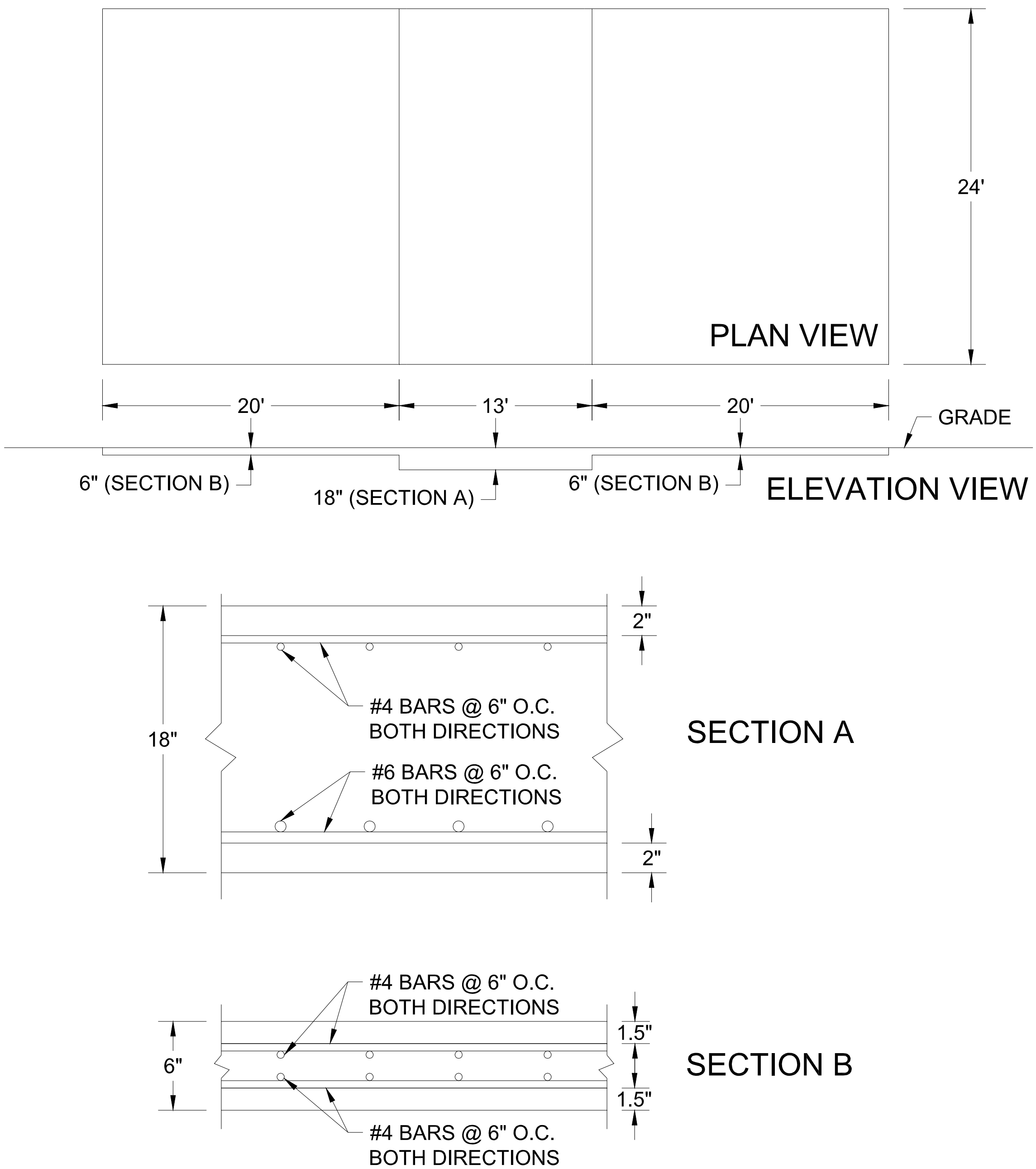

Figure A-25: Slab design details

APPENDIX B

Instrumentation

B.1 GENERAL

Table B-1: Glossary of instrumentation codes

Code	Description
N4, N3.5, … S4	Location of the gage according to the defined sections
WG	West Girder (Intact Girder)
WG1	West Girder (Western Edge of Bottom Flange)
WG2	West Girder (Eastern Edge of Bottom Flange)
RA, RB, RC	1st, 2nd and 3rd Component of the Rosette
OND	Outside North Diaphragm
IND	Inside North Diaphragm
OSD	Outside South Diaphragm
ISD	Inside South Diaphragm
EG	East Girder (Fractured Girder)
EG1	East Girder (Western Edge of Bottom Flange)
EG2	East Girder (Eastern Edge of Bottom Flange)
NCL or SCL	Just North or South of the CL
IEW	Inside East Web
OEW	Outside East Web
IWW	Inside West Web
OWW	Outside West Web
IBF	Inside Bottom Flange
OBF	Outside Bottom Flange
IF	Interior Top Flange of the Fractured Girder
TF	Exterior Top Flange of the Fractured Girder
ITF or InteriorTF	Interior Top Flange of the Fractured Girder
LP	Linear Potentiometer
SD	South Diaphragm
SP	String Potentiometer
TD	Top Deck
TC1	Transverse Concrete Gage (Western one)
TC5	Transverse Concrete Gage (Eastern one)
LC	Longitudinal Concrete Gage
ER	East Railing

WR	West Railing
MH	Middle Height of the Railing for sections N2, N1, S1, S2
MH	6 in. from Top Surface of the Railing for sections NCL, SCL
MH2	12 in. from Top Surface of the Railing for sections NCL, SCL

Table B-2: Typical gage models

Gage Type	Manufacturer	Model #	Gage Length
Bolt / Shear Stud	TML/Texas Measurements	BTM-6C	6 mm
Uni-axial steel	Vishay	CEA-06-250UN-350/P2	0.25 in.
Rosette steel	Vishay	CEA-06-250UR-350/P2	0.25 kn.
Uni-axial concrete	TML/Texas Measurements	PL-60-120-11-3LT	60 mm

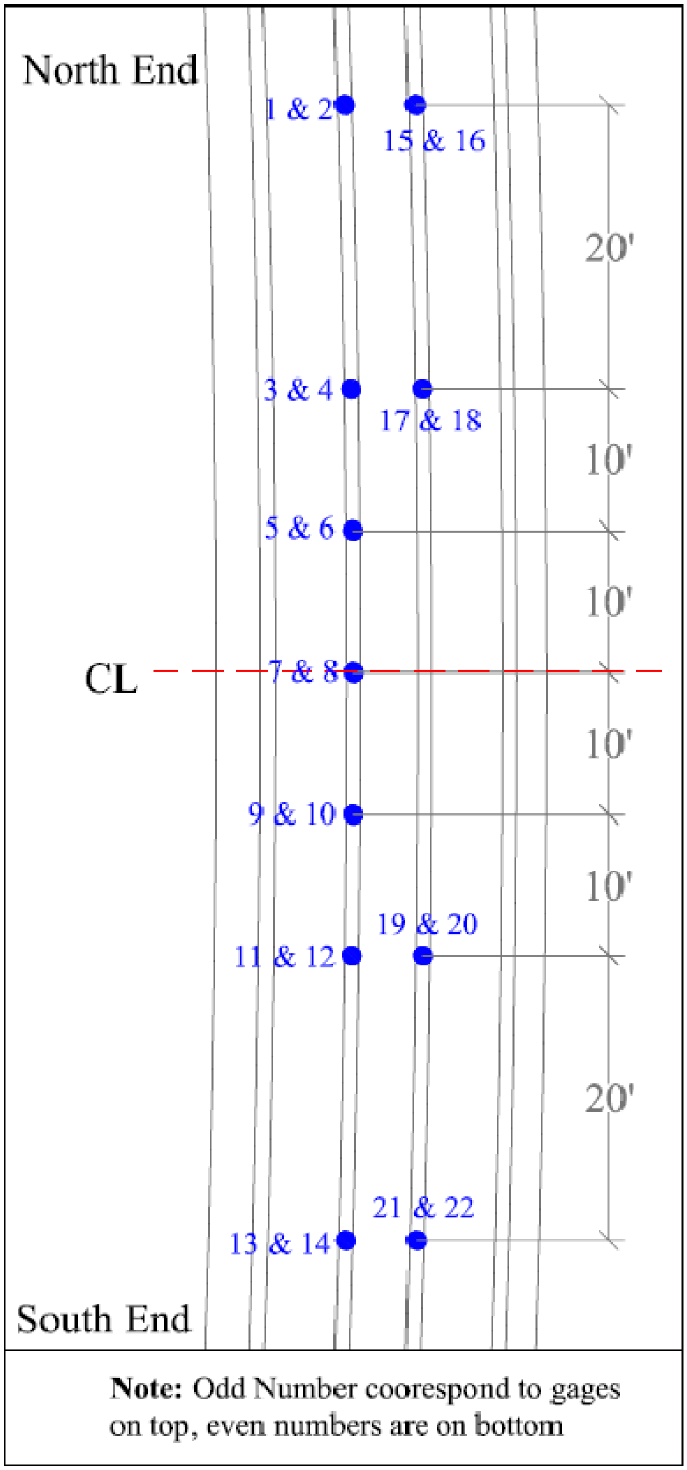

Figure B-1: Reinforcing bar foil gage locations

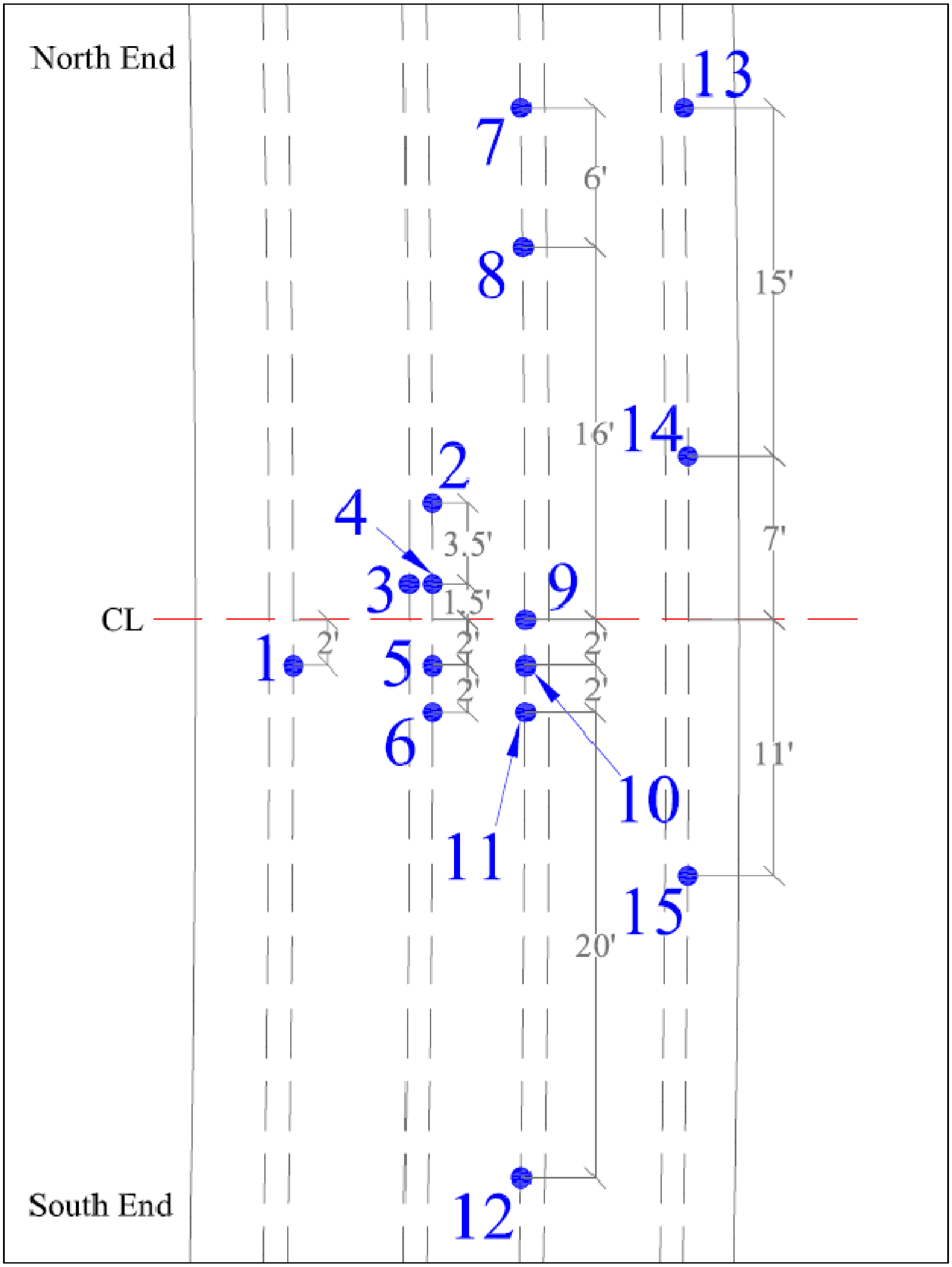

Figure B-2: Shear stud foil gage locations

B.2 FULL-SCALE TEST 1

Figure B-3: S1 foil and rosette gage locations (Test 1)

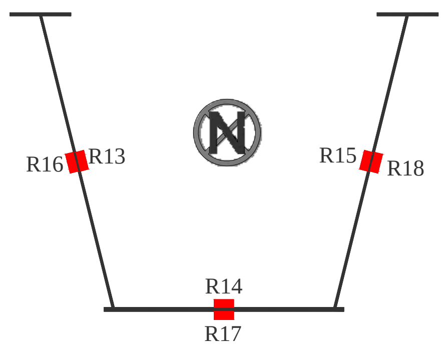

Figure B-4: N1 rosette gage locations (Test1)

Table B-3: Index of instrumentation channels (Test 1)

Gage Range	Location Information
FR1-22	Figure B-1
FS1-15	Figure B-2
R1-18	Figure B-3 Figure B-4
F1-18	Figure B-3

Index	Gage Name
0	FR 1
1	FR 2
2	FR 3
3	FR 4
4	FR 5
5	FR 6

Index	Gage Name
43	R 4a
44	R 4b
45	R 4c
46	R 5a
47	R 5b
48	R 5c

Index	Gage Name
86	R 18b
87	R 18c
88	DR 19a
89	DR 19b
90	DR 19c
91	DR 20a

6	FR 7
7	FR 8
8	FR 9
9	FR 10
10	FR 11
11	FR 12
12	FR 13
13	FR 14
14	FR 15
15	FR 16
16	FR 17
17	FR 18
18	FR 19
19	FR 20
20	FR 21
21	FR 22
22	FS 1
23	FS 2
24	FS 3
25	FS 4
26	FS 5
27	FS 6
28	FS 8
29	FS 9
30	FS 10
31	FS 11
32	FS 12
33	FS 15
34	R 1a
35	R 1b
36	R 1c
37	R 2a
38	R 2b
39	R 2c
40	R 3a
41	R 3b
42	R 3c

49	R 6a
50	R 6b
51	R 6c
52	R 7a
53	R 7b
54	R 7c
55	R 8a
56	R 8b
57	R 8c
58	R 9a
59	R 9b
60	R 9c
61	R 10a
62	R 10b
63	R 10c
64	R 11a
65	R 11b
66	R 11c
67	R 12a
68	R 12b
69	R 12c
70	R 13a
71	R 13b
72	R 13c
73	R 14a
74	R 14b
75	R 14c
76	R 15a
77	R 15b
78	R 15c
79	R 16a
80	R 16b
81	R 16c
82	R 17a
83	R 17b
84	R 17c
85	R 18a

92	DR 20b
93	DR 20c
94	DR 21a
95	DR 21b
96	DR 21c
97	DR 22a
98	DR 22b
99	DR 22c
100	Empty
101	Empty
102	Empty
103	Empty
104	F 1
105	F 2
106	F 3
107	F 4
108	F 5
109	F 6
110	F 7
111	F 8
112	F 9
113	F 10
114	F 11
115	F 12
116	F 13
117	F 14
118	F 15
119	F 16
120	F 17
121	F 18
122	F 19
123	F 20
124	F 21
125	F 22
126	F 23
127	F 24

B.3 FULL-SCALE TEST 2

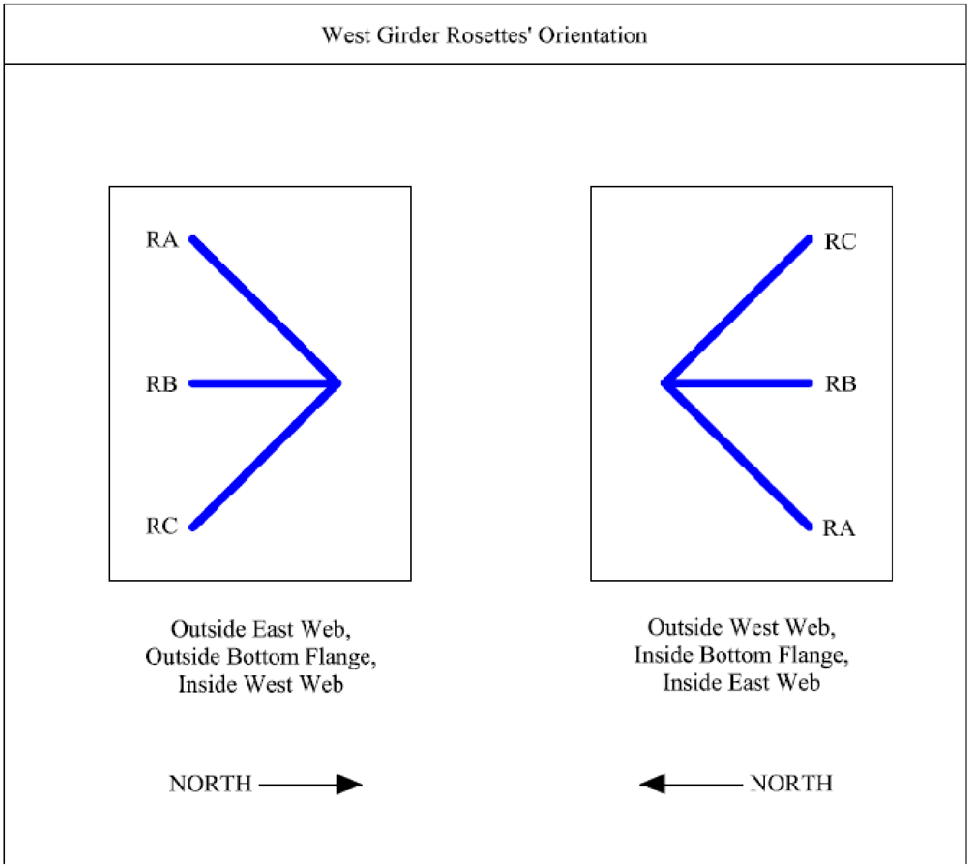

Figure B-5: Intact girder rosette orientation (Tests 2 and 3)

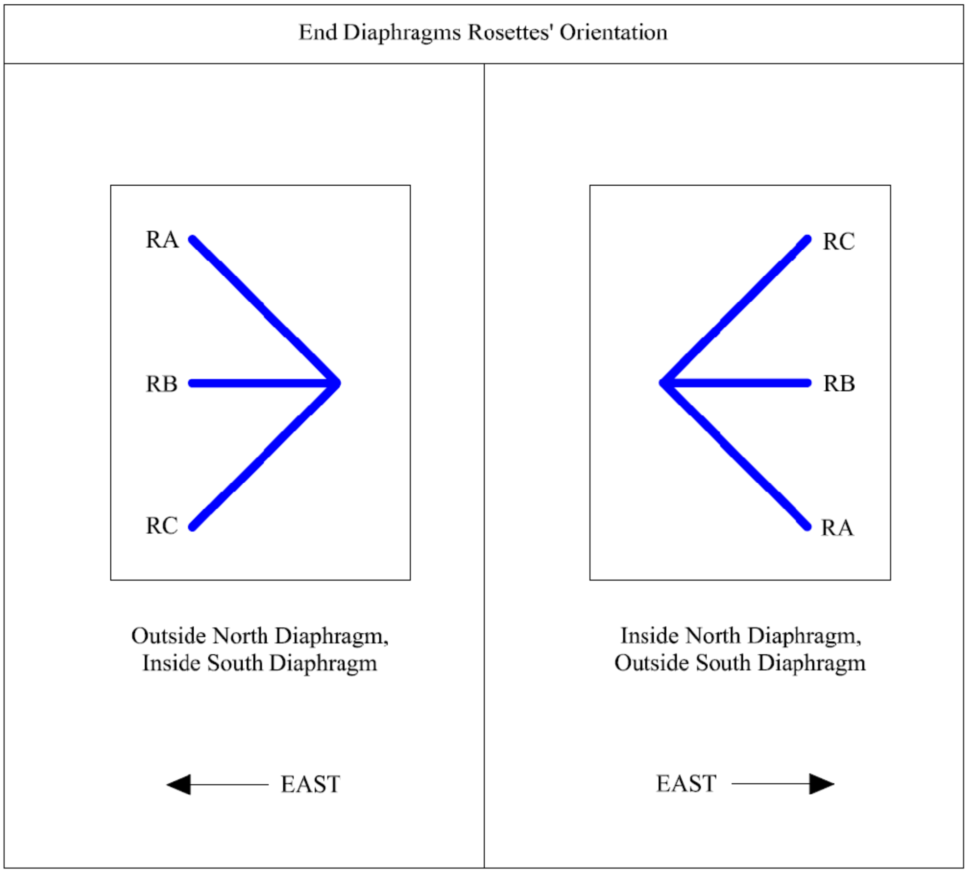

Figure B-6: End diaphragm rosette orientation (Tests 2 and 3)

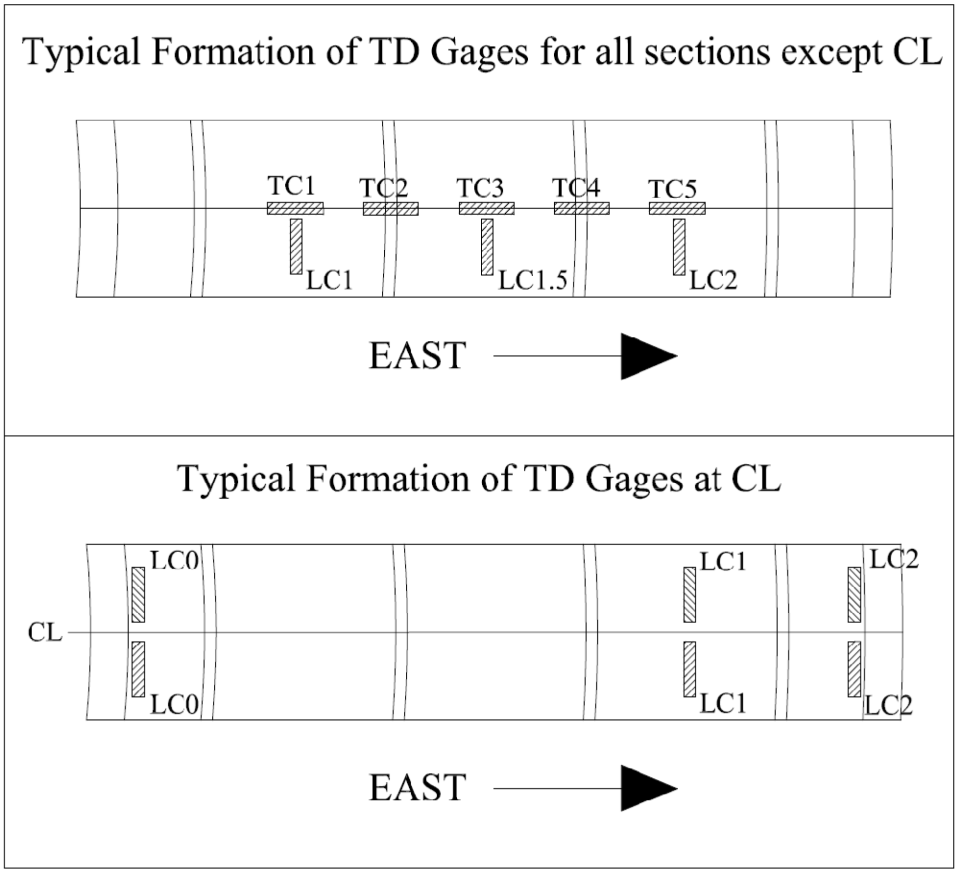

Figure B-7: Typical concrete deck gage locations (Tests 2 and 3)

Table B-4: Index of instrumentation channels (Test 2)

Index	Gage Name	Description
0	FR1	Foil Rebar Strain Gage
1	FR2	Foil Rebar Strain Gage
2	FR3	Foil Rebar Strain Gage
3	FR4	Foil Rebar Strain Gage
4	FR5	Foil Rebar Strain Gage
5	FR6	Foil Rebar Strain Gage
6	FR7	Foil Rebar Strain Gage
7	FR8	Foil Rebar Strain Gage
8	FR9	Foil Rebar Strain Gage
9	FR10	Foil Rebar Strain Gage
10	FR11	Foil Rebar Strain Gage

11	FR12	Foil Rebar Strain Gage
12	FR13	Foil Rebar Strain Gage
13	FR14	Foil Rebar Strain Gage
14	FR15	Foil Rebar Strain Gage
15	FR16	Foil Rebar Strain Gage
16	FR17	Foil Rebar Strain Gage
17	FR18	Foil Rebar Strain Gage
18	FR19	Foil Rebar Strain Gage
19	FR20	Foil Rebar Strain Gage
20	FR21	Foil Rebar Strain Gage
21	FR22	Foil Rebar Strain Gage
22	FS1	Shear Stud Strain Gage
23	FS2	Shear Stud Strain Gage
24	FS3	Shear Stud Strain Gage
25	FS4	Shear Stud Strain Gage
26	FS5	Shear Stud Strain Gage
27	FS6	Shear Stud Strain Gage
28	FS14	Shear Stud Strain Gage
29	FS9	Shear Stud Strain Gage
30	FS10	Shear Stud Strain Gage
31	FS11	Shear Stud Strain Gage
32	FS12	Shear Stud Strain Gage
33	FS15	Shear Stud Strain Gage
34	FS7	Shear Stud Strain Gage
35	WG-S1-IEW-RA	West Girder-Section S1-Inside East Web-Component A of the Rosette
36	WG-S1-IEW-RB	West Girder-Section S1-Inside East Web-Component B of the Rosette
37	WG-S1-IEW-RC	West Girder-Section S1-Inside East Web-Component C of the Rosette
38	WG-S1-IBF-RA	West Girder-Section S1-Inside Bottom Flange-Component A of the Rosette
39	FS13	Shear Stud Strain Gage
40	WG-S1-IBF-RB	West Girder-Section S1-Inside Bottom Flange-Component B of the Rosette
41	WG-S1-IBF-RC	West Girder-Section S1-Inside Bottom Flange-Component C of the Rosette
42	WG-S1-IWW-RA	West Girder-Section S1-Inside West Web-Component A of the Rosette
43	WG-S1-IWW-RB	West Girder-Section S1-Inside West Web-Component B of the Rosette

44	WG-S1-IWW-RC	West Girder-Section S1-Inside West Web-Component C of the Rosette
45	WG-S1-OEW-RA	West Girder-Section S1-Outside East Web-Component A of the Rosette
46	WG-S1-OEW-RB	West Girder-Section S1-Outside East Web-Component B of the Rosette
47	WG-S1-OEW-RC	West Girder-Section S1-Outside East Web-Component C of the Rosette
48	WG-S1-OBF-RA	West Girder-Section S1-Outside Bottom Flange-Component A of the Rosette
49	WG-S1-OBF-RB	West Girder-Section S1-Outside Bottom Flange-Component B of the Rosette
50	WG-S1-OBF-RC	West Girder-Section S1-Outside Bottom Flange-Component C of the Rosette
51	WG-S1-OWW-RA	West Girder-Section S1-Outside West Web-Component A of the Rosette
52	WG-S1-OWW-RB	West Girder-Section S1-Outside West Web-Component B of the Rosette
53	WG-S1-OWW-RC	West Girder-Section S1-Outside West Web-Component C of the Rosette
54	WG-N1-IEW-RA	West Girder-Section N1-Inside East Web-Component A of the Rosette
55	WG-N1-IEW-RB	West Girder-Section N1-Inside East Web-Component B of the Rosette
56	WG-N1-IEW-RC	West Girder-Section N1-Inside East Web-Component C of the Rosette
57	WG-N1-IBF-RA	West Girder-Section N1-Inside Bottom Flange-Component A of the Rosette
58	WG-N1-IBF-RB	West Girder-Section N1-Inside Bottom Flange-Component B of the Rosette
59	WG-N1-IBF-RC	West Girder-Section N1-Inside Bottom Flange-Component C of the Rosette
60	WG-N1-IWW-RA	West Girder-Section N1-Inside West Web-Component A of the Rosette
61	WG-N1-IWW-RB	West Girder-Section N1-Inside West Web-Component B of the Rosette
62	GO TO 172	
63	WG-N1-OEW-RA	West Girder-Section N1-Outside East Web-Component A of the Rosette
64	WG-N1-OEW-RB	West Girder-Section N1-Outside East Web-Component B of the Rosette
65	WG-N1-OEW-RC	West Girder-Section N1-Outside East Web-Component C of the Rosette
66	WG-N1-OBF-RA	West Girder-Section N1-Outside Bottom Flange-Component A of the Rosette

67	WG-N1-OBF-RB	West Girder-Section N1-Outside Bottom Flange-Component B of the Rosette
68	WG-N1-OBF-RC	West Girder-Section N1-Outside Bottom Flange-Component C of the Rosette
69	WG-N1-OWW-RA	West Girder-Section N1-Outside West Web-Component A of the Rosette
70	WG-N1-OWW-RB	West Girder-Section N1-Outside West Web-Component B of the Rosette
71	WG-N1-OWW-RC	West Girder-Section N1-Outside West Web-Component C of the Rosette
72	OND-RA	Outside North Diaphragm-Component A of the Rosette
73	OND-RB	Outside North Diaphragm-Component B of the Rosette
74	OND-RC	Outside North Diaphragm-Component C of the Rosette
75	IND-RA	Inside North Diaphragm-Component A of the Rosette
76	IND-RB	Inside North Diaphragm-Component B of the Rosette
77	IND-RC	Inside North Diaphragm-Component C of the Rosette
78	OSD-RA	Outside South Diaphragm-Component A of the Rosette
79	OSD-RB	Outside South Diaphragm-Component B of the Rosette
80	OSD-RC	Outside South Diaphragm-Component C of the Rosette
81	ISD-RA	Inside South Diaphragm-Component A of the Rosette
82	ISD-RB	Inside South Diaphragm-Component B of the Rosette
83	ISD-RC	Inside South Diaphragm-Component C of the Rosette
84	EG-N3-OBF-F	East Girder-Section N3-Outside Bottom Flange- Foil Gage
85	EG-N3-IBF-F	East Girder-Section N3-Inside Bottom Flange- Foil Gage
86	WG-N3-OEW-RA	West Girder-Section N3-Outside East Web-Component A of the Rosette
87	WG-N3-OEW-RB	West Girder-Section N3-Outside East Web-Component B of the Rosette
88	WG-N3-OEW-RC	West Girder-Section N3-Outside East Web-Component C of the Rosette
89	WG-N3-OBF-RA	West Girder-Section N3-Outside Bottom Flange-Component A of the Rosette
90	WG-N3-OBF-RB	West Girder-Section N3-Outside Bottom Flange-Component B of the Rosette
91	WG-N3-OBF-RC	West Girder-Section N3-Outside Bottom Flange-Component C of the Rosette
92	WG-N3-OWW-RA	West Girder-Section N3-Outside West Web-Component A of the Rosette
93	WG-N3-OWW-RB	West Girder-Section N3-Outside West Web-Component B of the Rosette
94	WG-N3-OWW-RC	West Girder-Section N3-Outside West Web-Component C of the Rosette
95	WG-N3-IEW-RA	West Girder-Section N3-Inside East Web-Component A of the Rosette

96	WG-N3-IEW-RB	West Girder-Section N3-Inside East Web- Component B of the Rosette
97	WG-N3-IEW-RC	West Girder-Section N3-Inside East Web- Component C of the Rosette
98	WG-N3-IBF-RA	West Girder-Section N3-Inside Bottom Flange- Component A of the Rosette
99	WG-N3-IBF-RB	West Girder-Section N3-Inside Bottom Flange- Component B of the Rosette
100	WG-N3-IBF-RC	West Girder-Section N3-Inside Bottom Flange- Component C of the Rosette
101	WG-N3-IWW-RA	West Girder-Section N3-Inside West Web- Component A of the Rosette
102	WG-N3-IWW-RB	West Girder-Section N3-Inside West Web- Component B of the Rosette
103	WG-N3-IWW-RC	West Girder-Section N3-Inside West Web- Component C of the Rosette
104	EG-N2-OBF-F	East Girder-Section N2-Outside Bottom Flange- Foil Gage
105	EG-N2-IBF-F	East Girder-Section N2-Inside Bottom Flange- Foil Gage
106	WG-N2-OEW-RA	West Girder-Section N2-Outside East Web- Component A of the Rosette
107	WG-N2-OEW-RB	West Girder-Section N2-Outside East Web- Component B of the Rosette
108	WG-N2-OEW-RC	West Girder-Section N2-Outside East Web- Component C of the Rosette
109	WG-N2-OBF-RA	West Girder-Section N2-Outside Bottom Flange- Component A of the Rosette
110	WG-N2-OBF-RB	West Girder-Section N2-Outside Bottom Flange- Component B of the Rosette
111	WG-N2-OBF-RC	West Girder-Section N2-Outside Bottom Flange- Component C of the Rosette
112	WG-N2-OWW-RA	West Girder-Section N2-Outside West Web- Component A of the Rosette
113	WG-N2-OWW-RB	West Girder-Section N2-Outside West Web- Component B of the Rosette
114	WG-N2-OWW-RC	West Girder-Section N2-Outside West Web- Component C of the Rosette
115	WG-N2-IEW-RA	West Girder-Section N2-Inside East Web- Component A of the Rosette
116	WG-N2-IEW-RB	West Girder-Section N2-Inside East Web- Component B of the Rosette
117	WG-N2-IEW-RC	West Girder-Section N2-Inside East Web- Component C of the Rosette
118	WG-N2-IBF-RA	West Girder-Section N2-Inside Bottom Flange- Component A of the Rosette
119	WG-N2-IBF-RB	West Girder-Section N2-Inside Bottom Flange- Component B of the Rosette

120	WG-N2-IBF-RC	West Girder-Section N2-Inside Bottom Flange-Component C of the Rosette
121	WG-N2-IWW-RA	West Girder-Section N2-Inside West Web-Component A of the Rosette
122	WG-N2-IWW-RB	West Girder-Section N2-Inside West Web-Component B of the Rosette
123	WG-N2-IWW-RC	West Girder-Section N2-Inside West Web-Component C of the Rosette
124	EG-N1-OBF-F	East Girder-Section N1-Outside Bottom Flange- Foil Gage
125	EG-N1-IBF-F	East Girder-Section N1-Inside Bottom Flange- Foil Gage
126	EG-S1-OBF-F	East Girder-Section S2-Outside Bottom Flange- Foil Gage
127	EG-S1-IBF-F	East Girder-Section S2-Inside Bottom Flange- Foil Gage
128	EG-S2-OBF-F	East Girder-Section S2-Outside Bottom Flange- Foil Gage
129	EG-S2-IBF-F	East Girder-Section S2-Inside Bottom Flange- Foil Gage
130	WG-S2-OEW-RA	West Girder-Section S2-Outside East Web-Component A of the Rosette
131	WG-S2-OEW-RB	West Girder-Section S2-Outside East Web-Component B of the Rosette
132	WG-S2-OEW-RC	West Girder-Section S2-Outside East Web-Component C of the Rosette
133	WG-S2-OBF-RA	West Girder-Section S2-Outside Bottom Flange-Component A of the Rosette
134	WG-S2-OBF-RB	West Girder-Section S2-Outside Bottom Flange-Component B of the Rosette
135	WG-S2-OBF-RC	West Girder-Section S2-Outside Bottom Flange-Component C of the Rosette
136	WG-S2-OWW-RA	West Girder-Section S2-Outside West Web-Component A of the Rosette
137	WG-S2-OWW-RB	West Girder-Section S2-Outside West Web-Component B of the Rosette
138	WG-S2-OWW-RC	West Girder-Section S2-Outside West Web-Component C of the Rosette
139	WG-S2-IEW-RA	West Girder-Section S2-Inside East Web-Component A of the Rosette
140	WG-S2-IEW-RB	West Girder-Section S2-Inside East Web-Component B of the Rosette
141	WG-S2-IEW-RC	West Girder-Section S2-Inside East Web-Component C of the Rosette
142	WG-S2-IBF-RA	West Girder-Section S2-Inside Bottom Flange-Component A of the Rosette
143	WG-S2-IBF-RB	West Girder-Section S2-Inside Bottom Flange-Component B of the Rosette
144	WG-S2-IBF-RC	West Girder-Section S2-Inside Bottom Flange-Component C of the Rosette

145	WG-S2-IWW-RA	West Girder-Section S2-Inside West Web-Component A of the Rosette
146	WG-S2-IWW-RB	West Girder-Section S2-Inside West Web-Component B of the Rosette
147	WG-S2-IWW-RC	West Girder-Section S2-Inside West Web-Component C of the Rosette
148	EG-S3-OBF-F	East Girder-Section S3-Outside Bottom Flange- Foil Gage
149	EG-S3-IBF-F	East Girder-Section S3-Inside Bottom Flange- Foil Gage
150	WG-S3-OEW-RA	West Girder-Section S3-Outside East Web-Component A of the Rosette
151	WG-S3-OEW-RB	West Girder-Section S3-Outside East Web-Component B of the Rosette
152	WG-S3-OEW-RC	West Girder-Section S3-Outside East Web-Component C of the Rosette
153	WG-S3-OBF-RA	West Girder-Section S3-Outside Bottom Flange-Component A of the Rosette
154	WG-S3-OBF-RB	West Girder-Section S3-Outside Bottom Flange-Component B of the Rosette
155	WG-S3-OBF-RC	West Girder-Section S3-Outside Bottom Flange-Component C of the Rosette
156	WG-S3-OWW-RA	West Girder-Section S3-Outside West Web-Component A of the Rosette
157	WG-S3-OWW-RB	West Girder-Section S3-Outside West Web-Component B of the Rosette
158	WG-S3-OWW-RC	West Girder-Section S3-Outside West Web-Component C of the Rosette
159	WG-S3-IEW-RA	West Girder-Section S3-Inside East Web-Component A of the Rosette
160	WG-S3-IEW-RB	West Girder-Section S3-Inside East Web-Component B of the Rosette
161	WG-S3-IEW-RC	West Girder-Section S3-Inside East Web-Component C of the Rosette
162	WG-S3-IBF-RA	West Girder-Section S3-Inside Bottom Flange-Component A of the Rosette
163	WG-S3-IBF-RB	West Girder-Section S3-Inside Bottom Flange-Component B of the Rosette
164	WG-S3-IBF-RC	West Girder-Section S3-Inside Bottom Flange-Component C of the Rosette
165	WG-S3-IWW-RA	West Girder-Section S3-Inside West Web-Component A of the Rosette
166	WG-S3-IWW-RB	West Girder-Section S3-Inside West Web-Component B of the Rosette
167	WG-S3-IWW-RC	West Girder-Section S3-Inside West Web-Component C of the Rosette
168	CD-F1	Inner Center Diaphragm of the Intact Girder-Foil Strain Gage

169	CD-F2	Inner Center Diaphragm of the Intact Girder- Foil Strain Gage
170	CD-F3	Inner Center Diaphragm of the Intact Girder- Foil Strain Gage
171	CD-F4	Inner Center Diaphragm of the Intact Girder- Foil Strain Gage
172	WG-N1-IWW-RC	West Girder-Section N1-Inside West Web- Component C of the Rosette
173	TD-N3-TC2	Top Deck-Section N3-Transverse Concrete Gage
174	TD-N3-TC3	Top Deck-Section N3-Transverse Concrete Gage
175	TD-N3-TC4	Top Deck-Section N3-Transverse Concrete Gage
176	TD-N3-TC5	Top Deck-Section N3-Transverse Concrete Gage
177	TD-N2-TC1	Top Deck-Section N2-Transverse Concrete Gage
178	TD-N2-TC2	Top Deck-Section N2-Transverse Concrete Gage
179	TD-N2-TC3	Top Deck-Section N2-Transverse Concrete Gage
180	TD-N2-TC4	Top Deck-Section N2-Transverse Concrete Gage
181	TD-N2-TC5	Top Deck-Section N2-Transverse Concrete Gage
182	TD-N1.5-TC1	Top Deck-Section N1.5-Transverse Concrete Gage
183	TD-N1.5-TC2	Top Deck-Section N1.5-Transverse Concrete Gage
184	TD-N1.5-TC3	Top Deck-Section N1.5-Transverse Concrete Gage
185	TD-N1.5-TC4	Top Deck-Section N1.5-Transverse Concrete Gage
186	TD-N1.5-TC5	Top Deck-Section N1.5-Transverse Concrete Gage
187	TD-N1-TC1	Top Deck-Section N1-Transverse Concrete Gage
188	TD-N1-TC2	Top Deck-Section N1-Transverse Concrete Gage
189	TD-N1-TC3	Top Deck-Section N1-Transverse Concrete Gage
190	TD-N1-TC4	Top Deck-Section N1-Transverse Concrete Gage
191	TD-N1-TC5	Top Deck-Section N1-Transverse Concrete Gage
192	TD-S1-TC1	Top Deck-Section S1-Transverse Concrete Gage
193	TD-S1-TC2	Top Deck-Section S1-Transverse Concrete Gage
194	TD-S1-TC3	Top Deck-Section S1-Transverse Concrete Gage
195	TD-S1-TC4	Top Deck-Section S1-Transverse Concrete Gage
196	TD-S1-TC5	Top Deck-Section S1-Transverse Concrete Gage
197	TD-S1.5-TC1	Top Deck-Section S1.5-Transverse Concrete Gage
198	TD-S1.5-TC2	Top Deck-Section S1.5-Transverse Concrete Gage
199	TD-S1.5-TC3	Top Deck-Section S1.5-Transverse Concrete Gage
200	TD-S1.5-TC4	Top Deck-Section S1.5-Transverse Concrete Gage
201	TD-S1.5-TC5	Top Deck-Section S1.5-Transverse Concrete Gage
202	TD-S2-TC1	Top Deck-Section S2-Transverse Concrete Gage
203	TD-S2-TC2	Top Deck-Section S2-Transverse Concrete Gage
204	TD-S2-TC3	Top Deck-Section S2-Transverse Concrete Gage

205	TD-S2-TC4	Top Deck-Section S2-Transverse Concrete Gage
206	TD-S2-TC5	Top Deck-Section S2-Transverse Concrete Gage
207	TD-S3-TC1	Top Deck-Section S3-Transverse Concrete Gage
208	TD-S3-TC2	Top Deck-Section S3-Transverse Concrete Gage
209	TD-S3-TC3	Top Deck-Section S3-Transverse Concrete Gage
210	TD-S3-TC4	Top Deck-Section S3-Transverse Concrete Gage
211	TD-S3-TC5	Top Deck-Section S3-Transverse Concrete Gage
212	TD-N2-LC1	Top Deck-Section N2-Longitudinal Concrete Gage
213	TD-N2-LC2	Top Deck-Section N2-Longitudinal Concrete Gage
214	TD-N1.5-LC1	Top Deck-Section N1.5-Longitudinal Concrete Gage
215	TD-N1-LC0	Top Deck-Section N1-Longitudinal Concrete Gage
216	TD-N1-LC1	Top Deck-Section N1-Longitudinal Concrete Gage
217	TD-N1-LC2	Top Deck-Section N1-Longitudinal Concrete Gage
218	TD-S1-LC0	Top Deck-Section S1-Longitudinal Concrete Gage
219	TD-S1-LC1	Top Deck-Section S1-Longitudinal Concrete Gage
220	TD-S1-LC2	Top Deck-Section S1-Longitudinal Concrete Gage
221	TD-S1.5-LC1	Top Deck-Section S1.5-Longitudinal Concrete Gage
222	TD-S2-LC1	Top Deck-Section S2-Longitudinal Concrete Gage
223	TD-S2-LC2	Top Deck-Section S2-Longitudinal Concrete Gage
224	ER-N3	East Railing-Section N3
225	ER-N2	East Railing-Section N2
226	ER-N1	East Railing-Section N1
227	ER-S1	East Railing-Section S1
228	ER-S2	East Railing-Section S2
229	ER-S3	East Railing-Section S3
230	LP-N3	Linear Potentiometer-Section N3
231	LP-N2	Linear Potentiometer-Section N2
232	LP-N1	Linear Potentiometer-Section N1
233	LP-CL	Linear Potentiometer-Section CL
234	LP-CL1	Linear Potentiometer-Across the fracture (West)
235	LP-CL2	Linear Potentiometer-Across the fracture (East)
236	LP-S1	Linear Potentiometer-Section S1
237	LP-S2	Linear Potentiometer-Section S2
238	LP-S3	Linear Potentiometer-Section S3
239	LP-SD1	Linear Potentiometer-South Diaphragm Exterior Tip of Bottom Flange (FG)
240	LP-SD2	Linear Potentiometer-South Diaphragm Interior Tip of Bottom Flange (FG)
241	LP-SD3	Linear Potentiometer-South Diaphragm Interior Tip of Bottom Flange (IG)

242	LP-SD4	Linear Potentiometer-South Diaphragm Exterior Tip of Bottom Flange (IG)
243	SP-CL	String Potentiometer-Mid-Width of Bottom Flange at CL of the Fracture Girder

B.4 FULL-SCALE TEST 3

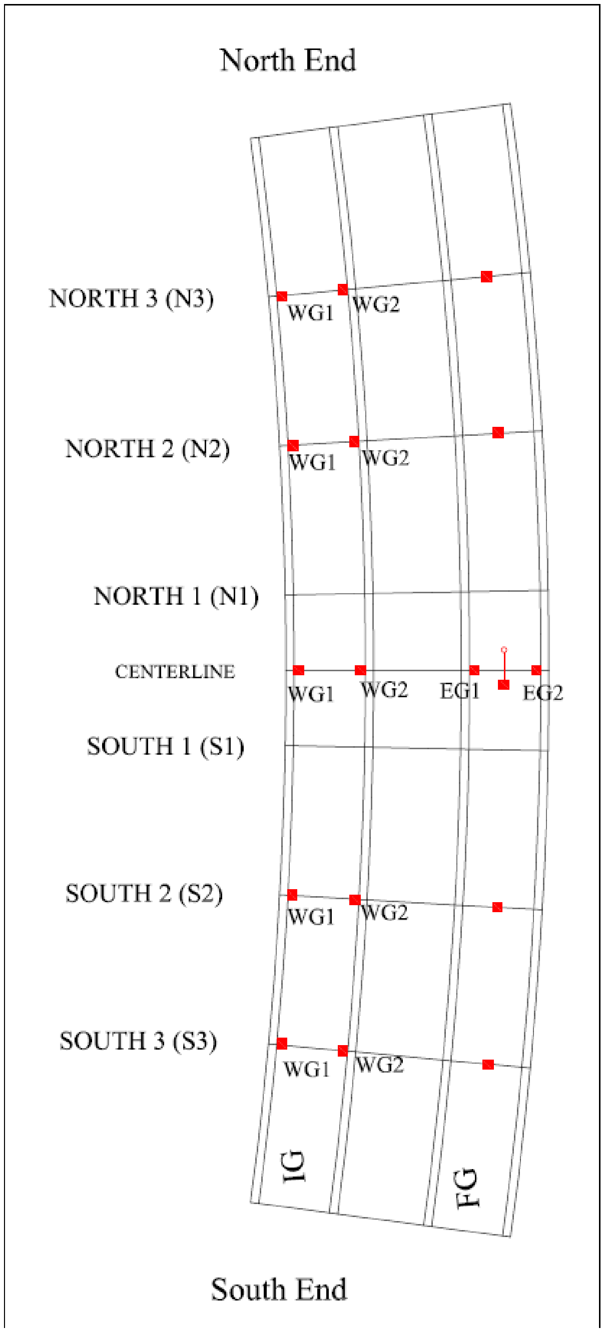

Figure B-8: String potentiometer locations (between girder bottom flanges and ground) (Test 3)

Table B-5: Index of instrumentation channels (Test 3)

National Instruments System		
Index	**Gage Name**	**Description**
0	FR1	Foil Rebar Strain Gage
1	FR2	Foil Rebar Strain Gage
2	FR3	Foil Rebar Strain Gage
3	FR4	Foil Rebar Strain Gage
4	FR5	Foil Rebar Strain Gage
5	FR6	Foil Rebar Strain Gage
6	FR7	Foil Rebar Strain Gage
7	FR8	Foil Rebar Strain Gage
8	FR9	Foil Rebar Strain Gage
9	FR10	Foil Rebar Strain Gage
10	FR11	Foil Rebar Strain Gage
11	FR12	Foil Rebar Strain Gage
12	FR13	Foil Rebar Strain Gage
13	FR14	Foil Rebar Strain Gage
14	FR15	Foil Rebar Strain Gage
15	FR16	Foil Rebar Strain Gage
16	FR17	Foil Rebar Strain Gage
17	FR19	Foil Rebar Strain Gage
18	FR20	Foil Rebar Strain Gage
19	FR21	Foil Rebar Strain Gage
20	FR22	Foil Rebar Strain Gage
21	FS1	Shear Stud Strain Gage
22	FS2	Shear Stud Strain Gage
23	FS13	Shear Stud Strain Gage
24	FS3	Shear Stud Strain Gage
25	FS4	Shear Stud Strain Gage
26	FS5	Shear Stud Strain Gage
27	FS6	Shear Stud Strain Gage
28	FS14	Shear Stud Strain Gage
29	WG-S1-IEW-RA	West Girder-Section S1-Inside East Web-Component A of the Rosette
30	WG-S1-IEW-RB	West Girder-Section S1-Inside East Web-Component B of the Rosette
31	WG-S1-IEW-RC	West Girder-Section S1-Inside East Web-Component C of the Rosette
32	WG-S1-IBF-RA	West Girder-Section S1-Inside Bottom Flange-Component A of the Rosette
33	WG-S1-IBF-RB	West Girder-Section S1-Inside Bottom Flange-Component B of the Rosette
34	WG-S1-IBF-RC	West Girder-Section S1-Inside Bottom Flange-Component C of the Rosette

35	WG-S1-IWW-RA	West Girder-Section S1-Inside West Web- Component A of the Rosette
36	WG-S1-IWW-RB	West Girder-Section S1-Inside West Web- Component B of the Rosette
37	WG-S1-IWW-RC	West Girder-Section S1-Inside West Web- Component C of the Rosette
38	EG-N3-TF-F	East Girder-Section N3-Exterior Top Flange- Foil Gage
39	EG-N2-TF-F	East Girder-Section N2-Exterior Top Flange- Foil Gage
40	EG-N1-TF-F	East Girder-Section N1-Exterior Top Flange- Foil Gage
41	EG-S2-InteriorTF-F	East Girder-Section S2-Interior Top Flange- Foil Gage
42	EG-S4-InteriorTF-F	East Girder-Section S4-Interior Top Flange- Foil Gage
43	WG-CL-IBF-F	West Girder-Section CL-Inside Bottom Flange-Foil Gage
44	WG-CL-OBF-F	West Girder-Section CL-Outside Bottom Flange-Foil Gage
45	WG-S1-OEW-RA	West Girder-Section S1-Outside East Web- Component A of the Rosette
46	WG-S1-OEW-RB	West Girder-Section S1-Outside East Web- Component B of the Rosette
47	WG-S1-OEW-RC	West Girder-Section S1-Outside East Web- Component C of the Rosette
48	WG-S1-OBF-RA	West Girder-Section S1-Outside Bottom Flange- Component A of the Rosette
49	WG-S1-OBF-RB	West Girder-Section S1-Outside Bottom Flange- Component B of the Rosette
50	WG-S1-OBF-RC	West Girder-Section S1-Outside Bottom Flange- Component C of the Rosette
51	WG-S1-OWW-RA	West Girder-Section S1-Outside West Web- Component A of the Rosette
52	WG-S1-OWW-RB	West Girder-Section S1-Outside West Web- Component B of the Rosette
53	WG-S1-OWW-RC	West Girder-Section S1-Outside West Web- Component C of the Rosette
54	WG-N1-IEW-RA	West Girder-Section N1-Inside East Web- Component A of the Rosette
55	WG-N1-IEW-RB	West Girder-Section N1-Inside East Web- Component B of the Rosette
56	WG-N1-IEW-RC	West Girder-Section N1-Inside East Web- Component C of the Rosette
57	WG-N1-IBF-RA	West Girder-Section N1-Inside Bottom Flange- Component A of the Rosette
58	WG-N1-IBF-RB	West Girder-Section N1-Inside Bottom Flange- Component B of the Rosette
59	WG-N1-IBF-RC	West Girder-Section N1-Inside Bottom Flange- Component C of the Rosette
60	WG-N1-IWW-RA	West Girder-Section N1-Inside West Web- Component A of the Rosette

61	WG-N1-IWW-RB	West Girder-Section N1-Inside West Web-Component B of the Rosette
62	WG-N1-IWW-RC	West Girder-Section N1-Inside West Web-Component C of the Rosette
63	WG-N1-OEW-RA	West Girder-Section N1-Outside East Web-Component A of the Rosette
64	WG-N1-OEW-RB	West Girder-Section N1-Outside East Web-Component B of the Rosette
65	WG-N1-OEW-RC	West Girder-Section N1-Outside East Web-Component C of the Rosette
66	WG-N1-OBF-RA	West Girder-Section N1-Outside Bottom Flange-Component A of the Rosette
67	WG-N1-OBF-RB	West Girder-Section N1-Outside Bottom Flange-Component B of the Rosette
68	WG-N1-OBF-RC	West Girder-Section N1-Outside Bottom Flange-Component C of the Rosette
69	WG-N1-OWW-RA	West Girder-Section N1-Outside West Web-Component A of the Rosette
70	WG-N1-OWW-RB	West Girder-Section N1-Outside West Web-Component B of the Rosette
71	WG-N1-OWW-RC	West Girder-Section N1-Outside West Web-Component C of the Rosette
72	OND-RA	Outside North Diaphragm-Component A of the Rosette
73	OND-RB	Outside North Diaphragm-Component B of the Rosette
74	OND-RC	Outside North Diaphragm-Component C of the Rosette
75	IND-RA	Inside North Diaphragm-Component A of the Rosette
76	IND-RB	Inside North Diaphragm-Component B of the Rosette
77	IND-RC	Inside North Diaphragm-Component C of the Rosette
78	OSD-RA	Outside South Diaphragm-Component A of the Rosette
79	OSD-RB	Outside South Diaphragm-Component B of the Rosette
80	OSD-RC	Outside South Diaphragm-Component C of the Rosette
81	ISD-RA	Inside South Diaphragm-Component A of the Rosette
82	ISD-RB	Inside South Diaphragm-Component B of the Rosette
83	ISD-RC	Inside South Diaphragm-Component C of the Rosette
84	EG-N3-OBF-F	East Girder-Section N3-Outside Bottom Flange- Foil Gage
85	EG-N3-IBF-F	East Girder-Section N3-Inside Bottom Flange- Foil Gage
86	WG-N3-OEW-RA	West Girder-Section N3-Outside East Web-Component A of the Rosette
87	WG-N3-OEW-RB	West Girder-Section N3-Outside East Web-Component B of the Rosette
88	WG-N3-OEW-RC	West Girder-Section N3-Outside East Web-Component C of the Rosette
89	WG-N3-OBF-RA	West Girder-Section N3-Outside Bottom Flange-Component A of the Rosette
90	WG-N3-OBF-RB	West Girder-Section N3-Outside Bottom Flange-Component B of the Rosette

91	WG-N3-OBF-RC	West Girder-Section N3-Outside Bottom Flange-Component C of the Rosette
92	WG-N3-OWW-RA	West Girder-Section N3-Outside West Web-Component A of the Rosette
93	WG-N3-OWW-RB	West Girder-Section N3-Outside West Web-Component B of the Rosette
94	WG-N3-OWW-RC	West Girder-Section N3-Outside West Web-Component C of the Rosette
95	WG-N3-IEW-RA	West Girder-Section N3-Inside East Web-Component A of the Rosette
96	WG-N3-IEW-RB	West Girder-Section N3-Inside East Web-Component B of the Rosette
97	WG-N3-IEW-RC	West Girder-Section N3-Inside East Web-Component C of the Rosette
98	WG-N3-IBF-RA	West Girder-Section N3-Inside Bottom Flange-Component A of the Rosette
99	WG-N3-IBF-RB	West Girder-Section N3-Inside Bottom Flange-Component B of the Rosette
100	WG-N3-IBF-RC	West Girder-Section N3-Inside Bottom Flange-Component C of the Rosette
101	WG-N3-IWW-RA	West Girder-Section N3-Inside West Web-Component A of the Rosette
102	WG-N3-IWW-RB	West Girder-Section N3-Inside West Web-Component B of the Rosette
103	WG-N3-IWW-RC	West Girder-Section N3-Inside West Web-Component C of the Rosette
104	EG-N2-OBF-F	East Girder-Section N2-Outside Bottom Flange- Foil Gage
105	EG-N2-IBF-F	East Girder-Section N2-Inside Bottom Flange- Foil Gage
106	WG-N2-OEW-RA	West Girder-Section N2-Outside East Web-Component A of the Rosette
107	WG-N2-OEW-RB	West Girder-Section N2-Outside East Web-Component B of the Rosette
108	WG-N2-OEW-RC	West Girder-Section N2-Outside East Web-Component C of the Rosette
109	WG-N2-OBF-RA	West Girder-Section N2-Outside Bottom Flange-Component A of the Rosette
110	WG-N2-OBF-RB	West Girder-Section N2-Outside Bottom Flange-Component B of the Rosette
111	WG-N2-OBF-RC	West Girder-Section N2-Outside Bottom Flange-Component C of the Rosette
112	WG-N2-OWW-RA	West Girder-Section N2-Outside West Web-Component A of the Rosette
113	WG-N2-OWW-RB	West Girder-Section N2-Outside West Web-Component B of the Rosette
114	WG-N2-OWW-RC	West Girder-Section N2-Outside West Web-Component C of the Rosette

115	WG-N2-IEW-RA	West Girder-Section N2-Inside East Web-Component A of the Rosette
116	WG-N2-IEW-RB	West Girder-Section N2-Inside East Web-Component B of the Rosette
117	WG-N2-IEW-RC	West Girder-Section N2-Inside East Web-Component C of the Rosette
118	WG-N2-IBF-RA	West Girder-Section N2-Inside Bottom Flange-Component A of the Rosette
119	WG-N2-IBF-RB	West Girder-Section N2-Inside Bottom Flange-Component B of the Rosette
120	WG-N2-IBF-RC	West Girder-Section N2-Inside Bottom Flange-Component C of the Rosette
121	WG-N2-IWW-RA	West Girder-Section N2-Inside West Web-Component A of the Rosette
122	WG-N2-IWW-RB	West Girder-Section N2-Inside West Web-Component B of the Rosette
123	WG-N2-IWW-RC	West Girder-Section N2-Inside West Web-Component C of the Rosette
124	EG-NCL-TF-F	East Girder-Section NCL-Exterior Top Flange- Foil Gage
125	EG-SCL-TF-F	East Girder-Section SCL-Exterior Top Flange- Foil Gage
126	EG-S1-TF-F	East Girder-Section S1-Exterior Top Flange- Foil Gage
127	EG-S2-TF-F	East Girder-Section S2-Exterior Top Flange- Foil Gage
128	EG-S2-OBF-F	East Girder-Section S2-Outside Bottom Flange- Foil Gage
129	EG-S2-IBF-F	East Girder-Section S2-Inside Bottom Flange- Foil Gage
130	WG-S2-OEW-RA	West Girder-Section S2-Outside East Web-Component A of the Rosette
131	WG-S2-OEW-RB	West Girder-Section S2-Outside East Web-Component B of the Rosette
132	WG-S2-OEW-RC	West Girder-Section S2-Outside East Web-Component C of the Rosette
133	WG-S2-OBF-RA	West Girder-Section S2-Outside Bottom Flange-Component A of the Rosette
134	WG-S2-OBF-RB	West Girder-Section S2-Outside Bottom Flange-Component B of the Rosette
135	WG-S2-OBF-RC	West Girder-Section S2-Outside Bottom Flange-Component C of the Rosette
136	WG-S2-OWW-RA	West Girder-Section S2-Outside West Web-Component A of the Rosette
137	WG-S2-OWW-RB	West Girder-Section S2-Outside West Web-Component B of the Rosette
138	WG-S2-OWW-RC	West Girder-Section S2-Outside West Web-Component C of the Rosette
139	WG-S2-IEW-RA	West Girder-Section S2-Inside East Web-Component A of the Rosette
140	WG-S2-IEW-RB	West Girder-Section S2-Inside East Web-Component B of the Rosette

141	WG-S2-IEW-RC	West Girder-Section S2-Inside East Web-Component C of the Rosette
142	WG-S2-IBF-RA	West Girder-Section S2-Inside Bottom Flange-Component A of the Rosette
143	WG-S2-IBF-RB	West Girder-Section S2-Inside Bottom Flange-Component B of the Rosette
144	WG-S2-IBF-RC	West Girder-Section S2-Inside Bottom Flange-Component C of the Rosette
145	WG-S2-IWW-RA	West Girder-Section S2-Inside West Web-Component A of the Rosette
146	WG-S2-IWW-RB	West Girder-Section S2-Inside West Web-Component B of the Rosette
147	WG-S2-IWW-RC	West Girder-Section S2-Inside West Web-Component C of the Rosette
148	EG-S3-OBF-F	East Girder-Section S3-Outside Bottom Flange- Foil Gage
149	EG-S3-IBF-F	East Girder-Section S3-Inside Bottom Flange- Foil Gage
150	WG-S3-OEW-RA	West Girder-Section S3-Outside East Web-Component A of the Rosette
151	WG-S3-OEW-RB	West Girder-Section S3-Outside East Web-Component B of the Rosette
152	WG-S3-OEW-RC	West Girder-Section S3-Outside East Web-Component C of the Rosette
153	WG-S3-OBF-RA	West Girder-Section S3-Outside Bottom Flange-Component A of the Rosette
154	WG-S3-OBF-RB	West Girder-Section S3-Outside Bottom Flange-Component B of the Rosette
155	WG-S3-OBF-RC	West Girder-Section S3-Outside Bottom Flange-Component C of the Rosette
156	WG-S3-OWW-RA	West Girder-Section S3-Outside West Web-Component A of the Rosette
157	WG-S3-OWW-RB	West Girder-Section S3-Outside West Web-Component B of the Rosette
158	WG-S3-OWW-RC	West Girder-Section S3-Outside West Web-Component C of the Rosette
159	WG-S3-IEW-RA	West Girder-Section S3-Inside East Web-Component A of the Rosette
160	WG-S3-IEW-RB	West Girder-Section S3-Inside East Web-Component B of the Rosette
161	WG-S3-IEW-RC	West Girder-Section S3-Inside East Web-Component C of the Rosette
162	WG-S3-IBF-RA	West Girder-Section S3-Inside Bottom Flange-Component A of the Rosette
163	WG-S3-IBF-RB	West Girder-Section S3-Inside Bottom Flange-Component B of the Rosette
164	WG-S3-IBF-RC	West Girder-Section S3-Inside Bottom Flange-Component C of the Rosette

165	WG-S3-IWW-RA	West Girder-Section S3-Inside West Web- Component A of the Rosette
166	WG-S3-IWW-RB	West Girder-Section S3-Inside West Web- Component B of the Rosette
167	WG-S3-IWW-RC	West Girder-Section S3-Inside West Web- Component C of the Rosette
168	EG-N4-InteriorTF-F	East Girder-Section N4-Interior Top Flange- Foil Gage
169	EG-N2-InteriorTF-F	East Girder-Section N2-Interior Top Flange- Foil Gage
170	TD-N3-LC1	Top Deck-Section N3-Longitudinal Concrete Gage
171	TD-N3-LC1.5	Top Deck-Section N3-Longitudinal Concrete Gage
172	TD-N3-LC2	Top Deck-Section N3-Longitudinal Concrete Gage
173	TD-N3-TC1	Top Deck-Section N3-Transverse Concrete Gage
174	TD-N3-TC2	Top Deck-Section N3-Transverse Concrete Gage
175	TD-N3-TC3	Top Deck-Section N3-Transverse Concrete Gage
176	TD-N3-TC4	Top Deck-Section N3-Transverse Concrete Gage
177	TD-N3-TC5	Top Deck-Section N3-Transverse Concrete Gage
178	TD-N2-TC1	Top Deck-Section N2-Transverse Concrete Gage
179	TD-N2-TC2	Top Deck-Section N2-Transverse Concrete Gage
180	TD-N2-TC3	Top Deck-Section N2-Transverse Concrete Gage
181	TD-N2-TC4	Top Deck-Section N2-Transverse Concrete Gage
182	TD-N2-TC5	Top Deck-Section N2-Transverse Concrete Gage
183	TD-N1.5-TC1	Top Deck-Section N1.5-Transverse Concrete Gage
184	TD-N1.5-TC3	Top Deck-Section N1.5-Transverse Concrete Gage
185	TD-N1.5-TC4	Top Deck-Section N1.5-Transverse Concrete Gage
186	TD-N1.5-TC5	Top Deck-Section N1.5-Transverse Concrete Gage
187	TD-N1-TC1	Top Deck-Section N1-Transverse Concrete Gage
188	TD-N1-TC3	Top Deck-Section N1-Transverse Concrete Gage
189	TD-N1-TC4	Top Deck-Section N1-Transverse Concrete Gage
190	TD-N1-TC5	Top Deck-Section N1-Transverse Concrete Gage
191	TD-S1-TC1	Top Deck-Section S1-Transverse Concrete Gage
192	TD-S1-TC3	Top Deck-Section S1-Transverse Concrete Gage
193	TD-S1-TC4	Top Deck-Section S1-Transverse Concrete Gage
194	TD-S1-TC5	Top Deck-Section S1-Transverse Concrete Gage
195	TD-S1.5-TC1	Top Deck-Section S1.5-Transverse Concrete Gage
196	TD-S1.5-TC3	Top Deck-Section S1.5-Transverse Concrete Gage
197	TD-N4-TC2	Top Deck-Section N4-Transverse Concrete Gage
198	TD-N4-TC4	Top Deck-Section N4-Transverse Concrete Gage
199	TD-N3.5-TC1	Top Deck-Section N3.5-Transverse Concrete Gage
200	TD-N3.5-TC2	Top Deck-Section N3.5-Transverse Concrete Gage
201	TD-S1.5-TC4	Top Deck-Section S1.5-Transverse Concrete Gage
202	TD-S1.5-TC5	Top Deck-Section S1.5-Transverse Concrete Gage
203	TD-S2-TC1	Top Deck-Section S2-Transverse Concrete Gage
204	TD-S2-TC2	Top Deck-Section S2-Transverse Concrete Gage
205	TD-S2-TC3	Top Deck-Section S2-Transverse Concrete Gage
206	TD-S2-TC4	Top Deck-Section S2-Transverse Concrete Gage
207	TD-S2-TC5	Top Deck-Section S2-Transverse Concrete Gage

208	TD-S3-TC1	Top Deck-Section S3-Transverse Concrete Gage
209	TD-S3-TC2	Top Deck-Section S3-Transverse Concrete Gage
210	TD-S3-TC3	Top Deck-Section S3-Transverse Concrete Gage
211	TD-S3-TC4	Top Deck-Section S3-Transverse Concrete Gage
212	TD-S3-TC5	Top Deck-Section S3-Transverse Concrete Gage
213	TD-N2-LC1	Top Deck-Section N2-Longitudinal Concrete Gage
214	TD-N2-LC2	Top Deck-Section N2-Longitudinal Concrete Gage
215	TD-N1-LC1	Top Deck-Section N1-Longitudinal Concrete Gage
216	TD-N1-LC2	Top Deck-Section N1-Longitudinal Concrete Gage
217	TD-S1-LC1	Top Deck-Section S1-Longitudinal Concrete Gage
218	TD-S1-LC2	Top Deck-Section S1-Longitudinal Concrete Gage
219	TD-S2-LC1	Top Deck-Section S2-Longitudinal Concrete Gage
220	TD-S2-LC2	Top Deck-Section S2-Longitudinal Concrete Gage
221	TD-N3.5-TC4	Top Deck-Section N3.5-Transverse Concrete Gage
222	TD-N3.5-TC5	Top Deck-Section N3.5-Transverse Concrete Gage
223	ER-N2	East Railing-Section N2
224	ER-N1	East Railing-Section N1
225	ER-S1	East Railing-Section S1
226	ER-S2	East Railing-Section S2
227	ER-N2-MH	East Railing-Section N2-Middle Height
228	LP-N3-ER	Linear Potentiometer-Section N3-East Railing
229	LP-S3-ER	Linear Potentiometer-Section S3-East Railing
230	LP-N3	Linear Potentiometer-Section N3
231	LP-N2	Linear Potentiometer-Section N2
232	LP-N1	Linear Potentiometer-Section N1
233	LP-CL	Linear Potentiometer-Section CL
234	SP-CL-EG1	String Potentiometer-Section CL-East Girder (Western Tip of Bottom Flange)
235	SP-CL-EG2	String Potentiometer-Section CL-East Girder (Eastern Tip of Bottom Flange)
236	LP-S1	Linear Potentiometer-Section S1
237	LP-S2	Linear Potentiometer-Section S2
238	LP-S3	Linear Potentiometer-Section S3
239	LP-N4-IF	Linear Potentiometer-Section N4-Interior Top Flange of the Fractured Girder
240	LP-N3-IF	Linear Potentiometer-Section N3-Interior Top Flange of the Fractured Girder
241	LP-S3-IF	Linear Potentiometer-Section S3-Interior Top Flange of the Fractured Girder
242	LP-S4-IF	Linear Potentiometer-Section S4-Interior Top Flange of the Fractured Girder
243	SP-CL	String Potentiometer-Across the Fracture

Agilent Systems System		
Index	**Gage Name**	**Description**
0	ER-N1-MH	East Railing-Section N1-Middle Height

1	ER-NCL-MH	East Railing-Section NCL-6" from the Top Surface
2	ER-NCL-MH2	East Railing-Section NCL-12" from the Top Surface
3	ER-SCL-MH	East Railing-Section SCL-6" from the Top Surface
4	ER-SCL-MH2	East Railing-Section SCL-12" from the Top Surface
5	ER-S1-MH	East Railing-Section S1-Middle Height
6	ER-S2-MH	East Railing-Section S2-Middle Height
7	ER-NCL	East Railing-Section NCL
8	ER-SCL	East Railing-Section SCL
9	WR-N2	West Railing-Section N2
10	WR-N1	West Railing-Section N1
11	WR-NCL	West Railing-Section NCL
12	WR-SCL	West Railing-Section SCL
13	WR-S1	West Railing-Section S1
14	WR-S2	West Railing-Section S2
15	LP-N2-IF	Linear Potentiometer-Section N2-Interior Top Flange of the Fractured Girder
16	LP-N1-IF	Linear Potentiometer-Section N1-Interior Top Flange of the Fractured Girder
17	LP-CL-IF	Linear Potentiometer-Section CL-Interior Top Flange of the Fractured Girder
18	LP-S1-IF	Linear Potentiometer-Section S1-Interior Top Flange of the Fractured Girder
19	LP-S2-IF	Linear Potentiometer-Section S2-Interior Top Flange of the Fractured Girder
20	SP-N3-WG1	String Potentiometer-Section N3-West Girder (Western Tip of Bottom Flange)
21	SP-N3-WG2	String Potentiometer-Section N3-West Girder (Eastern Tip of Bottom Flange)
22	SP-N2-WG1	String Potentiometer-Section N2-West Girder (Western Tip of Bottom Flange)
23	SP-N2-WG2	String Potentiometer-Section N2-West Girder (Eastern Tip of Bottom Flange)
24	SP-CL-WG1	String Potentiometer-Section CL-West Girder (Western Tip of Bottom Flange)
25	SP-CL-WG2	String Potentiometer-Section CL-West Girder (Eastern Tip of Bottom Flange)
26	SP-S2-WG1	String Potentiometer-Section S2-West Girder (Western Tip of Bottom Flange)
27	SP-S2-WG2	String Potentiometer-Section S2-West Girder (Eastern Tip of Bottom Flange)
28	SP-S3-WG1	String Potentiometer-Section S3-West Girder (Western Tip of Bottom Flange)
29	SP-S3-WG2	String Potentiometer-Section S3-West Girder (Eastern Tip of Bottom Flange)
30	SP-N3-EG	String Potentiometer-Section N3-East Girder (Mid-width of Bottom Flange)

31	SP-N2-EG	String Potentiometer-Section N2-East Girder (Mid-width of Bottom Flange)
32	SP-S2-EG	String Potentiometer-Section S2-East Girder (Mid-width of Bottom Flange)
33	SP-S3-EG	String Potentiometer-Section S3-East Girder (Mid-width of Bottom Flange)
34	EG-S3-TF-F	East Girder-Section S3-Exterior Top Flange-Foil Gage
35	TD-N2.5-TC1	Top Deck-Section N2.5-Transverse Concrete Gage
36	TD-N2.5-TC2	Top Deck-Section N2.5-Transverse Concrete Gage
37	TD-N2.5-TC4	Top Deck-Section N2.5-Transverse Concrete Gage
38	TD-N2.5-TC5	Top Deck-Section N2.5-Transverse Concrete Gage
39	TD-N2-LC1.5	Top Deck-Section N2-Longitudinal Concrete Gage
40	TD-N1-LC1.5	Top Deck-Section N1-Longitudinal Concrete Gage
41	TD-NCL-LC0	Top Deck-Section NCL-Longitudinal Concrete Gage
42	TD-NCL-LC1	Top Deck-Section NCL-Longitudinal Concrete Gage
43	TD-NCL-LC2	Top Deck-Section NCL-Longitudinal Concrete Gage
44	TD-SCL-LC0	Top Deck-Section SCL-Longitudinal Concrete Gage
45	TD-SCL-LC1	Top Deck-Section SCL-Longitudinal Concrete Gage
46	TD-SCL-LC2	Top Deck-Section SCL-Longitudinal Concrete Gage
47	TD-S1-LC1.5	Top Deck-Section S1-Longitudinal Concrete Gage
48	TD-S2-LC1.5	Top Deck-Section S2-Longitudinal Concrete Gage
49	TD-S2.5-TC1	Top Deck-Section S2.5-Transverse Concrete Gage
50	TD-S2.5-TC2	Top Deck-Section S2.5-Transverse Concrete Gage
51	TD-S2.5-TC4	Top Deck-Section S2.5-Transverse Concrete Gage
52	TD-S2.5-TC5	Top Deck-Section S2.5-Transverse Concrete Gage
53	TD-S3-LC1	Top Deck-Section S3-Longitudinal Concrete Gage
54	TD-S3-LC1.5	Top Deck-Section S3-Longitudinal Concrete Gage
55	TD-S3-LC2	Top Deck-Section S3-Longitudinal Concrete Gage
56	TD-S3.5-TC1	Top Deck-Section S3.5-Transverse Concrete Gage
57	TD-S3.5-TC2	Top Deck-Section S3.5-Transverse Concrete Gage
58	TD-S3.5-TC4	Top Deck-Section S3.5-Transverse Concrete Gage
59	TD-S3.5-TC5	Top Deck-Section S3.5-Transverse Concrete Gage
60	TD-S4-TC2	Top Deck-Section S4-Transverse Concrete Gage
61	TD-S4-TC4	Top Deck-Section S4-Transverse Concrete Gage

References

American Association of State Highway Transportation Officials. (2004). *AAHSTO LRFD Bridge Design Specifications.* Washington, D.C.

American Association of State Highway Transportation officials/American Welding Society. (2002). *AASHTO/AWS D1.5M/D1.5:2002 Bridge Welding Code*. AASHTO/AWS, Washington D.C./Miami, FL.

Barnard, Timothy. (2006). "Constructing a Full-Scale Horizontally-Curved Twin Steel Trapezoidal Box Girder Bridge Segment to Determine Redundancies in Fracture Critical Bridges." *Departmental Report, University of Texas at Austin.*

Connor, Robert J., Dexter, Robert, and Mahmoud, Hussam. (2005). "Inspection and Management of Bridges with Fracture-Critical Details." *National Cooperative Highway Research Program Synthesis 354.* Transportation Research Board, national Academy Press, Washington, D.C.

Espinoza, Omar. (2007). "Measurements of Deformations and Stresses due to Plate out-of-flatness in a Steel Twin Box Girder Bridge System." *Masters Thesis, University of Texas at Austin.*

Fisher, J.W., Pense, A.W., and Roberts, R. (1977). "Evaluation of Fracture of Lafayette Street Bridge." *Journal of the Structural Division,* ASCE, Vol. 103, No. 7, pp. 1339-1357.

Hovell, Catherine. (2007). "Evaluation of Redundancy in Trapezoidal Box-Girder Bridges Using Finite Element Analysis." *Masters Thesis, University of Texas at Austin.*

Idriss, R. L., White, K. R., Woodward, C. B., and Jauregui, D.V. (1995). "Evaluation and Testing of a Fracture Critical Bridge." *NDT&E International,* vol. 28, no. 6, pp. 339-347.

Kim, Janghwan. (2009). "Evaluating the Redundancy of Steel Bridges." *Doctoral Dissertation, University of Texas at Austin. In progress.*

Mouras, Joshua. (2008). "Evaluating the Redundancy of Steel Bridges: Improving the Strength and Behavior of Shear Stud Connections under Tensile Loading." *Masters Thesis, University of Texas at Austin.*

Quiel, Spencer. (2003). "Forensic Analysis of the Steel Girder Fracture in the I-95 Brandywine River Bridge." *Research Experience for Undergraduates Report, University of Notre Dame.*

Samaras, Vasilis. (2009). "Evaluating the Redundancy of Steel Bridges." *Masters Thesis, University of Texas at Austin. In progress.*

Scheffey, C.F. (1971). "Pt. pleasant Bridge Collapse: Conclusions of the Federal Study." *Civil Engineering*, Vol. 41, No. 7.

Schwendeman, L.P., and Hedgren, A.W. (1978). "Bolted repair of fractured I-79 girder." *Journal of the Structural Division*, ASCE, Vol. 104, No. 2, pp. 134-143.

Sutton, James P. (2007). "Evaluating the Redundancy of Steel Bridges: Effect of a Bridge Haunch on the Strength and Behavior of Shear Studs under Tensile Loading." *Masters Thesis, University of Texas at Austin.*

Sutton, James. P., Mouras, Joshua M., Frank, Karl H., and Williamson, Eric B. "The Tensile Capacity of Welded Shear Studs." *Center for Transportation Research at the University of Texas at Austin*. FHWA/TX-08/9-5498-R2. October, 2008.

Vita

Bryce Jacob Neuman was born on December 7, 1981 in Tucson, Arizona to Terry and Jerry Neuman. He is the fourth out of five children, appropriately referred to as the "Killer Bs." From oldest to youngest, their names are: Brenda, Brian, Bradley, Bryce, and Brooke. As of the time of this writing, he was the uncle to five amazing nieces and nephews named (from oldest to youngest) Isabella, Evan, Peighton, Mara, and Ethan.

After graduating from Catalina Foothills High School in Tucson, Arizona in 2000, Bryce enrolled at the University of Pennsylvania in Philadelphia, Pennsylvania, where he completed a Bachelors of Science in Economics from the Wharton School of Business in 2004. One year later, he re-entered school as a Post-Baccalaureate in Civil Engineering at Northern Arizona University in Flagstaff, Arizona, where he also performed research under the supervision of Dr. Joshua Hewes. After two years of undergraduate work, he began his graduate education in structural engineering at the University of Texas at Austin, where he participated in research at the Ferguson Structural Engineering Laboratory under the supervision of Dr. Eric Williamson and Dr. Karl Frank. Following the completion of his Master's degree in 2009, Bryce took his first full-time engineering position in San Francisco, California.

Outside of his family and academic pursuits, Bryce is passionate about pedal-biking for recreation and transportation, other outdoor adventures, music with spark, and foods of all kinds.

Permanent address: 5927 E Paseo Cimarron

Tucson, Arizona 85750

bjneuman@gmail.com

This thesis was typed by the author.